

**Valorisation of Citrus Fruit Peel Wastes and Blackcurrant
Pomace via Acid-free Microwave Hydrothermal Processes**

Xiangju Meng

Doctor of Philosophy

University of York

Chemistry

Green Chemistry Centre of Excellence

February 2022

Abstract

The chemical and allied-industries have been for too long reliant on crude oil and fossil fuels for their chemicals, materials and energy needs. These industries are significant contributors (approximately 4% of global CO₂ emissions) to anthropogenic-induced global warming. Future thinking requires consideration of alternative, carbon-neutral renewable feedstocks, such as biomass, that develop biorefineries in place of traditional petroleum refineries. Unavoidable food supply chain wastes, such as citrus peels and blackcurrant pomace, are exemplars of large volume, renewable feedstock, which can be exploited (valorised) for the production of biobased chemicals, materials and bioenergy.

Herein, the valorisation of citrus peels (orange and lemon) and blackcurrant pomace (BCP) via acid-free hydrothermal microwave processing, as opposed to conventional heating in acidic media, is reported. This valorisation approach formed two fractions: a hydrolysate which was rich in pectin (citrus) and antioxidants (BCP), and a solid fraction, giving microfibrillated cellulose (MFC) (citrus) and residues (BCP).

Citrus pectin is linear polysaccharide with smooth region (homogalacturonan, HG) and hairy region (rhamno-galacturonan, RG). Orange pectin processed at 160 °C resulting in an RG-I pectin rich in galactan, which proved that hydrothermal microwave processing of orange pectin at 160 °C is a selective degradation. MFC was successfully characterised as a nanostructured material with properties highly dependent on the treatment temperature.

BCP microwave hydrolysates (MHs) produced at low temperatures (<120 °C) were characterised as a complex mixture of variety compounds presenting antioxidant activity.

In conclusion, the presented valorisation of citrus peels and BCP confirmed its potential as a valuable bioresource for the production of pectin, MFC and antioxidants with numerous potential applications.

Abbreviations

AG	Arabinogalactan
Ara	Arabinose
ATR-IR	Attenuated Total Reflection Infra-Red
BBE	Blueberry Extract
BC	Blackcurrant
BCP	Blackcurrant Pomace
BPA	Biochar Pectin Alginate Hydrogel Beads
C3G	Cyanidin 3- <i>O</i> -glucoside
C3R	Cyanidin 3- <i>O</i> -rutinoside
CAN	Ceric Ammonium Nitrate
CEO	Clove Essential Oil
ChCl	Choline Chloride
CHN	Carbon Hydrogen Nitrogen
CHX	Chlorhexidine Digluconate-based Antibacterial Solution
CLSM	Confocal Laser Scanning Microscopy
CI	Crystalline Index
CNF	Cellulose Nano Fibres
COP26	2021 United Nations Climate Change Conference
COSY	¹ H/ ¹ H Correlation Spectroscopy
COVID-19	Coronavirus identified in 2019
CP-MAS	Cross Polarisation Magic Angle Spinning
CPG	Citrus Pectin Gel
CPW	Citrus Peel Waste
CSF	Chelator Soluble Fraction
D	Dispersity

D3G	Delphinidin 3- <i>O</i> -glucoside
D3R	Delphinidin 3- <i>O</i> -rutinoside
DCM	Dichloromethane
DE	Degree of Esterification
DEPT	Distortionless Enhancement by Polarisation Transfer
DF	Dietary Fibre
DLPR	Depectinated Lemon Peel Residue
DMSO	Dimethyl Sulfoxide
DOPR	Depectinated Orange Peel Residue
DPPH	2,2-diphenyl-1-picrylhydrazyl
EAE	Enzyme Assisted Extraction
EDTA	Ethylenediamine-tetraacetic Acid
E-Factor	Environmental Factor
EO	Essential Oil
EU	European Union
FAO	Food and Agriculture Organisation
FDCA	2,5-Furandicarboxylic Acid
FSCW	Food Supply Chain Waste
Gal	Galactose
Gal A	Galacturonic Acid
Gal-3	Galectin-3
GDP	Gross Domestic Product
GPC	Gel Permeation Chromatography
GRAS	Generally Recognised as Safe
HCA	Hydroxycinnamic Acid / Hierarchical Cluster Analysis
HD	Hydro-distillation

HG	Homogalacturonan
HHV	Higher Heating Value
HIUS	High-intensity Ultra-sonication
HMF	5-Hydroxymethylfurfural
HPLC	High-performance Liquid Chromatography
HSQC	Heteronuclear Single Quantum Correlation
Hy-MASS	Hydrothermal Microwave Assisted Selective Scissoring
IBA	International Blackcurrant Association
IR	Infrared
IV	Intrinsic Viscosity
IVn	Number Average Intrinsic Viscosity
LALS	Low angle light scattering
LEO	Lemon Essential Oil
LP	Lemon Peel
LRS	Lucozade-Ribena-Suntory
MAE	Microwave Assisted Extraction
MAHD	Microwave Assisted Hydro-distillation
MAP	Microwave Assisted Pyrolysis
MCP	Modified Citrus Pectin
MFC	Micro-fibrillated Cellulose
MH	Microwave Hydrolysate
MHG	Microwave Hydro-diffusion and Gravity
Mn	Number Average Molecular Weight
MR	Microwave Residue
MSD	Microwave Steam Distillation
MSDf	Microwave Steam Diffusion

Mw	Weight Average Molecular Weight
MW	Microwave
MWAs	Microwave Absorbers
NADES	Natural Deep Eutectic Solvent
NFC	Nano-fibrillated Cellulose
NMR	Nuclear Magnetic Resonance
OP	Orange Peel
OPW	Orange Peel Waste
PEF	Polyethylene Furanoate
PET	Polyethylene Terephthalate
PHAs	Polycyclic Aromatic Hydrocarbons
piDF	Pure Insoluble Dietary Fibre
PTFE	Polytetrafluoroethylene
RALS	Right angle light scattering
Rh	Hydrodynamic Radius
Rha	Rhamnose
RI	Refractive Index
RG-I	Rhamnogalacturonan I
RG-II	Rhamnogalacturonan II
RT	Retention Time
SA	Sodium Alginate
SD	Steam Distillation
SDGs	Sustainable Development Goals
SEM	Scanning Electron Microscopy
SFME	Solvent Free Microwave Extraction
SHDf	Steam Hydro-diffusion

SSNMR	Solid-state ¹³ C Nuclear Magnetic Resonance
STA	Simultaneous Thermal Analysis
SWE	Subcritical Water Extraction
TEM	Transmission Electron Microscopy
TEMPO	2,2,6,6-tetra-methylpiperidine-1-oxyl
TGA	Thermogravimetric Analysis
TMA	Total Monomeric Anthocyanins
TMP	Thermo-mechanical Pulp
TPC	Total Phenolic Content
UAE	Ultrasound Assisted Extraction
UFSCW	Unavoidable Food Supply Chain Waste
UK	United Kingdom
UN	United Nations
USA	United States of America
USD	United States Dollars
UV	Ultraviolet
WRV	Water Retention Value
WSF	Water Soluble Fraction
wsCQDs	water soluble carbon quantum dots
XRD	X-Ray Diffraction

List of Contents

Abstract	2
Abbreviations	3
List of Contents	8
List of Figures	14
List of Tables	20
Acknowledgement	22
Declaration	23
1. Introduction	24
1.1 Global Overview	24
1.2 Sustainable Development Goals (SDGs)	26
1.3 Green Chemistry, Biomass & Biorefinery	30
1.3.1 Biomass	32
1.3.2 Biorefineries	34
1.4 Food Supply Chain Waste (FSCW) and Unavoidable Food Supply Chain Waste (UFSCW).....	36
1.5 Citrus Fruit & Peel Waste.....	39

1.5.1	Opportunities from Orange Peel Waste.....	41
1.5.2	Essential Oils and D-limonene.....	43
1.5.3	Opportunities from Lemon Peel Waste	45
1.6	Blackcurrant Pomace	49
1.7	Aims	54
1.8	Microwaves	58
1.8.1	Pectin.....	62
1.8.2	Micro-fibrillated celluloses (MFCs)	72
1.8.3	Production of MFC	72
1.8.4	Applications of MFC	74
2.	Experimental	77
2.1	Materials & Reagents	77
2.2	Methodology	78
2.2.1	Acid-free microwave assisted pectin extraction (general method) ..	78
2.2.2	Microwave micro-fibrillated cellulose production (general method)	
	79	
2.2.3	Microwave assisted extraction (MAE) of BCP. (General method) ..	80

2.3	General Instrumental analysis	80
2.3.1	ATR-IR	80
2.3.2	Solid state ¹³ C Nuclear Magnetic Resonance (SSNMR)	81
2.3.3	Thermogravimetric Analysis (TGA)	81
2.3.4	Elemental analysis (CHN).....	82
2.4	Characterisation of Pectin	82
2.4.1	Degree of Esterification	82
2.4.2	Liquid ¹³ C NMR.....	83
2.4.3	High-performance Liquid Chromatography (HPLC).....	83
2.4.4	Gel Permeation Chromatography.....	84
2.5	Characterisation of MFC.....	84
2.5.1	MFC gel formation.....	84
2.5.2	Water retention value (WRV).....	85
2.5.3	Powder X-Ray Diffraction (XRD)	85
2.5.4	Scanning Electron Microscopy (SEM)	86
2.5.5	Transmission Electron Microscopy (TEM).....	86

2.5.6	Confocal Laser Scanning Microscopy (CLSM).....	86
2.6	Characterisation of BCP Hydrolysates.....	87
2.6.1	Total Phenol Content (TPC).....	87
2.6.2	Total Antioxidant Activity (DPPH method).....	88
2.6.3	¹ H NMR	89
2.6.4	2D NMR.....	89
2.6.5	HPLC-MS	89
3.	Results and Discussion.....	91
3.1	Part 1: Pectin Isolation and Characterisation	91
3.1.1	Pectin Isolation.....	91
3.1.2	Pectin Characterisation.....	94
3.1.3	Summary	111
3.2	Part 2: Production and Characterisation of Citrus Micro-fibrillated Cellulose (MFC) or Defibrillated Celluloses	112
3.2.1	MFC Production.....	112
3.2.2	MFC Characterisation	114
3.2.3	Potential Application of MFCs: Hydrogels.....	128

3.2.4	Summary	132
3.3	Part 3: Production and Characterisation of Blackcurrant Pomace Hydrolysates.....	132
3.3.1	BCP microwave hydrolysate (MH).....	133
3.3.2	Total phenol content & antioxidant activity of BCP and MHs.	136
3.3.3	¹ H NMR of BCP MHs.....	138
3.3.4	2D NMR of BCP MH-50	139
3.3.5	HPLC-MS of BCP hydrolysate	142
3.3.6	GPC of BCP Microwave Hydrolysates	153
3.3.7	BCP Microwave Residues (MR).....	155
3.3.8	Summary	158
4.	Conclusion.....	159
4.1	Regarding the Obtained Results.....	159
4.1.1	Valorisation of Citrus Peel Waste.....	159
4.1.2	Valorisation of Blackcurrant Pomace.....	160
4.2	Limitation and Future Work.....	161
4.2.1	Limitations of Citrus Valorisation.....	161

4.2.2	Future work - Soxhlet Pretreatment	162
4.2.3	Result of Soxhlet Pretreatment	163
4.2.4	Limitation of Blackcurrant Valorisation and Future Work.....	164
	References	166
	Appendices	182

List of Figures

Figure 1 Structure of Cellulose	32
Figure 2 Structure of Hemicellulose	33
Figure 3 Lignin monolignols.....	34
Figure 4 Overview of lignocellulosic biomass, sugar/starch crops and oil plants (feedstocks) and the biorefinery processes.	35
Figure 5 Split of EU food waste by sector.	38
Figure 6 Components of UFSCW and their potential products.	39
Figure 7 Global citrus fruit production in breeds (left) and orange production in countries (right).....	40
Figure 8 Cross Section of an Orange.	41
Figure 9 Stereoisomers of limonene.	43
Figure 10 Structures of lemon pigment main components.	46
Figure 11 The structure of lemon yellow #15.	47
Figure 12 Comparison of different routes from aldose to FDCA.	48
Figure 13 Blackcurrant (A) and blackcurrant pomace (B).....	49
Figure 14 Top 6 black and red currant producers (tonnes) in 2018 and 2019. IBA	

.....	50
Figure 15 The chemical structure of 4 main anthocyanins.	51
Figure 16 General process of microwave process of citrus peel waste.....	55
Figure 17 General process of microwave hydrothermal process of BCP from 50 °C to 160 °C to obtain hydrolysates and residues.	57
Figure 18 Microwave heating compared with conventional heating.	59
Figure 19 Schematic Structure of Pectin and structure of sugars.	64
Figure 20 Calibration of TPC, concentration of gallic acid vs absorbance at 765 nm.....	88
Figure 21 Summary of pectin yield (wt%, dry basis) from A) orange peel (OPR) and B) lemon peel (LPR).	92
Figure 22 Stacked IR spectra of pectins from direct processing OPR with respect to commercial citrus pectin (top) and LPR (bottom).	95
Figure 23 TGA of pectins from direct processing of OPR (top) and LPR (bottom).	98
Figure 24 ¹³ C NMR of orange OP1, OP2 and OP3 (*= solvent impurity)	99
Figure 25 Expansion of ¹³ C NMR of OP3-160 for chain length calculation.	100

Figure 26 ^{13}C NMR of lemon pectins. (*= solvent impurity).....	101
Figure 27 ^{13}C NMR of OP0-120, OP3-160, OP0-160 and OP3'-160.....	102
Figure 28 Galacturonic acid & galactose molar percent. (%).....	103
Figure 29 Mw, dispersity and intrinsic viscosity of pectin samples from GPC results.	106
Figure 30 Overlay Chromatograms for Orange Pectins. [RI (top left), Viscometer (top right), RALS (bottom left) and LALS (bottom right)].	107
Figure 31 Overlay Chromatograms for Lemon Pectins. [RI (top left), Viscometer (top right), RALS (bottom left) and LALS (bottom right)]	108
Figure 32 Mark-Houwink Plot for Orange Pectins	110
Figure 33 Mark-Houwink Plot for Lemon Pectins.	111
Figure 34 Yield of MFC production from LPR and OPR.....	113
Figure 35 Stacked IR spectra of orange and lemon MFCs.	114
Figure 36 STA of MFC samples.....	116
Figure 37 Solid state NMR of MFC samples.....	117
Figure 38 XRD of all MFCs.....	118
Figure 39 Crystallinity Index (CI) of all MFCs.	119

Figure 40 SEM of orange peel.	120
Figure 41 SEM images of MFC samples. (A. OMFC-120, B. OMFC-140, C. OMFC-160, D. OMFC-160', E. LMFC-120, F. LMFC-140, G LMFC-160, H. OMFC-120 with high magnification)	121
Figure 42 TEM images. A&B: OMFC-120, C: OMFC-160, D: OMFC-120 gel.	123
Figure 43 CLSM Reference. Cellulose & Pectin. Fluorescence strength vs wavelength (nm).....	125
Figure 44 CLSM of All MFCs. Green – cellulose, Red – lignin, Blue – pectin and mixed.....	126
Figure 45 HMF conversion pathway to humins.....	127
Figure 46 WRV of MFC samples. (g water per g MFC).....	128
Figure 47 Gel formation of orange (right) and lemon (left) MFCs. 120,140 and 160 from top to bottom.	131
Figure 48 Example SEM of a MFC gel.	131
Figure 49 Product and Yield of BCP MAE.....	133
Figure 50 BCP extractives and hydrolysates.....	134
Figure 51 BCP MAE hydrolysate water solution (5 mg/ml). From BCP-90 to	

BCP-160, left to right.....	135
Figure 52 HPLC result of BCP MAE hydrolysates. Mg/ml	136
Figure 53 Total phenol content of BCP hydrolysate. Mg GAE / g Hydrolysate (orange) or g BCP (blue).....	137
Figure 54 DPPH antioxidant inhibition of BCP hydrolysates.	137
Figure 55 Proton NMR of BCP hydrolysates.....	138
Figure 56 Proton NMR expansion of BCP MH-50. δ 3.24 (s), 3.01 – 2.77 (m).	139
Figure 57 2D NMR (HSQC) of BCP MH-50.	140
Figure 58 $^1\text{H}/^1\text{H}$ correlation spectroscopy (COSY) of BCP MH 50.....	141
Figure 59 DEPT spectra of BCP MH 50.....	142
Figure 60 All BCP MH samples HPLC-MS OVERLAY. (positive).....	142
Figure 61 Structures of compounds identified in BCP MH positive HPLC-MS.	143
Figure 62 All BCP MH samples HPLC-MS OVERLAY. (negative).....	147
Figure 63 Structures of compounds identified in BCP MH negative HPLC-MS.	148

Figure 64 Hierarchical cluster tree of identified compounds in hydrolysates. Top - Positive, Bottom – Negative.	152
Figure 65 Overlay Chromatograms for BCP MHs. (RI (top left), Viscometer (top right), RALS (bottom left) and LALS (bottom right). MH-100 (Red), MH- 110 (Purple), MH-120 (Green), MH-140 (Black) and MH-160 (Blue).....	154
Figure 66 Mark-Houwink Plot of MH-100 (Red), MH-110 (Purple), MH-120 (Green), MH-140 (Black) and MH-160 (Blue).....	155
Figure 67 CHN of BCP MAE residues.	156
Figure 68 Solid-state NMR of BCP and MAE residues (90-160 °C).....	156
Figure 69 STA of BCP MRs.....	157
Figure 71 Comparison of oven dried (vials) and freeze dried (bags) pectin samples.....	163
Figure 72 Hydrogel of freeze dried WMFC.....	164

List of Tables

Table 1 17 Sustainable Development Goals.....	27
Table 2 Citrus fruit production and processing in 2015 and 2016 (Million tonnes) (FAO 2017)	41
Table 3 Composition of sweet orange peel waste.	42
Table 4 Composition of a variety of essential oils extracted from oranges.	43
Table 5 Summary of reported heavy metal ions adsorption capacity of pectins..	70
Table 6 Citrus feedstock information.	77
Table 7 DE (%) of pectins from direct processing of OPR with respect to commercial citrus pectin and LPR.	96
Table 8 Monosaccharide content of pectin. Molar percent (%).	103
Table 9 Quantitative GPC results for analysis of pectin.	104
Table 10 Comparison of Pectin extraction conditions and yield of this thesis and literature.	112
Table 11 Top 14 compounds identified in BCP MHs. Positive.....	144
Table 12 Top 12 Compounds identified in BCP MHs. Negative.	149
Table 13 GPC result of BCP MH samples.	153

Table 14 Yield of Soxhlet pretreated WMFC and pectin.163

Acknowledgement

First and foremost, I'd like to thank my parents Fanzhi Meng and Peijun Qiu, who have always been offering me financial and mental support in my whole life. And girlfriend Yuli Zheng, really appreciate for her company in the past 3 years.

I would like to thank my supervisor Prof. Avtar Matharu and the Green Chemistry Centre of Excellence at the University of York for giving me the opportunity to be a PhD in an area I'm interested in, and for my supervisor's suggestions and guidance. I am grateful to Dr. Duncan Macquarrie as my Independent Panel Member (IPM) for his support and guidance.

I would also like to thank technician team of GCCE, Dr. Richard Gammons, Dr. Hannah Briers and Dr. Suranjana Bose for their help and training in the lab. Many thanks to university staff members: Dr. Heather Fish, Dr. Graeme McAllister, Dr. Meg Stark, Dr. Karen Hodgkinson and Dr. Joanne Marrison, for their expertise that brought many contributions to my work.

Special thanks to my friends Dr. Hao Xia, Dr. Long Zhou and Dr. Yang Gao, for their help in both my research work and daily life. Great thanks to everyone in GCCE for your help in the lab. It has been a great honour to be a member of GCCE.

Declaration

I declare that this thesis is a presentation of original work and I am the sole author.

This work has not previously been presented for an award at this, or any other,

University. All sources are acknowledged as References.

1. Introduction

1.1 Global Overview

Climate change is the biggest threat facing the future sustainability of our planet. Rising atmospheric carbon dioxide levels, rising global temperature, rising sea levels, receding arctic ice shelves and adverse weather conditions are all proxies for climate change. We urgently need to limit global temperature rise to within 1.5 °C with respect to pre-industrialisation levels by 2050, if not sooner.¹ The 2021 United Nations Climate Change Conference, also known as COP26, is already alerting the world to drastic action within this decade let alone by 2050.² Human or anthropogenic-induced activity due to industrialisation is a major cause of climate change. Anthropogenic activity can be mirrored with respect to global megatrends of increasing population and urbanisation and a commensurate need for resources that provide energy, materials and chemicals for our daily lifestyles. Global population has increased rapidly in the past seventy years from 2.5 billion (1950) to 7.8 billion (2020) and is predicted to increase to 9.7 billion by 2050.³ The populations of the 47 least developed countries are among the world's fastest growing, which may double in population in 2050. Heavy industrialisation, urbanisation and consumerism have seen global gross domestic product (GDP) increase from 50.1 trillion USD (2000) to 80.2 trillion USD (2017).⁴ We live in a linear or cradle to grave economy that exploits

natural resources for the manufacture of goods and articles that ultimately end up as *waste*. Our global material footprint, which refers to the total amount of raw materials extracted to meet final consumption demands, rose from 54 billion metric tonnes in 2000 to 92 billion in 2017. If unabated, then our global material footprint is projected to increase to 190 billion metric tonnes by 2060. The material footprint per capita is dependent on the wealth of a particular nation. High-income countries have a per capita material footprint of approximately 26 tonnes, whilst it is meagre 2 metric tonnes per capita for low-income countries. Nevertheless, the global material footprint is increasing at a faster rate than both population and economic output.⁵ We cannot sustain future resource requirements based on our current linear consumption rates.

Global development is often predicated to the discovery of crude oil for our energy needs but also, our ability to fractionate and convert it into a plethora of chemical building blocks, functional molecules and materials. The chemical industry contributes to 36% of total oil consumption and a considerable share of this serve as feedstock for producing chemicals and materials in addition to energy and heat. Interestingly, 96% of all manufactured organic compounds are derived from fossil fuels.⁶ The traditional chemical industry follows a linear pathway whereby crude oil feedstocks are pushed through a production chain that is based on reagents that are designed to be highly reactive, but usually residual and toxic. These processes always

generate waste, at rates higher than the intended product. The Environmental Factor (E-Factor) which is a measure of the amount of waste generated per unit of product produced for specialty chemicals is between 1-5 and 25-100 for pharmaceuticals.⁷

However, fossil fuel consumption needs to be controlled to keep global warming to within 1.5°C with respect to pre-industrialisation levels.^{2, 8, 9} [ENREF 7](#) Furthermore, crude oil is a non-renewable, finite, resource. It cannot guarantee our future energy, chemicals and materials needs. Alternative or renewable feedstocks need to be considered, such as biomass, preferably as waste and we also need to adhere to the principles of recycling and re-use, doing more with less, carbon neutrality and the United Nations 17 Sustainable Development Goals (SDGs), so that we develop circular thinking for a sustainable 21st Century.

1.2 Sustainable Development Goals (SDGs)

In 2015, the United Nations Sustainable Development Summit launched 17 Sustainable Development Goals (SDGs, see Table 1) as part of the resolution ‘*Transforming our world: the 2030 Agenda for Sustainable Development*’, aimed at protecting people and the planet, stimulating global prosperity and peace and developing global partnerships¹⁰.

Table 1 17 Sustainable Development Goals¹⁰

SDG	Definition
<i>Goal 1</i>	<i>End poverty in all its forms everywhere</i>
<i>Goal 2</i>	<i>End hunger, achieve food security and improved nutrition and promote sustainable agriculture</i>
<i>Goal 3</i>	<i>Ensure healthy lives and promote well-being for all at all ages</i>
<i>Goal 4</i>	<i>Ensure inclusive and equitable quality education and promote lifelong learning opportunities for all</i>
<i>Goal 5</i>	<i>Achieve gender equality and empower all women and girls</i>
<i>Goal 6</i>	<i>Ensure availability and sustainable management of water and sanitation for all</i>
<i>Goal 7</i>	<i>Ensure access to affordable, reliable, sustainable and modern energy for all</i>
<i>Goal 8</i>	<i>Promote sustained, inclusive and sustainable economic growth, full and productive employment and decent work for all</i>
<i>Goal 9</i>	<i>Build resilient infrastructure, promote inclusive and sustainable industrialisation and foster innovation</i>
<i>Goal 10</i>	<i>Reduce inequality within and among countries</i>
<i>Goal 11</i>	<i>Make cities and human settlements inclusive, safe, resilient and sustainable</i>
<i>Goal 12</i>	<i>Ensure sustainable consumption and production patterns</i>
<i>Goal 13</i>	<i>Take urgent action to combat climate change and its impacts</i>
<i>Goal 14</i>	<i>Conserve and sustainably use the oceans, seas and marine resources for sustainable development</i>
<i>Goal 15</i>	<i>Protect, restore and promote sustainable use of terrestrial ecosystems, sustainably manage forests, combat desertification, and halt and reverse land degradation and halt biodiversity loss</i>
<i>Goal 16</i>	<i>Promote peaceful and inclusive societies for sustainable development, provide access to justice for all and build effective, accountable and inclusive institutions at all levels</i>
<i>Goal 17</i>	<i>Strengthen the means of implementation and revitalise the global partnership for sustainable development</i>

The 2030 agenda is determined to end poverty and hunger, protect the planet from

degradation, ensure all human beings can enjoy the prosperity, foster peace and mobilise partnership between countries. The SDGs are inter-related and contain a broad range of issues that are further sub divided in to several targets. UN SDG 12, *Responsible Consumption and Production*, and targets 12.2, 12.3 and 12.5 are the most relevant to this thesis, i.e.,

Goal 12: Ensure sustainable consumption and production patterns.

Target 2: By 2030, achieve the sustainable management and efficient use of natural resources.

Target 3: By 2030, halve per capita global food waste at the retail and consumer levels and reduce food losses along production and supply chains, including post-harvest losses.

Target 5: By 2030, substantially reduce waste generation through prevention, reduction, recycling and reuse.

Total production and waste of citrus fruit and blackcurrant will be discussed later in Section 1.5 and 1.6.

However, the research within this thesis also partly interconnects with SDG 2 and 13, for example,

Goal 2: End hunger, achieve food security and improved nutrition and promote sustainable agriculture.

Target 3: By 2030, double the agricultural productivity and incomes of small-scale food producers, in particular women, indigenous peoples, family farmers,

*pastoralists and fishers, including through secure and equal access to land, other **productive resources** and inputs, knowledge, financial services, markets and opportunities for **value addition and non-farm** employment.*

***Target 4:** By 2030, ensure **sustainable food production systems** and implement resilient agricultural practices that increase productivity and production, that help maintain ecosystems, that strengthen capacity for adaptation to **climate change**, extreme weather, drought, flooding and other disasters and that progressively improve land and soil quality*

The utilisation of food supply chain waste (FSCW) can help to increase the income of small-scale food producers, provide opportunities for value addition and non-farm employment, build sustainable food production systems. The products isolated in the research, for example, pectin & cellulose, have the potential to be used in food industries, which shows a connection with ending hunger and achieving food security.

Goal 13: Take urgent action to combat climate change and its impacts.

Obviously, the use of renewable resources especially waste, whilst off-setting our reliance of crude oil, will positively impact climate change.

In 2019, the UN published the *Global Sustainable Development Report 2019*,¹¹ in which the SDG targets was classified into 3 groups. The first comprises the targets that are on track, the second comprises those need extra efforts and, the third comprises those SDGs where implementation is moving in the opposite direction.

Unfortunately, all the planet-related SDGs (goals 12-15) fell into the third category.

The latter are most worrisome either because implementation of the Goals has not yet

been able to reverse pre-existing deterioration of the planet, or because world recovery from the 2008 economic crisis has brought back negative trends.

Recently, the Food and Agricultural Organisation (FAO) released a report, “*Tracking progress on food and agriculture – related SDG indicators 2021*”,¹² looking at the impact of the global COVID-19 pandemic on food poverty. The pandemic and its forced lockdowns might have temporarily halted global greenhouse emissions but has pushed an additional 83-132 million people into chronic hunger.

Although green chemistry pre-dates the SDGs, there are many interconnects between the two and plays an important role in their attainment. Green chemistry provides a new circular pathway from renewable resources.¹³

1.3 Green Chemistry, Biomass & Biorefinery

Chemistry is always associated with danger, toxicity and pollution. In this case, a move towards green chemistry becomes very important.¹⁴ Green Chemistry is defined as the “*design of chemical products and processes to reduce or eliminate the use and generation of hazardous substances*”.¹⁵ An important aspect of Green Chemistry is at the design or concept stage. The design is a profession of human intention and one cannot design by accident.¹⁶ Green Chemistry is governed by 12 principles as first defined by *Anastas and Warner* which are highlighted as follows: ¹⁵.

1. *Prevention: Waste prevention is better than treatment or clean up.*
2. *Atom Economy: Chemical synthesis should maximise the incorporation of all starting materials.*
3. *Less Hazardous Chemical Synthesis: Chemical synthesis should ideally use and generate non-hazardous substances.*
4. *Designing Safer Chemicals: Chemical products should be designed to preserve efficacy of function while reducing toxicity.*
5. *Safer Solvents and Auxiliaries: The use of auxiliary substances (e.g., solvents, separation agents, etc.) should be made unnecessary wherever possible and, innocuous when used.*
6. *Design for Energy Efficiency: Energy demands in chemical syntheses should be minimised.*
7. *Use of Renewable Feedstocks: Raw materials should increasingly be renewable.*
8. *Reduce Derivatisations: Unnecessary derivatisation (use of blocking groups, protection/deprotection, temporary modification of physical/chemical processes) should be minimised or avoided, if possible, because such steps require additional reagents and can generate waste.*
9. *Catalysis: Catalytic reagents (as selective as possible) are superior to stoichiometric reagents.*
10. *Design for Degradation: Chemical products should break down into innocuous products.*
11. *Real time analysis for pollution prevention: Analytical methodologies need to be further developed to allow for real-time, in-process monitoring and control prior to the formation of hazardous substances.*
12. *Inherently Safer Chemistry for Accident Prevention: Chemical processes require better control with minimum potential for accidents.*

As we seek a future sustainable world through the practice of SDGs and the 12 principles of green chemistry, then the use of renewable feedstocks (Principle 7) is becoming more important for future chemical industries that were/are historically dependent on fossil fuels. The use of biomass as a feedstock for the chemical, fuel and

material industries is an attractive alternative to the use of fossil fuels, because of its availability in large volumes and renewability within reasonable timescales.

1.3.1 Biomass

Biomass is any organic material that comes from plants and animals based on land or in water. This thesis focuses on terrestrial plant or vegetal biomass, which comprises cellulose, hemicellulose and lignin in addition, to starch, oils and proteins.

1.3.1.1 Cellulose

Cellulose is a linear homopolymer of glucose residues connected by β -(1-4)-glycosidic bonds (Fig. 1) which thermally fragment above 300 °C. Cellulose is probably the most common organic polymer on the Earth with total production of 10^{11} - 10^{12} tonnes annually.¹⁷⁻¹⁹. Cellulose is biodegradable, renewable, undergoes decomposition rather than melting but is insoluble in most solvents due to extensive hydrogen bonding and a highly crystalline structure.^{19, 20} However, cellulosic-rich feedstocks, such as agricultural or forestry residues, are being exploited to produce bioethanol via hydrolysis and fermentation.²¹

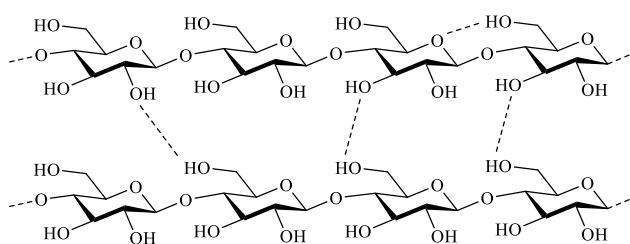


Figure 1 Structure of Cellulose

1.3.1.2 Hemicellulose

Hemicellulose(s) is/are complex short chain, amorphous, branched polysaccharides, composed of pentoses (xylose, arabinose), hexoses (mannose, glucose, galactose), and sugar acids (Fig. 2).²² Chain lengths of hemicellulose polymers are much shorter than those of cellulose.²³ Hemicelluloses contribute to strengthening the cell wall by interaction with cellulose and lignin.²⁴

Generally, hemicelluloses in hard wood such as birch, walnut and willow contain mostly xylans, whereas hemicelluloses in soft wood such fir, pine and spruce contain mostly glucomannans.²²

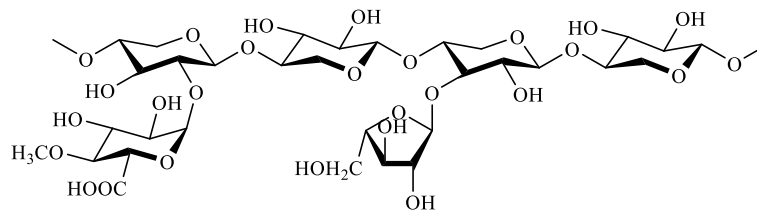


Figure 2 Structure of Hemicellulose

1.3.1.3 Lignin

Lignin is condensed phenolic-like aromatic polymer that binds and cross-links microcellulose fibres and hemicellulosic cell wall components.²⁵⁻²⁷ Lignin accounts for 30% by weight in softwood and 20% - 25% in hardwood.^{28,29} Lignin is mainly an amorphous tridimensional polymer of three primary cinnamyl units (Fig. 3): sinapyl (3,5-dimethoxy-4-hydroxycinnamyl), coniferyl (3-methoxy-4-hydroxycinnamyl), and

p-coumaryl (4-hydroxycinnamyl) alcohols, joined by ether and C-C linkages.²⁸ Lignin is an important source of biobased phenols but is often burnt for energy recovery.²⁶

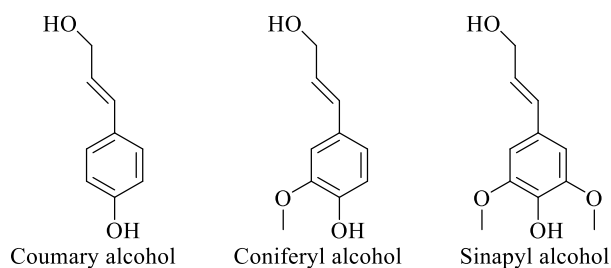


Figure 3 Lignin monolignols.

1.3.2 Biorefineries

A biorefinery is a facility that converts biomass and its constituents into smaller chemical moieties upon application of an appropriate technology or process (fermentation, pyrolysis, liquefaction) to yield potentially high-value downstream products (Fig. 4).³⁰⁻³³ Pyrolysis has been well-explored as a technology. Pyrolysis is a thermal process in the absence of oxygen that converts biomass into flammable gas, bio-oil and biochar.³⁴ Bio-oil is a liquid mixture of organic compounds including the sugar and sugar oligomers, carboxylic acid, aldehydes, ketones, esters, alcohols derived from cellulosic material and phenolics derived from lignin, as well as water.³⁵

Early biorefineries also known as first generation biorefineries focused on single technology and single feedstock such as vegetable oil or starch to biodiesel or bioethanol, respectively.³⁶ However, these biorefineries suffered public backlash because the feedstock used to make fuel was in direct competition with food and feed,

i.e., food versus feed versus fuel debate.³⁷ A second generation biorefinery does not compete with the food supply and is based on lignocellulosic biomass from agricultural residues and forestry waste. A third generation biorefinery is produces high-value chemicals or materials from algae or aquatic biomass.³⁶ In the future, biorefineries will be those based on commercially-viable technology, responsive to irregular supply of non-food feedstocks and flexible so that outputs are market demand driven.³⁸

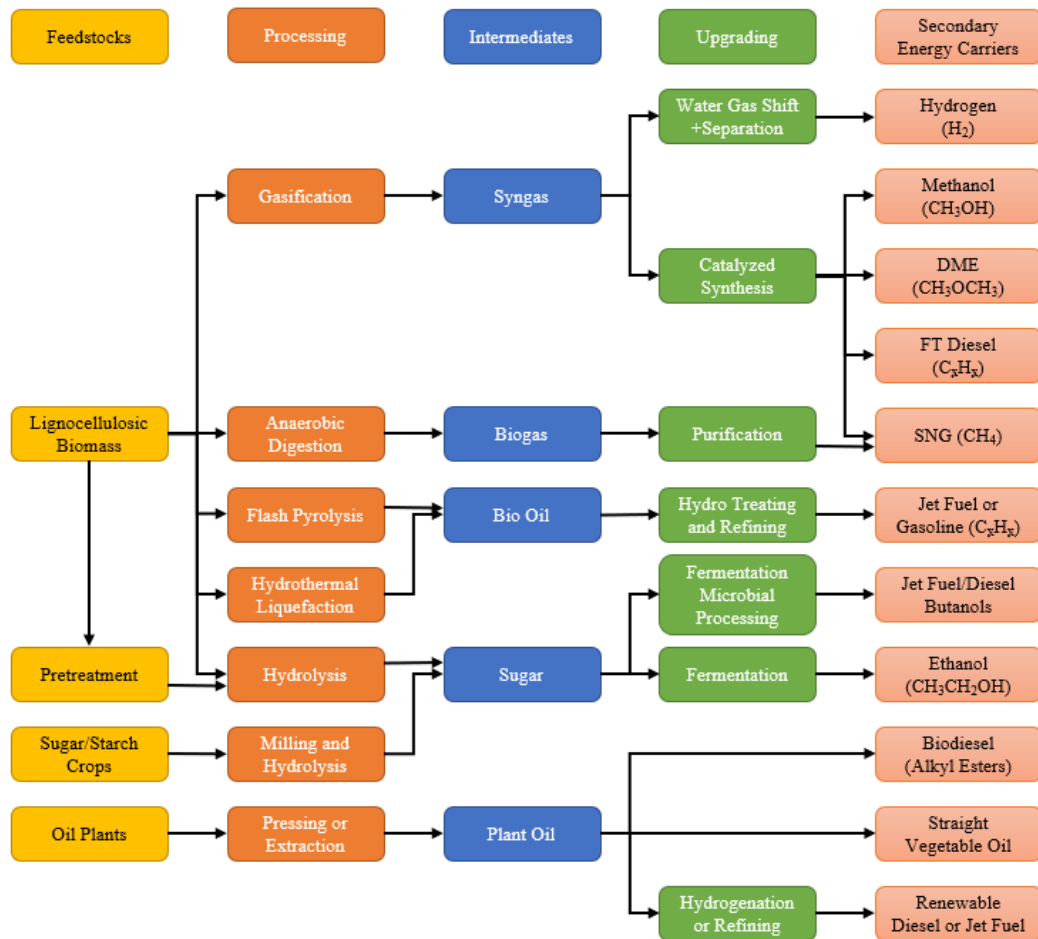


Figure 4 Overview of lignocellulosic biomass, sugar/starch crops and oil plants (feedstocks)

and the biorefinery processes. ³⁰⁻³³

Thus, the use of biomass provides two main benefits, namely: i. waste prevention, and; ii. As a carbon-neutral raw material for chemical, fuel and material industries.

Unavoidable food supply chain wastes (UFSW) have potential to serve as an important, high volume and renewable bio-based feedstock and, thus, are an interesting case study.

1.4 Food Supply Chain Waste (FSCW) and Unavoidable Food Supply Chain Waste (UFSCW)

Food supply chain waste (FSCW) is defined as “*the organic fraction produced for human consumption that has not been recycled or used for other purposes, or where the raw materials are less valuable than the cost of collection and recovery for reuse*”.³⁹ Further definitions attempt to split the food supply chain. For example, food loss “*is the decrease in the quantity or quality of food resulting from decisions and actions by food suppliers in the chain, excluding retail, food service providers and consumers*” and, food waste “*is the decrease in the quantity or quality of food resulting from decisions and actions by retailers, food services and consumers*”.⁴⁰

Much of food waste, food losses and food supply chain wastes are avoidable because of poor storage, over production and consumer non-acceptance due it being blemished or mis-shaped.

In 2015, the FAO estimated that roughly one-third of global food produced for human

consumption (or 1.3 billion tonnes) was lost or wasted annually. The carbon and water footprint of this significant amount of food waste were estimated to be 3.3 billion tonnes (or 8% of the world's total) of CO₂ equivalent and 250 km³ of blue water, respectively. It also equated to 1.4 billion hectares (or 28% of the world's total) of agriculture land use and an economic cost of about \$750 billion U.S. dollars (USD).⁴¹ Approximately 13.8% of global food waste occurs during harvesting, during transport and storage, and during processing, amounting to over \$400 billion USD lost revenues, annually.¹²

The European Union^f (EU) generates approximately 88 million tonnes of food waste per annum, equating to 173 kg of food waste per person, around 20% of total food production. Around 11% of EU food waste is generated at production sector, 19% from processing, 5% from wholesale and retail, 12% from food service and the largest portion 53% from household (Fig. 5).⁴² The disposal of food waste causes a large environmental problem. In the UK, approximately 15 million tonnes are wasted annually.⁴³

^f Data includes the UK which at the time was part of the EU.

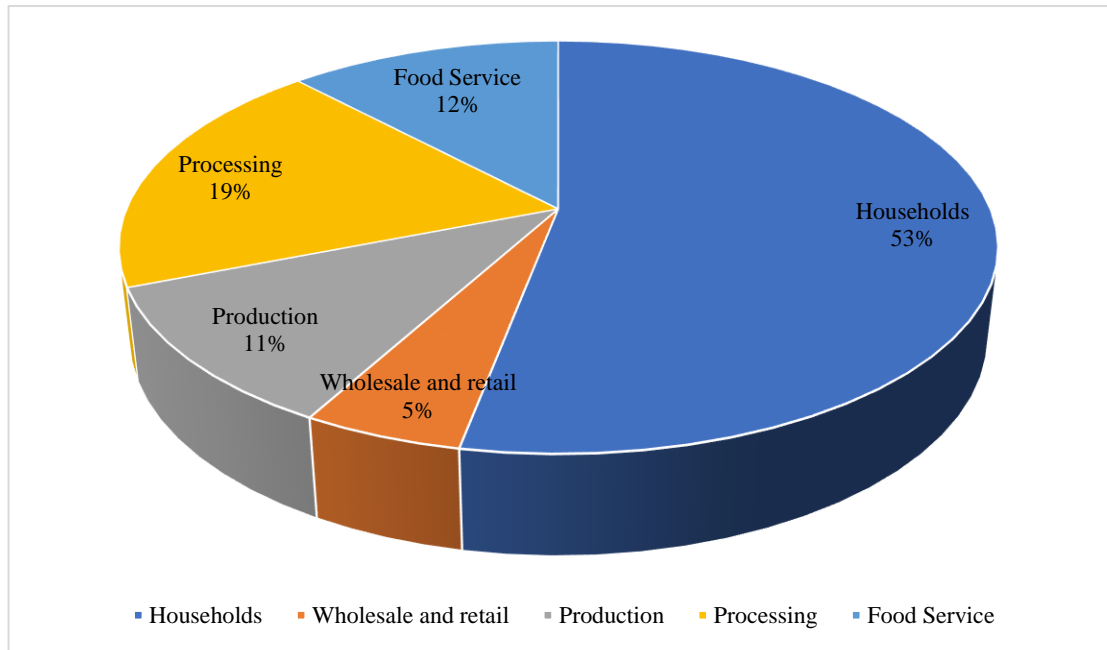


Figure 5 Split of EU food waste by sector.⁴²

However, less food is wasted today due to better storage and prevention strategies. Recent data from the UN Environment Programme revealed that 931 million tonnes of food was wasted in 2019 compared with 1.3 billion tonnes in 2015.⁴⁴

Unavoidable food supply chain waste (UFSCW) is the fraction of food waste resulting from the primary (harvesting) and secondary (chopping, peeling, scraping, etc) processing phases of the food supply chain.⁴⁵ Currently, UFSCW is used in animal feed, composting or biogas generation.^{46, 47} In developing countries which are highly agricultural, large amount of agricultural waste are burned impacting adversely on air, water and land pollution.⁴⁷ Usually, waste is burned at the source because it's not economical to transport it to a processing factory. For example, a biomass pelleting mill in the United States only collects the biomass waste from about a 50 km radius,

and even so, transportation accounts for 90% of their production cost.⁴⁸ In the EU, 19% of all biomass is used for energy and approximately 15% is for chemical and biomaterials production.⁴⁹ Bio-based chemicals are expected to generate revenues of approximately 103 billion USD in 2022.^{50, 51}

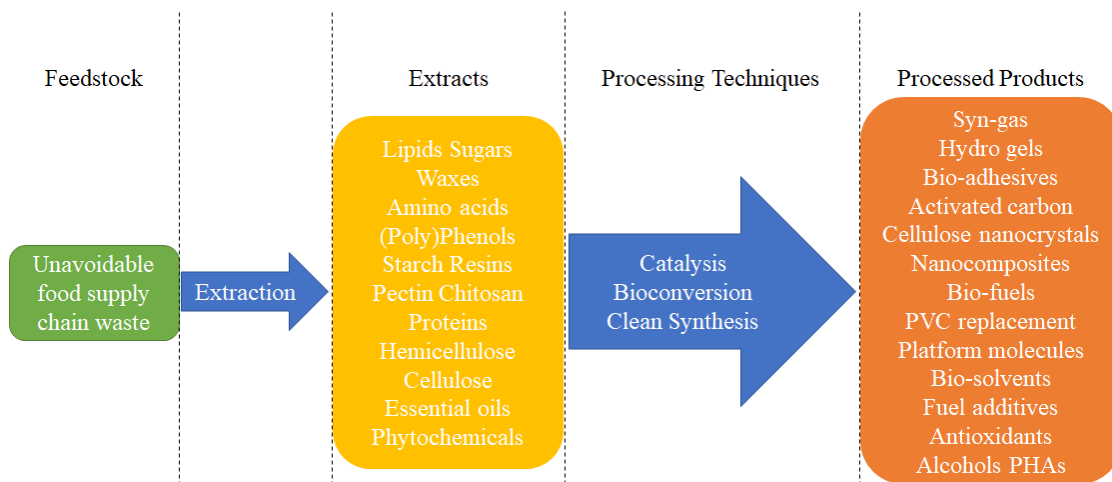


Figure 6 Components of UFSCW and their potential products.⁵²

UFSCW can be considered as “*Nature’s Periodic Table of fit for purpose biobased chemicals, applications and products with inherent structure and function*”⁴⁵ and is an abundant resource of fats and oils, flavours, aromas, pigments, proteins, polysaccharides, antioxidants and fibres (Fig. 6). A discussion on the potential of citrus and blackcurrant pomace as examples of UFSCW now follows.

1.5 Citrus Fruit & Peel Waste

The genus *Citrus* and related genera belong to the angiosperm subfamily

Aurantioideae of the Rutaceae family.⁵³ In 2015, global citrus production was over 130 million tonnes (Table 2).⁵⁴ Globally, the most common types of citrus fruit are oranges, tangerines, grapefruit, lemons and limes (Fig. 7, Left)

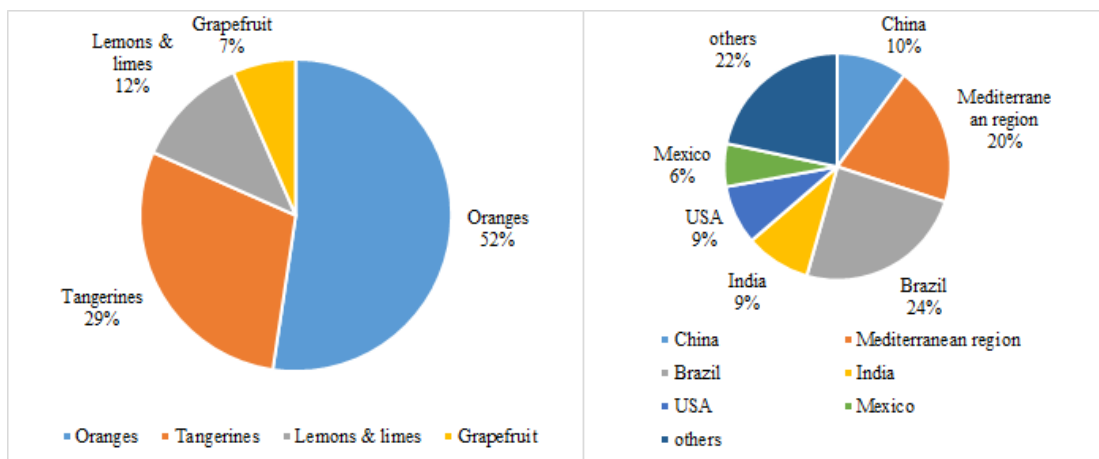


Figure 7 Global citrus fruit production in breeds (left) and orange production in countries (right).⁵⁵

Geographically, Brazil, Mediterranean region, China, India, USA and Mexico accounted for 78% of total oranges produced in 2015 (Fig. 7, Right). Unlike other countries, tangerine is the most popular citrus fruit in China. The production of tangerines in China alone represents almost 60% of global tangerine production. Typically, 20% of all citrus fruits are destined for processing industries, of which, 80% are oranges (Table 2).

The citrus fruit processing industry is an important component of the agro-industrial sector, producing citrus juice and essential oil but also generating wastewater and citrus peel waste (CPW). The latter represents approximately 50% w/w of the total

fruit (2016, 23.5 million tonnes), equating to 11.75 million tonnes per annum.

Table 2 Citrus fruit production and processing in 2015 and 2016 (Million tonnes) (FAO 2017)

<i>Type</i>	<i>Total Production</i>		<i>Used for Processing</i>	
	<i>2015</i>	<i>2016</i>	<i>2015</i>	<i>2016</i>
<i>Total Citrus</i>	<i>130.9</i>	<i>124.2</i>	<i>25</i>	<i>23.5</i>
<i>Oranges</i>	<i>68.6</i>	<i>67</i>	<i>19.9</i>	<i>18.5</i>
<i>Tangerines</i>	<i>38.3</i>	<i>33</i>	<i>1.8</i>	<i>1.8</i>
<i>Lemons & Limes</i>	<i>15.5</i>	<i>16</i>	<i>2.4</i>	<i>2.5</i>
<i>Grapefruit</i>	<i>8.6</i>	<i>8.3</i>	<i>0.8</i>	<i>0.8</i>

1.5.1 Opportunities from Orange Peel Waste

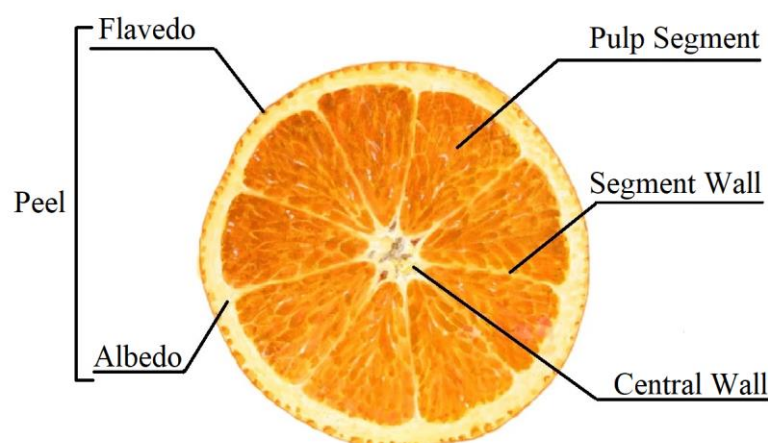


Figure 8 Cross Section of an Orange.

The cross-section of an orange comprises two main parts, outer peel and inner flesh (Fig. 8). The peel consists of the flavedo or exocarp (orange coloured) and the albedo or endocarp (white pith). The flavedo is mostly composed of cellulosic material but also other compounds like essential oils (limonene), waxes, steroids, fatty acids, pigments (carotenoids, chlorophylls, flavonoids) and enzymes. The albedo is rich in

pectin and cellulose.⁵⁶ Table 3 shows the typical composition of sweet orange peel waste derived from an industrial juicing operation.^{52, 57} A discussion on pectin and defibrillated celluloses is given later, see sections 1.8.1 and 1.8.2, respectively.

Table 3 Composition of sweet orange peel waste.⁵⁸

<i>Components</i>	<i>Weight % dry basis</i>
<i>Ash</i>	2.56 ± 0.10
<i>Sugar</i>	9.57 ± 0.22
<i>Fat</i>	4.00 ± 0.15
<i>Protein</i>	9.06 ± 0.38
<i>Flavonoid</i>	4.50 ± 0.15
<i>Pectin</i>	23.02 ± 2.12
<i>Lignin</i>	7.52 ± 0.59
<i>Cellulose</i>	37.08 ± 3.10
<i>Hemicellulose</i>	11.04 ± 0.66

Currently, traditional large-scale solutions for orange peel wastes (OPW) and other citrus wastes have been limited to low-value direct uses, such as landfilling, composting, animal feed, anaerobic digestions or fermentation.⁵⁹ As a landfill, OPW contains large amount of carbohydrates which can accelerate fermentation and uncontrollable methane production.⁶⁰ The moisture content (80-90%) of OPW is a huge problem for animal feed, the high energy demand for the dehydration process to <10% water content need to be considered. Meanwhile, with only 6% protein in dried OPW, it has low nutritional value and is a poor quality animal feed.⁶¹ OPW has been trialled for use in anaerobic digestion, but the presence of D-limonene inhibits the anaerobic digestion because of its antibacterial properties.⁶² Also, the direct disposal

of CPW can be potentially harmful to soil health because of the antimicrobial activity of D-limonene. On the other hand, the antimicrobial properties give citrus essential oil opportunities to be used in home and personal care industries.^{63, 64}

1.5.2 Essential Oils and D-limonene.

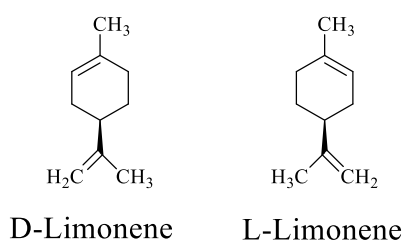


Figure 9 Stereoisomers of limonene.

Typically, oranges contain 0.5% by weight of essential oil. The composition of essential oils depends on the time of harvest, variety and location. The major component of orange essential oil is D-limonene (approximately 90% by weight).^{56, 65} Limonene (Figure 9), a monocyclic terpene comprising two isoprene units, is a secondary plant metabolite.⁶⁶

Table 4 Composition of a variety of essential oils extracted from oranges.

Feedstock	Method*	Yield %	Composition %			
			Terpenes	Limonene	Myrcene	Pinene
Gannan navel orange, China ⁶⁷	Cold press			85.32	5.11	1.95
Mexican oranges ⁶⁸	Hot water	5.23		74.43	4.27	1.45
Valencia	MAE	0.42	85.7	76.7	4.3	2.9

oranges ⁶⁹	Hot water	0.39	89.8	78.5	5.3	4.3
Valencia oranges ⁷⁰	HD	1.4 -	98.56	96.75	0.74	0.37
	MAHD	2.3	99.34	97.38	0.79	0.45
Sweet oranges from Spain ⁷¹ **	MSDf	1.17	97.4	93.9	1.7	0.8
	MSD	1.24	97.5	94.2	1.7	0.7
	SFME	1.42	97.7	94.2	1.7	0.9
	MHG	1.61	97.5	94.1	1.7	0.8
	SD	1.12	97.6	93.6	1.7	0.8
	SHDf	1.26	97.2	94.0	1.7	0.8

*: MAE: microwave assisted extraction; HD: hydro-distillation; MAHD: microwave assisted hydro-distillation; MSDf: microwave steam diffusion; MSD: microwave steam distillation; SFME: solvent free microwave extraction; MHG: microwave hydro-diffusion and gravity; SD: steam distillation; SHDf: steam hydro-diffusion.

** : Yield was calculated from reported η_{yield} and 7 ml EO from 400 g OP.

Hydro-distillation can be performed in three ways: water distillation, water and steam distillation and direct steam distillation. Water and steam act as main media to free compounds in the raw materials.

Steam distillation is to generate steam from bottom, condenser on the top of the vessel. Steam diffusion is to generate steam on the top, allows the extract to drop by earth gravity out of the reactor.

D-Limonene is a colourless oil slightly soluble in water (13.8 mg L⁻¹) with a sweet orange smell, widely used in food and cosmetic industries. It is typically obtained as by-product of citrus fruit juice industries, mainly by cold pressing then centrifugal separation or / and steam distillation. The oranges are squeezed first, the orange oil floats on the top of orange juice is food-grade D-limonene, the residues (OPW) are transferred to steam distillation for a second step essential oil production.⁷²

In 2013, global production of D-limonene was estimated to be over 70000 tonnes. The market for D-limonene is expected to reach over \$450 million USD by 2022 with

applications in flavours and fragrances and, biobased solvents.^{65, 72} The global flavour and fragrance market valued at over \$18.6 billion USD whilst the bio-based solvent market is expected to reach 13.74 billion USD by 2024.⁷³ D-Limonene can be used as alternative environmentally friendly bio-solvent replacing petroleum solvents such as toluene, *n*-hexane and dichloromethane.⁷² It is extensively used in different fields such as analytical chemistry, production of paint and eco-friendly cleaning agents.⁷⁴ The antimicrobial and antioxidant properties of D-limonene make it an antioxidant agent in food industry to preserve food and to avoid rot.⁷⁵ D-Limonene can be used safely in food as flavouring agent since it is considered as a Generally Recognised As Safe (GRAS) molecule.

1.5.3 Opportunities from Lemon Peel Waste

Lemon (*Citrus limon*) is the third most important cultivated citrus species. In 2015, 15.5 million tonnes of lemons and limes were harvested globally.⁵⁴ Lemon is mainly consumed as fresh fruit or processed to make juices or sliced,⁷⁶ each of which, generates a large amount of lemon wastes (peels, seeds, and pulps) accounting for 50% of the total lemon weight.⁷⁷ Compared with oranges, lemons are smaller and more acidic. The pH of lemon juice is 2.2-2.4 whilst the pH for orange juice is typically 3.1-4.1.⁷⁸

Martinez-Abad *et al.* recently reported a microwave assisted extraction (MAE) of essential oils and pigments from lemons.⁷⁹ Lemon essential oil (LEO) was extracted

from lemon peel waste (750 g) in water (225 ml) at 100 °C for 15 min (5 min ramp and 10 min holding) to give yield of $2.03 \pm 0.21\%$ by weight. The LEO-free residues were mixed with 80% (v/v) aqueous ethanol at 80 °C for 50 min, at a liquid-to-solid ratio of 1:10, and then filtered. The polysaccharides in the filtrate were precipitated by adding 96% (v/v) aqueous ethanol and were isolated by filtration. The mother liquor was rotary evaporated and freeze dried to afford crude lemon pigment (6 % by weight, see Figure 10) comprising diosmin (7.368%), eriocitrin (4.728%) and hesperidin (2.658%).

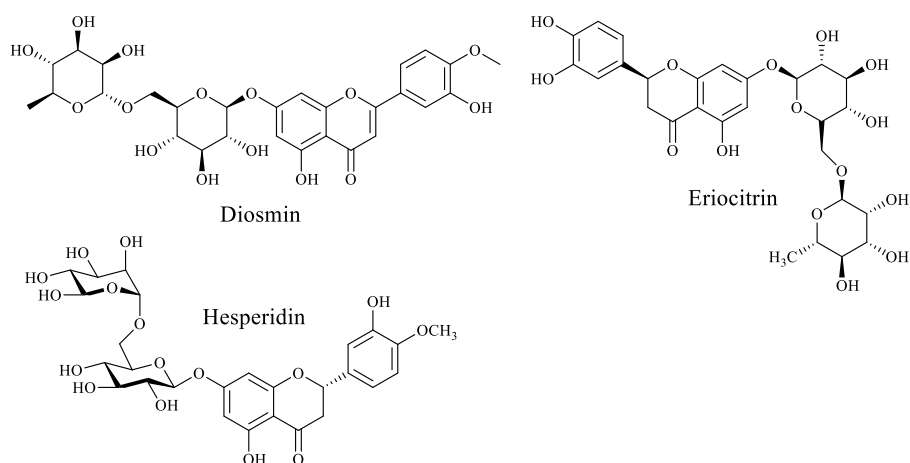


Figure 10 Structures of lemon pigment main components.

Herra-Barros *et al.* reported the use of siloxane-modified, titanium-enriched, lemon peel biomass for nickel adsorption from wastewater.⁸⁰ Lemon peel was washed, dried, milled (0.355, 0.5 and 1 mm), dispersed in dimethyl sulfoxide (DMSO), and reacted with tetraethyl orthosilicate and TiO₂. The adsorption capacity was tested with aqueous NiSO₄ solution (100 mg/L, 100 ml) showing that lemon peel was able to

adsorb over 78% of Ni(II) with an average adsorption capacity of 15.36 mg/g. The modified LP-TiO₂ nanoparticles increased Ni(II) adsorption capacity from 78% to 90%.

Chen *et al.* reported the extraction of lemon yellow #15 (Fig. 11), a natural colorant found in lemon peel.⁸¹ Lemon yellow #15 is more soluble in water and has better photostability than other natural colourants such as crocin and curcumin.⁸² Dried lemon peel was extracted successively with ethyl acetate (14.3%), ethanol (19.7%) and water (5.32%) in sonicator for 1 hour. The ethanol extract (5 g) from previous extraction was further purified (HPLC) to yield lemon yellow #15 (4 mg, 0.08%).

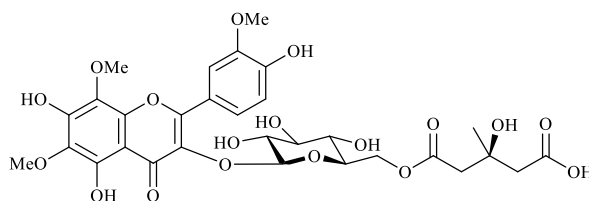


Figure 11 The structure of lemon yellow #15.

Abarna *et al.* reported a sol-gel synthesis of visible light active nano zinc oxide in presence of lemon peel.⁸³ Lemon peel was dried, ground into a powder and the desired weight (0.25, 0.5, 1 and 1.5 g) of LP mixed with zinc acetate (3 g) in ethanol (90 ml). Oxalic acid was added dropwise to form a colloidal suspension, which was calcined at 500°C to obtain the LP-ZnO. The latter shows a red shift in the UV spectrum (426 nm) compared with ZnO (400 nm), alone. The LP-ZnO was able to photodetoxify crystal violet dye (50 mM) within 2.5 h whilst ZnO as a control showed

nominal dye (10 nM) removal after 2.5 h.

Tyagi *et al.* reported the synthesis of water soluble carbon quantum dots (wsCQDs) from lemon peel for enhanced Cr(VI) sensing.⁸⁴ LP was washed with water, sulfuric acid (0.1 M) and sodium hypochlorite solution, successively, and autoclaved (200°C for 12 h) to afford wsCQDs. An aqueous solution of wsCQDs (125 µg mL⁻¹) can be used for sensitive and selective detection of Cr⁶⁺ at low concentration (~73 nM). The wsCQDs were able to degrade methylene blue (MB) 2.5 times faster than TiO₂ nanofibres.

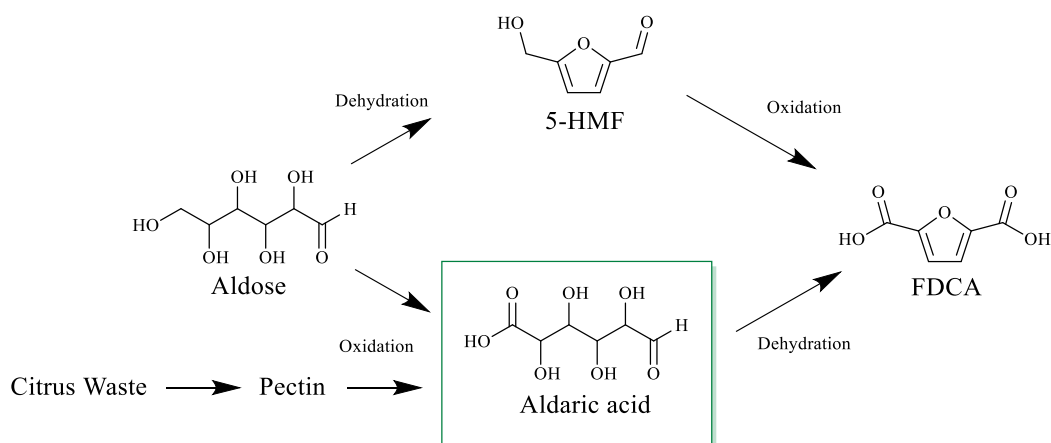


Figure 12 Comparison of different routes from aldose to FDCA.

In 2020, van Strien *et al.* reported the conversion of aldaric acids (the dehydration of aldaric acid (galactaric and glucaric acid) using silica-supported solid acid catalysts produced 2,5-furandicarboxylic acid (FDCA, Fig. 12) and its esters), which may come from pectin-rich feedstocks, to FDCA as a potential replacement for polyethylene terephthalate (PET).⁸⁵ The yield is up to 73% from galactaric acid and 70% from

glucaric acid. Currently, FDCA is synthesised from glucose or fructose via HMF, which is unstable under acidic conditions and converts into levulinic acid and humins.^{86, 87}

1.6 Blackcurrant Pomace

Blackcurrants (BC; *Ribes nigrum*) are small, dark purple fruits (Fig. 13A) that come from medium-sized woody shrubs native to colder climate areas such as northern Europe, northern Asia, and central Asia.⁸⁸



Figure 13 Blackcurrant (A) and blackcurrant pomace (B).

Russia is the biggest producer of BC in the world, but Poland is the primary exporter (80% to 90% of global exports) of fresh and processed BC.⁸⁹ The top 6 red and black currant producers in the world in 2018 and 2019 is Russia, Poland, Ukraine, Germany, UK and France.^f (See Fig. 14)

^f Source: International Blackcurrant Association (IBA)

BC are usually used for juice, wine and jam production yielding a large amount of blackcurrant residues or waste known as pomace (Fig. 13B). Although BC pomace (BCP) is commonly discarded after juice pressing, it can be used as food additive after drying and milling in the form of fruit powders.⁹⁰ Pomace is a valuable source of polyphenolic compounds, *e.g.* anthocyanins.

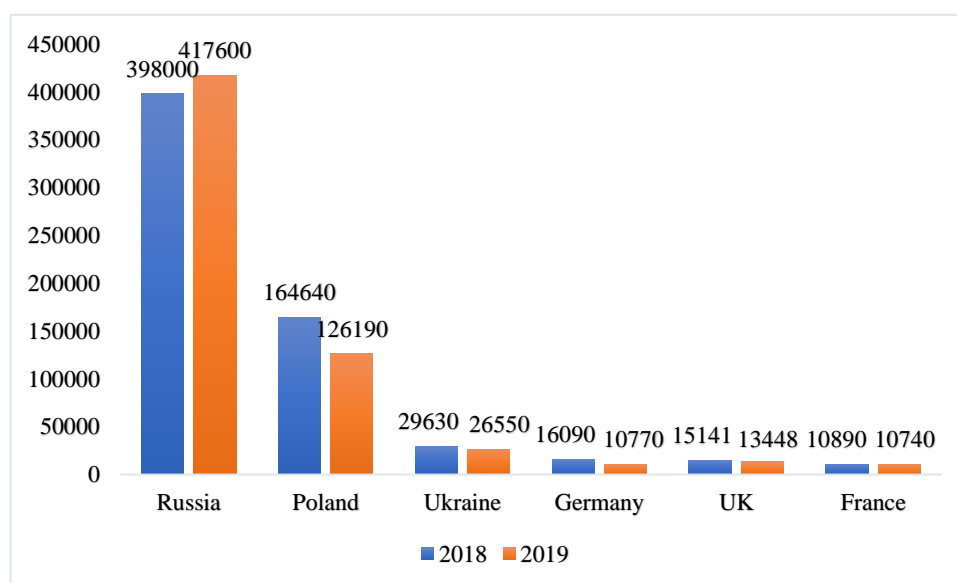


Figure 14 Top 6 black and red currant producers (tonnes) in 2018 and 2019. IBA

The skin of blackcurrants contains higher anthocyanins content than blackberries and blueberries, the content in blackcurrant skins is higher than flesh and seeds.^{91, 92} Anthocyanins are anti-oxidants and are associated with several health benefits.⁹³ BC and BCP contains four main anthocyanins (Fig. 15), namely: cyanidin 3-*O*-glucoside (C3G), delphinidin 3-*O*-glucoside (D3G), cyanidin 3-*O*-rutinoside (C3R) and

delphinidin 3-*O*-rutinoside (D3R).⁹⁴ The polar nature of these anthocyanins means that they be readily extracted in a variety of polar protic or hydroxylic solvents. For example, Nour *et al.*⁹⁵ macerated BC in food-grade aqueous ethanol in three concentrations (40% v/v, 60% v/v and 95% v/v). The extraction yield of individual anthocyanins was influenced by the ethanol concentration with 60% v/v aqueous ethanol affording the best yield of D3G, C3G and C3R.

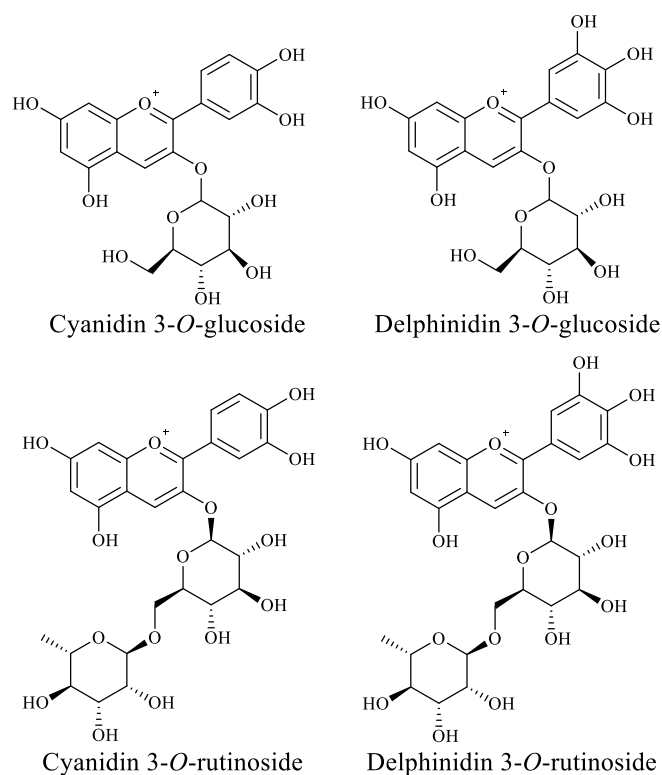


Figure 15 The chemical structure of 4 main anthocyanins.

Sojka *et al.* isolated phenolic extracts from industrial BCP.⁹⁶ The industrial BCP was firstly treated with hot water (70 °C) to remove sugars and acids followed by extraction with 45% (v/v) aqueous ethanol to obtain a crude BC extract. The latter was subjected to column chromatography eluting with water then 20% v/v aqueous

methanol and finally 100% methanol. The water eluted fraction contained over 50% of anthocyanins.

Recently, Azman *et al.* reported the influence of different drying methods (oven drying, industrial rotary kiln drying and freeze drying) on phenolic yield and antioxidant activity of BCP.⁹⁷ Each dried BCP was subjected to methanolic HCl (1% v/v in methanol) extraction for 24 hours. Freeze drying was shown to be the best method for retaining the integrity of temperature sensitive compounds such as hydroxycinnamic acids (HCA), whilst industrial rotary kiln dried BCP afforded the highest amount of anthocyanins. Oven drying at lower temperature and longer residence time prevented the degradation of total anthocyanins, whereas higher temperature and shorter residence time prevented the degradation of total HCA and flavanols.

Xu *et al.* reported the degradation of extracted polysaccharides from BC to yield cleaved polysaccharides with antioxidant and hypoglycemic activity.⁹⁸ BC were crushed, extracted with water at 80 °C, filtered and the filtrate was treated with ethanol to effect precipitation of polysaccharides. The latter were degraded in the presence of FeSO₄ and H₂O₂ to afford two main fractions (13 x10³ and 9.62 x10³ kDa). The smaller molecular weight fraction showed higher antioxidant and hypoglycemic activities.

Alba *et al.*⁹⁹ reported the isolation of dietary fibre (DF) from BCP as a potential food

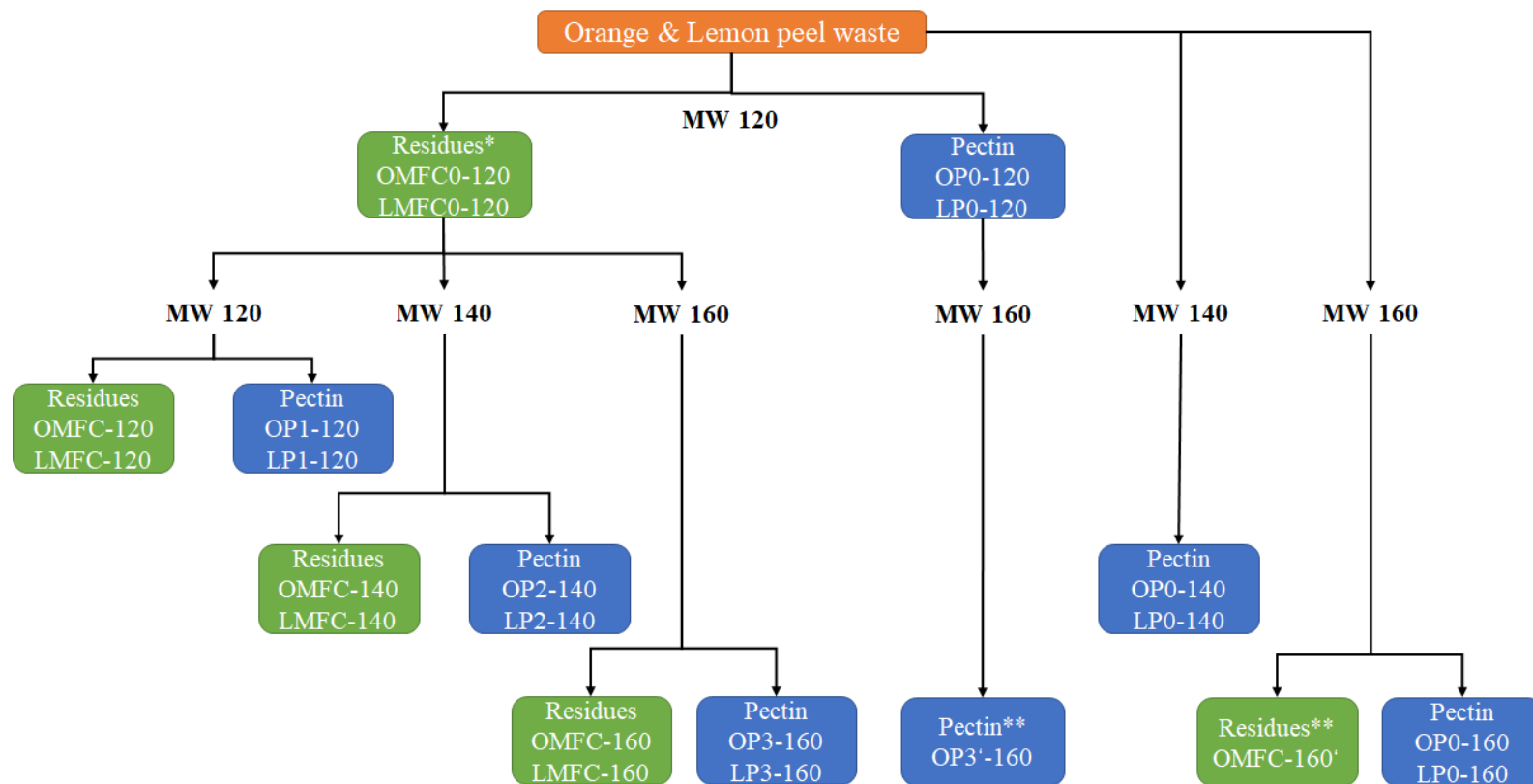
additive. After the removal of acid-soluble pectin and calcium-bound pectin from BC, the pure insoluble dietary fibre (piDF) was obtained. The piDF was further treated with H₂O₂ to separate cellulose, alkali-soluble hemicellulose and alkali-soluble lignin. The BCP is a potential source of DFs, could be used to obtain functional ingredients or to enhance the fibre content of food.

Anouti *et al.* reported hydrothermal liquefaction of BCP to afford bio-oils.¹⁰⁰ A BCP slurry (14 wt% dry matter to water ratio) was heated to 300 °C with 10 bar nitrogen, 35 min ramp time and 60 min holding time. After liquefaction, the aqueous layer was removed, whilst the solid residue was extracted with different solvents (ethyl acetate, hexane, acetone and isopropanol) to obtain bio-oils. Ethyl acetate in presence of sodium hydroxide extracted the highest oil yield (33%), whilst the hexane extract (17%) showed the highest higher heating value (HHV, 38.4 MJ kg⁻¹). This method is capable of producing high heating value bio-oils, however, the bio-oils are highly acidic (108-159 mg KOH per g bio-oil) and viscous (495 mPa·s). The solid residue (biochar) and aqueous were not mentioned in this report, these two fractions should be valuable as well. The same set of researchers later reported the reuse of the aqueous phase in the liquefaction of BCP.¹⁰¹ The aqueous phase was reused up to 6 times, showing an increase in oil yield from 26% to 31% and a slightly increased HHV of the bio-oils from 33.0 MJ kg⁻¹ to 35.2 MJ kg⁻¹.

1.7 Aims

The *global aim* of this thesis is to explore the valorisation of citrus fruit (oranges and lemons, Fig. 16) wastes and industrially-derived blackcurrant pomace (Fig. 17) as a source of biobased chemicals and materials using acid-free hydrothermal microwave processing as a central technology. Previously, researchers in the Green Chemistry Centre of Excellence, University of York, have undertaken significant research on acid-free microwave-assisted hydrothermal extraction of pectin from orange peel wastes.¹⁰² However, the resultant pectin-free residues were discarded until de Melo explored their microwave-assisted hydrothermal defibrillation in to micro- and nano-fibrillated celluloses and fibres.¹⁰³

Thus, the *primary aim* of the thesis is to explore the effect of direct acid-free microwave processing and/or sequential acid-free microwave reprocessing (see Fig 16) of citrus peel wastes (orange and lemon) at a variety of temperatures (120 °C, 140 °C and 160 °C) on the yield and nature of pectins and defibrillated celluloses produced.



Notes:

*: It's a continuous process, intermediate was not collected.

** : Product from orange peel only.

Figure 16 General process of microwave process of citrus peel waste.

The resultant materials will be analysed by a variety of techniques to ascertain their presence and purity. For example, ATR-IR (distinct carbonyl absorbance bands for pectin at approx. 1730 cm^{-1} ($-\text{CO}_2\text{Me}$) and 1610 cm^{-1} (COOH and/or COO^-)), TGA (distinct decomposition of pectins at approx. $190\text{-}230\text{ }^\circ\text{C}$, hemicellulose at approx. $260\text{-}300\text{ }^\circ\text{C}$, cellulose as approx. $310\text{-}360\text{ }^\circ\text{C}$), liquid ^{13}C NMR (distinct resonances for pectin at approx. 170 ppm ($-\text{C}=\text{O}$), $110\text{-}100$ (C1 anomeric carbons), approx. 55 ppm ($-\text{CO}_2\text{CH}_3$), ^{13}C NMR CPMAS (distinct for cellulose approx. 106 ppm (C1 anomeric carbon, 90 ppm (C-4 carbon) , $73\text{-}75\text{ ppm}$ (C-2,3,5) and 65 ppm (C-6, CH_2OH)). GPC will be used to track changes in the average molecular weight of the pectins with respect to temperature so as identify potential decomposition. SEM and TEM will be used to explore the surface morphology and aspect ratios, respectively, of the defibrillated fibres. The aspect ratio will enable classification of the defibrillated celluloses as micro and/or nanofibres and crystals.

Confocal laser microscopy will enable colour-sequential ‘mapping’ of cellulose, hemicellulose and lignin within the fibres. Defibrillated celluloses (micro- and nano-cellulose) are passive materials and are known to form hydrogels. The water retention value of defibrillated celluloses and their ability to form hydrogels will be investigated. A commentary on hydrogels is given in Chapter 3, Section 3.2.3.

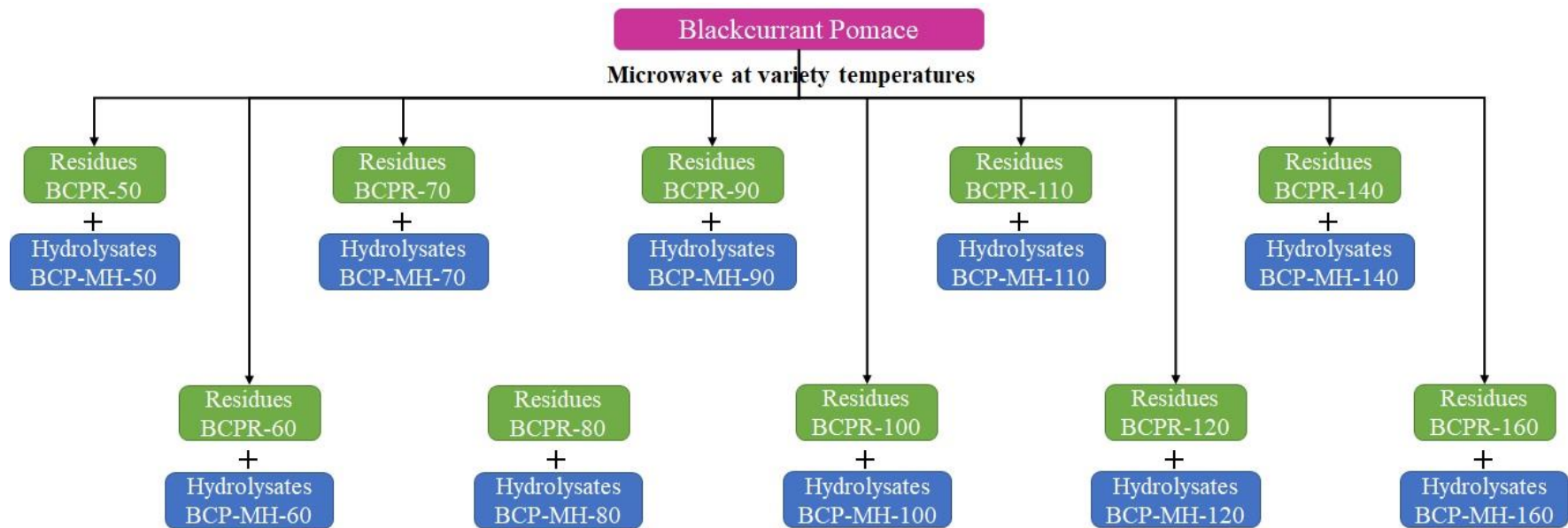


Figure 17 General process of microwave hydrothermal process of BCP from 50 °C to 160 °C to obtain hydrolysates and residues.

The *secondary aim* is to explore the effect of acid-free microwave-assisted hydrothermal processing of industrially-derived blackcurrant pomace from 50 °C to 160 °C at 10 °C intervals (Fig. 17) on the yield and composition of the resultant water extractives. The latter are expected to be rich in sugars, (poly)phenolics and anti-oxidants which will be mapped via LC-MS. The Total Phenolic Content (TPC) will be determined via the Folin-Ciocalteu method which is a colorimetric method for analysis of phenolics/ antioxidant activity by reduction of a molybdotungstophosphate complex. It was originally developed for analysing proteins, but adapted for determining polyphenols in wine by Singleton *et al.*¹⁰⁴ The metric produced by the test is a ‘gallic acid equivalent’ (GAE), a relative measure of performance compared with gallic acid. The anti-oxidancy will also be measured using the modified DPPH method as reported Azman *et al.*⁹⁷ The metric produced by the test is a “inhibition %” of DPPH absorbance at 517 nm.

As microwave technology, pectin and the formation of defibrillated celluloses (micro- and nanocellulose) are central to the work, a brief overview and their contextualisation is given in the following sections.

1.8 Microwaves

Microwaves are a form of electromagnetic radiation with wavelengths ranging from one metre to one millimetre; with frequencies between 300 MHz (100 cm) and 300

GHz (0.1 cm). Microwave heating has long been recognised as a rapid and energy-efficient mode of heating. Microwave heating is widely used in kitchens, laboratories and industries, operating at a frequency of 2.45 GHz.¹⁰⁵ Microwave irradiate directly on ions and polar molecules which convert electromagnetic energy into heat by dipole polarisation and ionic conduction, leading to rapid volumetric heating.¹⁰⁶

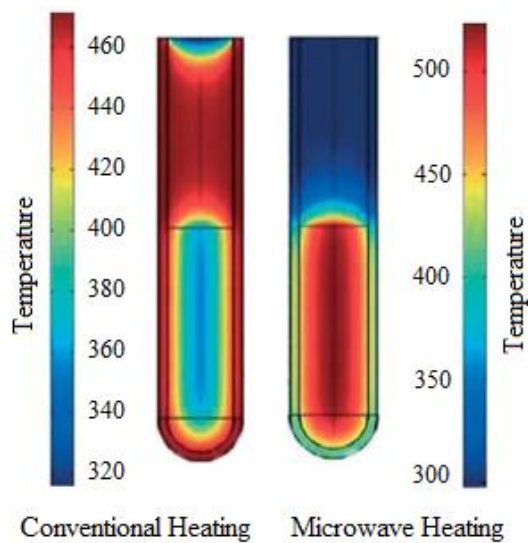


Figure 18 Microwave heating compared with conventional heating.¹⁰⁷

Compared with conventional heating, microwave heating can be more efficient because its rapid, selective, volumetric, and uniform.^{108, 109} The visualised difference between two heating methods is shown in Fig. 18.¹⁰⁷

Zeng *et al.* reported rapid extraction of polysaccharides via microwave-assisted extraction.¹¹⁰ The microwave irradiates deep within the structure of cell wall enabling rapid and efficient removal of polysaccharides from the raw-material.¹¹¹ MW

irradiation penetrates materials and causes rapid rotation of water molecules at high frequency and creates frictional heat. MW irradiation also cause polarisation in the structure of macromolecules resulting to breakage of hydrogen bond.¹¹²

Besides the isolation of polysaccharides, MAE has been used in the extraction of phenolic compounds from biomass. Cassol *et al.* reported MAE of anthocyanins from hibiscus flowers.¹¹³ The hibiscus flowers were treated with citric acid (2% w/v, biomass : acid ratio 1:5) under microwave irradiation at different powers (200, 300 and 700 W) and times (2, 5 and 8 min). The MAE methodology afforded total monomeric anthocyanins (TMA, up to 1.6mg g⁻¹) and total phenol content (TPC, up to 27 mg g⁻¹ GAE).

Pap *et al.* reported MAE of anthocyanins from blackcurrant marc (pomace).¹¹⁴ MAE was performed at various powers (from 140 to 700 W), pH (2 and 7) and extraction times (10 and 30) min. As a comparison, conventional extraction was carried out at 80 °C for 300 min at pH 2 (citric acid or hydrochloric acid). The total monomeric anthocyanins (TMA) were determined by UV measurement at 520 and 700 nm and HPLC was performed to determine the aqueous composition. Optimised MAE yielded a 20% increase of total anthocyanins extracted (from 16.7 to 20.4 mg g⁻¹) within 10 min compared to 300 min conventional extraction.

Acid or alkali hydrolysis of lignocellulosic materials is widely used to obtain pure cellulose. Higher alkali concentration and reaction temperature can remove more

lignin and increase purity.¹¹⁵ Liu *et al.* reported MW isolation of cellulose fibre from biomass.¹¹⁶ Wheat straw was pretreated by steam explosion, then microwave-assisted hydrolysis followed by micro-fluidisation, to obtain high-purity cellulose fibres. The product present high cellulose content (94.23%) and average individual diameter of 5.42 nm with crystallinity index of 58.62%. Besides combination with steam explosion, individual MW alkaline hydrolysis of wheat straw was reported,¹¹⁷ wheat straw was pretreated by HCl, then MW hydrolysed with various NaOH concentrations. The influence of temperature, duration and alkali concentration of fibres yield and cellulose concentration was determined. The purity of cellulose obtained from wheat straw under 140°C was up to 90.66%, MW was able to reduce 50%-75% of the reaction time or 67% of the chemicals than traditional treatments without MW.

Figuerola *et al.* reported MAE of bioactive polyphenols from avocado peel.¹¹⁸ Dried avocado peel powder was microwave extracted at 130 °C for 39 min in 36% v/v aqueous ethanol, the product presents TPC of 73.2 ± 3.8 mg/g GAE. 53 polar compounds were identified from the extracts, among them, dimers and trimers of procyanidin were the most abundant.

Golbargi *et al.* reported MAE of arabinan-rich pectic polysaccharides from melon peel.¹¹⁹ The highest yield (32.81%) was achieved with 20.94 ml/g water-solid ratio, 414.4 W MW power and 12.75 min. The product was pectic polysaccharide with a molecular weight of 5.71×10^4 kDa containing galacturonic acid (40.75%), arabinose

(30.13%), glucose (14.43%), galactose (8.29%) and rhamnose (1.24%).

Gautam *et al.* reported microwave-assisted pyrolysis of macroalgae.¹²⁰ Macroalgae (15 g) and activated carbon (5 g, microwave absorber) was pyrolysed under 560 W microwave radiation, the final temperature was 500 °C, holding time 15 min, resulting in bio-gas (26-32 wt%), bio-oil (41-46 wt%) and bio-char (22-33 wt%).

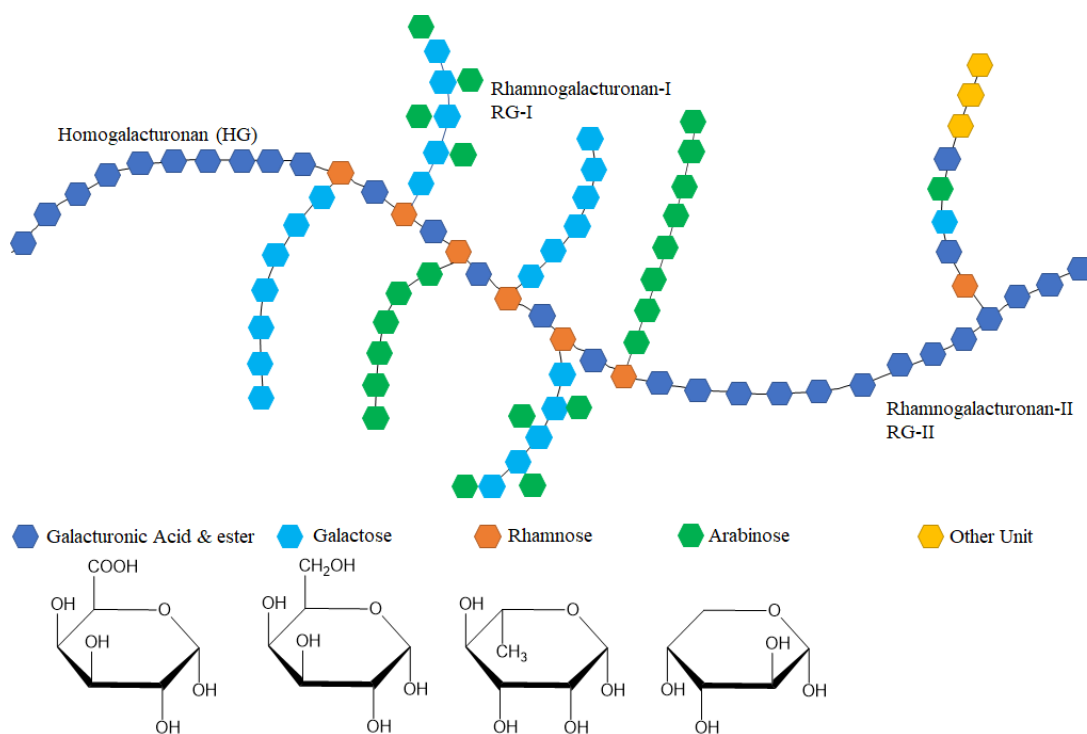
Melo *et al.* reported the hydrothermal microwave-assisted selective scissoring (Hy-MASS) of orange peel residues to afford defibrillated celluloses.¹⁰³ Melo *et al.* reprocessed depectinated orange peel residues using water and microwave radiation alone. The MW radiation selectively disintegrated cellulose fibre sheaves in the cell walls resulting in the formation cellulose nanofibres and nanocrystals as evidenced by transmission electron microscopy. Hy-MASS concept also showed selective decomposition of pectin at 160 °C resulting in RG-I domains and galactan branches, which was named as galactan-rich RG-I pectin. However, this was not further explored and is a main feature of this thesis providing new knowledge.

1.8.1 Pectin

Pectin is a polysaccharide present in the cell wall of plants especially fruit and vegetables.¹²¹ It is widely used as gelling, stabilising and thickening agent in food industry.¹²² Commercial pectin is a by-product of the juicing industry and is typically derived from apple pomace and citrus peel.¹²³ Pectin market has greatly grown in the

last decade. Price of pectin has increased from \$12 / kg USD in 2009 to \$21 / kg USD in 2016.¹²⁴ In 2019, the global pectin market was estimated to be worth \$1 billion USD equating to 77,611 tonnes of pectin. The market is projected to grow to \$1.5 billion USD (105,299 tonnes of pectin) by 2025. In 2018, the Food and Beverages segment accounted for more than 90% of pectin consumption globally. Europe was estimated to be the largest market for pectin valued about \$420 million USD.

Pectins possess high structural diversity.¹²⁵ Pectin is rich in D-galacturonic acid (Gal A) and is capable of trapping water to form gels at low concentration. Pectin can be complemented as dietary fibre, prebiotic and bioactive substances including fat replacer, functional ingredient and nutraceutical ingredient.¹²⁶⁻¹²⁸ Pectin contains structurally distinct regions including homogalacturonan (HG) which refers to “smooth region”, rhamno-galacturonan I (RG-I) and rhamnogalacturonan II (RG-II) which refer to “hairy region”. Approximately 65% of pectin is HG, is a linear polymer of α -1,4 linked galacturonic acid (Gal A) and is partially methyl esterified at C-6 or acetylated at C-2 and C-3.¹²⁹



ENREF 12

Figure 19 Schematic Structure of Pectin and structure of sugars. ¹²⁹⁻

¹³² ENREF 129 ENREF 127 ENREF 128

Typically, RG-I accounts for 20-35% of pectin and is composed of a repeating $[\rightarrow 2)\text{-}\alpha\text{-L-Rha-(1}\rightarrow 4)\text{-}\alpha\text{-D-Gal A-(1}\rightarrow]$ backbone with natural side chains attached to the *O*-4 of $\alpha\text{-L-Rha}$ backbone units.¹³⁰ Like HG, RG-I is also methylated and acetylated.¹³¹ The RG-I side chains including $\alpha\text{-L-1,5-arabinan}$, $\beta\text{-D-1,4-glactan}$ and arabinogalactan (AG-I & AG-II).¹³¹ RG-II, 2%-10% of pectin, is a HG backbone that is heavily branched with complex side chains of Rha, arabinose (Ara), galactose (Gal) and other minor sugars.¹³²

RG-I pectin exists in the fruits, roots, stems and leaves of plants, linking with

cellulose, hemicellulose and cell wall proteins,¹³³ plays an important role in the load-bearing structure of plant cell wall.¹³⁴

Conventionally, pectin is extracted by employing water acidified with strong mineral acids at elevated temperature. Since green chemistry concepts are widely approved, novel technologies, such as ultrasound assisted extraction (UAE)¹³⁵, microwave assisted extraction (MAE)¹³⁶ and subcritical water extraction (SWE)¹³⁷ have been developed and used as efficient eco-friendly technologies for recovery of valuable compounds (including pectin) from plants.¹²⁶

i. Conventional extraction

Conventional extraction of pectin is operated in acidic (pH 1.5-3) medium between 75-100 °C for 1-3 hours. Different conditions including temperature, pH, particle size, solid-liquid ratio and reaction time affect the yield and quality of extracted pectin. Hydrochloric and nitric acids were commonly used for pectin extraction.

Commercial pectins are extracted using hot acid, at pH ~2.¹³⁸ A study on the influence of extraction temperature on the properties of pectin reported that lower extraction temperature (below 40 °C) keeps the pectin molecule intact with more neutral sugar branches remaining.¹³⁸ However, water at room temperature solubilised pectin loosely attracted to the cell wall, but can't dissolve the tightly attracted pectin resulting in a very low yield.¹³⁹

ii. Microwave-assisted extraction (MAE)

As discussed earlier, microwave-assisted extraction requires shorter processing time, less solvent and produces higher yield and better-quality product. Rahmani *et al.* reported a Box-Behnken design of experiment to study the effect of conditions (irradiation time, microwave power and pH) on MAE of pectin from sour oranges.¹⁴⁰ Pectin presents $71.0 \pm 0.8\%$ galacturonic acid content and $1.5 \pm 0.2\%$ DE with a yield of 29.1% was achieved with 700W, 3 min and pH of 1.50 (citric acid).

iii. Ultrasound-assisted extraction (UAE)

Ultrasonic waves are mechanical vibrations ranging from 20 to 100 kHz and are often used in ultrasound-assisted extraction. Ultrasound form microbubbles which form microjets when collapsing, thereby disrupting cellular structures, improving solvent penetration, promote swelling and hydration, diffusion and mass transfer.¹⁴¹ Compared with conventional extraction, ultrasound-assisted extraction has been shown to reduce extraction time and temperature while increasing yield.¹²²

iv. Enzyme-assisted extraction (EAE)

The enzymes used for the extraction of pectin disrupt components of the plant cell wall with accurate specificity and selectivity, facilitating pectin release, reducing overall extraction time. The benefits of using EAE are (1) no acid requirements; (2) lower temperature is required, means lower energy demand; (3) specificity of enzymes

increased product quality.¹⁴²

Recently, the neutral sugar side-chains which are removed in pectin production, have attracted more attention due to their variety important bioactivities including inhibition of cell migration, immunological activities and prebiotic activities.¹⁴³

RG-I pectin is receiving more attention nowadays, there is an increasing interest in RG-I pectin extraction from by-products of agro-industry.¹⁴³ Normally, citrus pectin RG-I branches is rich in neutral sugars, especially arabinose.¹⁴⁴ RG-I region with specific sidechains is hard to isolate and thus, previous studies on RG-I bioactivity are normally based on HG and RG-I mixtures.¹⁴⁵

Colodel *et al.* reported the conventional acid extraction of pectin from Ponkan peel.¹⁴⁶ The ponkan peel was extracted with boiling nitric acid (pH 1.6) for 100 min to afford a yield of 25.6% of pectin. The resultant pectin was fully characterised including galacturonic acid content (84.5%), DE (85.7%) and average molar mass (80650 g mol⁻¹). The branches of RG-I region of ponkan pectin were mainly composed of galactans, but could not be isolated from the HG pectin.

However, Khodaei and Karboune successfully reported isolation of galactan-rich RG-I pectin from potatoes using microwaves¹³², and enzymatic cleavage to generate galactose-rich oligomers from potato RG-I.^{147,148} The potato pulp was pretreated by removing protein and starch, and the resultant potato cell wall material was extracted

with KOH by MAE. The optimised condition to obtain galactan-rich RG-I pectin was KOH (1.5 M), microwave power (41.1W per g cell wall matter), solid-liquid ratio (2.9% w/v) and 2 min. The resultant galactan-rich RG-I pectin (21.9%) contained 63.1 mol% of galactan with only 7.9 mol% galacturonic acid. The yield of pretreated potato cell wall material was not mentioned, so the yield of pectin based on potato was not able to calculate.

The most widely used application of pectin is as a rheology modifier or thickening agent in food, for example, jam. Generally, pectin gelation experiments were operated in present of sucrose and acid. Wang *et al.* reported an unexpected gelation behavior of citrus pectin.¹⁴⁹ High DE (80%) citrus pectin was able to form gel at 1 wt% with salt and alkaline (Na^+ and K^+). The gel strength and water holding capacity of citrus pectin gels (CPG) were related to monovalent cation, alkali condition and pectin concentration. Na^+ gels were more stable and stronger than those of K^+ . It was suggested that CPGs formed through the effects of de-esterification, self-aggregation, and entanglement of citrus pectin under alkaline conditions.

Some more novel applications are given as follows. Modified citrus pectin (MCP) has been shown to be effective against cancer.¹⁵⁰ The citrus pectin was modified with 3 M NaOH (pH 10) for 30 min followed by 3 M HCl (pH 3). Then the pH was adjusted to 6.3 with PBS buffer for 10 hours.¹⁵¹ The galactans present in MCP are responsible for anti-cancer effects. Galectin-3 (Gal-3), which is omnipresent human galectin, is β -

galactose binding protein present on the membranes of cells. Galectins binding to galactose-containing molecules on neighbouring cancer cells promote cell-cell interactions, to accelerate cancer. The amount of galectin increased the progression of cancer. Blocking Gal-3 expression led to reversion of the transformed phenotype and suppression of tumour growth in nude mice.^{150, 152-154}

Gouveia *et al.* reported biodegradable film made of thermoplastic pectin could be a potential alternative of eco-friendly and bio-based plastic.¹⁵⁵ Choline chloride (ChCl) and glycerol (1:2 w/w) were mixed and heated at 80 °C, the clear liquid formed was plasticiser named natural deep eutectic solvent (NADES). Pectin and plasticiser (NADES, ChCl or glycerol, 30 wt%) were mixed and heated to 80 °C for 30 min, then an equivalent of water was added to the paste. Finally, the resulted hot paste was thermo-compressed (120 °C, 196.1 kN, 20 and 25 min). The glycerol plasticised pectin based plastic film (0.35 mm thick) presented the highest tensile strength (18.41 MPa) and the lowest water vapor permeability ($1.45 \times 10^{-9} \text{ g} \cdot \text{m}^{-1} \cdot \text{s}^{-1} \cdot \text{Pa}^{-1}$). Unfortunately, this pectin based plastic film need to be kept away from moisture.

Pectic materials from variety of plants can be used as adsorbents for heavy metal. Wang *et al.* reported the adsorption capacity and selectivity of pectin for heavy metals depends on its origin.¹⁵⁶ For example, the adsorption capacity of Pb^{2+} was: citrus pectin (176 mg/g)¹⁵⁷; ‘nopal’ pectin (26.6 mg/g),¹⁵⁸ and; apple pectin (147-180 mg/g)¹⁵⁹. The adsorption capacity of pectin effected by metal ions selectively.^{158,160}

Meanwhile, the adsorption capacity was associated with method of preparation, variety of feedstock, time of harvest *et al.* Citrus pectin adsorption of Pb²⁺ was reported as 400 mg/g¹⁶¹ and 176 mg/g¹⁵⁷ with different preparation method. A summary of reported heavy metal adsorption capacity of pectins is listed in Table 5.

Table 5 Summary of reported heavy metal ions adsorption capacity of pectins.

Pectin	Metal	Adsorption Capacity	Adsorption Mechanism	References
Citrus	Pb ²⁺	0.85mmol/g	Ion exchange	Balaria and Schiewer (2008) ¹⁵⁷
Sugar beet	Al ³⁺	28.7 mg/g	Surface complexation	Kuljanin <i>et al.</i> (2014) ¹⁶²
	Ca ²⁺	179 mg/g	Electrostatic bonding	
'Nopal' pectin	Cr ³⁺	64.9 mg/g	Ionic interactions	Ibarra-Rodriguez <i>et al.</i> ¹⁵⁸
	Ca ²⁺	0.81 mg/g		
	Cu ²⁺	29.3 mg/g	Polar covalent bond	
	Cd ²⁺	11.4 mg/g		
	Ni ²⁺	42.4 mg/g		
	Pb ²⁺	26.6 mg/g		
	Zn ²⁺	25.1 mg/g		
Citrus	Fe ²⁺	0.191-0.523 mol/molGalA	"egg-box" model	Celus <i>et al.</i> (2017) ¹⁵⁸
Citrus with different DE	Zn ²⁺	0.208-0.520 mol/molGalA	Hydroxyl binding	Celus <i>et al.</i> (2018) ¹⁶³
	Ca ²⁺	0.147-0.501 mol/molGalA		
Sugar beet	Hg ²⁺	23.6 mg/g	Chelation	Ma <i>et al.</i> (2016) ¹⁶⁴
Commercial	Pb ²⁺	476.19-526.32 mg/g	"egg-box" model	Khotimchenko <i>et al.</i> (2017) ¹⁶⁵
Sea grass	Pb ²⁺	3.148mmol/g	"egg-box" model	Khozheanko <i>et al.</i> (2016) ¹⁶⁶
Sugar beet	Cd ²⁺	30.9 mg/g	Ion exchange and	Mata <i>et al.</i>

Ca-pectate Hydrogels & Xerogel	Pb ²⁺ Cu ²⁺ Cd ²⁺ Pb ²⁺ Cu ²⁺	129.9 mg/g 43.7 mg/g 56.9 mg/g 83.3 mg/g 31.3 mg/g	complexing between divalent cations in solution and calcium chelated or linked to carboxylic groups	(2009) ¹⁶⁷
---	--	--	---	-----------------------

Zhang *et al.* reported a combination of grapefruit derived pectin and bio-char.¹⁶⁸

Grapefruit peel was pyrolysed at 450 °C for 1 hour, yielded in 33.18% bio-char. Dried grapefruit peel powder were extracted by HCl (pH 1.5), the obtained pectin was de-esterified by NaOH, the yield of low esterified pectin was 12.3%. The pectin, bio-char and sodium alginate (SA) were mixed, then dropped into 5% (w/v) CaCl₂ solution via a syringe. The biochar / pectin / alginate hydrogel beads (BPA) were collected and freeze dried. The BPA was tested for adsorption of Cu²⁺, the maximum adsorption capacity of ~80.6 mg/ g, almost doubled the highest Cu²⁺ adsorption listed in Table 5.

The carboxyl group of galacturonic acid is the key point of heavy metal adsorption, heavy metal ions were bound with carboxyl by the chelation, makes pectic materials a potential alternative of heavy metal ion adsorption materials.^{157,161}

Koh *et al.* reported blueberry pectin including water soluble fraction (WSF) and chelator soluble fraction (CSF) extraction.¹⁶⁹ The freeze dried blueberry powder was extracted with acetate buffer (pH 5.2, 50mM) and acetate buffer containing ethylenediamine-tetraacetic acid (EDTA, respectively, then precipitate with ethanol. Blueberry extract (BBE) containing anthocyanins was extracted by acetate buffer (pH

4.0, 25mM) at 100°C for 15min. The CSF, rich in negative charge, low DE and high HG content attribute to greater binding activities with anthocyanins. The bound pectin contributes to stability of anthocyanins under gastrointestinal simulation.

1.8.2 Micro-fibrillated celluloses (MFCs)

The structures of defibrillated celluloses, *i.e.*, MFC and NFC, are often referred to as spaghetti-like strands and needles composed of both the crystalline and amorphous regions. The diameter of the fibres is usually < 10 nm while their length is > 1 µm. Unlike cellulose nanocrystals, MFCs have amorphous and crystalline domains¹⁷⁰. Their aspect ratio (L/d) is very high, which denotes a very low percolation threshold and an ability to form an advantageous rigid network, *i.e.*, they readily forms hydrogels and films upon drying.¹⁷¹

1.8.3 Production of MFC

MFCs can be produced via extensive mechanical and chemical treatments.¹⁷² Mechanical treatment is the primary disintegration technique for MFC and NFC production. These treatments include the following processes: high-pressure homogenisation, microfluidisation, super-grinding, cryo-crushing, steam explosion and high-intensity ultra-sonication (HIUS) can be used to reduce the particle size of fibres to micro or nano scale.¹⁷³

The use of high pressure homogenisation in MFC production was first reported in

early 1980s.^{174, 175} The homogeniser applied extremely high shearing force to the fibre-water suspension, with the synergy of turbulent flow and the frictional forces of the particles against each other, the cellulose fibre disintegrated.¹⁷⁶

Deepa *et al.* reported steam explosion as a treatment method. Wood pulp was exposed to high pressure steam followed by sudden decompression (explosion), resulting in substantial break down of the lignocellulosic structure, hydrolysis of hemicellulose fraction, depolymerisation of lignin and defibrillation.¹⁷⁷

The major challenge of mechanical disintegration of cellulosic fibres into MFC is the high energy consumption (20000-30000 kWh/tonne).¹⁷⁸ The combination of mechanical treatment with certain pre-treatments e.g., chemical or microwave or enzyme, is possible to decrease the energy cost.

Alkaline pre-treatment has been applied before mechanical treatment to remove lignin, remaining pectin and hemicelluloses.¹⁷⁹ Oxidation pre-treatment of cellulose by 2,2,6,6-tetra-methylpiperidine-1-oxyl (TEMPO) is a promising method for surface modification.¹⁸⁰ The oxidation of C-6 hydroxyl to carboxyl occurred only at the surface of the microfibrils under weakly acidic or neutral conditions. The TEMPO-oxidised cellulose present high negative ζ - potentials of -80 mV, this negative charge repulsed the nanofibres easing fibrillation.

Microwave pretreatment is energy efficient in MFC production from citrus waste.

Microwave radiation enhanced the disintegration of pectin, hemicellulose and cellulose with absence of any additional reagents.^{181, 182}

Enzymatic pretreatment is an alternative to chemical pretreatment. Enzymatic pretreatment on wood fibres reduces fibre clogging and energy demand.¹⁸³ Compared with acid hydrolysis, enzymatic hydrolysis of citrus waste materials yields in longer fibres with higher tensile strength.¹⁸⁴

1.8.4 Applications of MFC

The newly engineered micro-fibrillated cellulose (MFC) and nano-fibrillated cellulose (NFC) (or cellulose nanofibres, CNF) are known to have unusual properties such as high strength and stiffness, and thus can be used to improve the mechanical strength in paper-based products as well as to improve the gas barrier properties in films.¹⁸⁵⁻¹⁸⁷

MFC is also lightweight, translucent, strong and flexible.¹⁸⁸ Due to their properties, MFCs and NFCs are now found in cutting-edge applications in consolidated and innovative sectors, including food & cosmetics (rheology modifier), pharmaceutical & biomedical, pulp & paper, electronics & sensors and composites & packaging.¹⁸⁹⁻¹⁹²

MFC suspensions have mainly been converted to MFC films which show good barrier characteristics.¹⁷¹ MFC gels may succeed in improving the mechanical and barrier properties of paper, the air permeability and surface porosity of coated paper decreased with an MFC coating.¹⁹³

Ortiz *et al.* reported the addition of MFC (from phormium fibres) to soy protein based bio-films reinforced the protein matrix, which increased their mechanical strength and Young's modulus, improving their barrier properties to water vapor and oxygen.¹⁹⁴

Nathalie Lavoine *et al.*¹⁹⁵ reported MFC coating induces a slower and more progressive release of chlorhexidine digluconate-based antibacterial solution (CHX). These results are very promising with regards to future food-packaging applications.

MFC can be mixed directly into pulp in papermaking industries. Taipale *et al.* reported the addition of MFC to a pulp suspension which significantly increased the strength of paper. However, the drainage time was increased as well and this may be due to high ability of MFCs to hold water.¹⁹⁶ Morseburg *et al.* reported the synergistic effects of clay-MFC in the production of layered thermo-mechanical pulp (TMP) based sheets. The mechanical properties increased significantly with 10% for tensile index and 25% for strength.¹⁹⁷

Nanocellulose foams and aerogels can be used for controlled drug delivery.¹⁹¹ Cellulose nanofibre (CNF) based materials have been used as a matrix former for prolonged and controlled release of drugs in the stomach through to the upper small intestine.¹⁹⁸

Cellulose has a low solid thermal conductivity that makes MFC useful for thermal insulation. The aerogel made from cellulose nanofibres and bleached cellulose fibres

has been proved to be efficient to confine air to reduce thermal conductivity value to $23 \text{ mWm}^{-1}\text{K}^{-1}$.¹⁹⁹

2. Experimental

2.1 Materials & Reagents

A variety of oranges and lemons as detailed in Table 6 were bought from Morrisons, Foss Island, York, UK. All fruits were juiced and the post juicing residues comprising seed, peel, and segment membrane were collected. The latter were freshly milled (Retsch GM300 knife mill, 1600 rpm, 4 cycles of 30 s) and stored in a freezer (-20 °C) until further use. A fresh sample of milled residues was oven-dried at 105 °C for 2 days in order to determine its volatile content (Table 6).

Table 6 Citrus feedstock information.

Fruit	Origin	Size/mm	Weight/kg	Residue/kg	Solid/%
Valencia Oranges	Turkey	60-65	20	7.27	19.4
Lane Oranges	Spain	82-86	22	14.66	15.86
Lemons	Spain	53-63	5	3.45	11.34

All solvents and reagents used in work up procedures, *i.e.*, acetone, ethanol, ethyl acetate, magnesium sulfate, sodium hydroxide and sulfuric acid were obtained from Merck Ltd. (formerly Sigma-Aldrich Ltd.) and used as supplied without further purification.

Industrially-derived blackcurrant pomace was supplied by Lucozade-Ribena-Suntory (LRS, UK), containing stems, seeds and exocarp. The as-received pomace was further air-dried at ambient temperature for one week and then milled (coffee grinder) in to a

granular powder. A Milestone Synthwave microwave processor (1500 W) was used for hydrothermal treatment (see Appendix 1).

2.2 Methodology

2.2.1 Acid-free microwave assisted pectin extraction (general method)

A mixture of either orange or lemon peel residues (100 g) and deionised water (600 ml) were placed in a 750 ml PTFE microwave vessel and subjected to microwave processing at 120 °C or 140 °C or 160 °C for 30 minutes (15 min ramp time (from room temperature to desired temperature) and 15 min holding time) under 12 bar nitrogen atmosphere and 70% stirring. After the microwave processing was complete, the resultant reaction whilst still warm was filtered (120# stainless steel mesh) under vacuum. The solid fraction (MFC0-120) was isolated and kept aside for further MFC production whilst aqueous fraction was treated with one equivalent (based on the volume of hydrolysate) of ethanol and placed in a fridge overnight to expedite pectin precipitation. The following day, the resultant mixture comprising pectin precipitate was centrifuged (3900 rpm for 20 min, acceleration 9, deceleration 4). The supernatant was removed whilst the crude pectin pellet (1) was washed with ethanol (500 ml) and centrifuged again with the same conditions. The ethanol-washed pectin pellet (2) was further purified by stirring in hot ethanol (70 °C, 500 ml) for 20 min followed by hot vacuum filtration and drying to afford the desired pectin as an off-

white solid. Pectin samples are labelled with prefix OPNumber-XXX and LPNumber-XXX designating their origin from oranges and lemons, respectively. The 'number' refers to original or reprocessed material. XXX refers to the microwave processing temperature. For example, OP0-120 refers to orange pectin (OP), first microwave processing (0), at 120 °C (120).

2.2.2 Microwave micro-fibrillated cellulose production (general method)

MFC0 (150-200 g) collected from section 2.2.1 and deionised water (500-550 ml, total volume < 700 ml) were placed in a 750 ml PTFE microwave vessel and subjected to microwave processing at 120 °C or 140 °C or 160 °C for 30 minutes (15 min ramp time (from room temperature to desired temperature) and 15 min holding time) under 12 bar nitrogen atmosphere and 70% stirring. After the microwave processing was complete, the resultant reaction whilst still warm was filtered (120# stainless steel mesh) under vacuum. The hydrolysate (filtrate) was collected to isolate and purify a second crop of pectin with the same process as described in section 2.2.1. These second crop pectin samples are labelled as P1, P2 and P3 depending on reaction temperature. For example, OP1-120, refers to orange pectin from reprocessing of MFC0 at 120 °C. OP2-140, refers to orange pectin from reprocessing of MFC0 at 140°C. OP3-160, refers to orange pectin from reprocessing of MFC0 at 160 °C. The same coding is used for lemon pectin whereby OP is replaced with LP.

The solid residues were stirred with boiling water (1000 ml) for 10 min, filtered

(vacuum), washed with hot ethanol (2 x 500 ml, 70 °C, 10 min), cold ethanol (500 ml) and acetone (500 ml). The residue was then dried to obtain desired microfibrillated celluloses which were labelled as either OMFC-XXX or LMFC-XXX.

2.2.3 Microwave assisted extraction (MAE) of BCP. (General method)

A mixture of BCP (40 g) and deionised water (600 ml) was placed in a 750 ml PTFE microwave vessel and subjected to microwave processing at variety temperatures (from 50 °C to 160 °C) (15 min ramp time (from room temperature to desired temperature) and 15 min holding time) under 12 bar nitrogen atmosphere and 70% stirring. After the microwave processing was complete, the resultant reaction whilst still warm was filtered (120# stainless steel mesh) under vacuum. The aqueous fraction was centrifuged (3900 rpm, 10 min) to further remove small particles that were able to pass through the mesh and subsequently freeze-dried to afford the desired hydrolysate. The solid residues were oven dried and collected.

2.3 General Instrumental analysis

2.3.1 ATR-IR

Attenuated Total Reflection Infra-Red spectroscopy measurements were performed on a Perkin Elmer Spectrum 400 spectrometer. A small amount of sample (cover the window) was placed on the spectrometer and apply light pressure. The spectrum was taken from 4000 cm^{-1} to 650 cm^{-1} at 32 scans, with a spectral resolution of 2 cm^{-1} with

a blank window for background. The raw data was saved as an Excel file and was reprocessed by Origin 2018™ software.

2.3.2 Solid state ¹³C Nuclear Magnetic Resonance (SSNMR)

Solid state ¹³C Cross Polarisation Magic Angle Spinning (CP-MAS) NMR (SSNMR) spectra was acquired using a 400 MHz Bruker Avance III HD spectrometer equipped with a Bruker 4 mm H(F)/X/Y triple-resonance probe and 9.4T Ascend® superconducting magnet. The CP experiments employed a 1 ms linearly-ramped contact pulse, spinning rates of 10000 ± 2 Hz, optimised recycle delays of 5 seconds, 800 scans. Chemical shifts were reported with respect to tetramethylsilane (TMS) and were referenced using adamantane (29.5 ppm) as an external secondary reference. The spectrum was processed by MestReNova software.

2.3.3 Thermogravimetric Analysis (TGA)

TGA was performed on Stanton Redcroft STA-625 instrument. A small amount of sample (~10 mg) was accurately weighed into an aluminium STA cup and heated from room temperature to 625 °C at 10 °C min⁻¹ under a continuous nitrogen gas flow (50 ml min⁻¹). Time, temperature, weight and weight percent were recorded and saved in text document, reprocessed as a temperature vs weight percent and dTG figure via Origin 2018™ software.

2.3.4 Elemental analysis (CHN)

Elemental analyses were performed in-house by Dr. Graeme McAllister, Department of Chemistry, University of York using an Exeter Analytical Inc. CE-440 analyser. The sample was placed in a nickel sleeve and injected into a high temperature furnace (975 °C) and burnt in high purity oxygen under static conditions. The results reported are the average of duplicate.

2.4 Characterisation of Pectin

2.4.1 Degree of Esterification

The DE of pectin was calculated by different methods depending on the amount of sample available.

- 1) The absorbance band at around 1740 cm⁻¹ corresponds to esterified C=O bond, note this peak area as *a*. The peak at around 1600 cm⁻¹ corresponds to non-esterified carboxyl group, note this peak area as *b*.²⁰⁰ DE was calculated according to Equation 1.

$$DE = \frac{a}{a+b} * 100\% \text{ (Equation 1)}$$

- 2) Chemical titration: Dried pectin (~0.2 g) was weighted into a conical flask with aqueous propan-2-ol (1 ml, 65% v/v), distilled water (50 ml) is added and the flask is placed on a magnetic stirrer plate, stirred until pectin has dissolved.

Phenolphthalein (4-5 drops) was used as indicator. The solution was titrated with 0.1 M NaOH to pink, the volume of titrant consumed was noted as a ml. NaOH (15 ml, 0.1 M) was added to the solution, the flask is covered and stirred for 30 min. An amount of dilute sulfuric acid (0.1 M, ~7.5 ml, calibrated with NaOH previously) equals to 15 ml of 0.1M NaOH was added. The mixture was titrated with 0.1 M NaOH, the volume of titrant consumed again being noted as b ml. DE was calculated according to Equation 2.

$$DE = \frac{b}{a+b} * 100\% \text{ (Equation 2).}$$

2.4.2 Liquid ^{13}C NMR

^{13}C NMR spectra were recorded at 125 MHz on a Bruker AVIIIHD 500 spectrometer. Pectin (4 mg) was dissolved in deuterated water (1 ml, 4wt%), experiment was operated by Dr. Heather Fish as a service at 353 K (80 °C) with 30,000 scans and processed by MestReNova software.

2.4.3 High-performance Liquid Chromatography (HPLC)

HPLC analyses were performed in-house by Dr. Richard Gammons. Prior to submission each pectin sample (~5.5 mg) was digested in sulfuric acid (1 M, 1.5 ml) at 105 °C for 2.5 hours. The resultant hydrolysate was filtered (disk filter, 0.22 μm pore) and, thereafter analysed (injection volume, 5 μL ; run time 35 min) by Dr. Gammons using an Agilent 1260 HPLC instrument equipped with a reverse-phase Hi-

Plex H (300 x 7.7 mm, 8 µm particle size) column and refractive index detector (55 °C). 0.005 M H₂SO₄ was used as the mobile phase in isocratic mode (no gradient) with a flow-rate of 0.4 ml/min and column temperature at 60 °C.

2.4.4 Gel Permeation Chromatography

Gel permeation chromatography of pectin samples were analysed externally by Concept Life Sciences Ltd. using the method developed by Malvern Panalytical, whereby the samples were dissolved in phosphate-buffered saline (PBS) buffer at a concentration of 3 mg/ml, at room temperature, overnight, whilst being shaken gently. The samples did not fully dissolve, were filtered through 0.45 µm nylon syringe filters before tested by GPC.

2.5 Characterisation of MFC

2.5.1 MFC gel formation

MFC samples (25 mg, 50 mg, 75 mg, 100 mg and 150 mg) were placed in 7 ml sample vials, to which deionised water (5 ml) was added giving resulting in concentrations of 0.5%, 1%, 1.5%, 2% and 3% w/v, respectively. Each vial was homogenised (speed 10) for 3 min, allowed to stand for 5 mins and then inverted to qualitatively assess gel strength.

2.5.2 Water retention value (WRV)

The appropriate MFC sample (~0.1 g) was mixed with water (10 ml) contained in 35 ml vial and placed on roller mixer for 20 min at room temperature. The mixture was placed on a glass filter (the mass of glass filter was weighted as m_1), the filter was placed in 50 ml centrifuge tube then centrifuged (3900 rpm, 20 min) then weighted as m_2 (the mass of filter and wet MFC). The filter and sample were dried in the oven (105 °C, 2 days). The dried MFC and filter were weight as m_3 . The WRV was calculated using Equation 3.

$$WRV = \frac{m_2 - m_1}{m_3 - m_1} - 1 \text{ (Equation 3)}$$

2.5.3 Powder X-Ray Diffraction (XRD)

Powder XRD analysis was performed on a Bruker-AXS D8 Advance Diffractometer equipped with a Cu source producing a monochromatic K- α radiation at wavelength of 1.54184 Å and a PSD Lynx eye detector. Samples were ground to fine powders prior to analysis. Sample was placed on an aluminium plate with 0.75 mm depth, flattened with glass slide then inserted to the instrument. Samples were run with a rate of 2.5° min⁻¹ over a 2 θ range of 10 - 37.5° in a locked coupled theta-2 θ scan mode. Generator voltage and current were set to 40 kV and 40 mA respectively. Data was collected and processed via Origin including smoothing and background subtraction.

The crystalline index (CI) of MFC samples was calculated according to Segal's

equation (Equation 4).²⁰¹

$$CI = \frac{I_{200} - I_{am}}{I_{200}} \times 100 \text{ (Equation 4)}$$

I_{200} = intensity of the (200) peak ($2\theta = 22^\circ \pm 0.5$)

I_{am} = intensity of the amorphous contributions ($2\theta = 18^\circ \pm 0.5$)

2.5.4 Scanning Electron Microscopy (SEM)

SEM images were recorded by Dr. Meg Stark and Dr. Karen Hodgkinson, Department of Biology, University of York on a JEOL JSM SEM instrument. A water suspension of MFC sample (ca. 0.2% w/v) or a MFC gel sample was submitted for analysis.

2.5.5 Transmission Electron Microscopy (TEM)

TEM images were recorded by Dr. Meg Stark and Dr. Karen Hodgkinson, Department of Biology, University of York on a TEM Tecnai 12 BioTWIN coupled to a SIS Megaview 3 camera at an acceleration voltage of 120 kV.

2.5.6 Confocal Laser Scanning Microscopy (CLSM)

CLSM was performed in-house by Dr. Joanne Marrison, Department of Biology, University of York. A Carl Zeiss LSM 880 confocal microscope, fitted to an Axioimager, using a Plan Apochromat 20x/0.8 or 60x/1.4 oil objective with ZEN 3 software was used to capture the raw images. All samples were excited with a 405 nm laser using a 405 nm main beam splitter and emission collected from 410-695 nm in

bins of 8.9 nm using the spectral detector. Reference spectra of citrus pectin, lignin and cellulose (Sigma-Aldrich) were collected independently and used to spectrally unmix the experimental images. Images were averaged to reduce noise and increase the precision of the spectral unmixing which was performed using the in-built application within ZEN 3 on a pixel-to-pixel basis. This processing result in the image being split into 3 individual images corresponding to the cellulose, pectin and lignin content present in the sample.

2.6 Characterisation of BCP Hydrolysates

2.6.1 Total Phenol Content (TPC)

TPC of BCP hydrolysate was characterised by Folin-Ciocalteu method. (Details see section 1.7, *secondary aims*)

The appropriate BCP hydrolysate (5 mg) was reacted with Folin-Ciocalteu reagent (FCR) in presence of sodium carbonate in dark place at room temperature for 2 h. The absorbance at 765 nm was acquired by Jasco 550 UV-vis spectrometer. Gallic acid at specific concentration ranges from 49 – 52 mg/L was used as standard solution, 1-5 ml of gallic acid solution was diluted to 50 ml to acquire UV absorbance at 760 nm to form a standard absorbance vs concentration calibration. The result was shown as mg GAE / g BCP and mg GAE / g Hydrolysate.

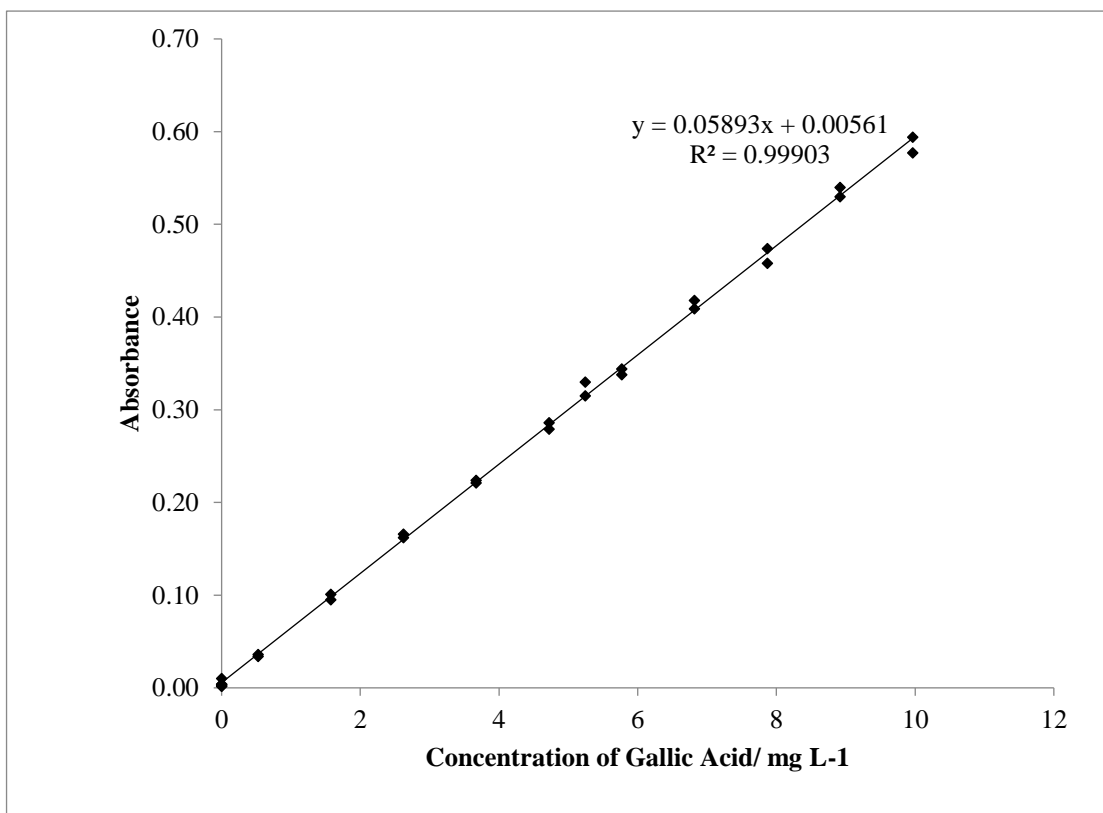


Figure 20 Calibration of TPC, concentration of gallic acid vs absorbance at 765 nm.

2.6.2 Total Antioxidant Activity (DPPH method)

DPPH (5 mg) was dissolved in ethanol absolute (50 ml) to form a 0.25 mmol/L, 0.1 mg/ml solution. The appropriate BCP hydrolysate (5 mg) was dissolved in distilled water (50 ml). The BCP aqueous solution (0.1 mg/ml, 1 ml) reacted with DPPH solution (0.1 mg/ml, 1 ml) for 30 min, absorbance at 517 nm was collected as A_b , DPPH ethanol solution (1 ml) was mixed with distilled water (1 ml) for 30 min, absorbance at 517 nm was acquired as A_0 , as reference. The inhibition (%) was calculated by the following equation.

$$\text{Inhibition \%} = \frac{A_0 - A_b}{A_0} \times 100 \quad (\text{Equation 5})$$

2.6.3 ¹H NMR

BCP MH (5 mg) was dissolved in D₂O (1 ml), submitted to NMR service in the teaching lab, Department of Chemistry, University of York. Spectra were recorded at 300 MHz on a Bruker AVIII 300 NB NMR, performed at 300K for 16 scans. The spectrum was processed by MestReNova software.

2.6.4 2D NMR

2D NMR was performed in-house by Dr. Heather Fish, Department of Chemistry, University of York. BCP MH-50 and 160 (30 mg) were dissolved in 1.5 ml D₂O, submitted to Dr. Fish at NMR centre.

Proton NMR spectra were recorded at 500 MHz on Bruker AVIIIHD 500 spectrometer, at 298K for 16 scans. ¹³C NMR spectra were recorded at 125 MHz on the same spectrometer at 298 K for 12776 scans. ¹H/¹H correlation spectroscopy (COSY) and heteronuclear single quantum coherence (HSQC) were recorded. DEPT spectrum was recorded at 125 MHz on Bruker AVIIIHD 500 spectrometer for 257 scans. The spectrum was processed by MestReNova software.

2.6.5 HPLC-MS

The BCP hydrolysates were analysed externally by Analytical Innovations, Ltd, Huddersfield, UK. The hydrolysates (50 mg) were dissolved in 20% aqueous methanol (2 ml), sonicated for 5 min at room temperature, centrifuged at 12,500 rpm

for 5 min and filtered through a 0.15 μm PTFE filter into an HPLC vial. The samples were analysed by Agilent 1290 Infinity II UHPLC and 6550 Q-ToF with iFunnel, with Agilent Eclipse Plus C18. 2.1 x 50 mm, 1.8 μM column, using 0.1% formic acid in water (A) and 0.1% formic acid in acetonitrile (B) as mobile phases, flow-rate of 0.3 ml/min, column temperature at 40°C, injection volume of 2 μl and runtime 8.5 min. The mass spectra of substances were compared with Metlin 8.0 database to identify possible structures.

3. Results and Discussion

This chapter is divided into 3 parts and is commensurate with the *global, primary* and *secondary* aims and objectives outlined in Chapter 1, section 1.7.

Part 1: Pectin Isolation and Characterisation.

Part 2: Production and Characterisation of Citrus Microfibrillated Cellulose (MFC) or Defibrillated Celluloses.

Part 3: Production and Characterisation of Blackcurrant Pomace Hydrolysates.

3.1 Part 1: Pectin Isolation and Characterisation

3.1.1 Pectin Isolation

The direct isolation of pectin, reported as yield (wt%, dry basis), from lemon and lane orange peel residues processed at 120 °C, 140 °C and 160 °C, and its subsequent re-processing is summarised in Fig. 21. The direct processing of OPR at 120 °C, 140 °C and 160 °C yielded OP0-120 (12.7%), OP0-140 (16.3%) and OP0-160 (5.5%). Thus, optimal extraction temperature was identified as 140 °C, whilst 160 °C gave the lowest yield inferring possible degradation. The sequential reprocessing of orange peel residues, generated from direct processing of OPR at 120 °C, *i.e.*, OMFC0-120, yielded additional pectin; 1.9% (OP1-120), 7.0% (OP2-140) and 3.2% (OP3-160) when processed at 120 °C, 140 °C and 160 °C, respectively.

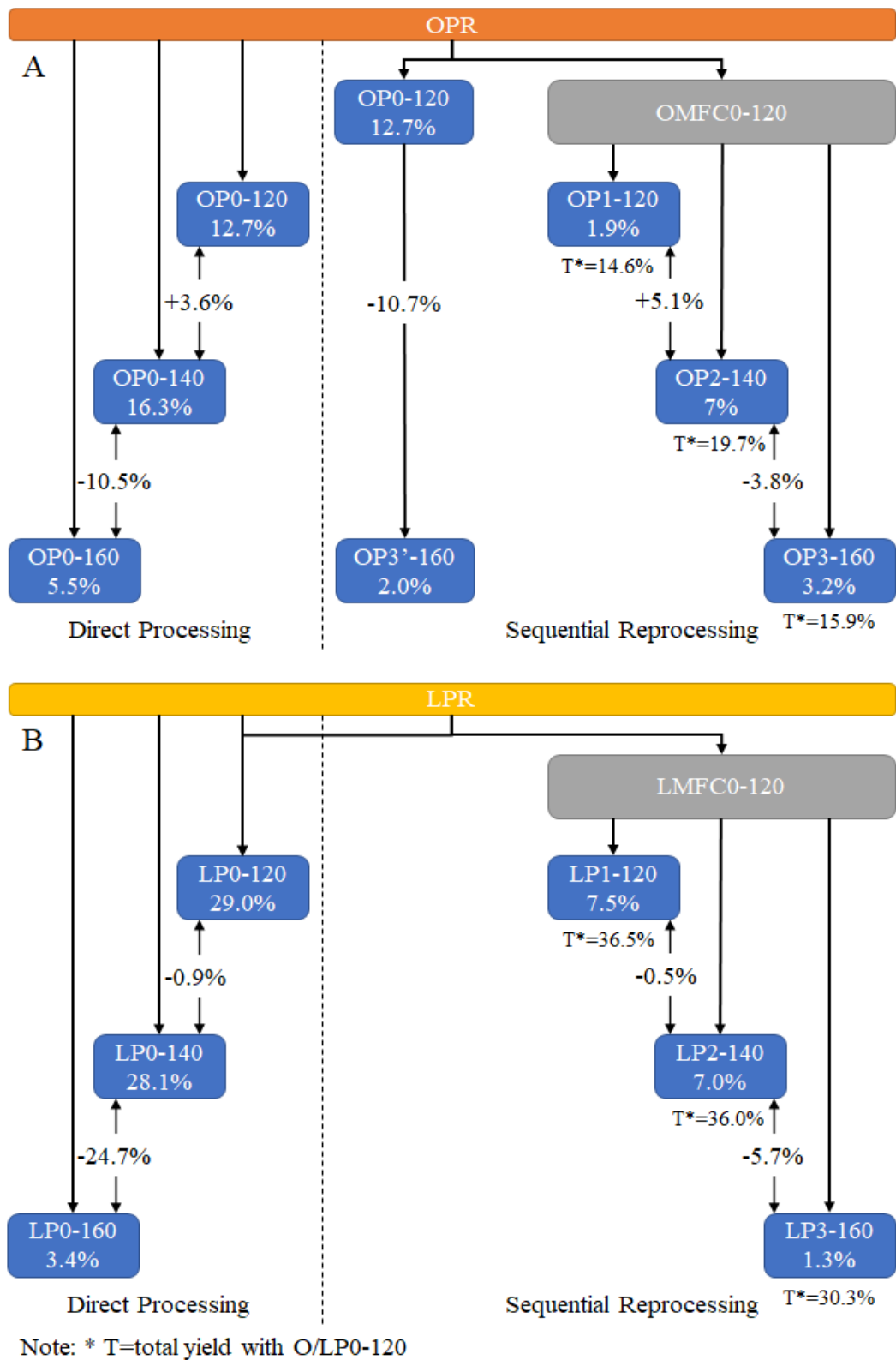


Figure 21 Summary of pectin yield (wt%, dry basis) from A) orange peel (OPR) and B) lemon peel (LPR).

Interestingly, sequential reprocessing at 140 °C (OP2-140) compared to direct processing at the same temperature (OP0-140) afforded highest total pectin yield (19.7%), *i.e.*, OPR to OP0-140 (16.3%) *versus* OPR to OP0-120 (12.7%) to OP2-140 (7.0%).

The sequential reprocessing of OP0-120 (12.7%) at 160 °C afforded OP3'-160 with a significantly lower yield (2%) again commensurate with pectin degradation. In fact, processing of any material above 140 °C is detrimental to pectin yield.

Compared with OPR, lemon peel residues contain more acidity due to their higher content of citric acid. The pH of oranges is calculated to be in the range of 3.5-4.3, whereas the pH of lemons is around 2- 2.6.⁷⁸ The naturally higher acidity of lemon peel residues is beneficial to acid-free microwave-assisted extraction of pectin. Thus, the isolation of pectins from lemon peel residues (LPR, Figure 21B) shows several differences and similarities with respect to pectin isolation from orange peel residues (OPR, Figure 21A), namely:

- i. More than double the amount of pectin is isolated from LPR than OPR at 120 °C, *i.e.*, LP0-120 (29.0%) *versus* OP0-120 (12.7%).
- ii. Direct processing of LPR at 140 °C compared with OPR at 140°C affords close to double the amount of pectin, *i.e.*, LP0-140 (28.1%) *versus* OP0-140 (16.3%).
- iii. Either direct processing of LPR or re-processing of LMFC0-120 at 160 °C shows

a drastic reduction in pectin yield similar to OPR or OP0-120. Again, this correlates with pectin degradation observed at higher than 140 °C

iv. The best route(s) for maximum pectin extraction of lemon residues is/are LPR to LP0-120 (29.0%) to LP2-140 (7.0%) [total, 36.0%] or LPR to LP0-120 (29.0%) to LP1-120 (7.5%) [total, 36.5%].

3.1.2 Pectin Characterisation

3.1.2.1 ATR-IR

The stacked ATR-IR spectra of isolated pectins after direct processing of OPR and LPR at 120 °C (OP0-120 or LP0-120), 140 °C (OP0-140 or LP0-140) and 160 °C (OP0-160 or LP0-160) and, of commercial citrus pectin (Sigma-Aldrich) are shown in Fig. 22. All spectra comprise a wide, broad, absorbance between 3600 and 3000 cm^{-1} corresponding to the O-H stretching vibration coupled with inter- and intramolecular hydrogen bonding. The absorbance bands around 2900-2800 cm^{-1} refer to C-H stretching vibration of sp^3 -hybridised carbons. Importantly, the absorbances occurring between 1750-1730 cm^{-1} and at approximately 1600 cm^{-1} are indicative of esterified carbonyl (C=O) and free carboxylate stretching band (COOH) synonymous with pectin, respectively.²⁰² The ratio of the peak area of these to absorbances forms the basis of calculating degree of esterification of pectin as outlined earlier in section 2.4.1 degree of esterification. The absorbance band at 1150 cm^{-1} refers to COO-

asymmetric valence vibration and the medium to sharp, strong absorbance at 1033 refers to C-O valence vibration.²⁰³

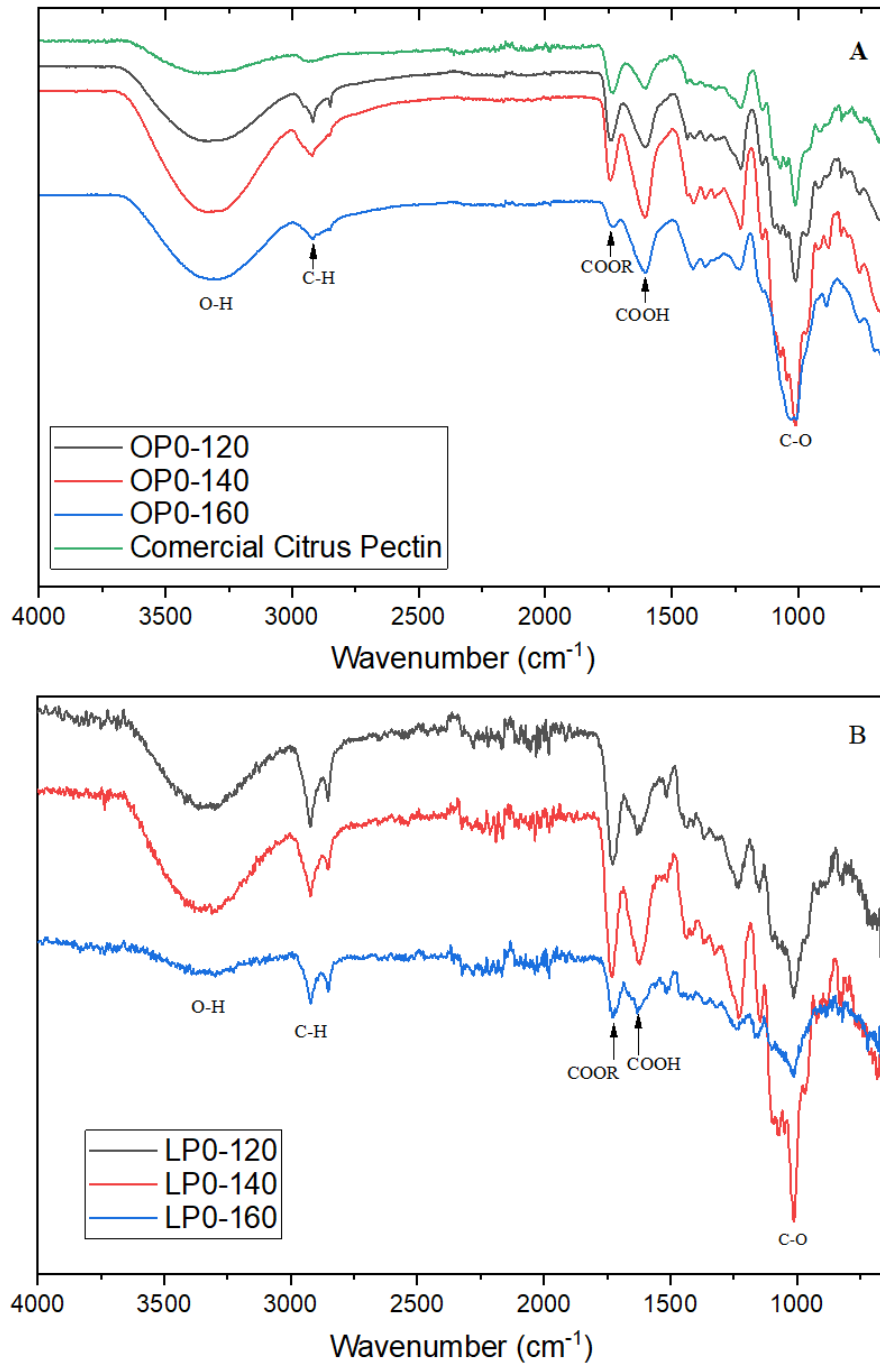


Figure 22 Stacked IR spectra of pectins from direct processing OPR with respect to commercial citrus pectin (top) and LPR (bottom).

3.1.2.2 Degree of Esterification (DE)

Degree of esterification (% DE) of pectin samples was determined by the IR method and the titration method are reported in Table 7.

Table 7 DE (%) of pectins from direct processing of OPR with respect to commercial citrus pectin and LPR.

Sample	DE (%)	
	IR	Titration
OP0-120	43.5	96.8
OP0-140	30.5	94.6
OP0-160	11.7	90.9
Commercial	59.0	75.1
LP0-120	60.9	82.5
LP0-140	55.3	86.1
LP0-160	58.9	N/A

DE of the pectin samples from the two methods shows huge variation. The IR method, although quick and easy, is less reliable than the titration method because it is influenced by water content within the sample which can artificially exaggerate the intensity of the O-H absorbance band in water at approx. 1600 cm^{-1} , which coincides with the carbonyl stretching vibration of the free carboxylic acid, resulting in a lower DE. However, although more reliable, the chemical titration method was seriously influenced by sample insolubility. Despite soaking the isolated pectins in water overnight prior to titration, insoluble particulate matter was still evident which was

not removed by filtration. However, these solids dissolved in the presence of sulfuric acid (second step of the titration) which may have led to much higher degree of esterification. Nevertheless, both the IR and titration method show the same trend for orange pectins, *i.e.*, decreasing DE with respect to increasing processing temperature.

3.1.2.3 TGA of Pectin Sample

The thermogravimetric profiles of orange and lemon pectin samples are shown in Fig. 23. All profiles show an initial mass loss from 25 °C to approximately 180 °C corresponding to moisture loss (7-15%). Thereafter, the next mass loss is characteristic of pectin which typically occurs at approximately 220 °C. For example, OP0-120 and OP0-140 show rate of maximum decomposition (dTG) at 220 °C. However, OP0-160 does not show dTG at 220 °C but, instead, at approx. 280 °C inferring that is a different material. The further characterisation of this material is reported later in this thesis. Lemon pectin samples show similar dTG at 230 °C coupled with a small decomposition at 340 °C (LP0-160) which may be due to carryover of residual cellulose.

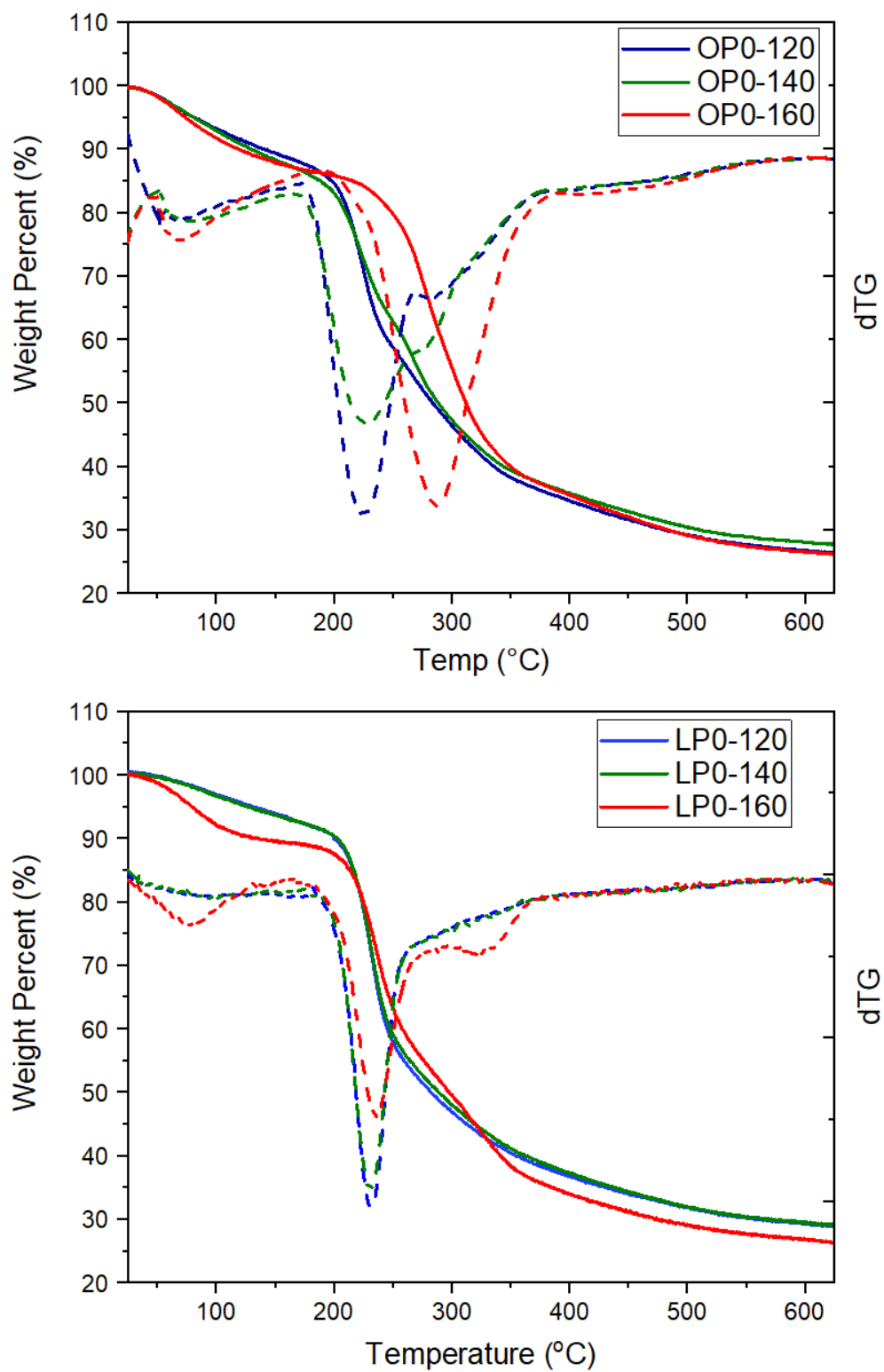


Figure 23 TGA of pectins from direct processing of OPR (top) and LPR (bottom).

3.1.2.4 Liquid ^{13}C NMR of pectins.

Further characterisation of pectin samples was carried out by liquid ^{13}C NMR (Fig. 24).

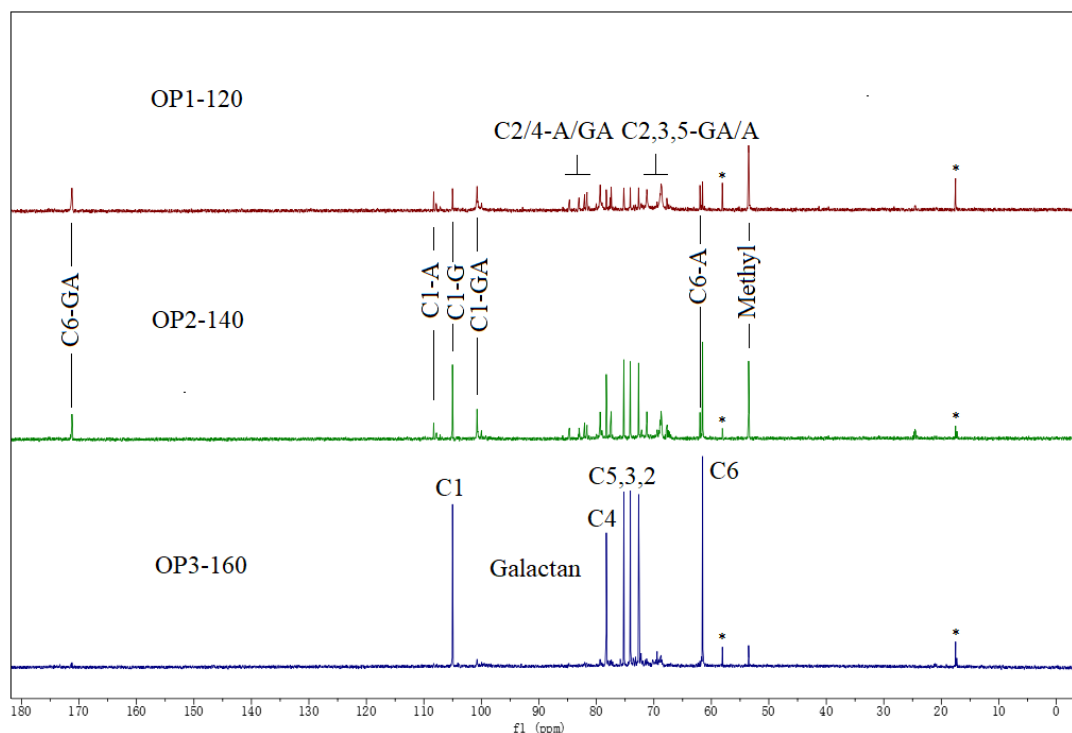


Figure 24 ^{13}C NMR of orange OP1, OP2 and OP3 (*= solvent impurity)

The resonance at 171 ppm refers to C-6 of galacturonic acid (GA), resonances at 108, 105 and 101 ppm correspond to C1 (anomeric) of arabinose (A), galactose (G) and GA. The resonances at from 85 ppm to 65 ppm are for the remaining ring carbons. Importantly, the resonance at 53.5ppm refers to methyl group of galacturonic acid methyl ester. This resonance (as well as the 171ppm resonance) is conspicuous in spectrum of OP1-120 and OP2-140, but almost negligible in OP3-160. Unlike OP1-

120 and OP2-140, the ^{13}C NMR spectrum of OP3-160 shows a clear spectrum of galactan.²⁰⁴ According to our knowledge of pectin structure, at 160 °C under microwave radiation, the degradation of the HG region of pectin is observed; the carbon resonances of Gal A and the methyl group are very small in OP3-160. Furthermore, the resonances of arabinose and rhamnose also become negligible suggestion further degradation of the ‘hairs’ or ‘hairy region’ of pectin. The material following microwave processing at 160 °C is predominantly rich in galactan-like hairs.

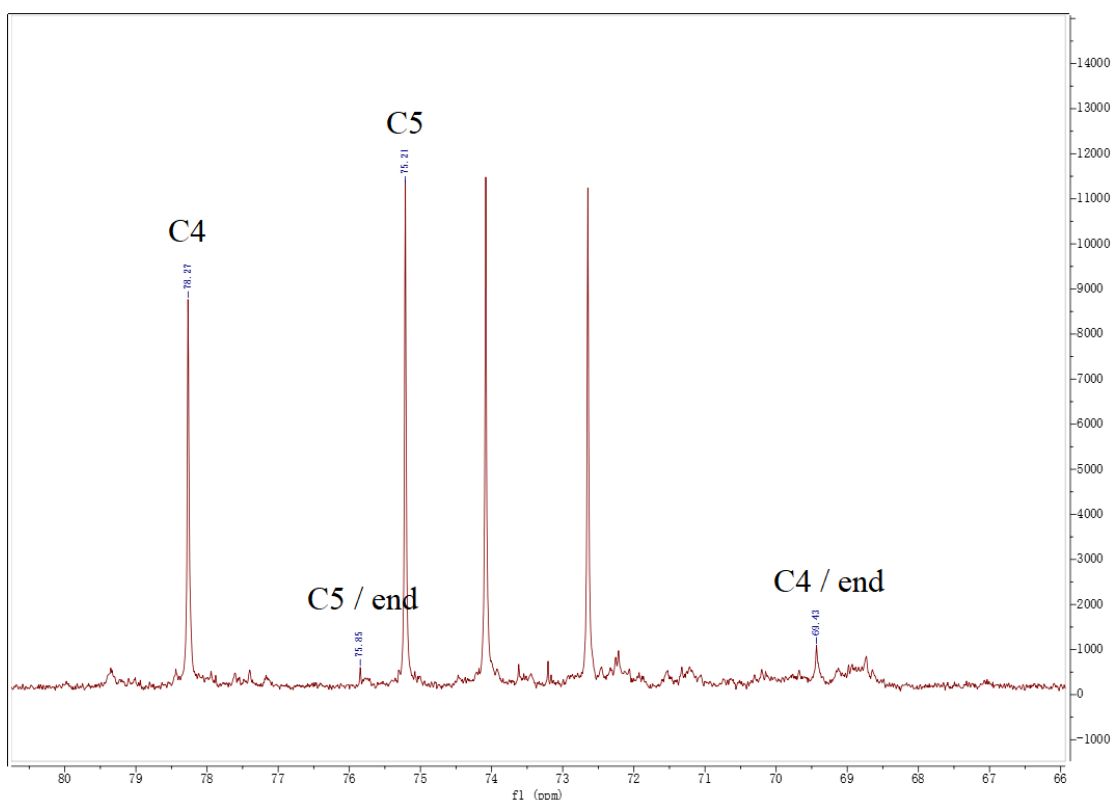


Figure 25 Expansion of ^{13}C NMR of OP3-160 for chain length calculation.

The extent of the branched galactan chain length can be calculated according to the method of Gunning *et al.*²⁰⁵. The resonances at 78.27 and 75.21 ppm correspond to C-

4 and C-5 of galactose in the galactan chain, which could be considered as number of galactose units. The non-reducing end of galactose has different signals (C-4 at 69.43 ppm and C-5 at 75.85 ppm), which could be considered as the number of branches. The chain length equals the number of galactose (the integral of C4 + C5) / number of branches (the integral of ending C4 + C5). According to Fig.25, it is ~12.

Similarly, all pectin samples isolated from lemon peel showed similar complex ^{13}C NMR spectra (Fig. 26). However, the resonance at 53.5 ppm corresponding to methyl group of galacturonic acid methyl ester, is much stronger than C-6 of Gal A suggesting the presence of other unknown substances. A small resonance at 17.2 ppm refers to $-\text{CH}_3$ of rhamnose, suggesting a very small RG-I region in lemon pectins.

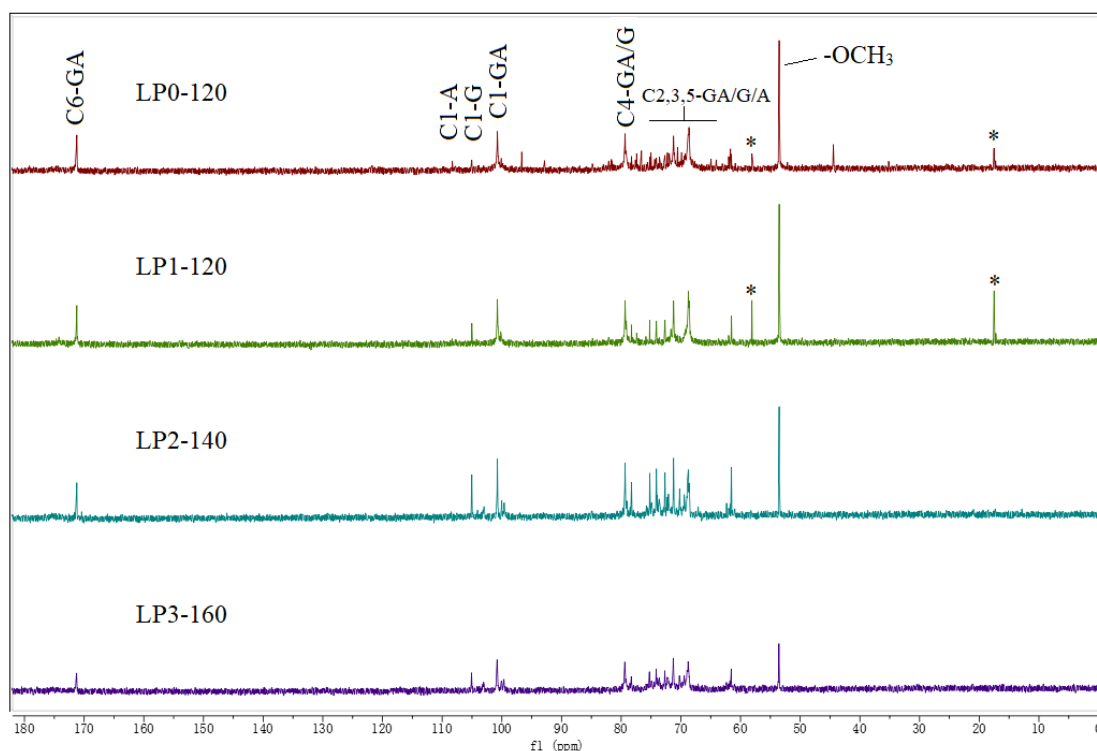


Figure 26 ^{13}C NMR of lemon pectins. (*= solvent impurity)

Trying to find out whether OP3-160 is newly extracted from MFC0-120 at 160 °C or it comes from degradation of OP0-120, the aqueous fraction of MW step-1 pectin isolation was treated by MHT at 160 °C again to obtain P3'. In order to save time and solvent, pectin (OP0-120) was not precipitate from the aqueous fraction, directly submitted to the microwave processor. The ^{13}C NMR spectrum (shown in Fig. 27) shows OP0-160, OP3-160 and OP3'-160 are similar materials containing galactan. This also proves that the orange pectin being treated at 160 °C with microwave hydrothermal process is part of orange pectin, RG-I and galactan branches, which can be named as galactan-rich RG-I pectin.

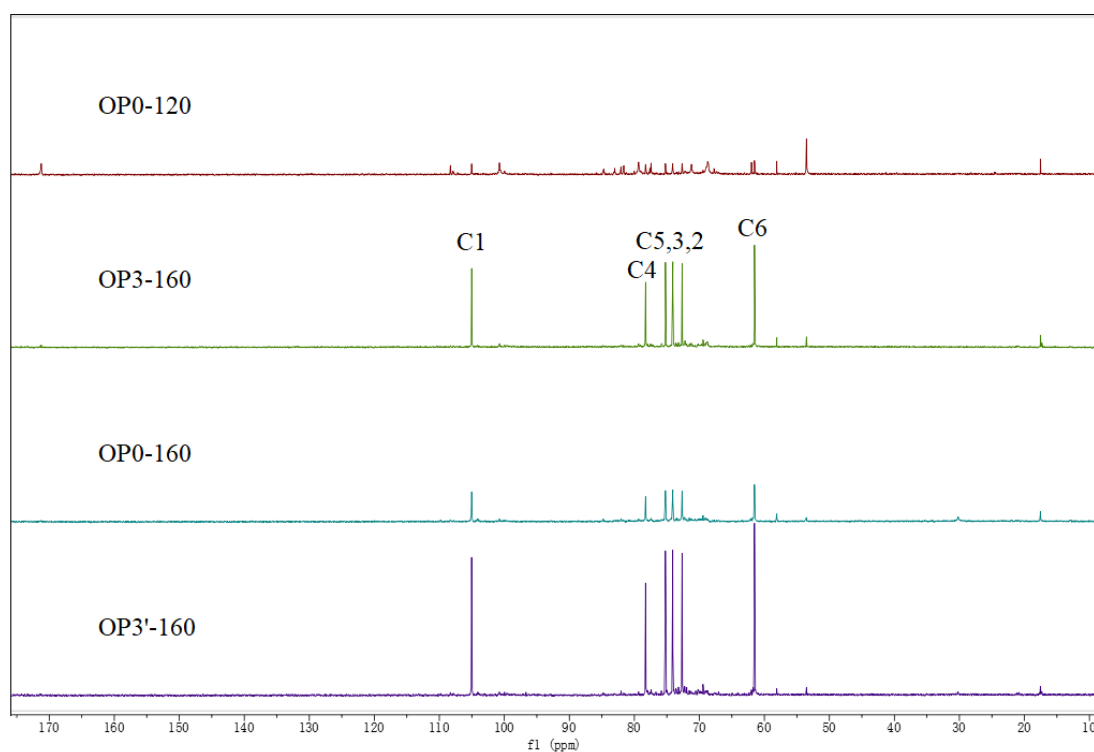


Figure 27 ^{13}C NMR of OP0-120, OP3-160, OP0-160 and OP3'-160.

3.1.2.5 Monosaccharide content analysis (HPLC)

To further ascertain the composition of pectins isolated from OPR and LPR, they were acid-digested into its monomer sugars and the monosaccharide content is shown in Table 8 and displayed graphically in Fig. 28.

Table 8 Monosaccharide content of pectin. Molar percent (%).

Sample	Galacturonic Acid	Galactose	Rha & Ara
OP0-120	56.47	25.66	17.87
OP0-140	45.25	38.27	16.48
OP0-160	14.84	77.73	7.43
OP1	67.32	19.98	12.7
OP2	48.10	35.64	16.26
OP3	18.48	75.60	5.92
LP0-120	79.67	11.85	8.48
LP0-140	82.84	13.55	3.61
LP0-160	76.87	21.31	1.82

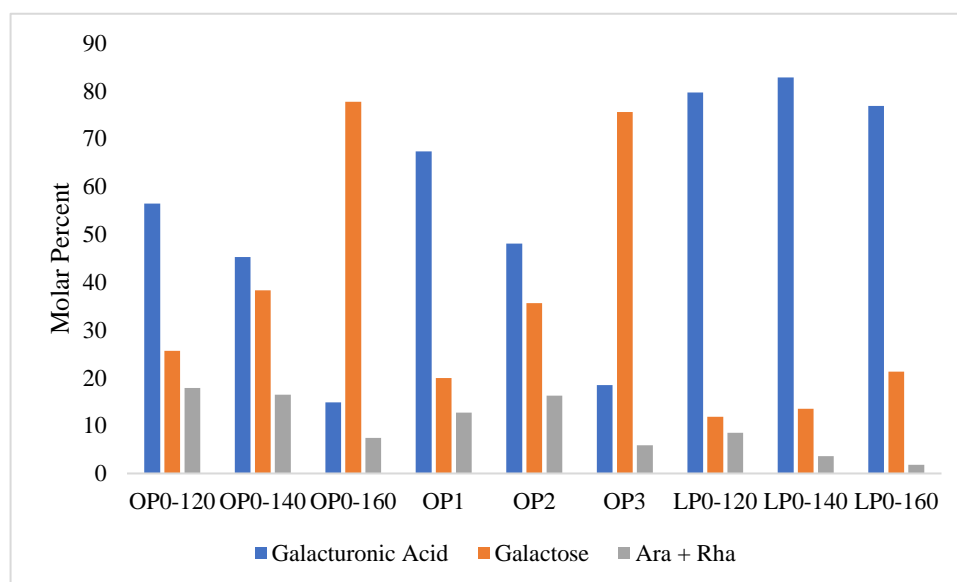


Figure 28 Galacturonic acid & galactose molar percent. (%)

Orange pectins were significantly changed in their galacturonic acid (down) and galactose (up) molar percentage when microwave temperature was increased, which corresponds to our thinking of selective degradation of orange pectin at 160 °C.

The galactose content in lemon pectins increased from 11.85% at 120 °C to 21.31% at 160 °C. Meanwhile, the arabinose & rhamnose percentage decreased to only 1.82% which corresponds to decomposition of RG-I back bone and arabinan branches. This is further evidence of galactan branches in RG-I region of pectin presenting higher thermal stability in microwave hydrothermal treatment processes.

3.1.2.6 Gel Permeation Chromatography (GPC)

GPC was conducted to further assess the potential degradation and changes in pectin. Samples were sent for external analysis (see section 2.4.4). The quantitative results of GPC data of pectin samples are shown in Table 9.

Table 9 Quantitative GPC results for analysis of pectin.

Sample	Mw (g/mol)	Mn (g/mol)	D	IVn (dl/g)	Rh (nm)	Recovery (%)
OP0-120	387,874	61,079	6.35	1.44	16.1	46.3
OP0-140	267,375	34,980	7.7	0.19	5.44	80.97
OP1	379,438	42,552	8.92	0.92	13.8	44.9
OP2	121,596	19,918	6.11	0.34	7.1	38.0
OP3	31,037	12,384	2.51	0.16	3.9	52.9
OP0-160	46,702	19,493	2.4	0.17	4.7	46.3
OP3'	81,075	23,972	3.39	0.18	5.2	41.9

LP0-120	146,310	54,809	2.67	2.63	16.4	41.7
LP0-140	284,615	11,809	24.1	0.16	3.46	89.25
LP1	84,914	30,045	2.83	1.38	10.7	36.9
LP2	32,622	16,168	2.02	0.44	5.4	47.3
LP3	10,500	4,779	2.2	0.14	2.7	36.1
LP0-160	9,488	7,121	1.33	0.16	2.8	45.4

Mw = weight average molecular weight (g/mol)

Mn = number average molecular weight (g/mol)

D = dispersity of the sample (Mw/Mn)

IVn = number average intrinsic viscosity (dL/g)

Rh = hydrodynamic radius (nm)

Recovery = ratio of the detected concentration to the expected concentration.

$$M_w = \frac{\sum N_i M_i^2}{\sum N_i M_i} \quad M_n = \frac{\sum N_i M_i}{\sum N_i} \quad (\text{Equation 6})$$

The number average molecular weight, Mn, and the weight average molecular weight, Mw, were determined according to equation 6, where, *i* refers to a specific molecule, Ni means the number of this molecule, Mi means the molecular weight of the molecule.

For a more visualised comparison, GPC results including Mw, Mn, dispersity and intrinsic viscosity of pectin samples are shown in Fig. 29. The average molecular weight including Mw and Mn of citrus pectins decreased significantly when the reaction temperature increases, from over 380,000 g/mol to lower than 20,000 g/mol (orange pectin) and from over 140,000 g/mol to lower than 5,000 g/mol (lemon pectin)

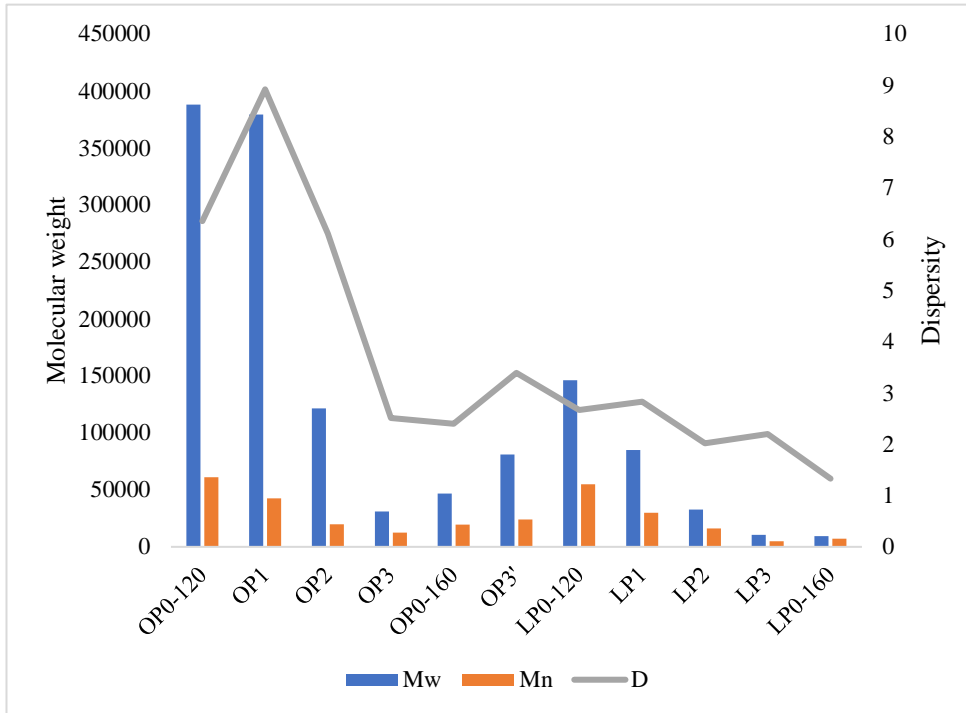


Figure 29 Mw, dispersity and intrinsic viscosity of pectin samples from GPC results.

Figures 30 and 31 show the overlay chromatograms for the orange pectins and lemon pectins, respectively.

RI = Refractive Index

RALS = Right angle light scattering

LALS = Low angle light scattering

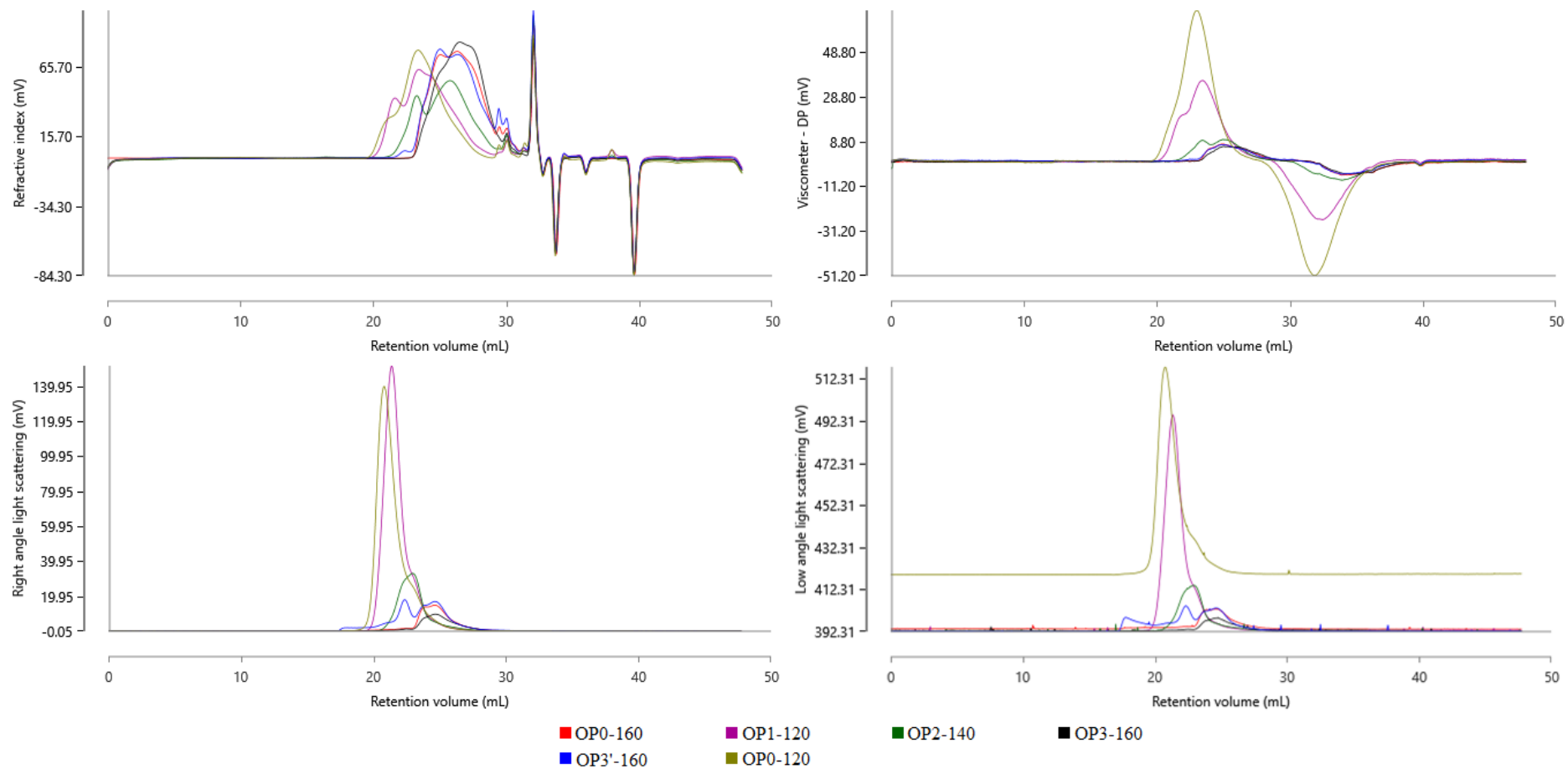


Figure 30 Overlay Chromatograms for Orange Pectins. [RI (top left), Viscometer (top right), RALS (bottom left) and LALS (bottom right)].

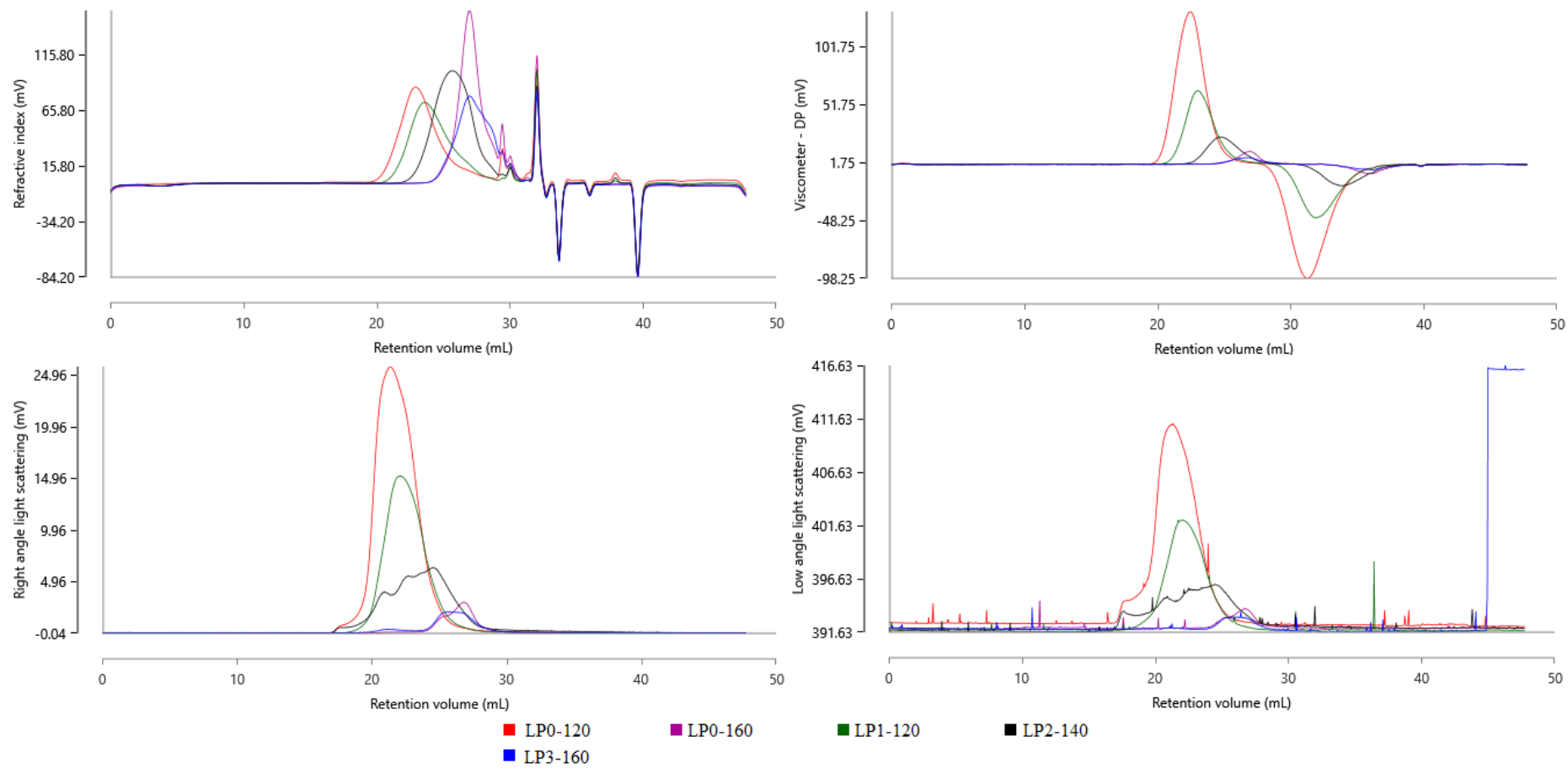


Figure 31 Overlay Chromatograms for Lemon Pectins. [RI (top left), Viscometer (top right), RALS (bottom left) and LALS (bottom right)]

These demonstrate that the samples are not similar as the retention volume and peak shape of each differs in all detectors (RI, viscometer, RALS and LALS). The samples OP1-120, LP0-120 and OP0-120 elute earlier on the refractive index (RI) chromatogram than the other samples suggesting that they contain bigger size components than other samples.

The difference in response for each of the detectors corresponds to the different parameters to which each detector responds. All of the samples have a similar peak area for RI, as this detector corresponds to sample concentration, whereas, in addition to concentration the viscometer and light scattering detectors respond to the sample's intrinsic viscosity and molecular weight respectively. Individual distribution plots for each sample showing the molecular weight distribution, hydrodynamic size (R_h) and intrinsic viscosity (IV) were listed in Appendices 2-12.

The Mark-Houwink plots show in Figure 32 and 33 plot intrinsic viscosity as a function (measured by the viscometer detector) of molecular weight (measured by the light scattering detector). Through the Mark-Houwink plot, structural and conformational differences between samples can be identified. At a constant slope, the intercept value (often referred to as the k value) directly relates to the density of the backbone structure per repeat unit length. The slope of the Mark-Houwink plot (commonly referred to as the Mark-Houwink a value) is related to the way chains are added to the backbone of the molecule. The stiffer the chain the steeper will be the

slope. A branched molecule will have a lower slope depending on the degree and type of branching. For materials that are composed of different chain lengths of the same subunit, we would expect to see a linear relationship between the IV and the Mw.

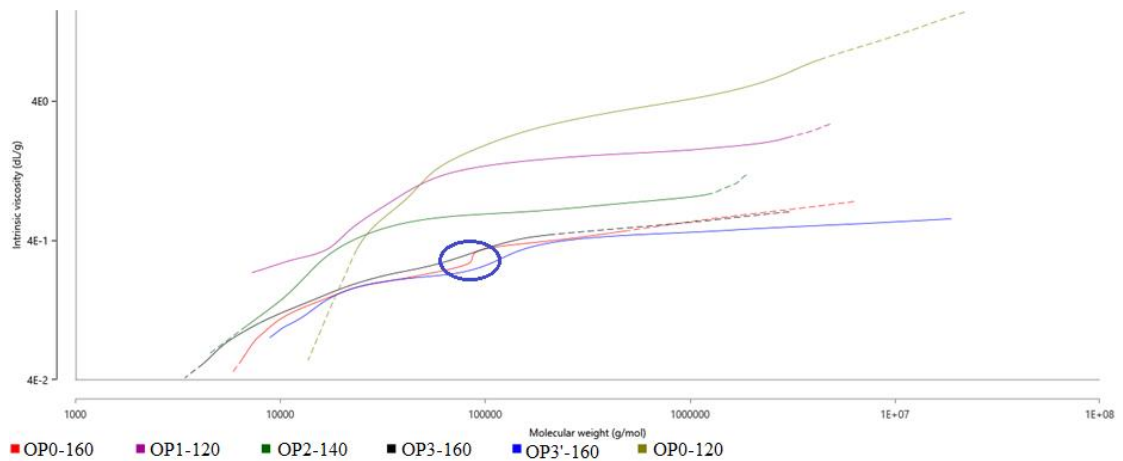


Figure 32 Mark-Houwink Plot for Orange Pectins

The Mark-Houwink plot in Fig. 32 compares all the orange based pectins. The plot suggests that if all of the orange pectins have the same chemical composition then the samples with the lower intrinsic viscosity (IV), in particular samples OP0-160, OP3-160 and OP3'-160, gave a denser structure. Sample OP3-160 only appears to have a single slope whereas OP1-120, OP2-140 and OP0-120 exhibit 2 distinct slopes at 17,000 g/mol, 14,000 g/mol and 18,000 g/mol, respectively. Samples OP0-160 and OP3'-160 exhibit 3 distinct slopes, at 19,000 g/mol and 10,200 g/mol for sample OP3'-160, this is particularly prevalent in sample OP0-160 as the slope becomes very steep across a narrow molecular weight range at 19,000 g/mol and 19,500 g/mol for OP0-160 (see circle on Fig.32). A slope change is indicative of a change in structure

within the sample. For example, in these samples the steep slope would be typical of the chain growing linearly and the shallow slope could be the aggregation of polymer chains or a polymer chain growing in a branched fashion.

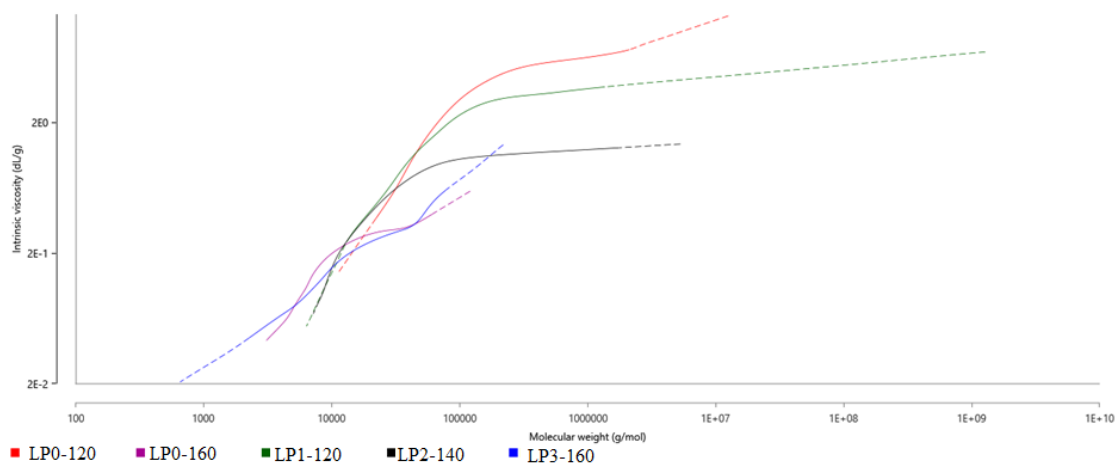


Figure 33 Mark-Houwink Plot for Lemon Pectins.

The Mark-Houwink plot in Fig. 33 compares all the lemon based pectins. The plot suggests that if all of the lemon pectins have the same chemical composition then the samples with the lower intrinsic viscosity (IV), in particular samples LP0-160 and LP3-160 have a denser structure. Sample LP3-160 appears to have 3 distinct slopes, at 10,500 g/mol and 14,000 g/mol, whereas the other samples all appear to have 2 distinct slopes (LP0-120 = 101,000 g/mol, LP0-160 = 10,000 g/mol, LP1-120 = 100,500 g/mol, LP2-140 = 15,000 g/mol).

3.1.3 Summary

Thus, to summarise *Part 1: Pectin Isolation and Characterisation*, pectins were successfully isolated from orange and lemon peels using acid-free microwave

processing. There are a variety of routes to pectin extraction dependent on temperature and/or direct or sequential reprocessing. The optimum extraction temperature is 140 °C, thereafter, significant decomposition of pectin is observed to afford a material which is rich in galactan residues.

Table 10 Comparison of Pectin extraction conditions and yield of this thesis and literature.

Feedstock	Method	Temperature/ °C	Time / min	Acid	pH	Yield / %
Orange Peel	MAE	120-160	30	N/A		14.6-19.7
Lemon Peel	MAE	120-160	30	N/A		30.3-36.5
Orange Peel ¹²¹	MAE		7	HCl	1.2	28.0
Orange Peel ²⁰⁶	MAE		1.5	HCl	1.5	15.79
Orange Peel ¹³⁶	MAE		3	Citric	1.5	29.1
Orange Peel ²⁰⁷	MAE	80	21	N/A		18.13
	THE	80	60	N/A		15.47
	UHPE	45	10	N/A		20.44

THE: Traditional hot extraction; UHPE: Ultra high-pressure extraction;

3.2 Part 2: Production and Characterisation of Citrus Micro-fibrillated Cellulose (MFC) or Defibrillated Celluloses

3.2.1 MFC Production

The yield (dry basis) of MFCs from lemon and orange peel residues processed at 120 °C, 140 °C and 160 °C are shown in Figure 34. As expected, the yield of MFC decreases with respect to increasing processing temperature since pectinaceous and hemicellulosic matter is removed progressively from the biomass. Additionally, especially at 160 °C, noticeable darkening of the MFC is observed corresponding to

onset of degradation and Maillard reaction between sugars and proteins.

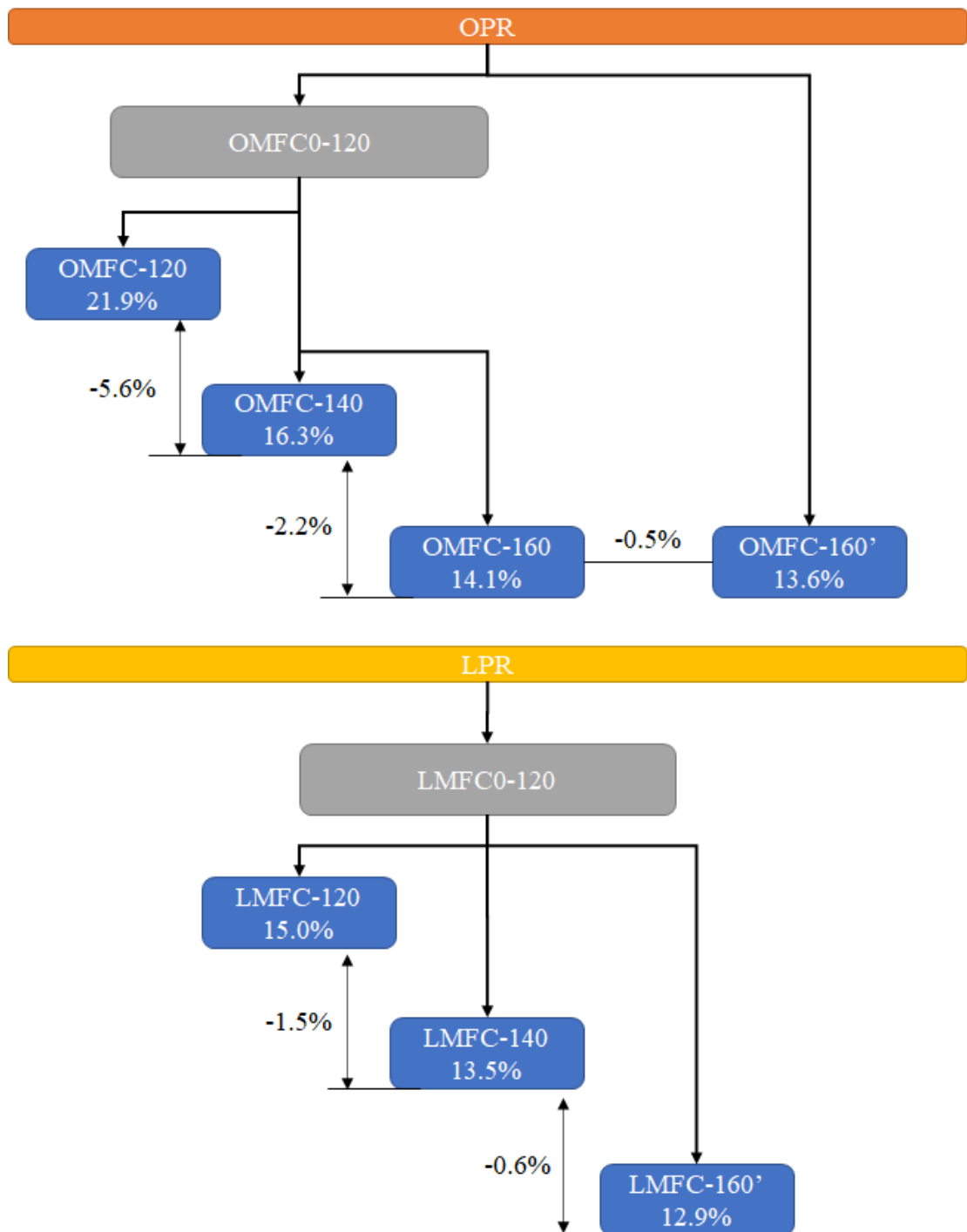


Figure 34 Yield of MFC production from LPR and OPR.

3.2.2 MFC Characterisation

3.2.2.1 ATR-IR

The stacked ATR-IR spectra of all MFC samples are shown in Fig. 35. All of orange and lemon MFC samples present strong absorptions typical of cellulose.²⁰³

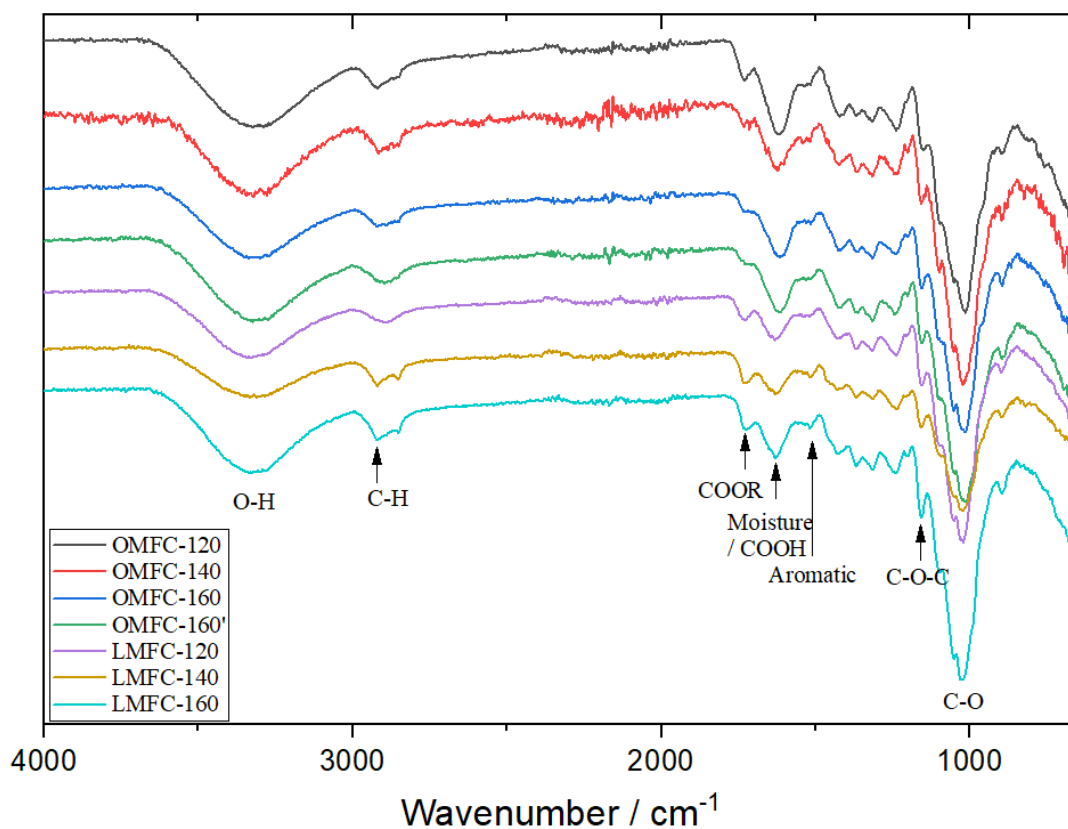


Figure 35 Stacked IR spectra of orange and lemon MFCs.

The broad absorbance band centred at 3341 cm⁻¹ comprised in all MFC samples corresponding to the O-H stretching vibration coupled with inter- and intramolecular hydrogen bonding. The absorbance bands around 2900-2800 cm⁻¹ refer to C-H stretching vibration of sp³-hybridised carbons. The absorbance at 1730 cm⁻¹ refers to

the C=O valence vibration of acetyl- or COOH- group in residual pectin. The absorbance at 1630 cm^{-1} refers to absorbed water and/or residual pectin, three absorbances at 1428 cm^{-1} , 1370 cm^{-1} and 1318 cm^{-1} are corresponding to C-H scissoring, deformation vibration and rocking vibration. The absorbance band at 1150 cm^{-1} refers to COO- asymmetric valence vibration and the medium to sharp, strong absorbance at 1033 refers to C-O valence vibration.²⁰³

3.2.2.2 TGA of MFC

The mass loss thermograms of all orange and lemon MFC samples are shown in Fig. 36. There is a shoulder in the dTG at about $250\text{ }^{\circ}\text{C}$ of both orange and lemon MFC-120 which corresponds to degradation of residual pectin and hemicellulose. The large peaks (dTG) at $350\text{-}360\text{ }^{\circ}\text{C}$ respond to cellulose degradation. To further ascertain the *purity* of cellulose, *i.e.*, free-from pectin, solid state NMR studies were conducted as discussed in the next section.

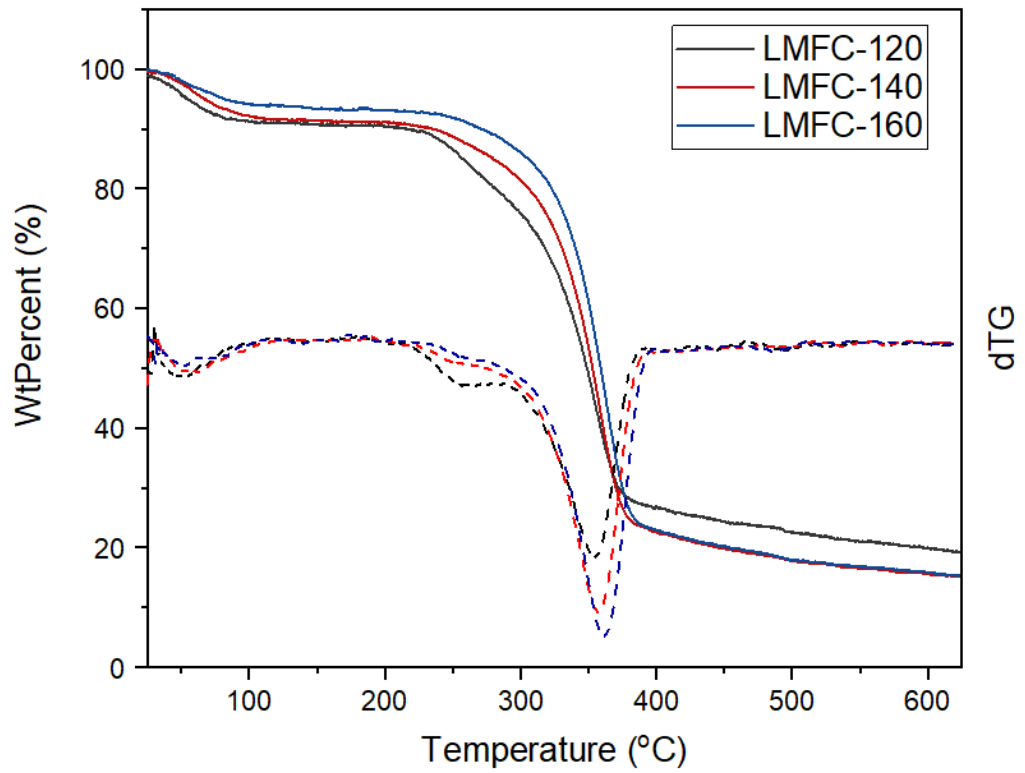
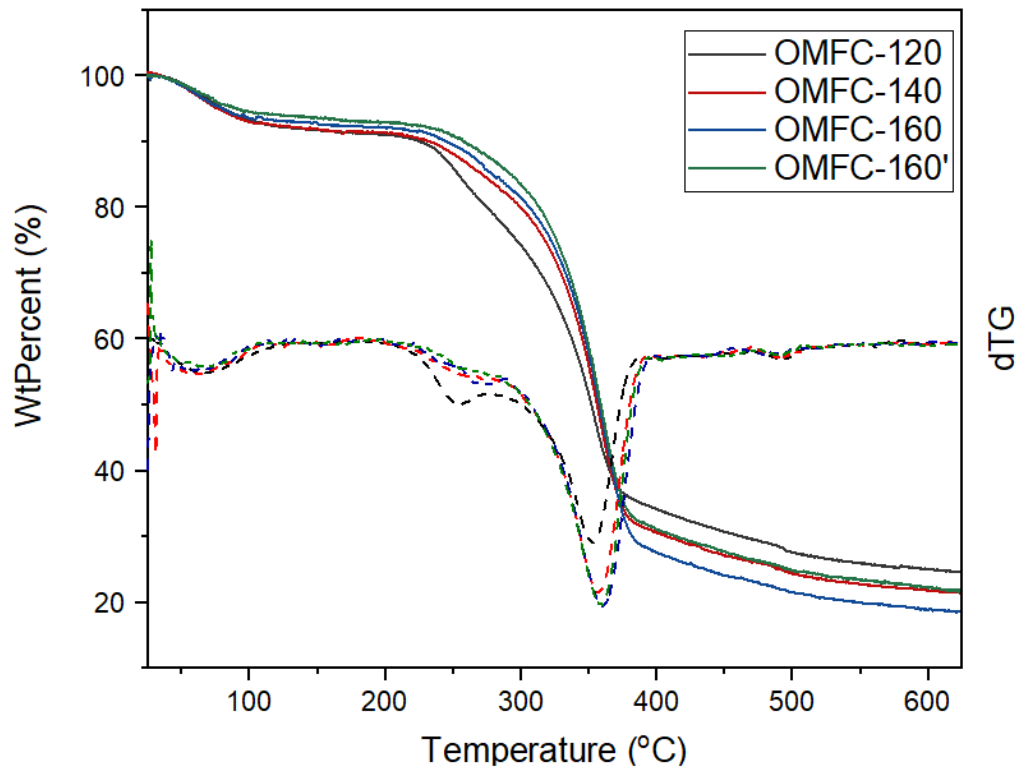


Figure 36 STA of MFC samples.

3.2.2.3 Solid state NMR

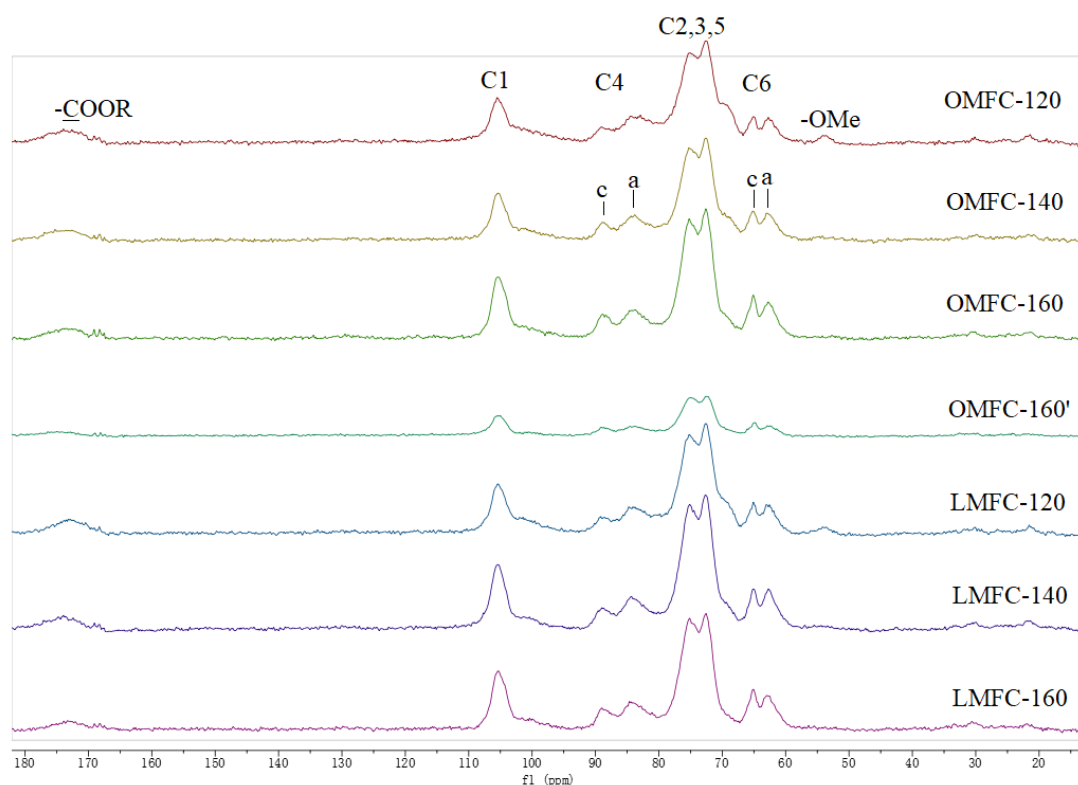


Figure 37 Solid state NMR of MFC samples.

The solid-state ^{13}C NMR spectra of MFCs is shown in Fig. 37. The resonances at 105.5 ppm, 89-85 ppm, 76-72 ppm and 65-62 ppm correspond to C-1, C-4, C-2,3,5 and C-6 of cellulose, respectively. The resonances at 173.4 and 53.6 ppm refer to C-6 of carbonyl (acid or ester) and methyl ester of galacturonic acid in pectin.²⁰⁸ Resonances at 89.0, 84.5, 65.0 and 62.7 ppm refer to C-4/6 of crystalline (c) and amorphous (a) cellulose, the ratio between the a and c signals proved that MFC-160 from both orange and lemon peel presents higher crystallinity. In order to confirm an enhancement in crystallinity, the degree of crystallinity or the crystallinity (CI) was

determined via XRD as outlined in the next section.

3.2.2.4 XRD

The powder X-ray diffraction (XRD) spectra of MFCs is presented in Fig. 38. A diffraction pattern typical of semicrystalline cellulose type-I containing crystalline regions with main 2θ peak at 16° , 22° and 34.5° and an amorphous contribution at 18° can be observed in all samples.²⁰⁹

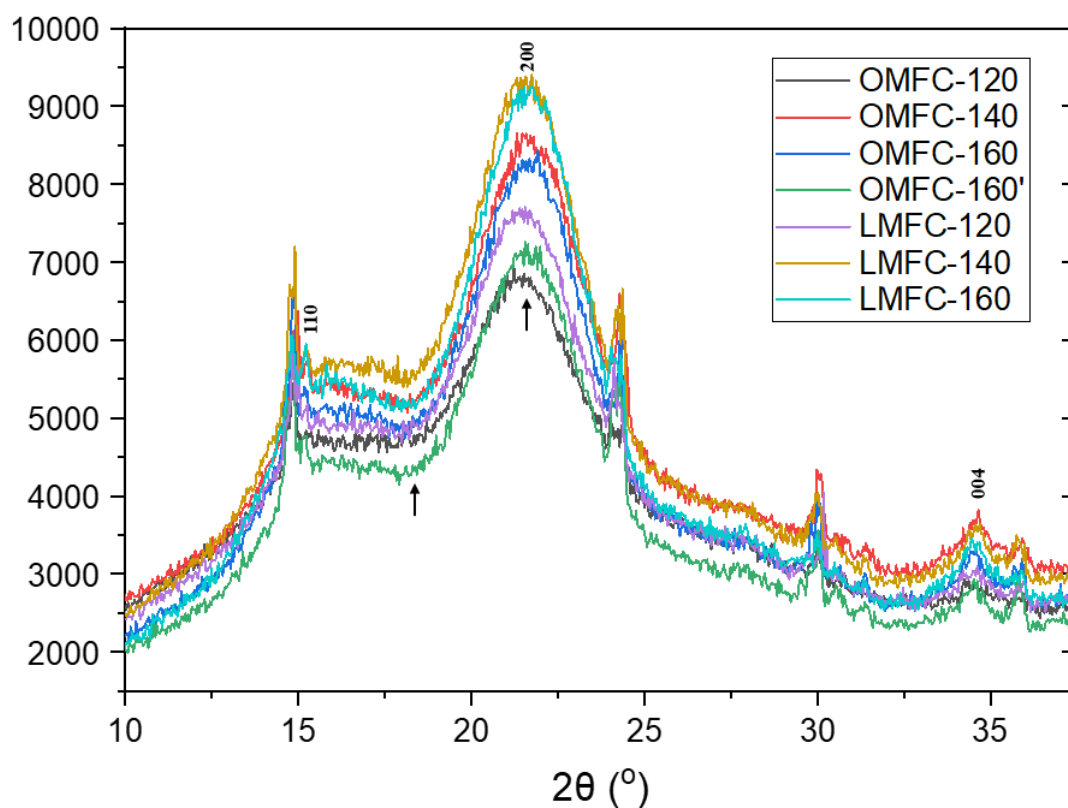


Figure 38 XRD of all MFCs.

The crystalline peaks of cellulose present in the samples become sharper with increasing reaction temperature. Other diffraction peaks (15° , 24.5° , 30° , 35.5°) observed in the spectrum are probably caused by impurities in MFCs such as mineral

salts.

Cellulose crystallinity is an important parameter to evaluate cellulose-based materials, affecting biodegradability, saccharification and thermal and mechanical properties of the materials. Crystallinity index (CI) is a measurement of the amount of crystallinity in cellulose, which can be measured by Segal's²⁰¹ method based on XRD data, was calculated by Equation 4 (Section 2.5.3), presented in Fig. 39. The CI of MFC samples increased when reaction temperature increased, from 32.72% and 39.28% at 120 °C to 41.38% and 45.13% at 160 °C for orange and lemon MFCs respectively.

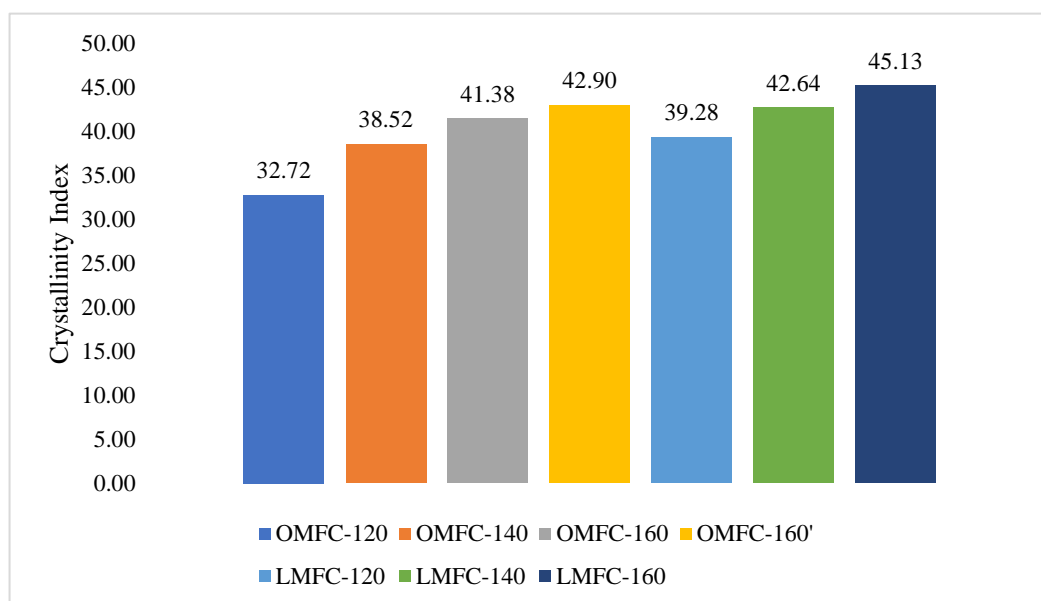


Figure 39 Crystallinity Index (CI) of all MFCs.

Lemon MFCs always present higher CI than orange MFCs produced at the same temperature, we assume that higher citric acid content of lemon peel residues accelerated the crystallisation of cellulose in citrus peel residues. In the meantime, the

CI of MFC-160' is 42.90% higher than that of MFC-160 (41.38%), in the two-step microwave procedure of MFC-160 production, the first step at 120 °C was under the same acidic condition as the one-step MFC-160' procedure, but the second step of DOPR and water suspension reacted at 160 °C was lower acidic (higher pH), which means acidity is a stronger variate than temperature influence CI in MFC production. The resultant fibres were imaged via SEM, TEM and confocal laser microscopy to evidence defibrillation and pectin distribution as outlined in the following section.

3.2.2.5 SEM and TEM

Fig. 40 shows SEM image (x500) of freeze-dried orange peel, highly heterogeneous pores within orange peel particles were observed.

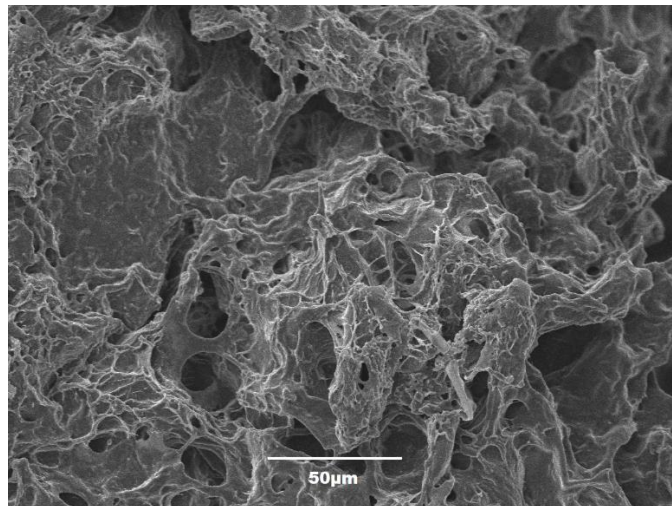


Figure 40 SEM of orange peel.

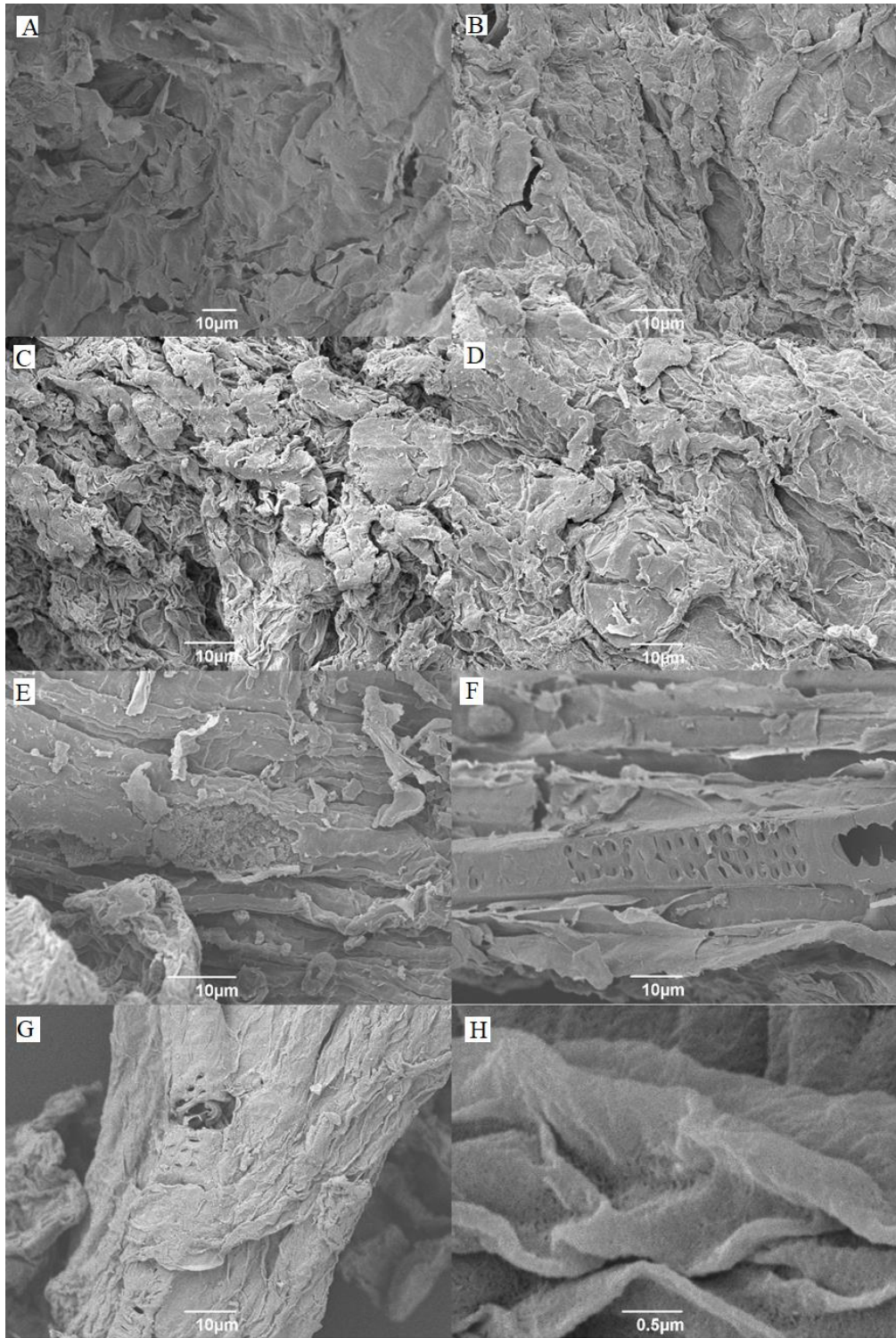


Figure 41 SEM images of MFC samples. (A. OMFC-120, B. OMFC-140, C. OMFC-160, D. OMFC-160', E. LMFC-120, F. LMFC-140, G LMFC-160, H. OMFC-120 with high magnification)

The SEM images of MFC samples are shown in Fig.41. A to G are the low magnification images (x1000-x1500) of orange and lemon MFCs, show the surface of MFC. Compared with SEM of orange peel in Fig.40, MFCs' SEM images show less amorphous matrix which probably containing pectin and hemicellulose. The microwave temperature seemed to apply tiny influence to MFC macro structure, the differences between the images can be considered as heterogeneous composition of citrus peel residues and the sample selection when taking the images.

The image F (LMFC-140) shows lemon peel pith cell wall structures like xylems (*ca.* 10 μm wide) and some macrofibres fragments. When we keep zooming in the microscopy to x35000 (Fig.41-H), the MFC pieces formed by microfibrils can be easily observed, the width of the fibres can be nanoscale.

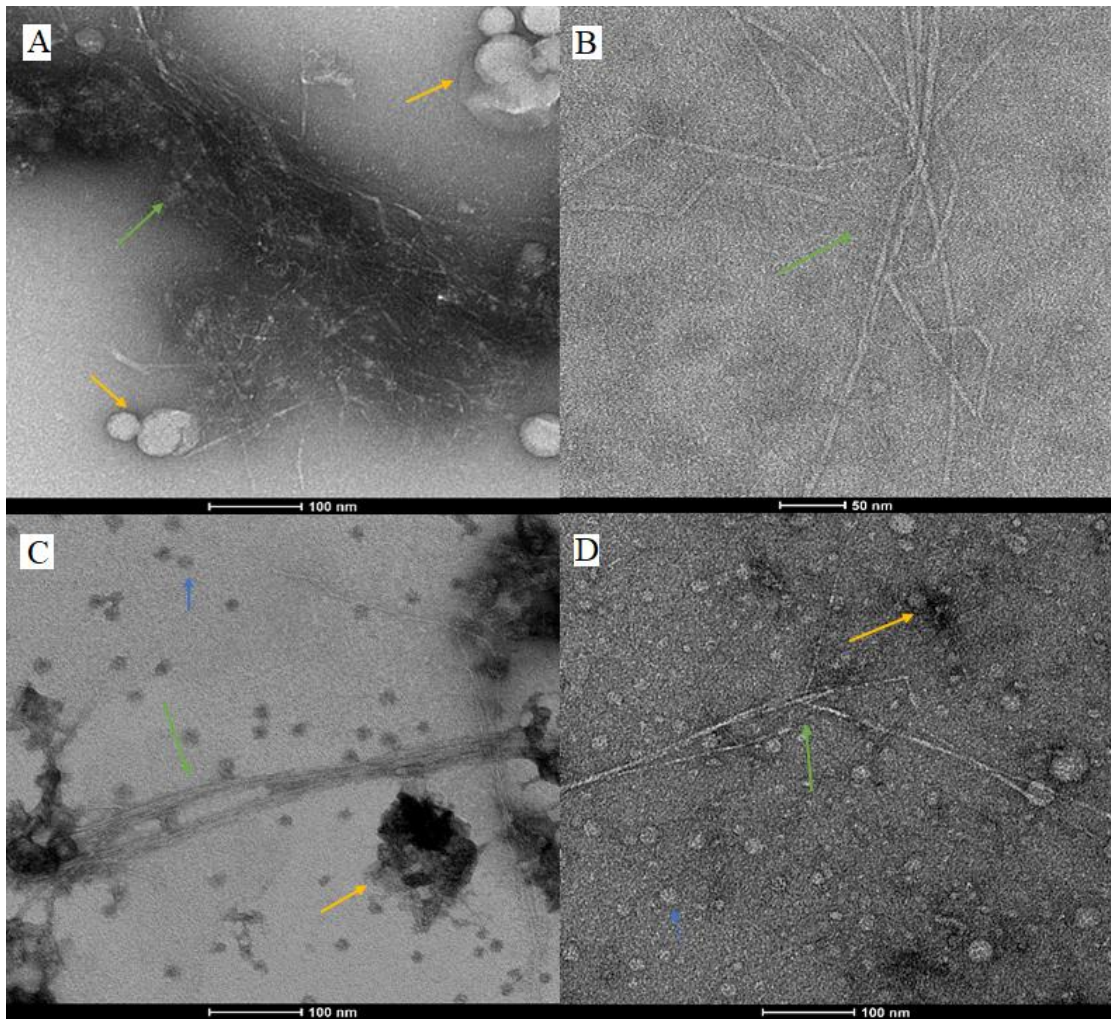


Figure 42 TEM images. A&B: OMFC-120, C: OMFC-160, D: OMFC-120 gel.

TEM images with higher resolution provide more evidence of MFCs' micro- or nano-structures. The TEM images of MFCs (Fig. 42) clearly show high levels of fibrillation of cellulose. The length of the fibres (green arrows) is over $1\mu\text{m}$ that is not able to be fully presented in TEM image, the width $<10\text{ nm}$, which means the fibre can be named either micro- or nano- fibrillated cellulose from two dimensions. Some amorphous matters can be observed from TEM images (yellow arrows in Fig. 42), which might correspond to amorphous cellulose, hemicellulose or residual pectin. The

dots (blue arrows) in OMFC-160 TEM image might be pseudo-lignin nanospheres, but the ones in OMFC-120 gel image are more likely bubbles because of the low reaction temperature. The pseudo-lignin is degradation by-product of cellulose pyrolysis, normally appears at higher temperature *e.g.*, 160 °C.

3.2.2.6 Confocal Laser Scanning Microscopy (CLSM)

Confocal Laser Scanning Microscopy (CLSM) is a powerful tool to study three-dimensional structural of biological cells and tissues, perform three-dimensional imaging of materials, provide accurate analysis of spatial distribution of fluorophores in biomass.^{210, 211} As a complement of electron microscopies (SEM & TEM), CLSM helps to identify the chemical composition on the surface of MFCs including cellulose, pectin and lignin. Commercial cotton cellulose and citrus pectin purchased from Sigma-Aldrich and citrus lignin isolated from DOPR by Dr. Melo in GCCE are used as references (Fig.43). All CLSM images were divided into 4 portions, green for cellulose, red for lignin, blue for pectin and a mixed all in one figure. CLSM image of 7 MFC samples is shown in Fig.44.

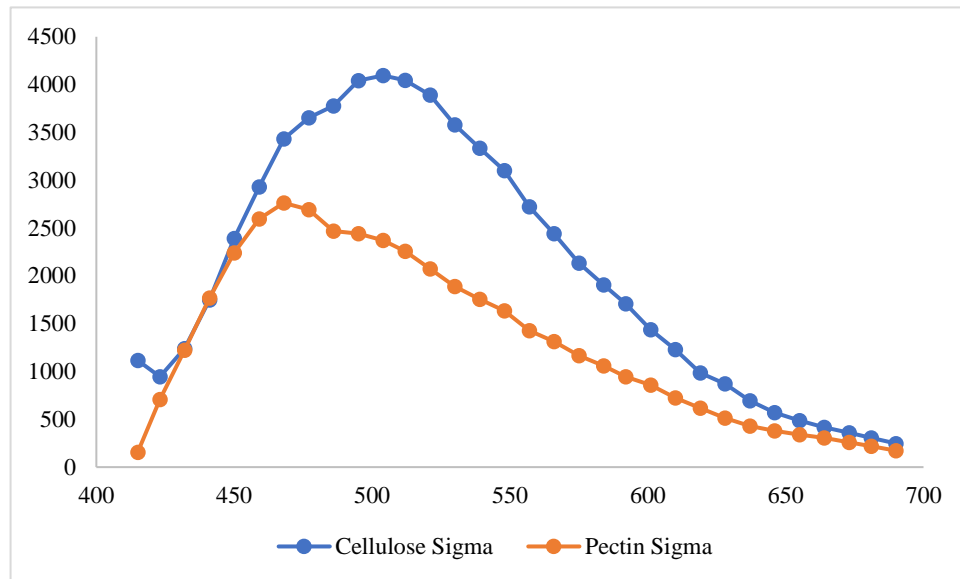


Figure 43 CLSM Reference. Cellulose & Pectin. Fluorescence strength vs wavelength (nm).

With the increasing temperature of microwave treatment, residual pectin content should decrease rapidly, but this trend is not shown in Fig. 44, the blue portion of pectin seems no difference in MFCs of different temperatures. When pectin and cellulose were excited by 405 nm laser, fluorescence of similar wavelength was emitted, the detector was not able to separate these to component clearly, some cellulose could be recognised as pectin by mistake. There is no (or very small amount) lignin in citrus peel waste, lignin can be hardly detected at low temperature MFCs, but three MFC samples produced 160 °C presented significant amount of lignin-like component, these lignin-like component are newly formed at 160 °C in microwave hydrothermal process, we name it ‘pseudo lignin’.

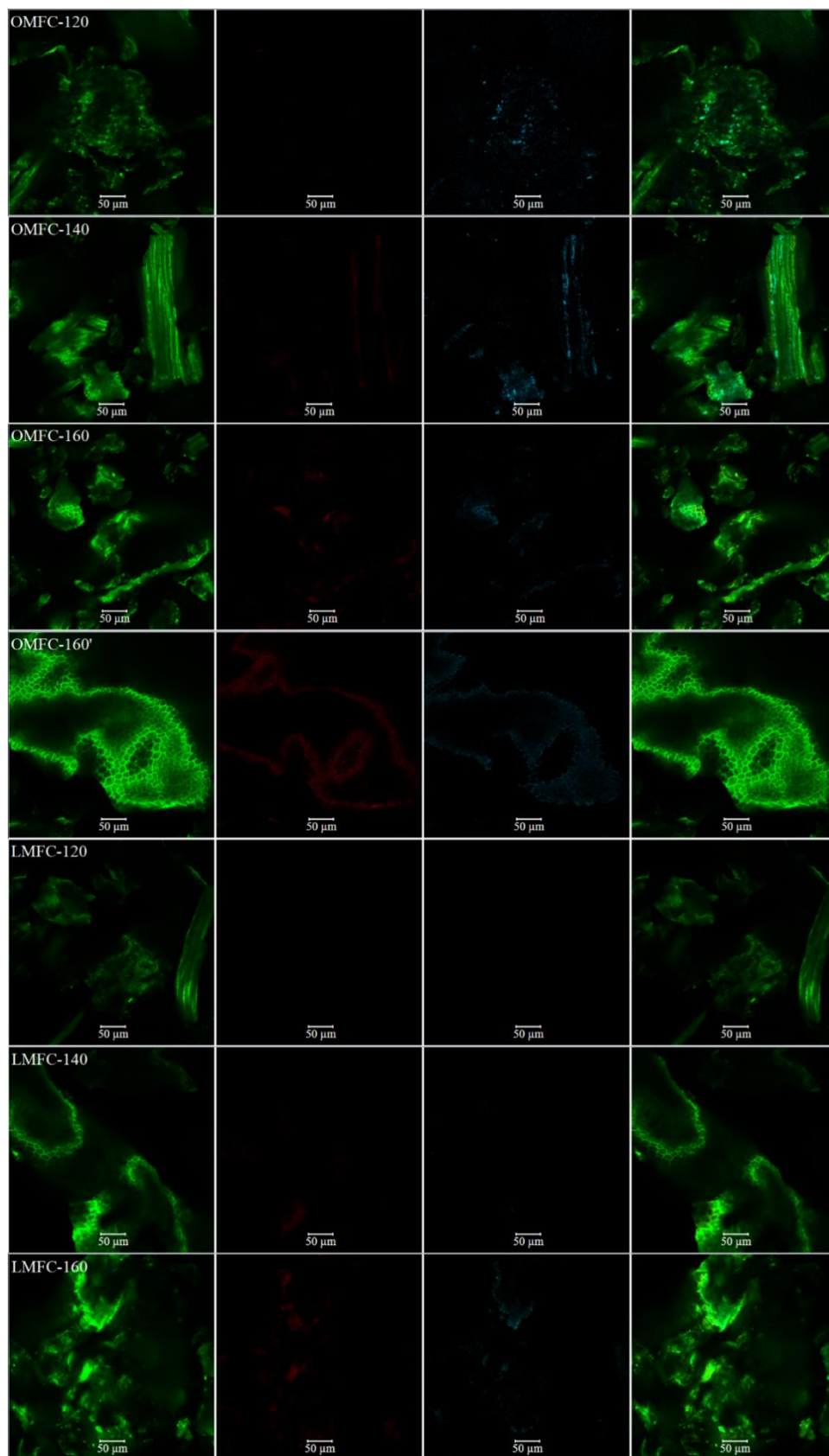


Figure 44 CLSM of All MFCs. Green – cellulose, Red – lignin, Blue – pectin and mixed.

‘Pseudo lignin’ also known as humins, is a complex material containing carbonyl, carboxylic, aromatic and aliphatic functional groups formed by degradation of polysaccharides.²¹² In utilisation of biomass resources, one of the most important route is hydrolysis of cellulose to glucose, followed by dehydration of glucose to 5-hydroxymethyl furfural (HMF), with subsequent rehydration of HMF to levulinic acid. However, humins is by-product of this route under microwave assisted subcritical conditions in our experiments.²¹³ (Pathway shown in Fig.45)²¹⁴

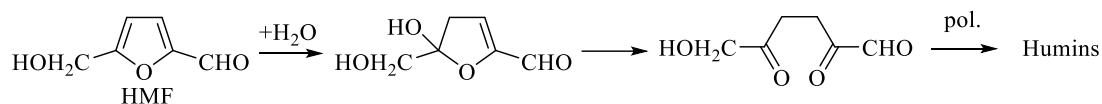


Figure 45 HMF conversion pathway to humins.

3.2.2.7 Water retention value (WRV)

Water retention value (WRV) measures the ability of MFC sample to retain water, which is widely used in the pulp and paper industries.²¹⁵ WRV is a measure of the amount of water retained by fibres including the amount of water in pores and thin layer on fibre external surfaces.²¹⁶ The usage of centrifuge in WRV measurements is to reduce the amount of bulk water on fibre surfaces to acquire more accurate result. WRV of all MFC samples is shown in Fig. 46.

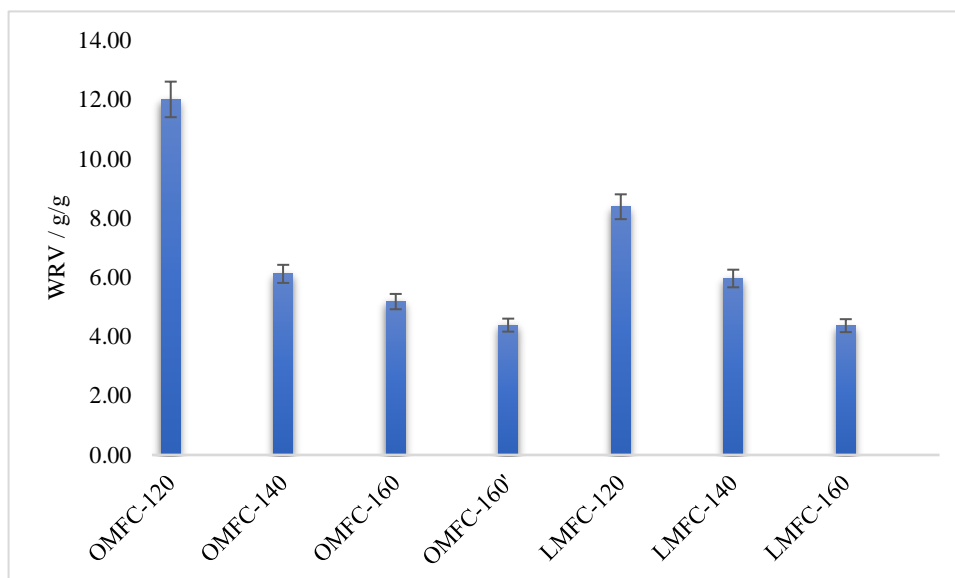


Figure 46 WRV of MFC samples. (g water per g MFC).

In general, MFC samples produced at lower temperature (120 °C) presented higher WRV for both orange and lemon MFCs. When the reaction temperature was increased, WRV decreased. This trend corresponds to previous results of water holding capacity (WHC), showing that WRV is highly influenced by the temperature of hydrothermal treatment, higher values are achieved at lower temperatures.²¹⁷

3.2.3 Potential Application of MFCs: Hydrogels

Hydrogels are three-dimensional networks consisting of cross-linked polymers. The polymers in the networks can associate with large quantities of water due to hydrophilic functional groups are able to retain a significant fraction of water within their structure in swollen state without being dissolved.²¹⁸ Hydrogels are often described as soft and wet materials based on physical appearance, which alludes to

their two major material attributes: high water absorbency and low stiffness.²¹⁹

Cellulose has numerous hydroxyl groups which can form hydrogen bonding linked network to drive gel formation, via either physical or chemical stabilisation of aqueous solution with specific concentration.²²⁰

The highly porous structure enables hydrogels to absorb small molecules inside physical structure, provides hydrogels applications as drug delivery carriers.²²¹ The hydrogel network allows loading and unloading drug molecules at a constant rate depending on the diffusion coefficient.²²²

Skin is the largest organ of human, it's in direct contact with environment. Skin injuries require an effective treatment to prevent serious illnesses or even death.²²³

Wound dressing is a simple and practical way of keeping the wounds clean and protect them from bacterial infection. Hydrogels have received special attention due to their properties of high absorbability, good air permeability, easy replacement and controlled drug release.

High adsorption capacity makes hydrogels application in waste water purification.

High mechanical strength, high surface area and hydrophilic nature are key points for hydrogels to trap selective contaminants including cationic and anionic dyes and heavy metal ions from waste water. MFCs have high adsorption capacity to heavy metal ions owing to the negative charge of carboxylic groups on the surface.^{224, 225}

Pectin based hydrogels have been utilised for water purification.¹⁵⁶ Fares *et al.* reported polyacrylic acid grafted pectin hydrogel.²²⁶ The pectin was treated with ceric ammonium nitrate (CAN) to form free radicals followed by polymerisation with acrylic acid. The polyacrylic acid branched pectin was crosslinked by glutaraldehyde to obtain the final product. The grafted pectin hydrogel adsorption capacity of Cd^{2+} was 0.26 mmol/g, meanwhile the desorption is 0.24 mmol/g, which means the grafted pectin hydrogel was reusable.

Lessa *et al.*²²⁷ reported beads made from cellulose/pectin microfibrils used for removal of metal ions from water. Reported adsorption capacities of Cd^{2+} , Cu^{2+} and Fe^{2+} were 192.3 mg/g, 88.5 mg/g and 98 mg/g respectively. Pectin and cellulose fibres were extracted from OPW.²²⁸ A pectin/CF aqueous dispersion was dropped into CaCl_2 solution, the beads were formed due to ionic crosslinking of pectin and calcium. The beads were kept in solution for 4 hours, followed by vacuum drying.

3.2.3.1 Gel formation

All MFC samples from orange and lemon were suspended in water at variety concentrations, homogenised and test for lowest concentration to form a gel. Lowest gelation concentration of lemon & orange MFC samples at 120°C, 140 °C and 160 °C are shown in Fig. 47, all MFC samples were able to form stable gel at 1.5 wt%, some can form gel at 1 wt%, but the gels lasted for about 10 min.

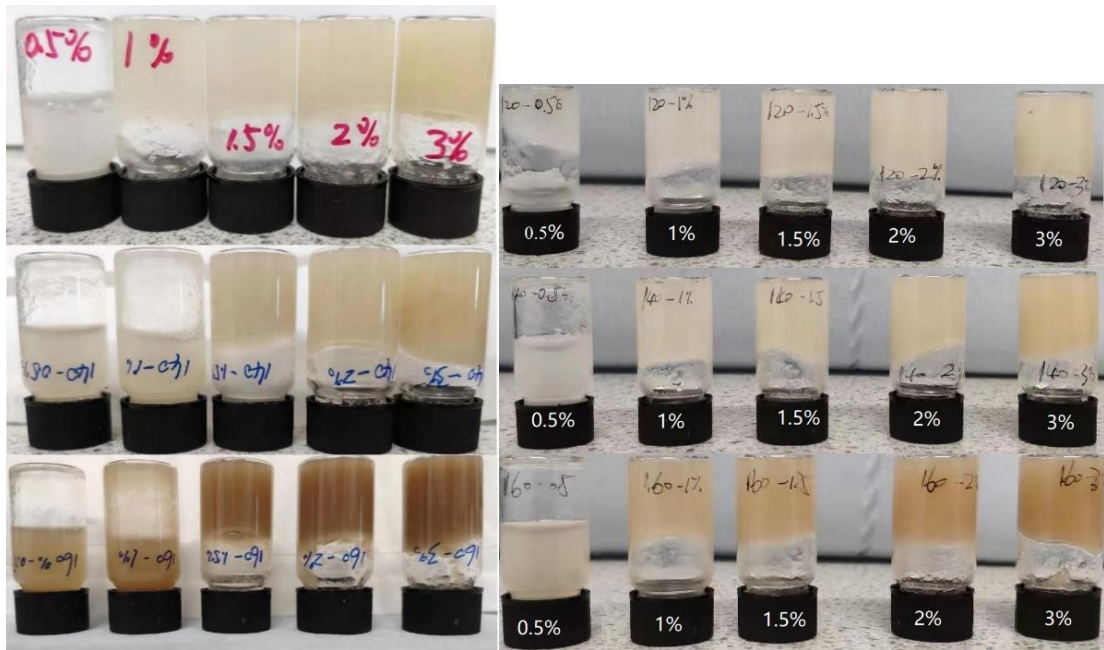


Figure 47 Gel formation of orange (right) and lemon (left) MFCs. 120,140 and 160 from top to bottom.

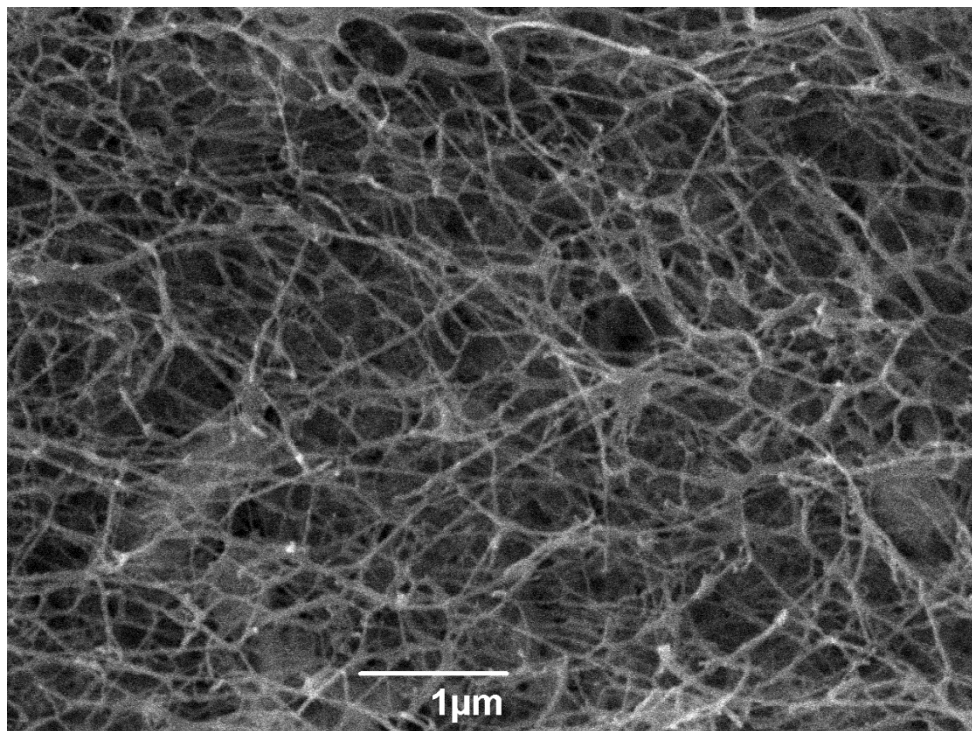


Figure 48 Example SEM of a MFC gel.

Unlike heterogeneous MFC samples show different SEM images (Fig.41, section 3.2.2.5), the homogenised MFC gels present very similar crosslinked microfibrils structures, image is shown in Fig.48. This structure corresponds to the stability of MFC hydrogels – a homogeneous mixture of MFC and water.

3.2.4 Summary

To summarise *part 2: Production and Characterisation of Citrus Microfibrillated Cellulose (MFC) or Defibrillated Celluloses*, MFCs were successfully produced from orange and lemon peel via acid-free microwave hydrothermal treatment. MFC products obtained at lower temperature (120 °C) present residual pectic content, lighter color, higher WRV but lower CI. Products at higher temperature (160 °C) with lower yields present no pectic residues, darker colour, lower WRV but higher CI. Which means our products at different temperatures can be used in different applications.

3.3 Part 3: Production and Characterisation of Blackcurrant Pomace Hydrolysates

Blackcurrants are usually used for juice, wine and jam production yielding a large amount of blackcurrant residues or waste known as pomace. BCP is commonly discarded after juice pressing but it is a valuable source of polyphenolic compounds. Part 3 is an attempt towards utilisation of BCP to help our collaborators from Suntory.

BCP was microwave extracted at variety of temperatures (50-160 °C) for 30 min, the aqueous fraction was separated and freeze-dried to obtain BCP microwave hydrolysates.

3.3.1 BCP microwave hydrolysate (MH).

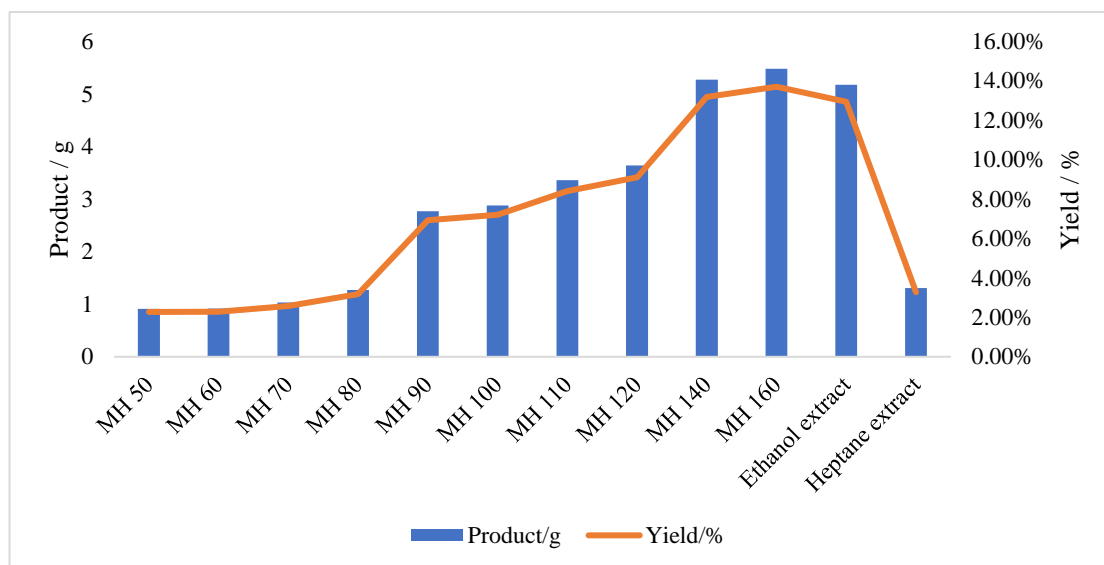


Figure 49 Product and Yield of BCP MAE.

The yield of BCP extracts (ethanol and heptane) and MH (water) is shown in Fig.49. Ethanol gave 4 times extraction yield than heptane, the polarity of ethanol offered the ability of extraction polar compounds *e.g.*, pigments and sugars. The yield of MH increased when temperature increased, exhibit 3 distinct slopes at 90 °C and 140 °C, correspond to new compounds start to be extracted at 90 and 140 °C.

The extractives and hydrolysates (MH-90 to MH-160) are shown in Fig.50. The heptane extractives are dark green waxes, ethanol extracts are gels may contain sugars and pigments. The MH-160 present a significant colour change (brown), which

corresponds to degradation of pigments and the pyrolysis of cellulose.

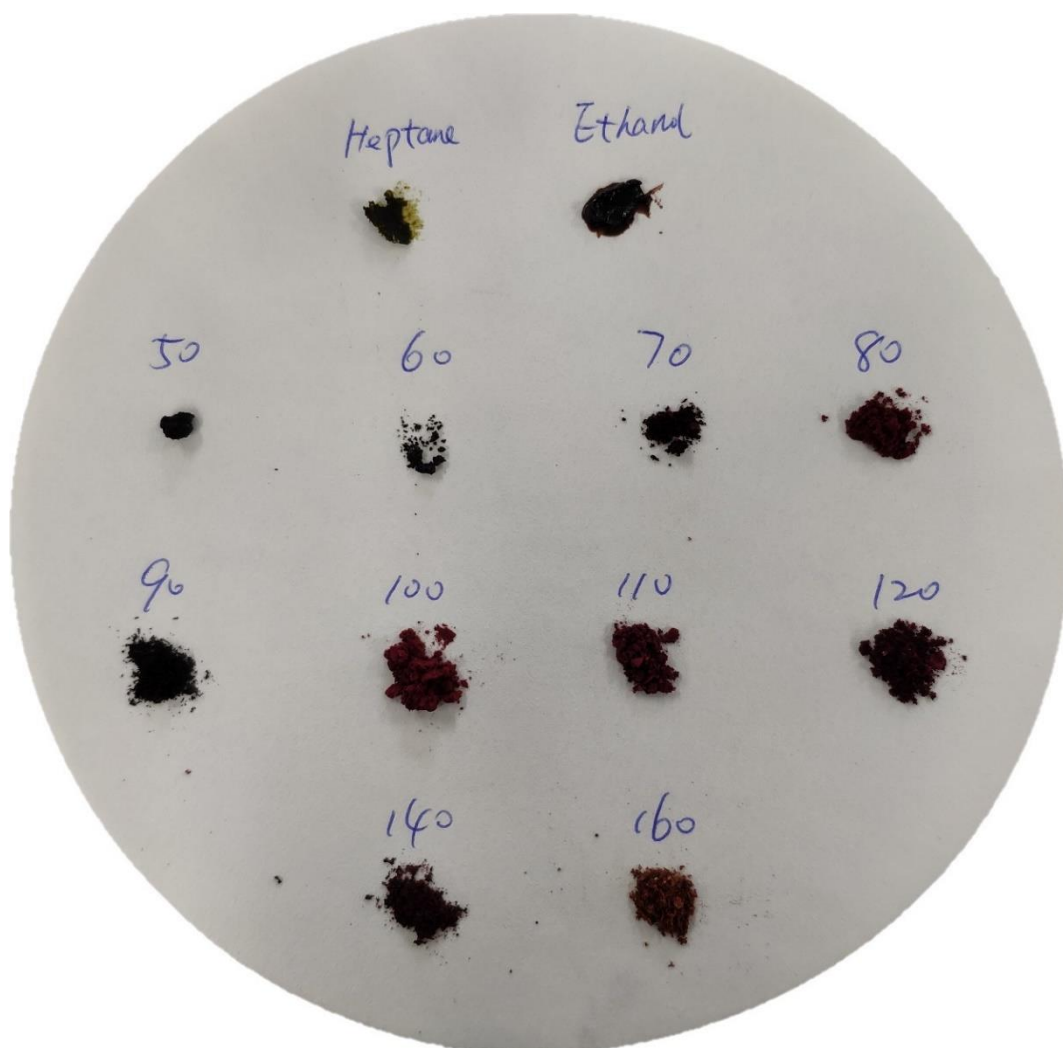


Figure 50 BCP extractives and hydrolysates.

The hydrolysates were dissolved in water 5% w/v for HPLC, shown in Fig.51. The colour of solutions slightly changes from MH-90 to MH-120, unlike hydrolysate, the aqueous solution colour changed obviously from MH-140.

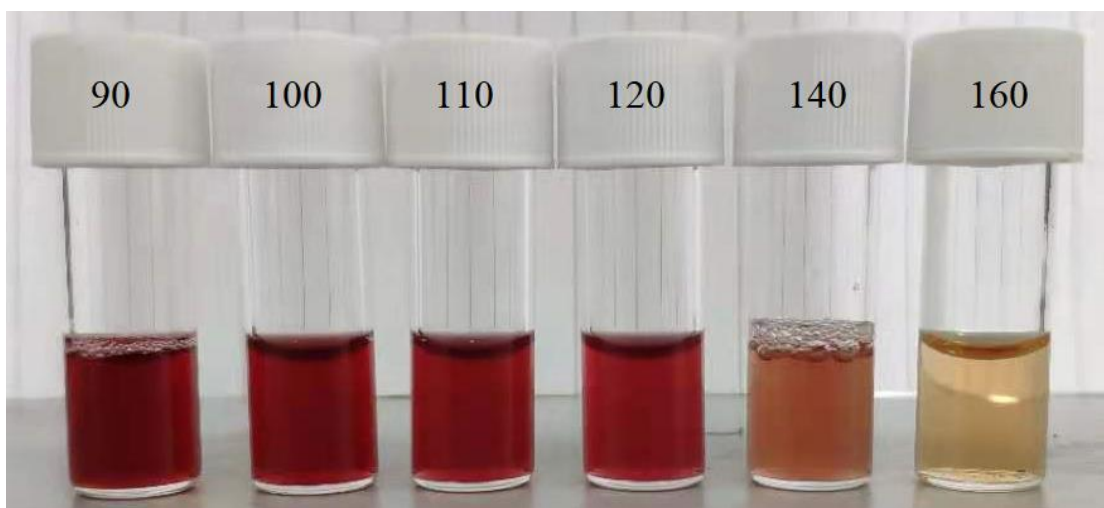


Figure 51 BCP MAE hydrolysate water solution (5 mg/ml). From BCP-90 to BCP-160, left to right.

The sugar content of BCP-MH samples determined by HPLC is shown in Fig.52. The glucose content increases when temperature increased from 90 °C to 140 °C, corresponds to cellulose hydrolysis enhanced by temperature increase. However, glucose content decreased at 160 °C, refers to cellulose/glucose degradation or pyrolysis at 160 °C, which fits the CLSM result on section 3.2.2.6, pseudo lignin content in MFC-160 samples. The concentration of galacturonic acid significantly decreased as the temperature goes up, presents low thermal stability of galacturonic acid and HG pectin. The concentration of arabinose / rhamnose increased along with temperature, this also fit our thinking or RG-I pectin presents stronger thermal stability in section 3.1.2 pectin characterisation.

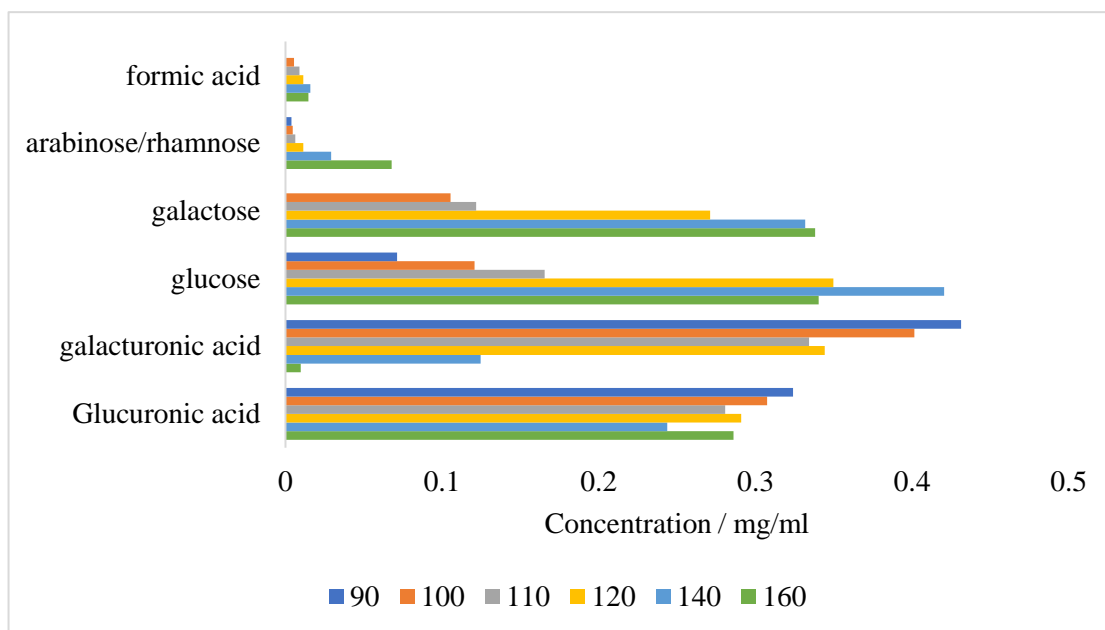


Figure 52 HPLC result of BCP MAE hydrolysates. Mg/ml

3.3.2 Total phenol content & antioxidant activity of BCP and MHs.

Total phenol content (TPC) of BCP hydrolysates was carried out by Folin-Ciocalteu method, results are quantified as gallic acid equivalent (GAE, mg/g), as shown in Fig. 53. A general trend of increasing TPC with respect to increasing temperature is noted but with slight variations. This is interesting in its own right as it suggests possible selective extraction of phenolic compounds and flavonoids. Although, the detailed analysis of these compounds is not the scope of this thesis, an attempt was made in collaboration with Analytical Innovations Ltd, Huddersfield (see later, section 3.3.5).

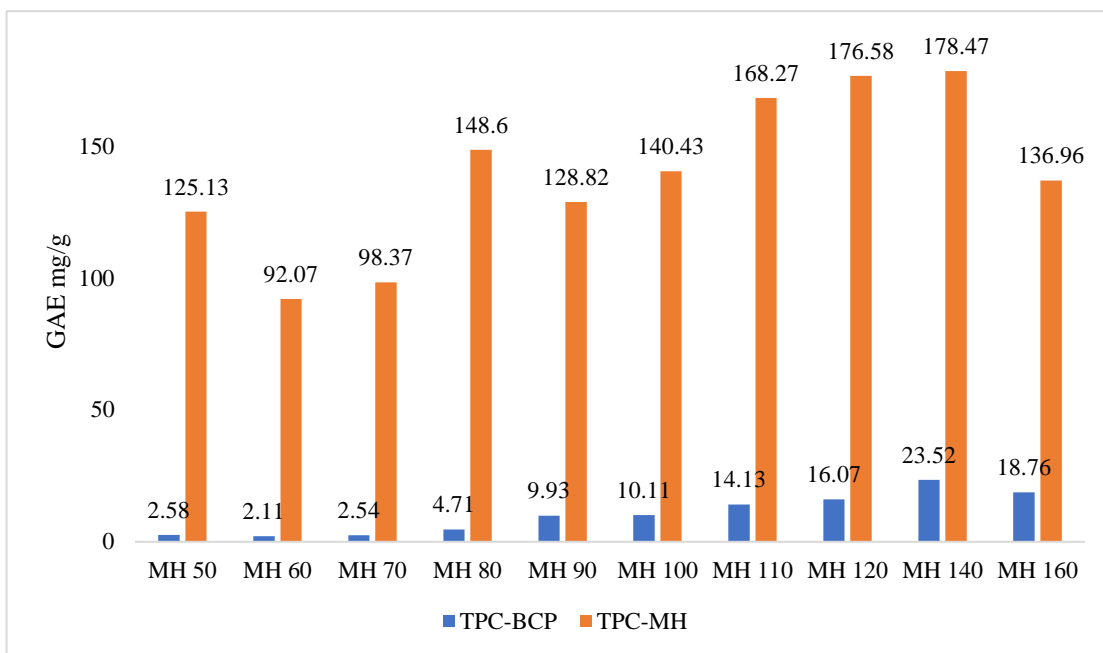


Figure 53 Total phenol content of BCP hydrolysate. Mg GAE / g Hydrolysate (orange) or g BCP (blue).

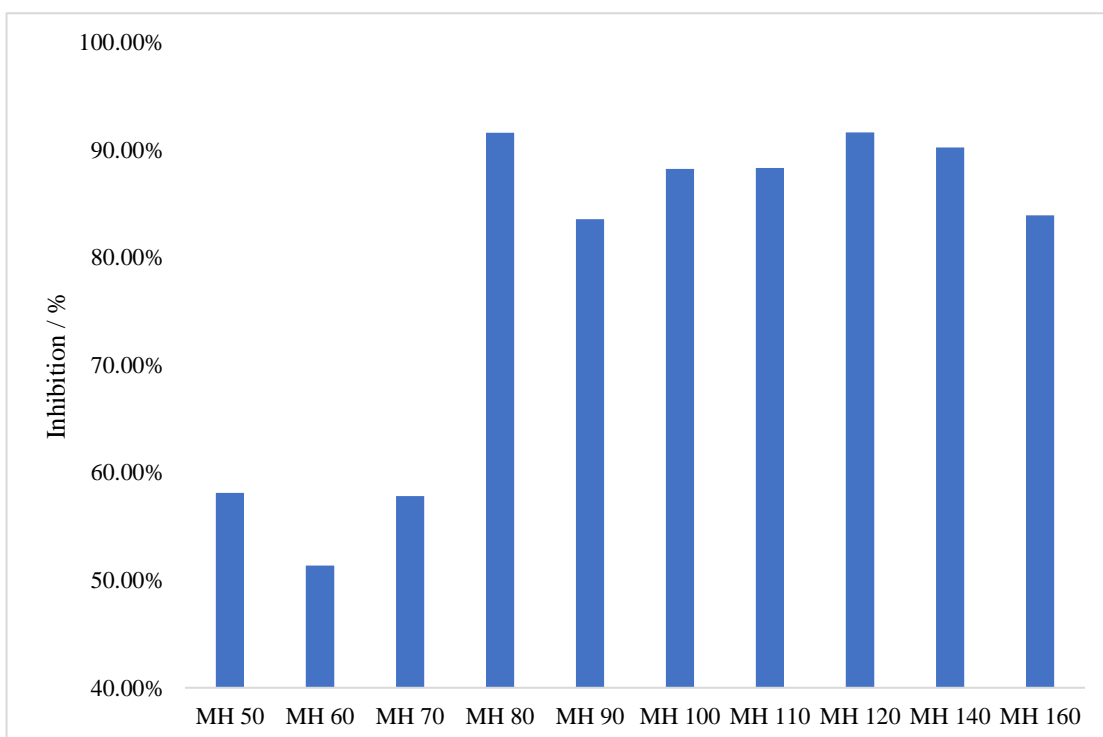


Figure 54 DPPH antioxidant inhibition of BCP hydrolysates.

Total antioxidant activity of BCP hydrolysate was measured by DPPH method (Fig.54). Like total phenol content, the DPPH inhibition presents similar trend. MH 50 and MH 80 exhibited unexpected high inhibition. With our in-house capabilities, an NMR investigation was undertaken to explore changes a macro-level in the composition of the extractives as outlined in the next section

3.3.3 ^1H NMR of BCP MHs

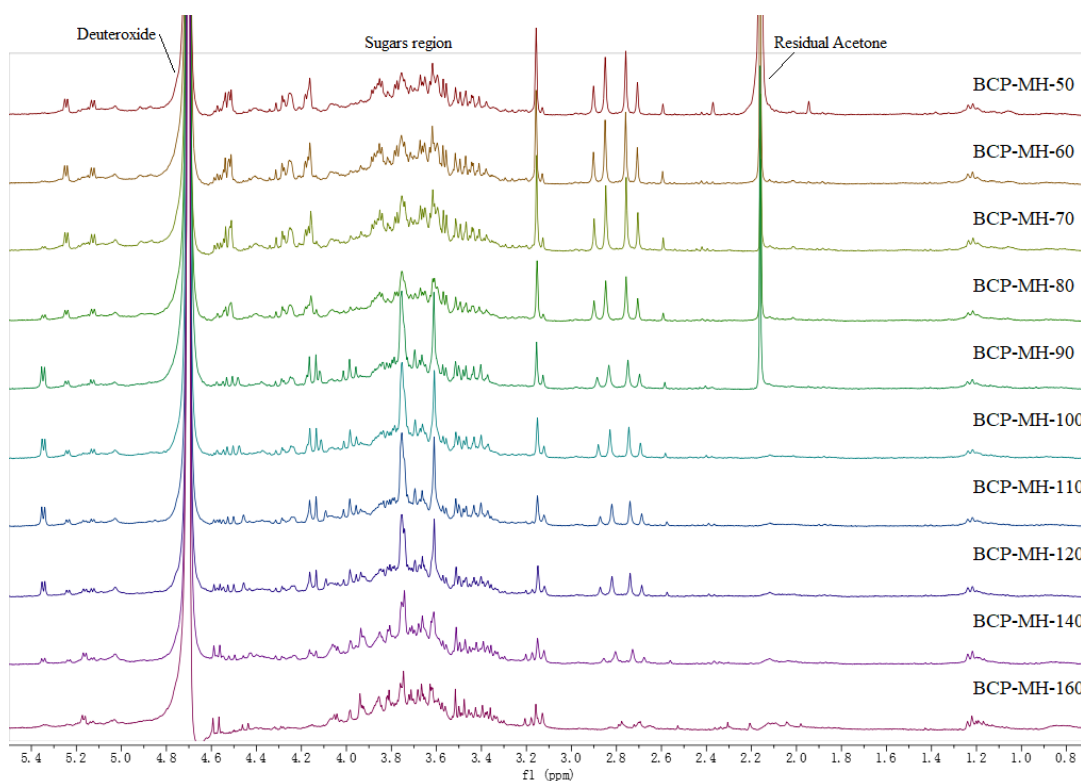


Figure 55 Proton NMR of BCP hydrolysates.

The proton NMR spectrum of BCP hydrolysates is shown in Fig.55. The resonances at 2.16 ppm and 4.7 ppm refer to residual acetone and the solvent (D_2O), can be ignored.

The signals crowded in the region 3.3-5.3 were typical signals of polysaccharides. The singlets at 3.70 and 3.84 ppm and the *doublet* at 5.43 and 5.44 ppm were assumed to be signals of pectin which show stronger resonances in samples MH 90 to MH120. The singlet at 3.24 ppm and *quartet* from 2.79 to 2.99 ppm (see Fig 56 for expansion) present the most obvious decreasing trend when temperature of MAE increased. These resonances correspond to a compound or a series of similar compounds with low thermal stability, decomposed at high temperatures. The anthocyanins' sugar protons resonances were included in the sugars' region, other protons' resonances of delphinidin, cyanidin, kaempferol, myricetin and quercetin were in the range between 6.5-9 ppm, was not shown in the figure.²²⁹

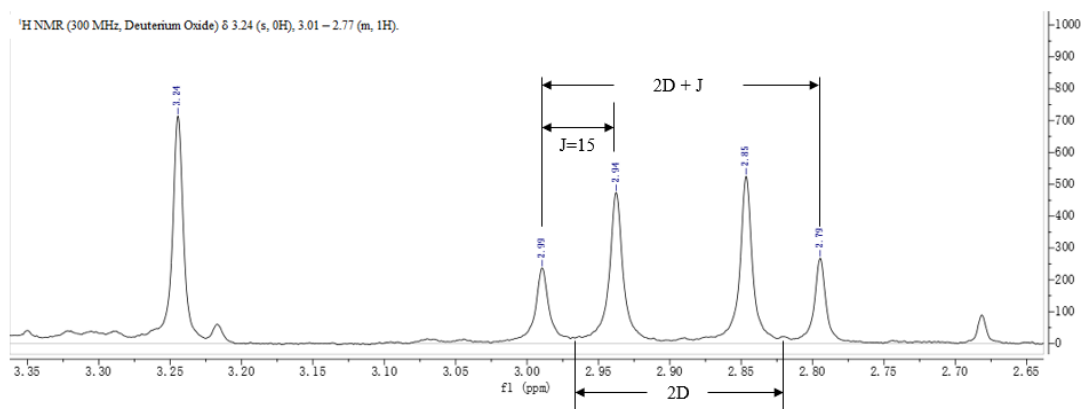


Figure 56 Proton NMR expansion of BCP MH-50. δ 3.24 (s), 3.01 – 2.77 (m).

3.3.4 2D NMR of BCP MH-50

2D NMR was employed for further characterisation of the BCP MH extractives as shown in Fig. 57. Signals of ethanol and acetone are as solvent impurities and not part

of the sample.

The cluster of $^1\text{H}/^{13}\text{C}$ cross-peaks in the range of 3.4-4.7 / 68-96 ppm was assigned to protons and carbons of sugars and their derivatives. The group of resonances range from 4.8-5.4 / 91-108 ppm shows the presence of sugar anomeric protons (H-1) and carbons (C-1).

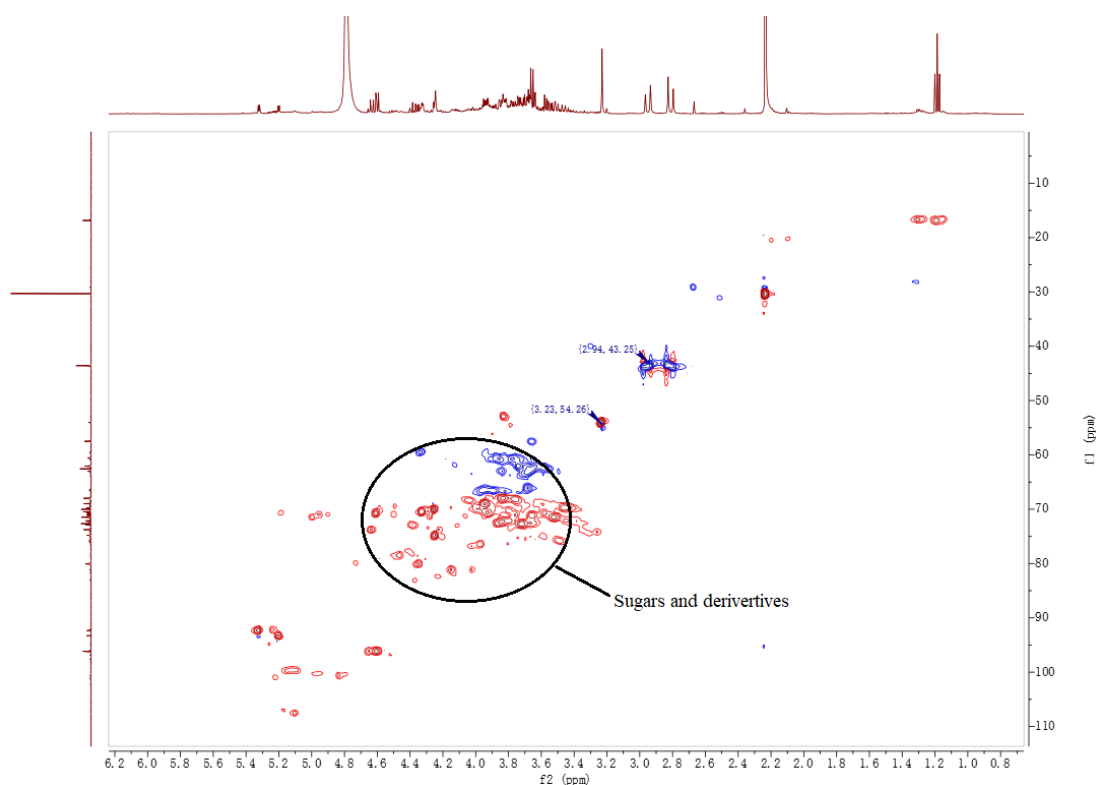


Figure 57 2D NMR (HSQC) of BCP MH-50.

The *quartet* at δ 2.97 – 2.80 ppm corresponds to hydrogen connected with carbon at 43.58 ppm, the *singlet* at 3.23 ppm refers to the proton connected with carbon at 54.26 ppm.

The $^1\text{H}/^1\text{H}$ correlation spectroscopy (COSY) spectra is shown in Fig. 58. The protons

in CH₂ at δ 3.01 – 2.77 were mainly coupling with themselves (blue circle), slightly coupled with proton at 4.5 ppm (arrows). The proton at δ 3.24 (s) was coupling with itself and proton at 4.65 ppm. The proton at 4.65 ppm was connected with the carbon at 96 ppm (Fig. 55 HSQC), which could be C-8 in delphinidin & cyanidin²³⁰, coupled with sugar derivatives.

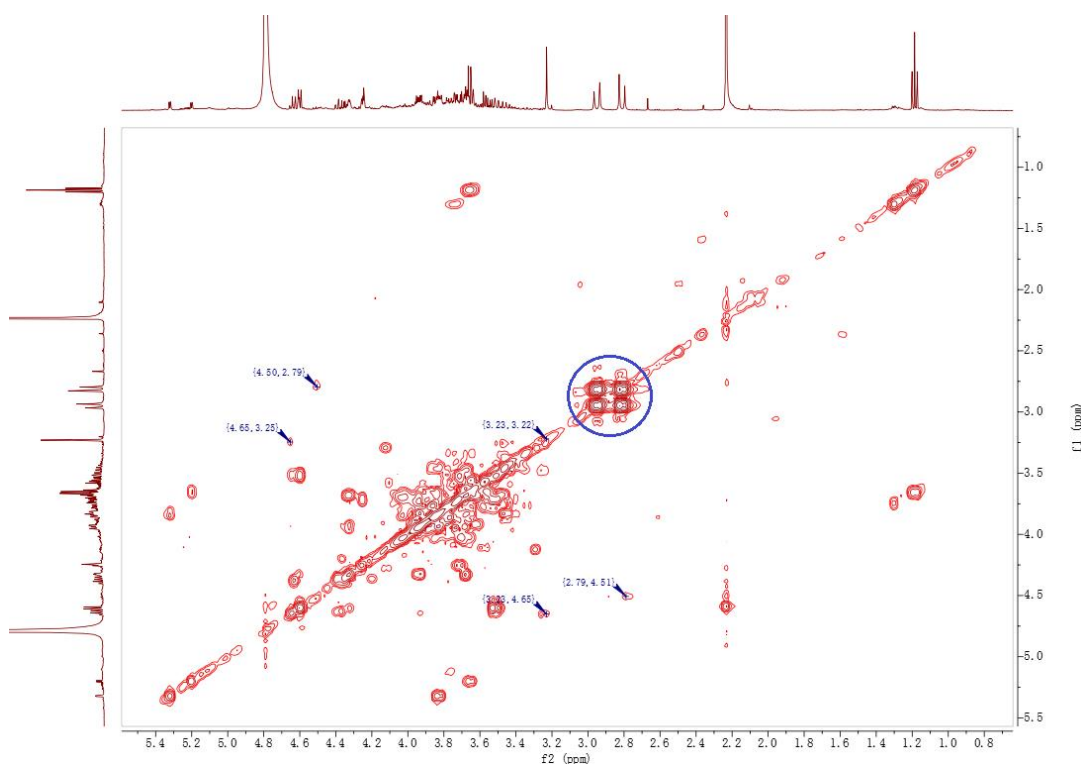


Figure 58 ¹H/¹H correlation spectroscopy (COSY) of BCP MH 50.

The DEPT spectra of BCP MH-50 is shown in Fig. 59, allowed identification of odd and even hydrogen containing carbons. Thus, the resonances at 43.58 and 54.01 ppm correspond to -CH₂ and CH, respectively.

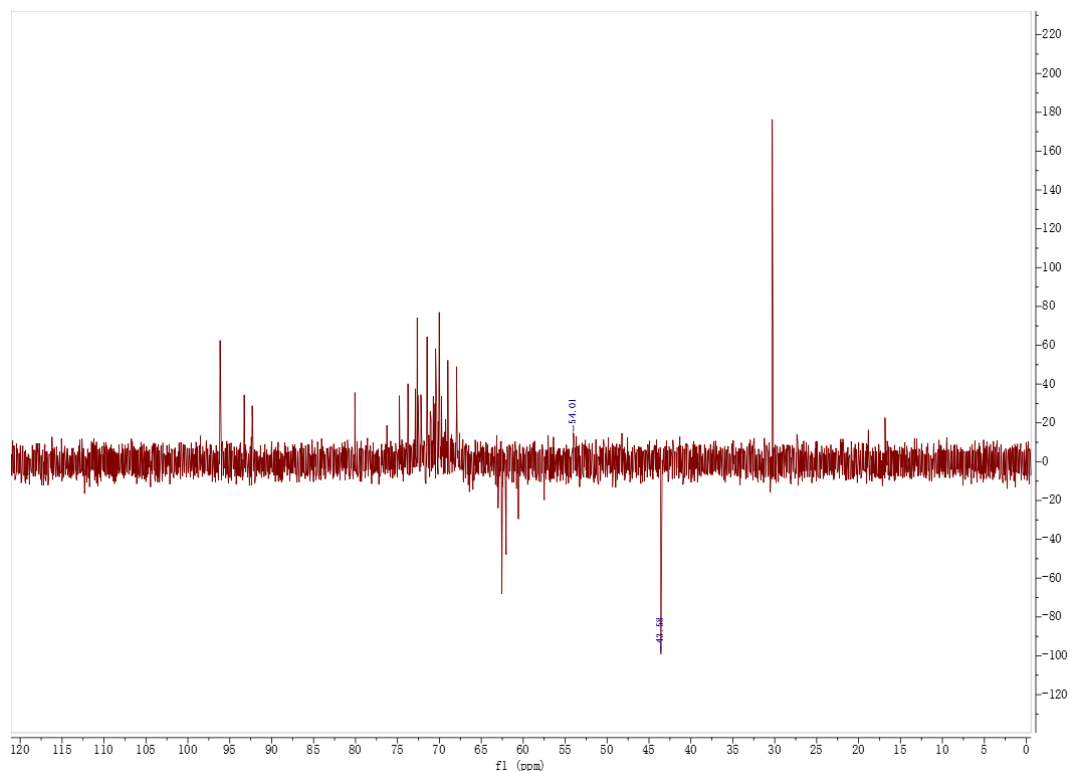


Figure 59 DEPT spectra of BCP MH 50.

3.3.5 HPLC-MS of BCP hydrolysate

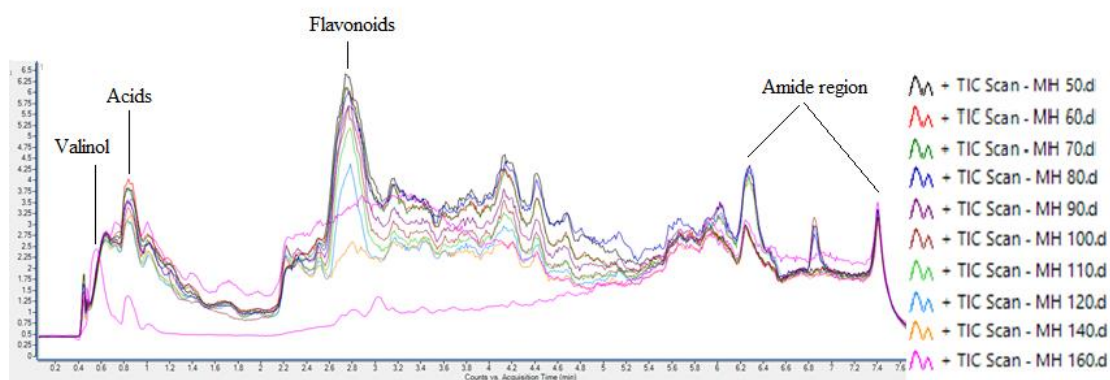


Figure 60 All BCP MH samples HPLC-MS OVERLAY. (positive)

The stacked HPLC-MS (positive overlay) of all BCP MH extracts is shown in Fig. 60.

The pink line on the bottom was named as standard BCP extracts by our collaborators

at Suntory, which was BCP extracted by 10% methanol under sonication at room temperature as a comparison to our microwave hydrolysates (MHs). The most common compounds identified in BCP MH samples by HPLC-MS are listed in Table 11.

2-Amino-3-methyl-1-butanol (also known as valinol, structure in Fig. 61), was detected in all samples except BCP 100 and 160. The major peak of standard sample at 0.525 min is identified as valinol as well.

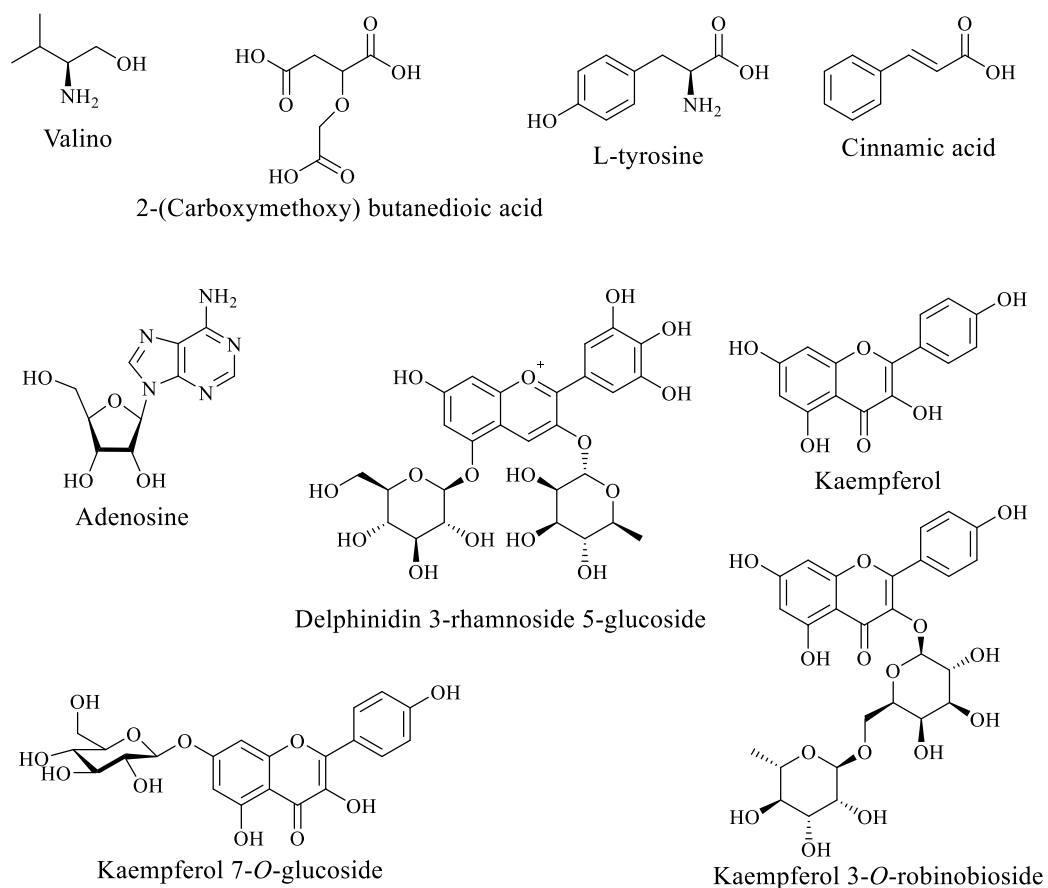


Figure 61 Structures of compounds identified in BCP MH positive HPLC-MS.

Table 11 Top 14 compounds identified in BCP MHs. Positive.

RT	Compound	Formula	Molecular Weight	Probability	Detected Samples
0.576	2-Amino-3-methyl-1-butanol	C ₅ H ₁₃ NO	103.10	>99%	50, 60, 70, 80, 90, 110, 120, 140
0.856	Carboxy-methoxy-succinate	C ₆ H ₈ O ₇	192.03	95-98%	50, 60, 70, 90, 100, 140
0.898	L-Tyrosine	C ₉ H ₁₁ NO ₃	181.07	98.6%	140, 160
1.174 / 1.415	Adenosine	C ₁₀ H ₁₃ N ₅ O ₄	267.10	96-97%	100, 160
2.23	Cinnamic acid	C ₉ H ₈ O ₂	148.05	>99%	90, 100, 110, 120, 140
2.67	Delphinidin 3-glucoside	C ₂₁ H ₂₁ O ₁₂	465.10	>99%	50, 60, 70, 90, 100, 110, 120
2.69	Delphinidin 3-rhamnoside 5-glucoside	C ₂₇ H ₃₁ O ₁₆	611.16	97.5->99%	50, 60, 70, 80, 90, 100, 110, 120
2.79	Cyanidin 3-glucoside	C ₂₁ H ₂₁ O ₁₁ ⁺	449.38	>99%	60, 70, 80, 100, 110
2.79	Kaempferol 7-O-glucoside	C ₂₁ H ₂₀ O ₁₁	448.1	>99%	50, 90, 120,
2.80	Kaempferol	C ₁₅ H ₁₀ O ₆	286.05	>99%	50, 60, 70, 80, 90, 100, 110, 120
2.814	Biorobin	C ₂₇ H ₃₀ O ₁₅	594.16	97->99%	50, 60, 70, 80, 90, 100, 110, 120, 140
4.4	Withaperuvine B	C ₂₈ H ₄₀ O ₉	520.27	68-94%	All
6.47	Palmitic amide	C ₁₆ H ₃₃ NO	255.26	96-97%	All
6.94	Stearamide	C ₁₈ H ₃₇ NO	283.29	93-98%	50, 60, 70, 80, 90, 120, 140, 160
7.4	Oleamide	C ₁₈ H ₃₅ NO	281.27	83-85%	50, 60, 80, 90, 100, 110, 120, 140, 160

The peak at 0.8-0.9 min corresponds to a series of acids, namely, 2-(carboxymethoxy) butanedioic acid which is also known as (carboxymethoxy) succinic acid. L-Tyrosine appears at 0.898 min and is one of the 20 standard amino acid in proteins. L-Tyrosine was only identified in high temperature samples suggesting hydrolysis of proteins.

Adenosine is one of the four nucleosides building blocks to DNA and RNA, its derivatives are the energy carriers adenosine mono-, di- and triphosphate, also known as AMP, ADP and ATP. It was identified in samples 100 and 160 at 1.174 and 1.451 min, respectively. Cinnamic acid and its derivatives are widely distributed throughout the plant kingdom, closely associated with flavonoids.²³¹ Cinnamic acid was reported in blackcurrant leaves by Chrzanowski *et al.*²³²

Peaks from 2.67 min to 2.79 min are anthocyanins (Delphinidin 3-*O*-glucoside, Delphinidin 3-rhamnoside 5-glucoside and Cyanidin 3-*O*-glucoside) which are most expected compounds from blackcurrant pomace.^{95, 233} (Structures of D3G and C3G are shown in Fig. 15, section 1.6, structure of D3R5G is shown in Fig.61)

Kaempferol 7-*O*-glucoside is a flavonol glucoside derived from kaempferol, is normally found in *Cassia* species, presenting significant antimicrobial activities.²³⁴

C3G and K7G present similar molecular weight and formula, identified in different samples, appeared at the same time (RT 2.79 min). It is possible that the instrument may have misrecognised one compound as another, as there is no literature proof of

K7G in blackcurrant. C3G is more reliable in BCP hydrolysates.

Kaempferol is a natural flavonoid.²³⁵ Kaempferol was isolated and identified from blackcurrant by Määttä-Riihinen *et al.* in 2004.²³⁶ Kaempferol 3-*O*-robinobioside also known as biorobin, was isolated and identified from herbal folk medicine (*Gynura formosana* Kiamnra) by Hou *et al.* in 2005.²³⁷

The proton NMR resonances of biorobin were listed in the paper and tentatively correspond to our proton NMR spectrum in Fig.55. Doublets at 5.33 and 5.03 ppm refer to H-1 of Rha and Gal, doublet at 1.17 ppm corresponds to H-6 of Rha. Due to the similarity of flavonoids, the resonances above can be referred to other compounds. The largest peak from 2.7-2.9 min in the chromatogram is the combination of all these compounds. From the chromatogram (Fig.60) and other separated chromatograms (see Appendices 13-15), the peak height of flavonoids (RT 2.8 min) decreased when temperature increased. This trend also concurs with the depletion of NMR resonances reported earlier (see Fig.55, section 3.3.3).

Interestingly, the peaks at 4.1 and 4.4 min all identified as Withaperuvin B in all samples with probability varying from 68% to 94%. Withaperuvin B was first reported in 1982 following its extraction from *physalis perwiana* roots.²³⁸ Recently, Ghisoni *et al.* reported Withaperuvin B identified in extra-virgin-olive oils.²³⁹

The peaks at 6.47, 6.94 and 7.4 min are palmitic amide, stearamide and oleamide

respectively.

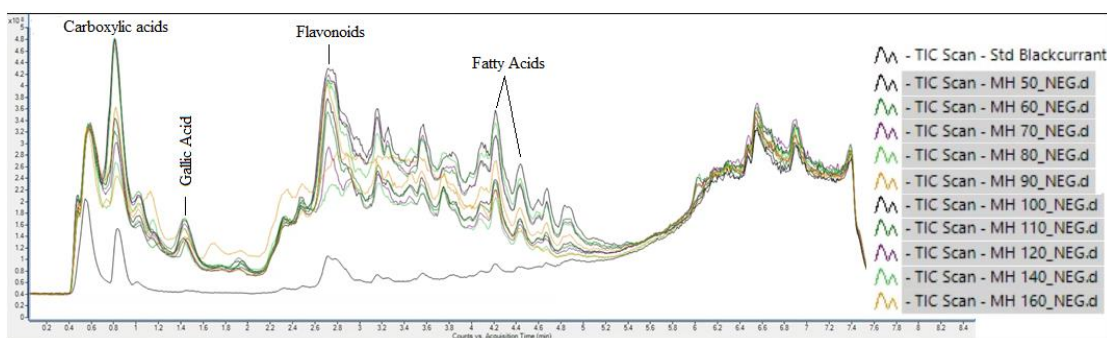


Figure 62 All BCP MH samples HPLC-MS OVERLAY. (negative)

The negative mode HPLC-MS chromatogram of all samples is shown in Fig. 62 and the most common compounds identified are listed in Table 12. The structures of these compounds are shown in Fig.63. The peaks before and around 1 min correspond to carboxylic acids, including gulonic acid and L-altruronic acid, or sugars and sugar derivatives.

Gulonic acid and its derivative 2-keto-L-gulonic acid are intermediate of metabolism from D-glucose to L-ascorbic acid.²⁴⁰ L-Altruronic acid is an isomer of galacturonic acid and glucuronic acid. It was identified in all sample except BCP-160. The HPLC analysis reported earlier also showed that galacturonic acid concentration was lowest in BCP-160 (shown in Fig. 52, section 3.3.1). Thus, it may be plausible to assume that the peak 0.554 min is galacturonic acid from pectin decomposition.

The peak at 1.439 min is assumed to be gallic acid (structure shown above), which is a natural plant phenol and a strong antioxidant.²⁴¹

The volume percent of gallic acid present even level from 50 °C to 110 °C (6-8%), significantly increased from 8.4% to 15.4% when temperature increased from 120 °C to 160 °C.

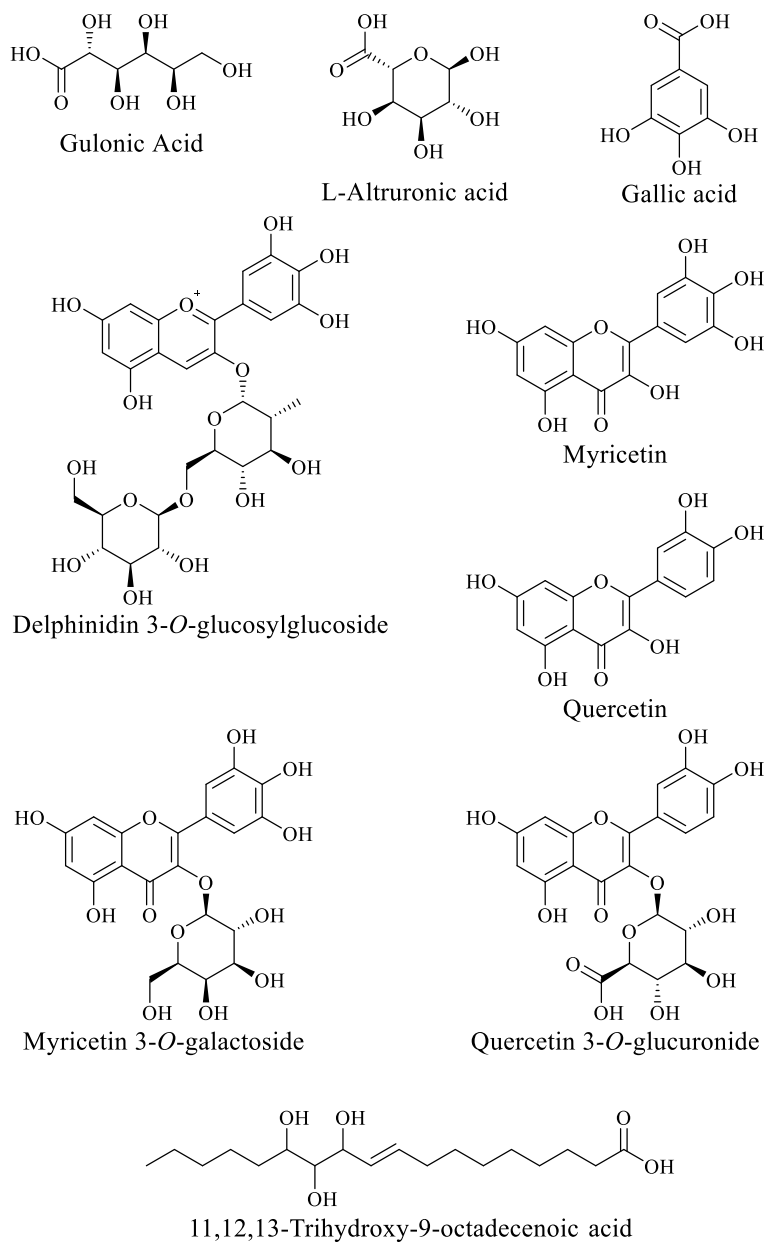


Figure 63 Structures of compounds identified in BCP MH negative HPLC-MS.

Table 12 Top 12 Compounds identified in BCP MHs. Negative.

RT	Compound	Formula	Molecular Weight	Probability	Detected Samples
0.546	Gulonic acid	C ₆ H ₁₂ O ₇	196.06	96-97%	All except 110
0.554	L-Altruronic acid	C ₆ H ₁₀ O ₇	194.04	82-84%	All except 160
0.75-0.8	Unknown		391.06		50, 80, 100
0.85	Unknown	C ₆ H ₈ O ₇	192.03	90%	60, 80, 100, 120
1.43	Gallic acid	C ₇ H ₆ O ₅	170.02	96-98%	All
2.70	Delphinidin 3-rhamnoside 5-glucoside	C ₂₇ H ₃₁ O ₁₆	611.16	69-72%	50, 60, 70, 80, 90, 100, 110, 120
2.71	Delphinidin 3- <i>O</i> -glucosylglucoside	C ₂₇ H ₃₁ O ₁₇	627.16	>95%	50, 60, 70, 80, 90, 100, 110
2.72	Myricetin 3- <i>O</i> -galactoside	C ₂₁ H ₂₀ O ₁₃	480.10	>99%	100, 110, 120,
2.80	Luteolin 7-neohesperidoside	C ₂₇ H ₃₀ O ₁₅	594.16	70%	60, 70, 80, 100, 110
3.11	Quercetin 3- <i>O</i> -glucuronide	C ₂₁ H ₂₀ O ₁₃	480.10	82-97%	50, 60, 70, 80, 90, 100
3.57	Myricetin	C ₁₅ H ₁₀ O ₈	318.04	94-98%	All
3.85	Quercetin	C ₁₅ H ₁₀ O ₇	302.04	99%	50, 70, 80, 100, 110, 140
4.22-4.44	11,12,13-trihydroxy-9-octadecenoic acid	C ₁₈ H ₃₄ O ₅	330.24	98->99%	All

The large peak from 2.7 min to 2.9 min comprises a branch of flavonoids including D3R5G, delphinidin 3-glucosylglucoside, myricetin 3-*O*-galactoside and C3R. Delphinidin 3-glucosylglucoside (D3GG) is an anthocyanin, which is a sugar derivative of delphinidin.

Peaks range from 3 to 4 min refer to a series of flavonoids including myricetin, quercetin and myricetin 3-*O*-galactoside, these flavonoids with antioxidant activities were reported from blackcurrant.²⁴² Quercetin 3-*O*-glucuronide has been reported in blackberry, raspberry and bilberry leaves and may be present at 7 mg/g in dry blackberry leaves and as the main flavonol in bilberry leaves.²⁴³ There is no evidence shows that quercetin 3-*O*-glucuronide can be identified in blackcurrant, but its reduction product quercetin 3-*O*-glucoside was reported 0.038-0.085 mg/g in dry blackcurrant leaves.²⁴³

The peaks at 4.2 min and 4.4 min are both assumed to be 11,12,13-trihydroxy-9-octadecenoic acid and other similar fatty acids.

11,12,13-Trihydroxy-9-octadecenoic acid, also known as 11,12,13-TriHOME, trihydroxyoctadecenoic acids (Tri-HOMEs) are linoleic acid-derived lipid mediators, are classified as oxylipins.²⁴⁴ Oxylipins are a group of fatty acid metabolites produced via oxygenation of polyunsaturated fatty acids.²⁴⁵

There were some peaks at 0.774 min of MH 50, 0.756 min and 0.818 min of MH 80

and 0.804 min of MH 100 correspond to an unknown compound which was identified molecular weight is 391.044. This compound was assumed to be a phenol with antioxidant activity, which initiated the uncommon TPC and DPPH antioxidant inhibition of MH 50 and MH 80 (Fig. 53 and 54, section 3.3.2).

Another unknown compound was isolated at 0.846 min in samples MH 60, 80, 100 and 120, molecular weight is 192.03, the formula was assumed to be $C_4H_8N_4O_3S$, $C_{12}H_4N_2O$ and $C_6H_8O_7$ with probability of 71%, 81% and 90.1%, respectively. The most common compound in fruit with the formula $C_6H_8O_7$ is citric acid. Citric acid was commonly found in citrus fruit, blackcurrant juice contains citric acid as well.²⁴⁶

The complex raw data from HPLC-MS was processed by hierarchical cluster analysis (HCA) to evaluate the quality differences among BCP MHs. HCA is a multivariate analysis method for studying classification problems which has been widely used for quality evaluation of biomass extractives.²⁴⁷ The hierarchical cluster tree of 10 batches of BCP MH and one standard BCP extractives sample was displayed in Fig. 64. The tree shows how the individual samples are grouped together, which samples are more similar to each other. Three main groups identified aligned with the yield findings.

The 11 batches of samples could be divided into 2 main clusters: Std, MH 140 and MH 160 were in cluster A, the rest of samples were in cluster B. The cluster B could be divided into 2 secondary clusters: MH 50, MH60 and MH 70 were in cluster B1,

MH 80, MH 90, MH 100, MH 110 and MH 120 were in cluster B2. The yield of BCP MHs shown in Fig.49 (section 3.3.1) could be divided into 3 main groups, MH 50-80 were in group 1, MH 90-120 were in group 2, MH 140 and MH 160 were in group 3, compared with hierarchical cluster tree, only MH 80 was in different group.

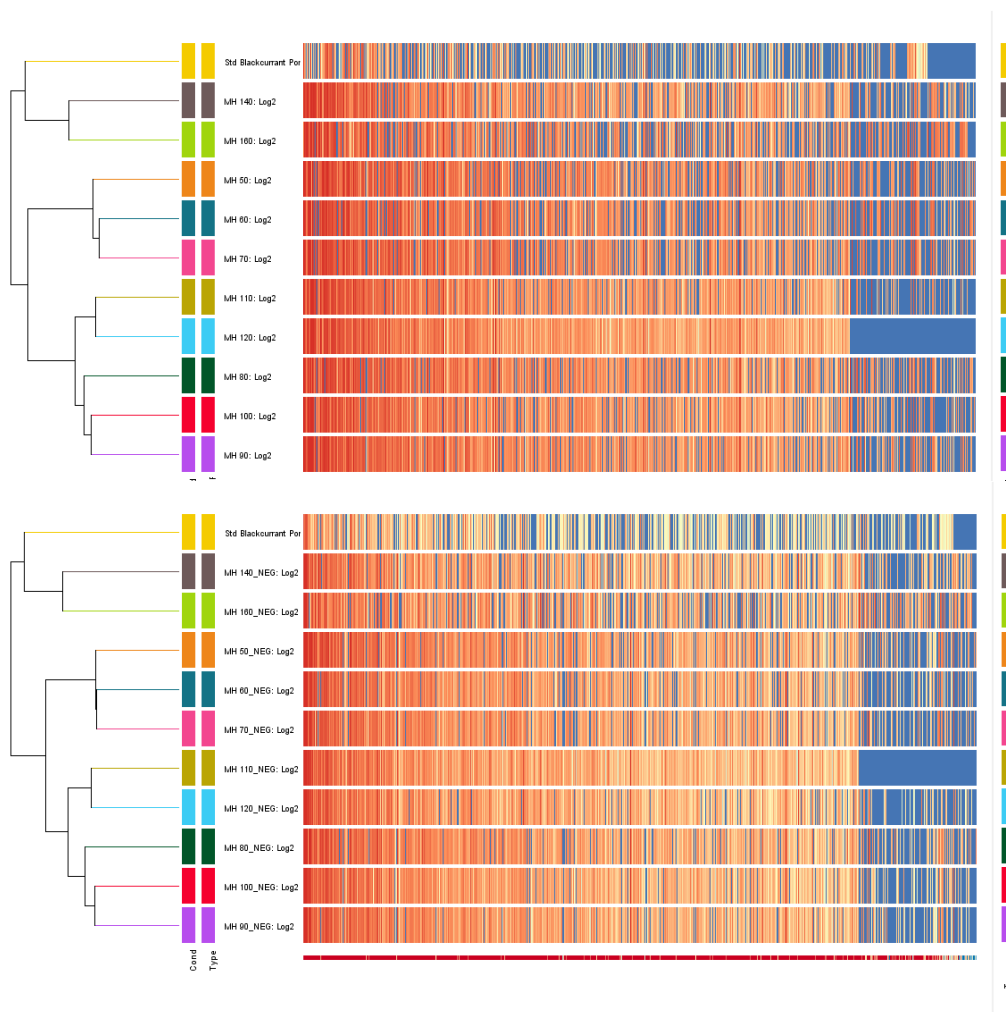


Figure 64 Hierarchical cluster tree of identified compounds in hydrolysates. Top - Positive, Bottom – Negative.

Full list of identified compounds of all BCP MHs was attached in Appendices 16-35.

3.3.6 GPC of BCP Microwave Hydrolysates

Considering microwave hydrothermal treatment was able to extract pectin from biomass, the MH samples at high temperatures (100°C-160 °C) were sent to Concept Life Sciences company for gel permeation chromatography as well. Results are shown in Table 13.

Table 13 GPC result of BCP MH samples.

Sample ID	Mn (g/mol)	Mw (g/mol)	D	IVn (dL/g)	Rh (nm)
BCP-MH-100 Peak 1	20591	205374	13.9	0.2838	4.80
BCP-MH-100 Peak 2	7841	28516065	3177.4	0.0425	1.80
BCP-MH-110 Peak 1	19251	262141	13.6	0.3375	4.96
BCP-MH-110 Peak 2	3291	6439	2.0	0.0503	1.34
BCP-MH-120	138484	289949	2.1	0.6551	11.82
BCP-MH-140	71804	113653	1.6	0.3268	7.37
BCP-MH-160 Peak 1	40221	158197	3.9	0.1875	5.35
BCP-MH-160 Peak 2	7359	15755	1.8	0.0343	1.59

The BCP MH samples all exhibited atypical distributions as the RALS/LALS detection contained a large peak distribution at 15-25 mL retention volumes whereas the RI detected peaks at 25-30 mL retention volumes. This discrepancy has prohibited the instrument software from being able to accurately calculate the data. Where possible, both peaks have been integrated and the data for both provided, however in some instances the later eluting peak did not provide a significant enough response to allow the software to integrate this peak, therefore only the peak at ~25 mL retention volume has been integrated. Due to this atypical chromatography the recovery of the

BCP samples is low, particularly when only one peak is integrated, as only a fraction of the sample has been included in the calculation.

The RI response is dependent on concentration of the components but the RALS/LALS response is dependent upon the size of the component. (Fig. 65) Hence, the atypical chromatography suggests that the BCP samples contain a small concentration of molecules which are large in size, therefore not detected by the RI but which are detected by the RALS/LALS, alongside a large concentration of small molecules.

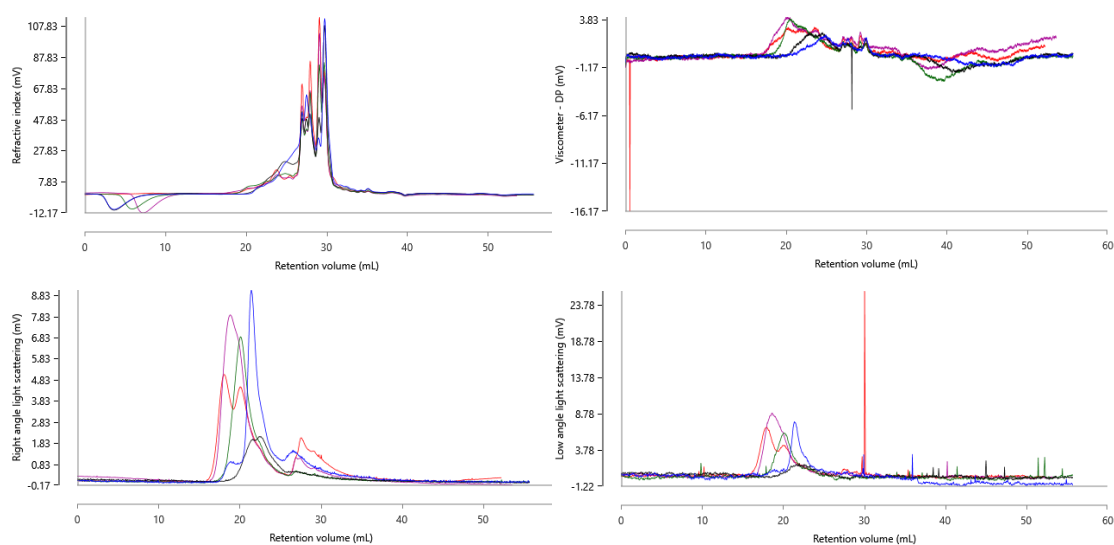


Figure 65 Overlay Chromatograms for BCP MHs. (RI (top left), Viscometer (top right), RALS (bottom left) and LALS (bottom right). MH-100 (Red), MH-110 (Purple), MH-120 (Green), MH-140 (Black) and MH-160 (Blue)

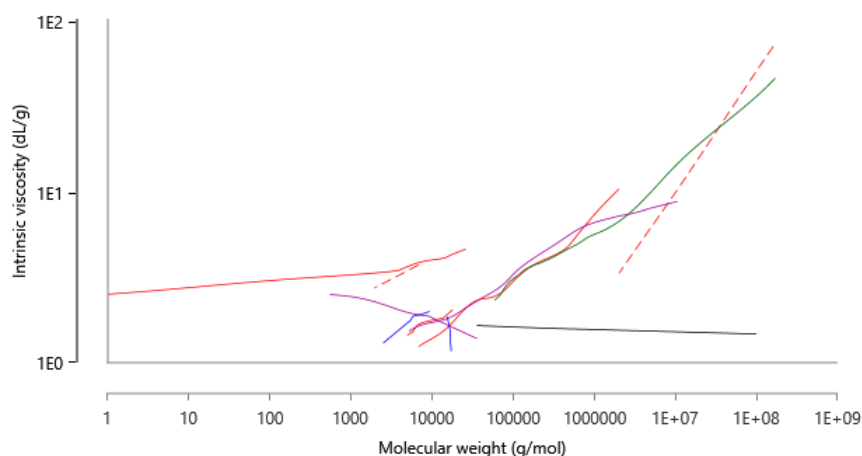


Figure 66 Mark-Houwink Plot of MH-100 (Red), MH-110 (Purple), MH-120 (Green), MH-140 (Black) and MH-160 (Blue)

The Mark-Houwink plot in Fig. 66 compares the BCP samples. This is included for reference only as the software has been unable to accurately extrapolate this data due to the atypical chromatography for these samples.

Besides BCP MHs, the residues were also collected and characterised, shown in next section.

3.3.7 BCP Microwave Residues (MR)

The elemental analysis (CHN) of BCP MR is shown in Fig. 67. Lignocellulosic materials will not degrade at low temperatures, only residues of high temperature samples (from 90 °C to 160 °C) were submitted for CHN analysis. Considering the pyrolysis of cellulose there should be an increasing trend for carbon content when microwave temperature increased, but the differences shown in the figure are within the error range.

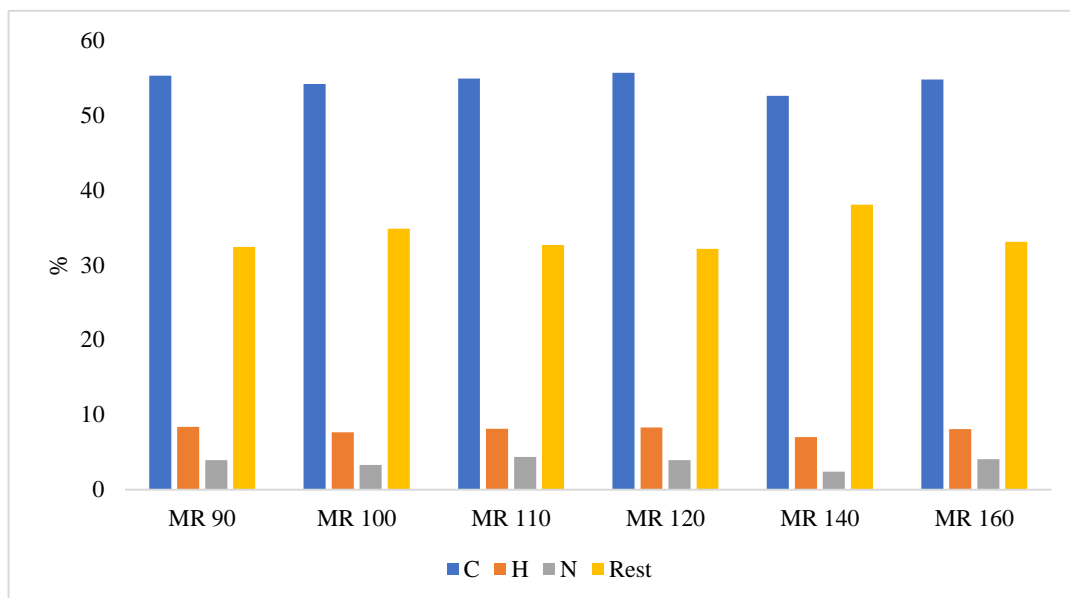


Figure 67 CHN of BCP MAE residues.

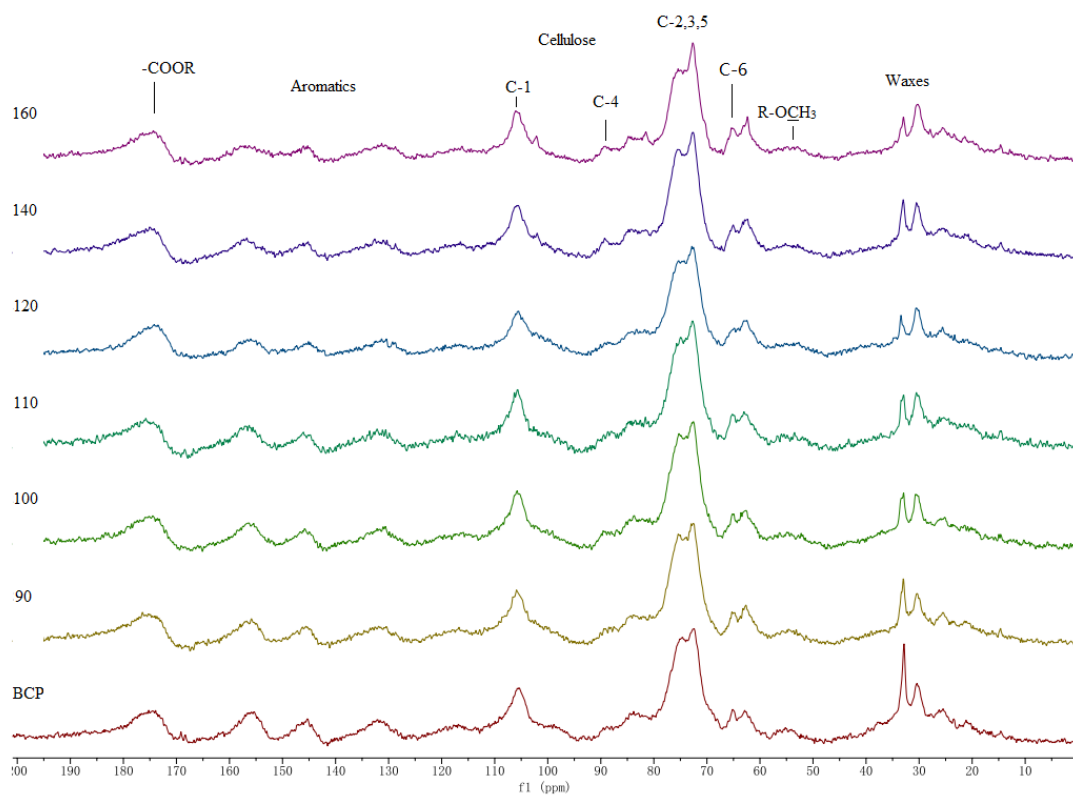


Figure 68 Solid-state NMR of BCP and MAE residues (90-160 °C)

The solid-state NMR of BCP and its MRs (90-160) is shown in Fig.68. The

resonances at 106, 89, 73-76 and 62-65 ppm correspond to C1, C4, C2,3,5 and C6 of cellulose. The resonances at 174 and 54 ppm correspond to galacturonic acid and methoxy group of pectin. The resonances between 120-160 ppm are aromatics of flavonoids and lignin. The resonance at 33 ppm shows the most significant decrease from BCP to high temperature residues, corresponds to waxes.

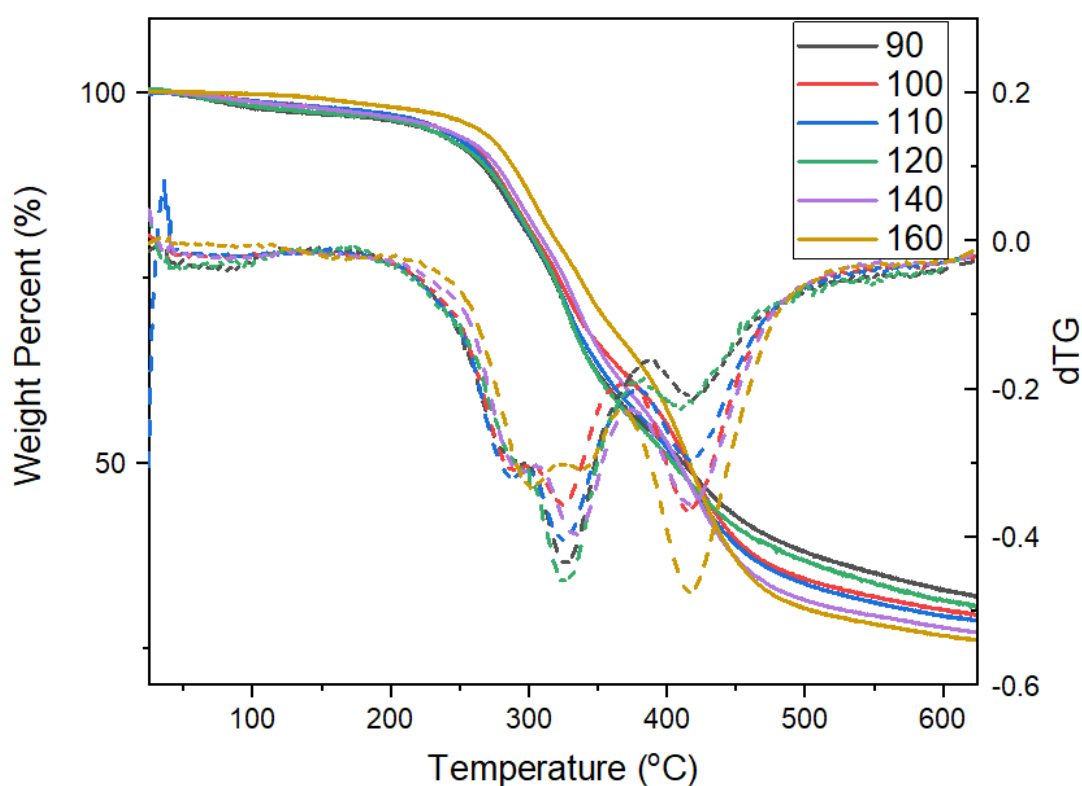


Figure 69 STA of BCP MAE Residues.

TGA of BCP residues (90-160) is shown in Fig. 69. The small shoulder in the dTG at around 280 °C was assumed to be degradation of hemicellulose. The dTG peak at 330 °C refers to degradation of cellulose and the mass lost over 400 °C corresponds to lignin decomposition. The TGA OF BCP MR 160 shows significant change in

cellulose and lignin composition. This may be attributed to 2 reasons: 1. Decomposition of cellulose at 160 °C under microwave irradiation; 2. Formation of pseudo lignin (humins) as discussed previously (section 3.2.2.6).

3.3.8 Summary

To summarise *Part 3: Production and Characterisation of Blackcurrant Pomace Hydrolysates*, microwave hydrolysates (MHs) were isolated from BCP which present TPC up to 178.5 mg/g GAE and 91.6% DPPH inhibition. A multitude of components are extracted which only become evident via HPLC-MS analysis. Some are plausible, for example, derivatives of delphinidin and cyanidin, whereas others (Kaempferol 7-*O*-glucoside, K7G) require further investigation as there is no literature precedence for the occurrence in BCP. The best temperature for MHs isolation should be below 120 °C, when temperature is higher than 120 °C, antioxidants degraded and sugars became main components.

4. Conclusion

4.1 Regarding the Obtained Results

4.1.1 Valorisation of Citrus Peel Waste

As presented in the Introduction, previous works have been undertaken on microwave based valorisation of citrus peel waste.^{79, 121, 136, 140} However, these studies neither considered a fully-integrated process nor the green impact of acidic catalyst. In this work, a new approach based on acid-free hydrothermal microwave treatment was designed, with focus on valorisation of pectin and cellulosic residues of citrus peel waste. This valorisation approach resulted in the sequential production of citrus pectin and MFC.

For pectin isolation, the yield was up to 19.7% for orange pectin and 36.5% for lemon pectin, it proved that this approach was able to achieve similar yield compared with those ones with acid catalyst (see Table 10, section 3.1.3). The most exciting discovery of this work was the hydrothermal microwave-assisted selective scissoring (Hy-MASS) of orange pectin at 160 °C, which was named as Hy-MASS-p. The characterisation of orange pectin samples produced at 160 °C via TGA, ¹³C NMR, HPLC and GPC has confirmed our thinking of selective decomposing of orange pectin at 160 °C under microwave radiation. This is the first report of producing galactan-rich RG-I pectin from orange peel waste and avoids the use of complicated,

bespoke, enzymatic techniques

MFC was successfully characterised as a nanostructure material with excellent ability to form hydrogels at low concentrations. The MFC samples processed at different temperatures presented different properties. For example, lower temperature products (120 °C) present residual pectic content, whiter, higher WRV but lower CI. Products at higher temperature (160 °C) with lower yields present no pectic residues, brown colour, lower WRV but higher CI. This approach was able to offer products for different applications by changing processing temperature.

In summary, acid-free hydrothermal microwave treatment applied to production of pectin and MFC is a quick and efficient process to isolate pectin. This approach was able to produce galactan-rich RG-I pectin and brown MFC with higher crystallinity with one-step direct process, or normal citrus pectin and white MFC with higher water retention value with a two-step sequential reprocess. If a *cleaner* MFC is needed, then another option may be Soxhlet pretreatment prior to microwave processing. This is discussed further in section 4.2.

4.1.2 Valorisation of Blackcurrant Pomace

As presented in the Introduction, previous works have been undertaken on valorisation of blackcurrant pomace (BCP). Those studies focus on antioxidant activity of polysaccharide from alkaline extraction,²⁴⁸ acid extraction,⁹⁷ bio-oil from

hydrothermal liquefaction¹⁰¹ and dietary fibres production.⁹⁹ In this work, a new approach based on acid-free hydrothermal microwave treatment was designed, with focus on valorisation of BCP hydrolysates with antioxidant activities. BCP MHs was characterised as hydrolysates with antioxidant activities, total phenol content up to 178.5 mg/g GAE. Considering yield, appearance, antioxidant and HPLC-MS results, the BCP MHs obtained from variety temperatures can be divided into 3 main groups: 1) MH 50-80, containing small molecules and flavonoids; 2) MH 90-120, containing small molecules, flavonoids and pectin; 3) MH 140 and MH 160, mainly metabolise of lignocellulosic materials.

4.2 Limitation and Future Work

There were some limitations identified with the purpose to direct and motivate future work.

4.2.1 Limitations of Citrus Valorisation

The pectin isolation from the hydrolysate after MHT was performed by ethanol precipitation, followed by ethanol solvent exchange to remove pigments, The melting point of ethanol is -114.1 °C, which means this product is not suitable for freeze drying (normally performed at -55 °C), resulting in stone-like pectin product (see Appendix 36) after oven drying (30-40 °C). These pectin products were extremely hard to grind and dissolve. Thus, this may have influenced DE titration, gel formation

and GPC results as these require complete solubility of the sample in the desired analytical solvent.

Meanwhile, the final step in MFC production was solvent exchange as well. A 60 °C oven dry may cause thermal degradation and tighten of cellulose (hornification), resulting in darkening of the product. It may be that removal of pigments from citrus peel prior to MHT, may negate the need to several hot ethanol washes Towards the end of this research period, a preliminary Soxhlet extraction pre-treatment study was undertaken to produce to obtain a *whiter* orange peel residue (WOPR) as reported in section 4.4.2. The benefit of WOPR for our experiments is the final solvent washing process is no longer necessary, and organic solvent usage was saved to make the experiment greener.

4.2.2 Future Work - Soxhlet Pretreatment

Orange peel waste (80-100 g) was placed in a Soxhlet thimble, ethanol (250 ml) was added into round bottom flask, reflux until the OPR is visually colourless (normally 2-3 hours). The WOPR was oven dried for further MHT.

The MHT of Soxhlet pretreated WOPR was slightly different from the general method. A mixture of WOPR (30-40 g) and water (700 ml) were used in pectin MHT. (Details in sections 2.2.1 and 2.2.2) When pectin is isolated from aqueous fraction, the pectin pellet was placed in a round bottom flask and dissolved in water, rotary evaporate to

remove residual ethanol, then freeze dried. The solid fraction was washed by boiling water twice then freeze dried to obtain a white and loose WMFC. The average yield of Soxhlet pretreated WOPR from fresh Valencia OPR was 11% (56.7% dry basis). Due to azeotropic distillation of ethanol and water, solvent in Soxhlet extractor always contains water, sugars in OPR can be extracted.

4.2.3 Result of Soxhlet Pretreatment

The yield of Soxhlet pretreated pectin and MFC was shown in Table 13.

Table 14 Yield of Soxhlet pretreated WMFC and pectin.

Name	Weight/g	Yield / %	Dry method
WMFC-1	24.41	61%	Oven
WMFC-1-P0	2.96	7.4	Oven
WMFC-1-P1	3.24	8.1	Oven
WMFC-2	23.23	77.4%	Freeze dry
WMFC-2-P0	2.21	7.4	Freeze dry
WMFC-2-P1	2.5	8.3	Freeze dry

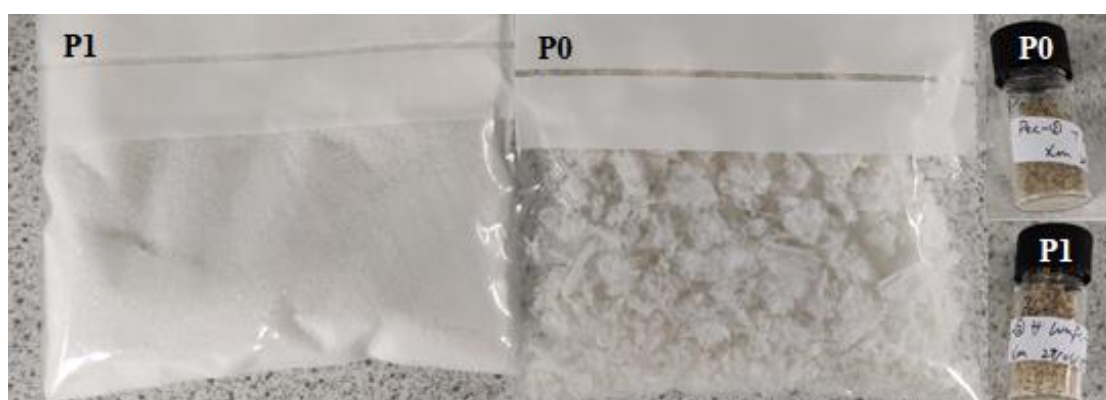


Figure 70 Comparison of oven dried (vials) and freeze dried (bags) pectin samples.

A picture of pectin product from Soxhlet pretreated WOPR compared with respect to freeze-dried pectin is shown in Fig. 70. The freeze dried pectin shows an entirely different form, *i.e.*, white and fluffy.

The hydrogel formation of freeze dried WMFC is shown in Fig. 71, the lowest concentration of gelation is 2%. The hydrogels of WMFC much whiter than gels of normal MFC as shown earlier in Fig. 47, section 3.2.3.1. Thus, the initial aim of producing a *cleaner* MFC was achieved.

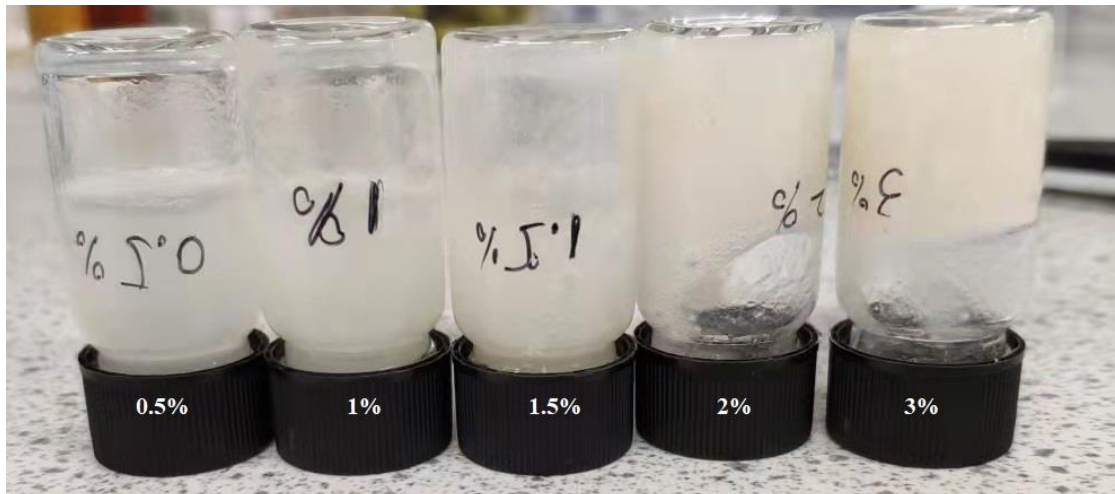


Figure 71 Hydrogel of freeze dried WMFC.

4.2.4 Limitation of Blackcurrant Valorisation and Future Work

Microwave residues (MR) in this project were briefly characterised without further valorisation. Considering the high lignin content in BCP⁹⁹ and MRs (Fig 69, section 3.3.7), the residues were not suitable for MFC production. A sequential microwave assisted pyrolysis reprocessing at high temperatures (over 200 °C) could be a potential

to obtain bio-oils containing high-value chemicals and bio-char from blackcurrant pomace.

References

1. Paris agreement, *Report of the Conference of the Parties to the United Nations Framework Convention on Climate Change (21st Session, 2015: Paris)*. https://unfccc.int/files/essential_background/convention/application/pdf/english_paris_agreement.pdf, 2015, (Accessed 22/02/2022).
2. United Nations Climate Change Conference 2021, *COP26-Explained*, <https://ukcop26.org/wp-content/uploads/2021/07/COP26-Explained.pdf>, 2021, (Accessed 22/02/2022).
3. Department of Economic and Social Affairs, United Nations, *World Population Prospects 2019.*, <https://population.un.org/wpp/>, 2019, (Accessed 22/02/2022).
4. World Bank, *World Bank Open Data*, <https://data.worldbank.org/indicator/NY.GDP.MKTP.CD.>, 2020, (Accessed 22/02/2022).
5. United Nations, *Sustainable Development Goals Review*, <https://unstats.un.org/sdgs/report/2019/Overview/>, 2019, (Accessed 22/02/2022).
6. J. B. Binder and R. T. Raines, *Journal of the American Chemical Society*, 2009, **131**, 1979-1985.
7. R. A. Sheldon, *Green Chemistry*, 2017, **19**, 18-43.
8. M. Lazarus and H. van Asselt, Springer, Editon edn., 2018.
9. P. Le Billon and B. Kristoffersen, *Environment and Planning A: Economy and Space*, 2020, **52**, 1072-1092.
10. U. Nations, *Transforming Our World: The 2030 Agenda for Sustainable Development*, sustainabledevelopment.un.org.
11. P. Messerli, E. Murniningtyas, P. Eloundou-Enyegue, E. G. Foli, E. Furman, A. Glassman, G. Hernández Licona, E. M. Kim, W. Lutz and J.-P. Moatti, 2019.
12. Food and Agriculture Organization of the United Nations, *Tracking progress on food and agriculture-related SDG indicators 2021*, <http://www.fao.org/sdg-progress-report/2021/en/>, 2021, (Accessed 22/02/2022).
13. J. B. Zimmerman, P. T. Anastas, H. C. Erythropel and W. Leitner, *Science*,

- 2020, **367**, 397-400.
14. J. H. Clark, *Green Chemistry*, 1999, **1**, 1-8.
 15. P. T. Anastas and J. C. Warner, *Green chemistry: Theory and practice*, 1998, 29-56.
 16. P. Anastas and N. Eghbali, *Chemical Society Reviews*, 2010, **39**, 301-312.
 17. K. Perepelkin, *Fibre Chemistry*, 2004, **36**, 161-176.
 18. V. Kocherbitov, S. Ulvenlund, M. Kober, K. Jarring and T. Arnebrant, *The Journal of Physical Chemistry B*, 2008, **112**, 3728-3734.
 19. V. Gupta, P. Carrott, R. Singh, M. Chaudhary and S. Kushwaha, *Bioresource technology*, 2016, **216**, 1066-1076.
 20. A.-F. Metaxa, E. K. Efthimiadou, N. Boukos and G. Kordas, *Journal of colloid and interface science*, 2012, **384**, 198-206.
 21. M. Kuglarz, M. Alvarado-Morales, D. Karakashev and I. Angelidaki, *Bioresource technology*, 2016, **200**, 639-647.
 22. B. C. Saha, *Journal of Industrial Microbiology and Biotechnology*, 2003, **30**, 279-291.
 23. L. J. Gibson, *Journal of the Royal Society Interface*, 2012, **9**, 2749-2766.
 24. H. V. Scheller and P. Ulvskov, *Plant Biology*, 2010, **61**, 263.
 25. P. T. Martone, J. M. Estevez, F. Lu, K. Ruel, M. W. Denny, C. Somerville and J. Ralph, *Current Biology*, 2009, **19**, 169-175.
 26. A. J. Ragauskas, G. T. Beckham, M. J. Biddy, R. Chandra, F. Chen, M. F. Davis, B. H. Davison, R. A. Dixon, P. Gilna and M. Keller, *Science*, 2014, **344**, 1246843.
 27. C. Amen-Chen, H. Pakdel and C. Roy, *Bioresource Technology*, 2001, **79**, 277-299.
 28. C. Li, X. Zhao, A. Wang, G. W. Huber and T. Zhang, *Chem. Rev.*, 2015, **115**, 11559-11624.
 29. F. G. Calvo-Flores and J. A. Dobado, *ChemSusChem*, 2010, **3**, 1227-1235.
 30. S. Palamae, P. Dechatiwongse, W. Choorit, Y. Chisti and P. Prasertsan, *Carbohydrate polymers*, 2017, **155**, 491-497.
 31. B. C. Saha, N. N. Nichols, N. Qureshi, G. J. Kennedy, L. B. Iten and M. A. Cotta, *Bioresource technology*, 2015, **175**, 17-22.

32. Y. H. Chan, S. Yusup, A. T. Quitain, R. R. Tan, M. Sasaki, H. L. Lam and Y. Uemura, *Energy Conversion and Management*, 2015, **104**, 180-188.
33. M. Hu, X. Wang, J. Chen, P. Yang, C. Liu, B. Xiao and D. Guo, *Energy conversion and management*, 2017, **135**, 453-462.
34. D. Chen, Y. Wang, Y. Liu, K. Cen, X. Cao, Z. Ma and Y. Li, *Fuel*, 2019, **252**, 1-9.
35. X. Hu and M. Gholizadeh, *Renewable and Sustainable Energy Reviews*, 2020, **134**, 110124.
36. V. Aristizábal-Marulanda and C. A. Cardona Alzate, *Biofuels, Bioproducts and Biorefining*, 2019, **13**, 789-808.
37. R. Luque, L. Herrero-Davila, J. M. Campelo, J. H. Clark, J. M. Hidalgo, D. Luna, J. M. Marinas and A. A. Romero, *Energy & Environmental Science*, 2008, **1**, 542-564.
38. S. N. Joglekar, P. D. Pathak, S. A. Mandavgane and B. D. Kulkarni, *Environmental Science and Pollution Research*, 2019, 1-10.
39. C. S. K. Lin, L. A. Pfaltzgraff, L. Herrero-Davila, E. B. Mubofu, S. Abderrahim, J. H. Clark, A. A. Koutinas, N. Kopsahelis, K. Stamatelatou and F. Dickson, *Energy & Environmental Science*, 2013, **6**, 426-464.
40. Food and Agriculture Organization of the United Nations, *The State of Food and Agriculture*, <https://www.fao.org/3/ca6030en/ca6030en.pdf>, 2019, (Accessed 22/02/2022).
41. Food Agriculture Organization of the United Nations, *Food wastage footprint: impacts on natural resources: summary report*, <https://www.fao.org/3/i3347e/i3347e.pdf>, 2013, (Accessed 22/02/2022).
42. Å. Stenmarck, C. Jensen, T. Quested, G. Moates, M. Buksti, B. Cseh, S. Juul, A. Parry, A. Politano and B. Redlingshofer, *Estimates of European food waste levels*, IVL Swedish Environmental Research Institute, 2016.
43. The Waste and Resources Action Programme, *Estimates of Food and Packaging Waste in the UK Grocery Retail and Hospitality Supply Chains*, https://www.givergy.com/wpcontent/uploads/2020/03/Estimates_20in_the_UK_Jan17.pdf, 2015, (Accessed 22/02/2022).
44. United Nations Environment Programme, T. Q. H. Forbes, C. O'Connor, *Food Waste Index Report 2021*, <https://www.unep.org/resources/report/unep-food-waste-index-report-2021>, 2021, (Accessed 22/02/2022).

45. A. S. Matharu, E. M. de Melo and J. A. Houghton, *Bioresource technology*, 2016, **215**, 123-130.
46. J. S. Hargreaves, I. D. Pulford, M. Balakrishnan and V. S. Batra, *Conversion of large scale wastes into value-added products*, CRC Press, 2013.
47. M. Z. Jacobson, *Journal of Geophysical Research: Atmospheres*, 2014, **119**, 8980-9002.
48. Massachusetts Institute of Technology, K. Kung, *The dirty secret of biomass waste*, <https://tatacenter.mit.edu/2015/12/07/the-dirty-secret-of-biomass-waste/>, 2015, (Accessed 22/02/2022).
49. Nova Institute, M. Carus and L. Dammer, *The “circular bioeconomy”– concepts, opportunities and limitations*, <https://bioplasticfeedstockalliance.org/?mdocsfile=1285>, 2018, (Accessed 22/02/2022).
50. D. A. Teigiserova, L. Hamelin and M. Thomsen, *Resources, Conservation and Recycling*, 2019, **149**, 413-426.
51. M. Alexandri and J. Venus, *Current Opinion in Green and Sustainable Chemistry*, 2017, **8**, 24-29.
52. L. A. Pfaltzgraff, E. C. Cooper, V. Budarin and J. H. Clark, *Green Chemistry*, 2013, **15**, 307-314.
53. G. A. Wu, J. Terol, V. Ibanez, A. López-García, E. Pérez-Román, C. Borredá, C. Domingo, F. R. Tadeo, J. Carbonell-Caballero and R. Alonso, *Nature*, 2018, **554**, 311.
54. Food and Agriculture Organization of the United Nations, *Citrus Fruit Statistics 2015*, <http://www.fao.org/3/a-i5558e.pdf>, 2015, (Accessed 22/02/2022).
55. Food and Agriculture Organization of the United Nations, *FAO Citrus Fruit Fresh and Processed Statistical Bulletin 2016*, <https://www.fao.org/3/i8092e/i8092e.pdf>, 2017, (Accessed 22/02/2022).
56. D. Mamma and P. Christakopoulos, *Waste and Biomass Valorization*, 2014, **5**, 529-549.
57. M. Boukroufa, C. Boutekedjiret, L. Petigny, N. Rakotomanomana and F. Chemat, *Ultrasonics Sonochemistry*, 2015, **24**, 72-79.
58. F. R. Marín, C. Soler-Rivas, O. Benavente-García, J. Castillo and J. A. Pérez-Alvarez, *Food chemistry*, 2007, **100**, 736-741.

59. V. Negro, B. Ruggeri, D. Fino and D. Tonini, *Resources, Conservation and Recycling*, 2017, **127**, 148-158.
60. V. Ferreira-Leitao, L. M. F. Gottschalk, M. A. Ferrara, A. L. Nepomuceno, H. B. C. Molinari and E. P. Bon, *Waste and Biomass Valorization*, 2010, **1**, 65-76.
61. V. Negro, G. Mancini, B. Ruggeri and D. Fino, *Bioresource Technology*, 2016, **214**, 806-815.
62. F. Battista, G. Remelli, S. Zanzoni and D. Bolzonella, *ACS Sustainable Chemistry & Engineering*, 2020, **8**, 6834-6843.
63. A. Czech, E. Zarycka, D. Yanovych, Z. Zasadna, I. Grzegorzcyk and S. Kłys, *Biological Trace Element Research*, 2020, **193**, 555-563.
64. S. Rafiq, R. Kaul, S. Sofi, N. Bashir, F. Nazir and G. A. Nayik, *Journal of the Saudi Society of Agricultural Sciences*, 2018, **17**, 351-358.
65. I. John, K. Muthukumar and A. Arunagiri, *International Journal of Green Energy*, 2017, **14**, 599-612.
66. J. Mann, R. S. Davidson, J. B. Hobbs, D. Banthorpe and J. B. Harborne, *Natural products: their chemistry and biological significance*, Longman Scientific & Technical, 1994.
67. Q. Guo, K. Liu, W. Deng, B. Zhong, W. Yang and J. Chun, *Food Science & Nutrition*, 2018, **6**, 1431-1437.
68. J. R. Ayala, G. Montero, H. E. Campbell, C. García, M. A. Coronado, J. A. León, C. A. Sagaste and L. J. Pérez, *Journal of Essential Oil Bearing Plants*, 2017, **20**, 897-914.
69. M. A. Ferhat, B. Y. Meklati, J. Smadja and F. Chemat, *Journal of Chromatography A*, 2006, **1112**, 121-126.
70. J. Bustamante, S. van Stempvoort, M. García-Gallarreta, J. A. Houghton, H. K. Briers, V. L. Budarin, A. S. Matharu and J. H. Clark, *Journal of Cleaner Production*, 2016, **137**, 598-605.
71. S. E. Razzaghi, A. Arabhosseini, M. Turk, T. Soubrat, A. Cendres, M. H. Kianmehr, S. Perino and F. Chemat, *Journal of food engineering*, 2019, **241**, 26-32.
72. R. Ciriminna, M. Lomeli-Rodriguez, P. D. Cara, J. A. Lopez-Sanchez and M. Pagliaro, *Chemical Communications*, 2014, **50**, 15288-15296.
73. B. Ozturk, J. Winterburn and M. Gonzalez-Miquel, *Biochemical engineering journal*, 2019, **151**, 107298.

74. M. Lohrasbi, M. Pourbafrani, C. Niklasson and M. J. Taherzadeh, *Bioresource technology*, 2010, **101**, 7382-7388.
75. M. Viuda-Martos, Y. Ruiz-Navajas, J. Fernández-López and J. Pérez-Álvarez, *Food control*, 2008, **19**, 1130-1138.
76. N. Besil, S. Rezende, N. Alonzo, M. V. Cesio, F. Rivas and H. Heinzen, *SN Applied Sciences*, 2019, **1**, 618.
77. M. Russo, I. Bonaccorsi, G. Torre, M. Sarò, P. Dugo and L. Mondello, *journal of functional foods*, 2014, **9**, 18-26.
78. W. McGlynn, *Importance of Food pH in Commerical Canning Operations*, https://shareok.org/bitstream/handle/11244/50205/oksd_fapc_118_2010-07.pdf?sequence=1 2003, (Accessed 22/02/2022).
79. A. Martínez-Abad, M. Ramos, M. Hamzaoui, S. Kohnen, A. Jiménez and M. C. Garrigós, *Foods*, 2020, **9**, 1493.
80. A. Herrera-Barros, N. Bitar-Castro, Á. Villabona-Ortíz, C. Tejada-Tovar and Á. D. González-Delgado, *Sustainable Chemistry and Pharmacy*, 2020, **17**, 100299.
81. X. Chen, Y. Ding, B. Forrest, J. Oh, S. M. Boussert and M. T. Hamann, *Food chemistry*, 2019, **270**, 251-256.
82. R. Ciriminna, B. Forest, F. Meneguzzo, M. Pagliaro and M. T. Hamann, *Applied Sciences*, 2020, **10**, 6812.
83. B. Abarna, T. Preethi and G. Rajarajeswari, *Journal of Environmental Chemical Engineering*, 2019, **7**, 102742.
84. A. Tyagi, K. M. Tripathi, N. Singh, S. Choudhary and R. K. Gupta, *RSC advances*, 2016, **6**, 72423-72432.
85. N. van Strien, S. Rautiainen, M. Asikainen, D. A. Thomas, J. Linnekoski, K. Niemelä and A. Harlin, *Green Chemistry*, 2020.
86. M. Sajid, X. Zhao and D. Liu, *Green chemistry*, 2018, **20**, 5427-5453.
87. R.-J. van Putten, J. C. Van Der Waal, E. De Jong, C. B. Rasrendra, H. J. Heeres and J. G. de Vries, *Chemical reviews*, 2013, **113**, 1499-1597.
88. V. Corrigan, D. Hedderley, G. Langford and C. Zou, *New Zealand Journal of Crop and Horticultural Science*, 2014, **42**, 247-264.
89. A. Michalska, A. Wojdyło, G. P. Łysiak, K. Lech and A. Figiel, *Advanced Powder Technology*, 2017, **28**, 1340-1348.

90. A. Horszwald, H. Julien and W. Andlauer, *Food Chemistry*, 2013, **141**, 2858-2863.
91. R. E. Cortez and E. Gonzalez de Mejia, *Journal of food science*, 2019, **84**, 2387-2401.
92. M. Vagiri, E. Johansson and K. Rumpunen, X International Rubus and Ribes Symposium 946, 2011.
93. T. Röhrig, V. Kirsch, D. Schipp, J. Galan and E. Richling, *Journal of agricultural and food chemistry*, 2019, **67**, 6792-6797.
94. S. G. Lee, T. M. Vance, T.-G. Nam, D.-O. Kim, S. I. Koo and O. K. Chun, *Plant foods for human nutrition*, 2015, **70**, 427-432.
95. V. Nour, F. Stampar, R. Veberic and J. Jakopic, *Food chemistry*, 2013, **141**, 961-966.
96. M. Sojka, S. Guyot, K. Kołodziejczyk, B. Król and A. Baron, *The Journal of Horticultural Science and Biotechnology*, 2009, **84**, 100-106.
97. E. M. Azman, A. House, D. Charalampopoulos and A. Chatzifragkou, *International Journal of Food Science & Technology*, 2020.
98. Y. Xu, X. Niu, N. Liu, Y. Gao, L. Wang, G. Xu, X. Li and Y. Yang, *Food chemistry*, 2018, **243**, 26-35.
99. K. Alba, W. Macnaughtan, A. Laws, T. J. Foster, G. Campbell and V. Kontogiorgos, *Food Hydrocolloids*, 2018, **81**, 398-408.
100. S. Anouti, G. Haarlemmer, M. Déniel and A. Roubaud, *Energy & Fuels*, 2016, **30**, 398-406.
101. M. Deniel, G. Haarlemmer, A. Roubaud, E. Weiss-Hortala and J. Fages, *Energy & Fuels*, 2016, **30**, 4895-4904.
102. L. S. Mackenzie, H. Tyrrell, R. Thomas, A. S. Matharu, J. H. Clark and G. A. Hurst, *Journal of Chemical Education*, 2019, **96**, 3025-3029.
103. E. M. De Melo, J. H. Clark and A. S. Matharu, *Green Chemistry*, 2017, **19**, 3408-3417.
104. V. L. Singleton, R. Orthofer and R. M. Lamuela-Raventós, *Methods in enzymology*, 1999, **299**, 152-178.
105. G. Yang and S.-J. Park, *Materials*, 2019, **12**, 1177.
106. C. O. Kappe, *Angewandte Chemie International Edition*, 2004, **43**, 6250-6284.

107. M. R. Rosana, J. Hunt, A. Ferrari, T. A. Southworth, Y. Tao, A. E. Stiegman and G. B. Dudley, *The Journal of organic chemistry*, 2014, **79**, 7437-7450.
108. T. Appleton, R. Colder, S. Kingman, I. Lowndes and A. Read, *Applied energy*, 2005, **81**, 85-113.
109. V. L. Budarin, Y. Zhao, M. J. Gronnow, P. S. Shuttleworth, S. W. Breeden, D. J. Macquarrie and J. H. Clark, *Green Chemistry*, 2011, **13**, 2330-2333.
110. W.-C. Zeng, Z. Zhang, H. Gao, L.-R. Jia and W.-Y. Chen, *Carbohydrate Polymers*, 2012, **89**, 694-700.
111. K. Bélafi-Bakó, P. Cserjési, S. Beszédes, Z. Csanádi and C. Hodúr, *Food and bioprocess technology*, 2012, **5**, 1100-1105.
112. A. de la Hoz, A. Diaz-Ortiz and A. Moreno, *Chemical Society Reviews*, 2005, **34**, 164-178.
113. L. Cassol, E. Rodrigues and C. P. Z. Noreña, *Industrial Crops and Products*, 2019, **133**, 168-177.
114. N. Pap, S. Beszédes, E. Pongrácz, L. Myllykoski, M. Gábor, E. Gyimes, C. Hodúr and R. L. Keiski, *Food and Bioprocess Technology*, 2013, **6**, 2666-2674.
115. A. L. M. P. Leite, C. D. Zanon and F. C. Menegalli, *Carbohydrate polymers*, 2017, **157**, 962-970.
116. Q. Liu, Y. Lu, M. Aguedo, N. Jacquet, C. Ouyang, W. He, C. Yan, W. Bai, R. Guo and D. e. Goffin, *ACS Sustainable Chemistry & Engineering*, 2017, **5**, 6183-6191.
117. Q. Liu, W.-Q. He, M. Aguedo, X. Xia, W.-B. Bai, Y.-Y. Dong, J.-Q. Song, A. Richel and D. Goffin, *Carbohydrate Polymers*, 2020, **253**, 117170.
118. J. G. Figueroa, I. Borrás-Linares, R. Del Pino-García, J. A. Curiel, J. Lozano-Sánchez and A. Segura-Carretero, *Food Chemistry*, 2021, **352**, 129300.
119. F. Golbargi, S. M. T. Gharibzahedi, A. Zoghi, M. Mohammadi and R. Hashemifesharaki, *Carbohydrate Polymers*, 2021, **256**, 117522.
120. R. Gautam, S. Shyam, B. R. Reddy, K. Govindaraju and R. Vinu, *Sustainable Energy & Fuels*, 2019, **3**, 3009-3020.
121. D.-L. Su, P.-J. Li, S. Y. Quek, Z.-Q. Huang, Y.-J. Yuan, G.-Y. Li and Y. Shan, *Food chemistry*, 2019, **286**, 1-7.
122. B. B. V. Guandalini, N. P. Rodrigues and L. D. F. Marczak, *Food Research International*, 2019, **119**, 455-461.

123. Z. J. Kermani, A. Shpigelman, H. T. T. Pham, A. M. Van Loey and M. E. Hendrickx, *Food Hydrocolloids*, 2015, **44**, 424-434.
124. C. L. Petkowicz and P. A. Williams, *Food Hydrocolloids*, 2020, **107**, 105930.
125. E. G. Maxwell, N. J. Belshaw, K. W. Waldron and V. J. Morris, *Trends in Food Science & Technology*, 2012, **24**, 64-73.
126. F. Naqash, F. Masoodi, S. A. Rather, S. Wani and A. Gani, *Carbohydrate polymers*, 2017, **168**, 227-239.
127. W. Wang, X. Wu, T. Chantapakul, D. Wang, S. Zhang, X. Ma, T. Ding, X. Ye and D. Liu, *Food Research International*, 2017, **102**, 101-110.
128. Y. Zouambia, N. Moulai-Mostefa and M. Krea, *Carbohydrate polymers*, 2009, **78**, 841-846.
129. D. Mohnen, *Current opinion in plant biology*, 2008, **11**, 266-277.
130. L. Cui, J. Wang, R. Huang, Y. Tan, F. Zhang, Y. Zhou and L. Sun, *International journal of biological macromolecules*, 2019, **128**, 459-467.
131. L. Sun, D. Ropartz, L. Cui, H. Shi, M.-C. Ralet and Y. Zhou, *Carbohydrate polymers*, 2019, **203**, 119-127.
132. N. Khodaei, S. Karboune and V. Orsat, *Food chemistry*, 2016, **190**, 495-505.
133. L. Tan, S. Eberhard, S. Pattathil, C. Warder, J. Glushka, C. Yuan, Z. Hao, X. Zhu, U. Avci and J. S. Miller, *The Plant Cell*, 2013, **25**, 270-287.
134. S. E. Broxterman and H. A. Schols, *Carbohydrate polymers*, 2018, **197**, 269-276.
135. D. Liu, L. Zhang, Y. Xu and X. Zhang, *Proceedings of Meetings on Acoustics ICA2013*, 2013.
136. S. S. Hosseini, F. Khodaiyan and M. S. Yarmand, *Carbohydrate polymers*, 2016, **140**, 59-65.
137. H.-m. Chen, X. Fu and Z.-g. Luo, *Food chemistry*, 2015, **168**, 302-310.
138. C. D. May, *Carbohydrate polymers*, 1990, **12**, 79-99.
139. M. F. Basanta, N. M. Ponce, A. M. Rojas and C. A. Stortz, *Carbohydrate polymers*, 2012, **89**, 230-235.
140. Z. Rahmani, F. Khodaiyan, M. Kazemi and A. Sharifan, *International Journal of Biological Macromolecules*, 2020, **147**, 1107-1115.
141. A. Ilghami, S. Ghanbarzadeh and H. Hamishehkar, *Pharmaceutical Sciences*,

- 2015, **21**, 46-50.
142. M. Marić, A. N. Grassino, Z. Zhu, F. J. Barba, M. Brnčić and S. R. Brnčić, *Trends in Food Science & Technology*, 2018, **76**, 28-37.
 143. D. Wu, J. Zheng, G. Mao, W. Hu, X. Ye, R. J. Linhardt and S. Chen, *Critical reviews in food science and nutrition*, 2019, 1-23.
 144. H. Zhang, J. Chen, J. Li, L. Yan, S. Li, X. Ye, D. Liu, T. Ding, R. J. Linhardt and C. Orfila, *Food Hydrocolloids*, 2018, **79**, 579-586.
 145. G. Mao, D. Wu, C. Wei, W. Tao, X. Ye, R. J. Linhardt, C. Orfila and S. Chen, *Trends in Food Science & Technology*, 2019, **94**, 65-78.
 146. C. Colodel, L. C. Vriesmann, R. F. Teófilo and C. L. de Oliveira Petkowicz, *International journal of biological macromolecules*, 2018, **117**, 385-391.
 147. N. Khodaei and S. Karboune, *Food chemistry*, 2016, **197**, 406-414.
 148. N. Khodaei, B. Fernandez, I. Fliss and S. Karboune, *Carbohydrate polymers*, 2016, **136**, 1074-1084.
 149. H. Wang, L. Wan, D. Chen, X. Guo, F. Liu and S. Pan, *Carbohydrate polymers*, 2019, **212**, 51-58.
 150. V. V. Glinsky and A. Raz, *Carbohydrate research*, 2009, **344**, 1788-1791.
 151. K. J. Pienta, H. Nailk, A. Akhtar, K. Yamazaki, T. S. Replogle, J. Lehr, T. L. Donat, L. Tait, V. Hogan and A. Raz, *JNCI: Journal of the National Cancer Institute*, 1995, **87**, 348-353.
 152. C. L. Jackson, T. M. Dreaden, L. K. Theobald, N. M. Tran, T. L. Beal, M. Eid, M. Y. Gao, R. B. Shirley, M. T. Stoffel and M. V. Kumar, *Glycobiology*, 2007, **17**, 805-819.
 153. R. S. do Nascimento, L. de Freitas Pedrosa, L. T. H. Diethelm, T. Souza, T. M. Shiga and J. P. Fabi, *Food Research International*, 2020, **137**, 109747.
 154. W. Zhang, P. Xu and H. Zhang, *Trends in Food Science & Technology*, 2015, **44**, 258-271.
 155. T. I. Gouveia, K. Biernacki, M. C. Castro, M. P. Gonçalves and H. K. Souza, *Food Hydrocolloids*, 2019, **97**, 105175.
 156. R. Wang, R. Liang, T. Dai, J. Chen, X. Shuai and C. Liu, *Trends in Food Science & Technology*, 2019, **91**, 319-329.
 157. A. Balaria and S. Schiewer, *Separation and Purification Technology*, 2008, **63**, 577-581.

158. D. Ibarra-Rodríguez, J. Lizardi-Mendoza, E. A. López-Maldonado and M. T. Oropeza-Guzmán, *Chemical Engineering Journal*, 2017, **323**, 19-28.
159. L. Kupchik, E. Bogdanov, O. Bogdanova and M. Kupchik, *Russian journal of applied chemistry*, 2006, **79**, 457-460.
160. V. Dronnet, C. Renard, M. Axelos and J.-F. Thibault, *Carbohydrate polymers*, 1996, **30**, 253-263.
161. M. Khotimchenko, V. Kovalev and Y. Khotimchenko, *Journal of hazardous materials*, 2007, **149**, 693-699.
162. T. A. Kuljanin, L. R. Jevrić, B. L. Ćurčić, M. R. Nićetin, V. S. Filipović and J. P. Grbić, *Hemijska industrija*, 2014, **68**, 89-97.
163. M. Celus, C. Kyomugasho, L. Salvia-Trujillo, J. Van Audenhove, A. M. Van Loey, T. Grauwet and M. E. Hendrickx, *Food hydrocolloids*, 2018, **79**, 319-330.
164. X. Ma, D. Li, Z. Wu, H. Zhang, X. Chen and Z. Liu, *Chemical Engineering & Technology*, 2016, **39**, 371-377.
165. M. Khotimchenko, K. Makarova, E. Khozhaenko and V. Kovalev, *International journal of biological macromolecules*, 2017, **97**, 526-535.
166. E. Khozhaenko, V. Kovalev, E. Podkorytova and M. Khotimchenko, *Science of the total environment*, 2016, **565**, 913-921.
167. Y. Mata, M. Blázquez, A. Ballester, F. González and J. Muñoz, *Chemical Engineering Journal*, 2009, **150**, 289-301.
168. W. Zhang, J. Song, Q. He, H. Wang, W. Lyu, H. Feng, W. Xiong, W. Guo, J. Wu and L. Chen, *Journal of hazardous materials*, 2020, **384**, 121445.
169. J. Koh, Z. Xu and L. Wicker, *Food chemistry*, 2020, **302**, 125343.
170. J. Lu, T. Wang and L. T. Drzal, *Composites Part A: Applied Science and Manufacturing*, 2008, **39**, 738-746.
171. N. Lavoine, I. Desloges, A. Dufresne and J. Bras, *Carbohydrate polymers*, 2012, **90**, 735-764.
172. W. Li, J. Yue and S. Liu, *Ultrasonics sonochemistry*, 2012, **19**, 479-485.
173. S. H. Osong, S. Norgren and P. Engstrand, *Cellulose*, 2016, **23**, 93-123.
174. F. W. Herrick, R. L. Casebier, J. K. Hamilton and K. R. Sandberg, *J. Appl. Polym. Sci.: Appl. Polym. Symp.*; (United States), 1983.

175. A. F. Turbak, F. W. Snyder and K. R. Sandberg, *J. Appl. Polym. Sci.: Appl. Polym. Symp.*:(United States), 1983.
176. S. Kalia, S. Boufi, A. Celli and S. Kango, *Colloid and Polymer Science*, 2014, **292**, 5-31.
177. B. Deepa, E. Abraham, B. M. Cherian, A. Bismarck, J. J. Blaker, L. A. Pothan, A. L. Leao, S. F. De Souza and M. Kottaisamy, *Bioresource technology*, 2011, **102**, 1988-1997.
178. I. Siró and D. Plackett, *Cellulose*, 2010, **17**, 459-494.
179. B. Wang, M. Sain and K. Oksman, *Applied Composite Materials*, 2007, **14**, 89-103.
180. T. Saito, M. Hirota, N. Tamura, S. Kimura, H. Fukuzumi, L. Heux and A. Isogai, *Biomacromolecules*, 2009, **10**, 1992-1996.
181. A. S. Matharu, E. M. de Melo, J. Remón, S. Wang, A. Abdulina and E. Kontturi, *CHEMSUSCHEM*, 2018.
182. T. Impoolsup, N. Chiewchan and S. Devahastin, *Carbohydrate Polymers*, 2020, **230**, 115630.
183. M. Pääkkö, M. Ankerfors, H. Kosonen, A. Nykänen, S. Ahola, M. Österberg, J. Ruokolainen, J. Laine, P. T. Larsson and O. Ikkala, *Biomacromolecules*, 2007, **8**, 1934-1941.
184. M. Mariño, L. Lopes da Silva, N. Durán and L. Tasic, *Molecules*, 2015, **20**, 5908-5923.
185. S. Yoo and J. S. Hsieh, *Industrial & Engineering Chemistry Research*, 2010, **49**, 2161-2168.
186. S. Ahola, X. Turon, M. Osterberg, J. Laine and O. Rojas, *Langmuir*, 2008, **24**, 11592-11599.
187. M. Henriksson, G. Henriksson, L. Berglund and T. Lindström, *European Polymer Journal*, 2007, **43**, 3434-3441.
188. A. Dufresne, *Materials today*, 2013, **16**, 220-227.
189. A. Serpa, J. Velásquez-Cock, P. Gañán, C. Castro, L. Vélez and R. Zuluaga, *Food Hydrocolloids*, 2016, **57**, 178-186.
190. T. Abitbol, A. Rivkin, Y. Cao, Y. Nevo, E. Abraham, T. Ben-Shalom, S. Lapidot and O. Shoseyov, *Current opinion in biotechnology*, 2016, **39**, 76-88.
191. N. Lavoine and L. Bergström, *Journal of Materials Chemistry A*, 2017, **5**,

- 16105-16117.
192. H. M. Azeredo, M. F. Rosa and L. H. C. Mattoso, *Industrial Crops and Products*, 2017, **97**, 664-671.
 193. C. Aulin, M. Gällstedt and T. Lindström, *Cellulose*, 2010, **17**, 559-574.
 194. C. M. Ortiz, P. R. Salgado, A. Dufresne and A. N. Mauri, *Food Hydrocolloids*, 2018, **79**, 416-427.
 195. N. Lavoine, I. Desloges, C. Sillard and J. Bras, *Cellulose*, 2014, **21**, 4429-4442.
 196. T. Taipale, M. Österberg, A. Nykänen, J. Ruokolainen and J. Laine, *Cellulose*, 2010, **17**, 1005-1020.
 197. K. Mörseburg and G. Chinga-Carrasco, *Cellulose*, 2009, **16**, 795-806.
 198. A. J. Svagan, J.-W. Benjamins, Z. Al-Ansari, D. B. Shalom, A. Müllertz, L. Wågberg and K. Löbmann, *Journal of Controlled Release*, 2016, **244**, 74-82.
 199. B. Seantier, D. Bendahou, A. Bendahou, Y. Grohens and H. Kaddami, *Carbohydrate polymers*, 2016, **138**, 335-348.
 200. M. Monsoor, U. Kalapathy and A. Proctor, *Journal of Agricultural and Food chemistry*, 2001, **49**, 2756-2760.
 201. L. Segal, J. J. Creely, A. Martin Jr and C. Conrad, *Textile research journal*, 1959, **29**, 786-794.
 202. R. Gnanasambandam and A. Proctor, *Food chemistry*, 2000, **68**, 327-332.
 203. M. Schwanninger, J. Rodrigues, H. Pereira and B. Hinterstoisser, *Vibrational Spectroscopy*, 2004, **36**, 23-40.
 204. F. H. Larsen, I. Byg, I. Damager, J. Diaz, S. B. Engelsen and P. Ulvskov, *Biomacromolecules*, 2011, **12**, 1844-1850.
 205. A. P. Gunning, R. J. Bongaerts and V. J. Morris, *The FASEB Journal*, 2009, **23**, 415-424.
 206. A. B. Kute, D. Mohapatra, N. Kotwaliwale, S. K. Giri and B. Sawant, *Agricultural Research*, 2020, **9**, 241-248.
 207. X. Guo, D. Han, H. Xi, L. Rao, X. Liao, X. Hu and J. Wu, *Carbohydrate polymers*, 2012, **88**, 441-448.
 208. S. Gårdebjer, A. Bergstrand, A. Idström, C. Börstell, S. Naana, L. Nordstierna and A. Larsson, *Composites Science and Technology*, 2015, **107**, 1-9.
 209. S. Park, J. O. Baker, M. E. Himmel, P. A. Parilla and D. K. Johnson,

- Biotechnology for biofuels*, 2010, **3**, 1-10.
210. Q.-Y. Zhou, C. Fan, C. Li, Y.-L. Wang, Z.-Q. Chen, Q. Yu and M.-Q. Zhu, *Materials Horizons*, 2018, **5**, 474-479.
211. X. Teng, F. Li and C. Lu, *Chemical Society Reviews*, 2020, **49**, 2408-2425.
212. S. D. Shinde, X. Meng, R. Kumar and A. J. Ragauskas, *Green Chemistry*, 2018, **20**, 2192-2205.
213. H. Shen, H. Shan and L. Liu, *ChemSusChem*, 2020, **13**, 513-519.
214. S. K. Patil and C. R. Lund, *Energy & Fuels*, 2011, **25**, 4745-4755.
215. F. Gu, W. Wang, Z. Cai, F. Xue, Y. Jin and J. Zhu, *Cellulose*, 2018, **25**, 2861-2871.
216. X. Luo, J. Zhu, R. Gleisner and H. Zhan, *Cellulose*, 2011, **18**, 1055-1062.
217. A. S. Matharu, E. M. de Melo, J. Remón, S. Wang, A. Abdulina and E. Kontturi, *ChemSusChem*, 2018, **11**, 1344-1353.
218. F. Ahmadi, Z. Oveisi, S. M. Samani and Z. Amoozgar, *Research in pharmaceutical sciences*, 2015, **10**, 1.
219. J. Nie, Z. Wang, K. Zhang and Q. Hu, *RSC Advances*, 2015, **5**, 37346-37352.
220. W. Wang, X. Zhang, A. Teng and A. Liu, *International journal of biological macromolecules*, 2017, **103**, 226-233.
221. Y. Liu, W. He, Z. Zhang and B. P. Lee, *Gels*, 2018, **4**, 46.
222. J. Li and D. J. Mooney, *Nature Reviews Materials*, 2016, **1**, 1-17.
223. H. Du, W. Liu, M. Zhang, C. Si, X. Zhang and B. Li, *Carbohydrate polymers*, 2019, **209**, 130-144.
224. M. Ahmad, S. Ahmed, B. L. Swami and S. Ikram, *Langmuir*, 2015, **79**, 109-155.
225. J. Shojaeiarani, D. Bajwa and A. Shirzadifar, *Carbohydrate polymers*, 2019, **216**, 247-259.
226. M. M. Fares, Y. R. Tahboub, S. T. Khatatbeh and Y. M. Abul-Haija, *Journal of Polymers and the Environment*, 2011, **19**, 431.
227. E. F. Lessa, A. L. Medina, A. S. Ribeiro and A. R. Fajardo, *Arabian Journal of Chemistry*, 2020, **13**, 709-720.
228. E. F. Lessa, M. S. Gularte, E. S. Garcia and A. R. Fajardo, *Carbohydrate*

- Polymers*, 2017, **157**, 660-668.
229. Y. Lu and L. Y. Foo, *Food Chemistry*, 2003, **80**, 71-76.
230. S. Farooque, P. M. Rose, M. Benohoud, R. S. Blackburn and C. M. Rayner, *Journal of agricultural and food chemistry*, 2018, **66**, 12265-12273.
231. J. B. Fernandes, D. W. Griffith and H. Bain, *Phytochemical Analysis*, 1996, **7**, 97-103.
232. G. Chrzanowski, C. Sempruch and I. Sprawka, *Electronic Journal of Polish Agricultural Universities*, 2007, **10**, 42.
233. C. M. Statham, R. Crowden and J. Harborne, *Phytochemistry*, 1972, **11**, 1083-1088.
234. D. Singh, S. Sharma, R. Rani, S. Mishra and R. Sharma, *Int J Pharm Clin Res*, 2011, **3**, 30-34.
235. J. M Calderon-Montano, E. Burgos-Morón, C. Pérez-Guerrero and M. López-Lázaro, *Mini reviews in medicinal chemistry*, 2011, **11**, 298-344.
236. K. R. Määttä-Riihinen, A. Kamal-Eldin, P. H. Mattila, A. M. González-Paramás and A. R. Törrönen, *Journal of agricultural and food chemistry*, 2004, **52**, 4477-4486.
237. W. C. Hou, R. D. Lin, T. H. Lee, Y. H. Huang, F. L. Hsu and M. H. Lee, *Journal of the Science of Food and Agriculture*, 2005, **85**, 615-621.
238. M. Sahai, P. Neogi and A. B. Ray, *Heterocycles*, 1982, **19**, 37-40.
239. S. Ghisoni, L. Lucini, F. Angilletta, G. Rocchetti, D. Farinelli, S. Tombesi and M. Trevisan, *Food Research International*, 2019, **121**, 746-753.
240. C. Evans, A. Conney, N. Trousof and J. Burns, *Biochimica et biophysica acta*, 1960, **41**, 9-14.
241. G.-C. Yen, P.-D. Duh and H.-L. Tsai, *Food chemistry*, 2002, **79**, 307-313.
242. M. Sandell, O. Laaksonen, R. Jarvinen, N. Rostiala, T. Pohjanheimo, K. Tiitinen and H. Kallio, *Journal of Agricultural and Food Chemistry*, 2009, **57**, 3718-3728.
243. A.-V. Ferlemi and F. N. Lamari, *Antioxidants*, 2016, **5**, 17.
244. D. Fuchs, X. Tang, A.-K. Johnsson, S.-E. Dahlen, M. Hamberg and C. E. Wheelock, *Biochimica et Biophysica Acta (BBA)-Molecular and Cell Biology of Lipids*, 2020, **1865**, 158611.

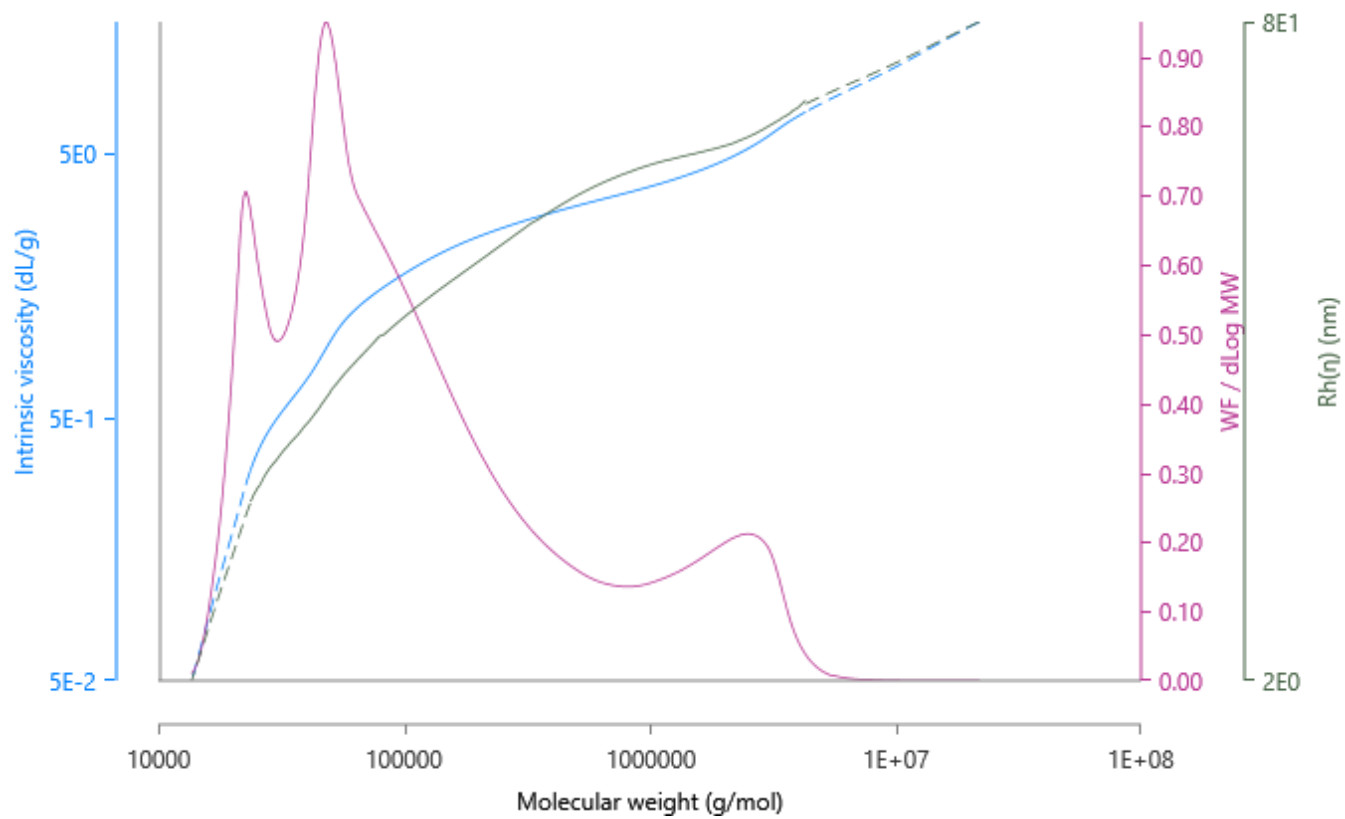
245. S. P. Caligiuri, M. Parikh, A. Stamenkovic, G. N. Pierce and H. M. Aukema, *American Journal of Physiology-Heart and Circulatory Physiology*, 2017, **313**, H903-H918.
246. A. Ibarz, J. Pagan and R. Miguelsanz, *Journal of Food Engineering*, 1992, **15**, 63-73.
247. Y. Hong, X. Liao and Z. Chen, *Journal of Pharmaceutical Analysis*, 2021, **11**, 465-471.
248. S. Duan, M. Zhao, B. Wu, S. Wang, Y. Yang, Y. Xu and L. Wang, *International journal of biological macromolecules*, 2020, **155**, 1114-1122.

Appendices

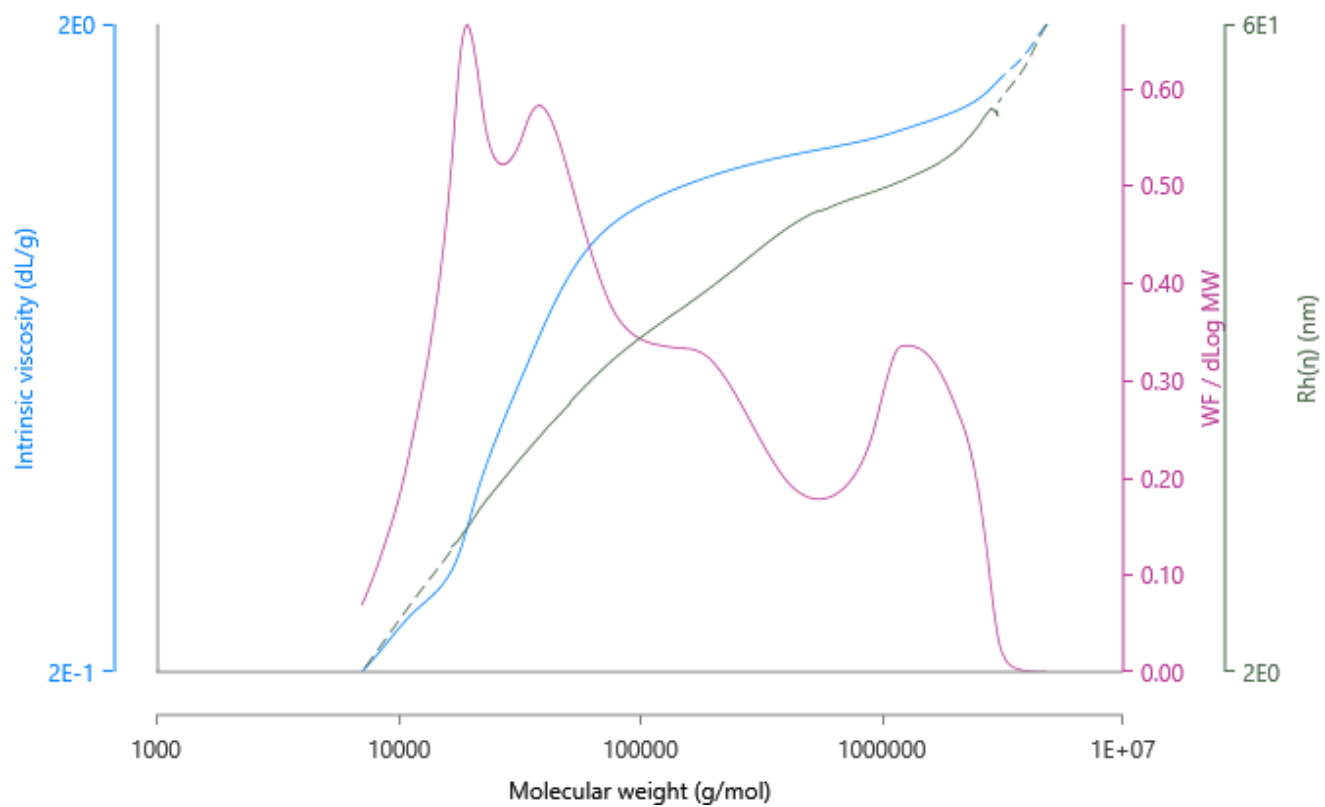
Appendix 1 Milestone Synthwave microwave reactor.



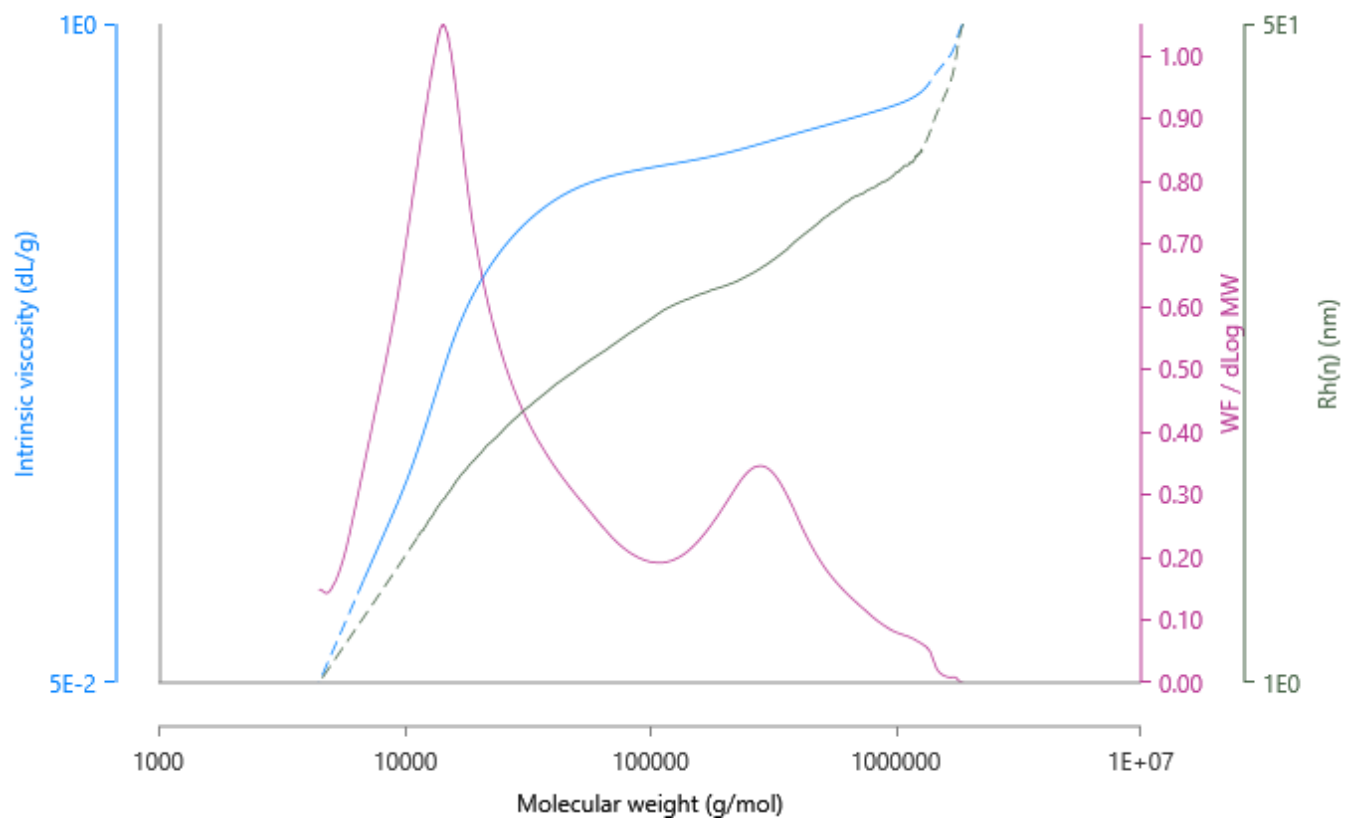
Appendix 2 Molecular Weight m (g/mol) vs Intrinsic viscosity (dL/g), Molecular Weight Distribution (WF/dLog MW) and Hydrodynamic Size (nm) Plot for OP0-120.



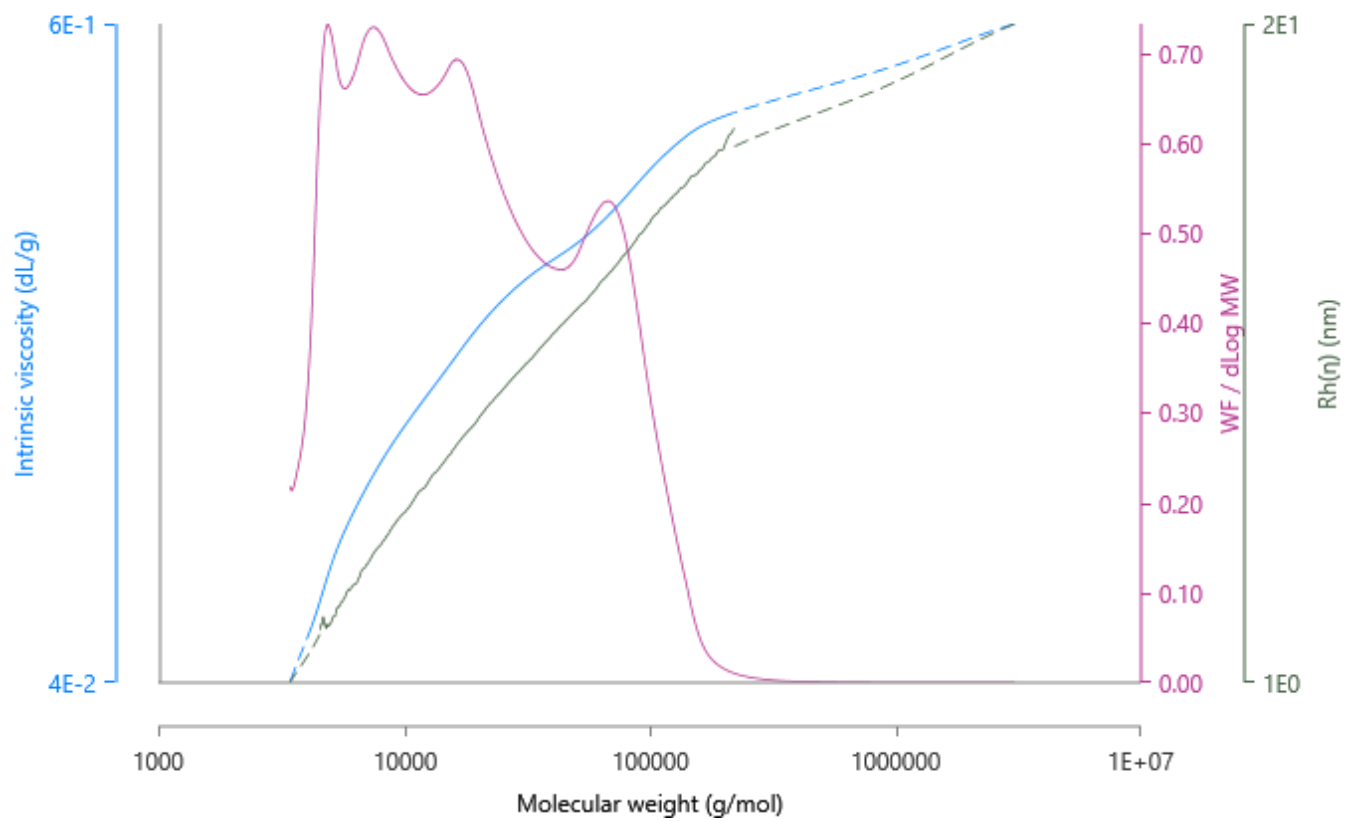
Appendix 3 Molecular Weight m (g/mol) vs Intrinsic viscosity (dL/g), Molecular Weight Distribution (WF/dLog MW) and Hydrodynamic Size (nm) Plot for OP1-120.



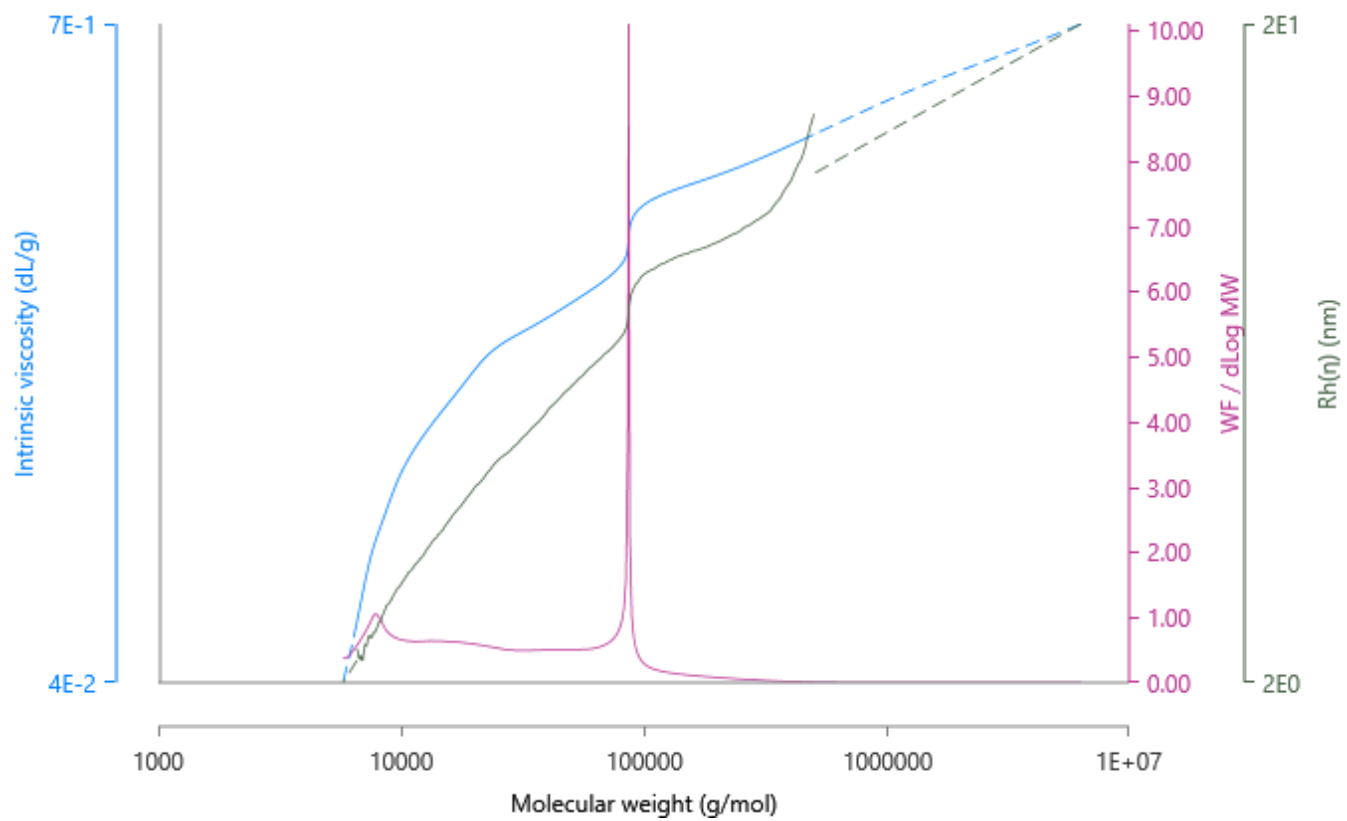
Appendix 4 Molecular Weight m(g/mol) vs Intrinsic viscosity (dL/g), Molecular Weight Distribution (WF/dLog MW) and Hydrodynamic Size (nm) Plot for OP2-140.



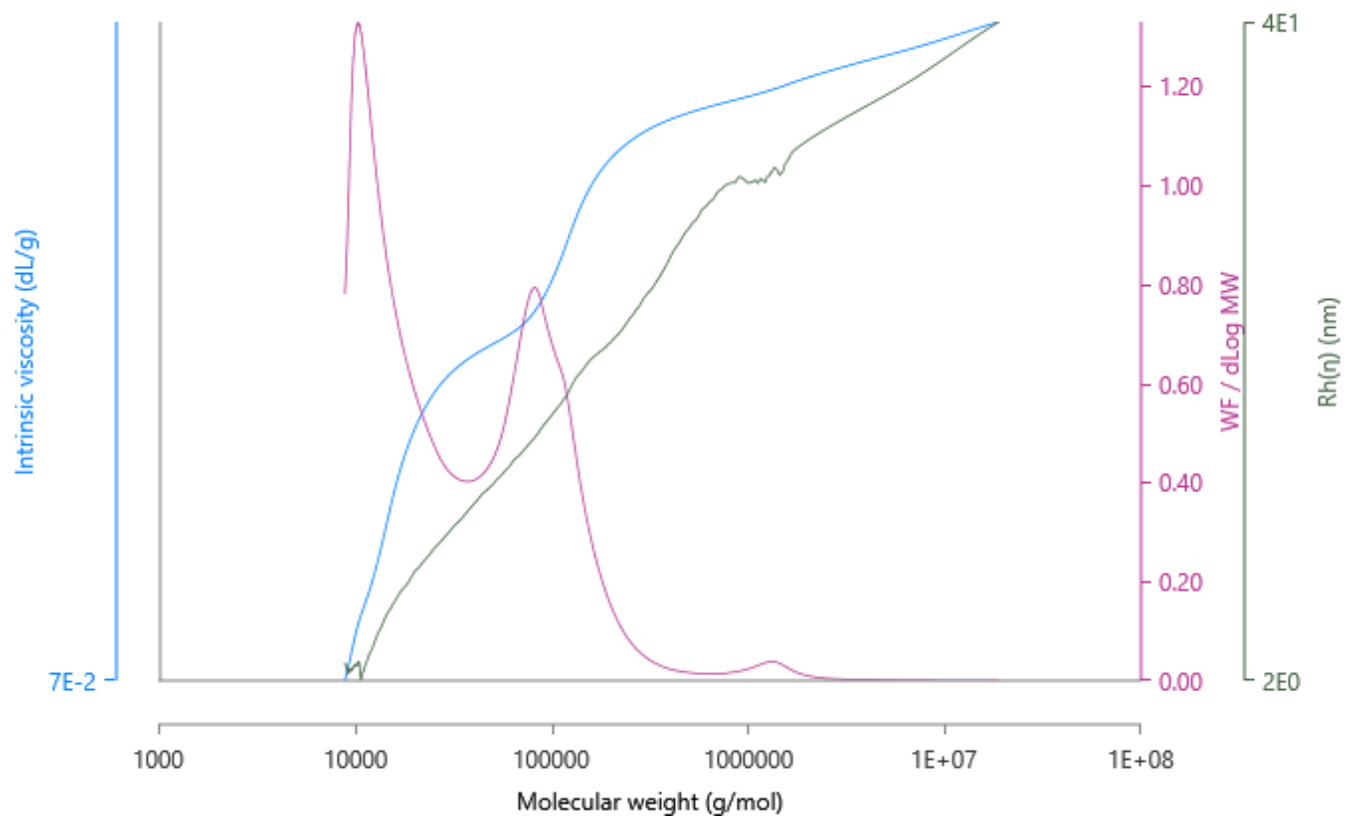
Appendix 5 Molecular Weight m(g/mol) vs Intrinsic viscosity (dL/g), Molecular Weight Distribution (WF/dLog MW) and Hydrodynamic Size (nm) Plot for OP3-160.



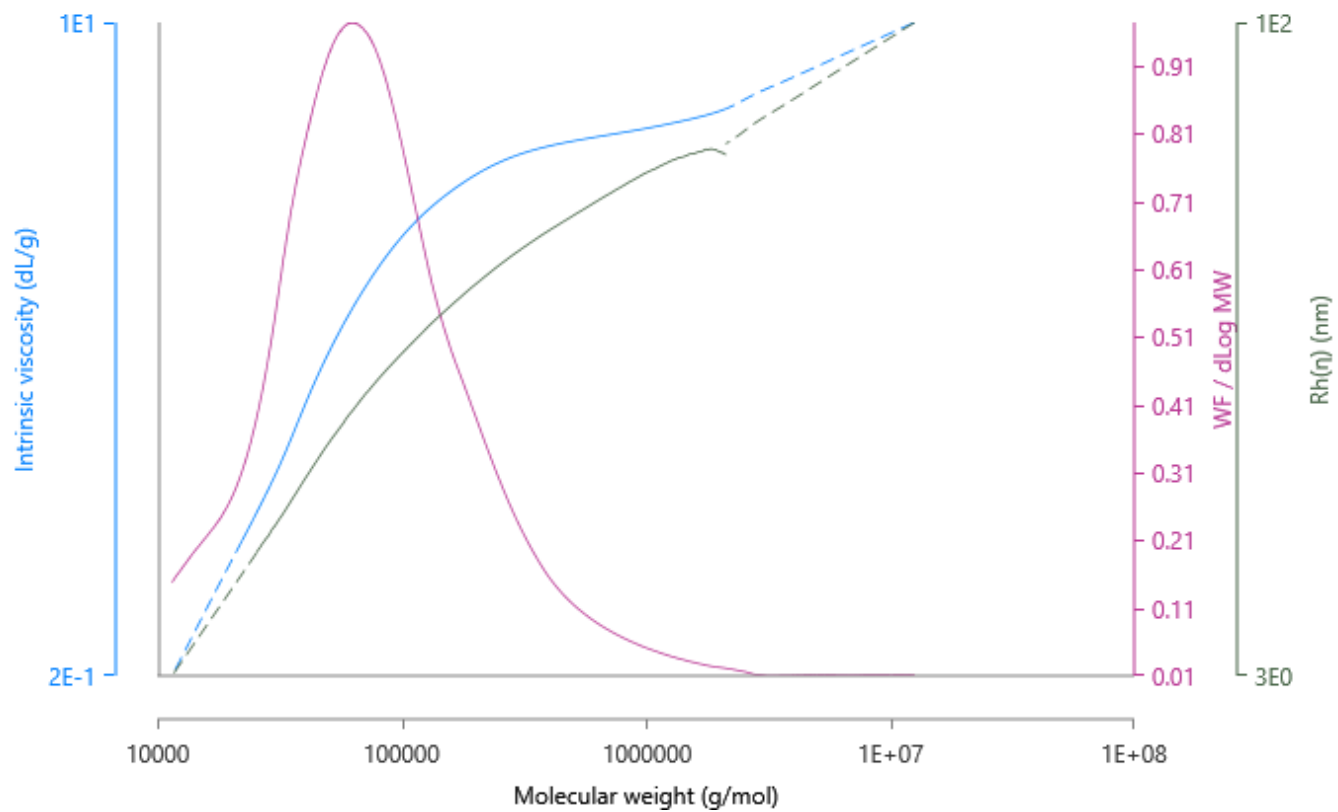
Appendix 6 Molecular Weight m(g/mol) vs Intrinsic viscosity (dL/g), Molecular Weight Distribution (WF/dLog MW) and Hydrodynamic Size (nm) Plot for OP0-160.



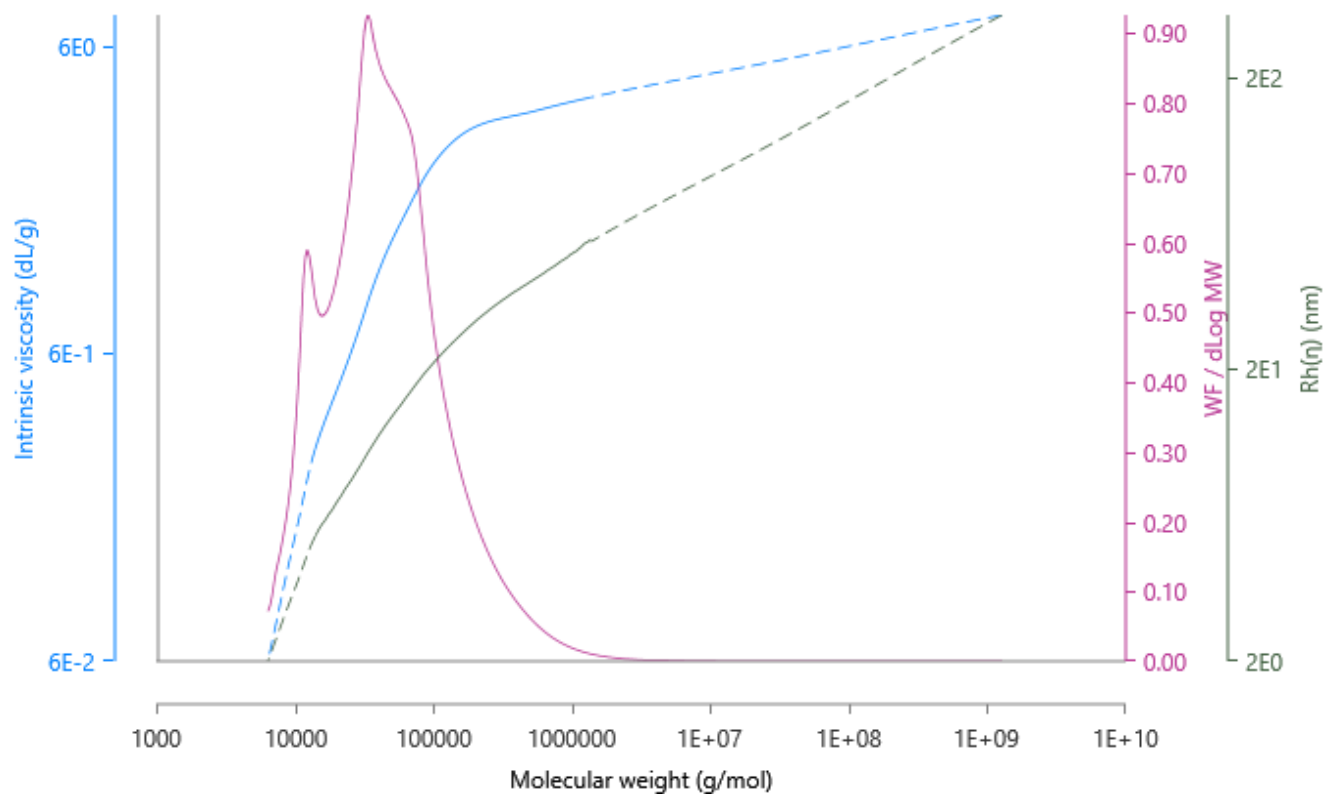
Appendix 7 Molecular Weight m(g/mol) vs Intrinsic viscosity (dL/g), Molecular Weight Distribution (WF/dLog MW) and Hydrodynamic Size (nm) Plot for OP3'-160.



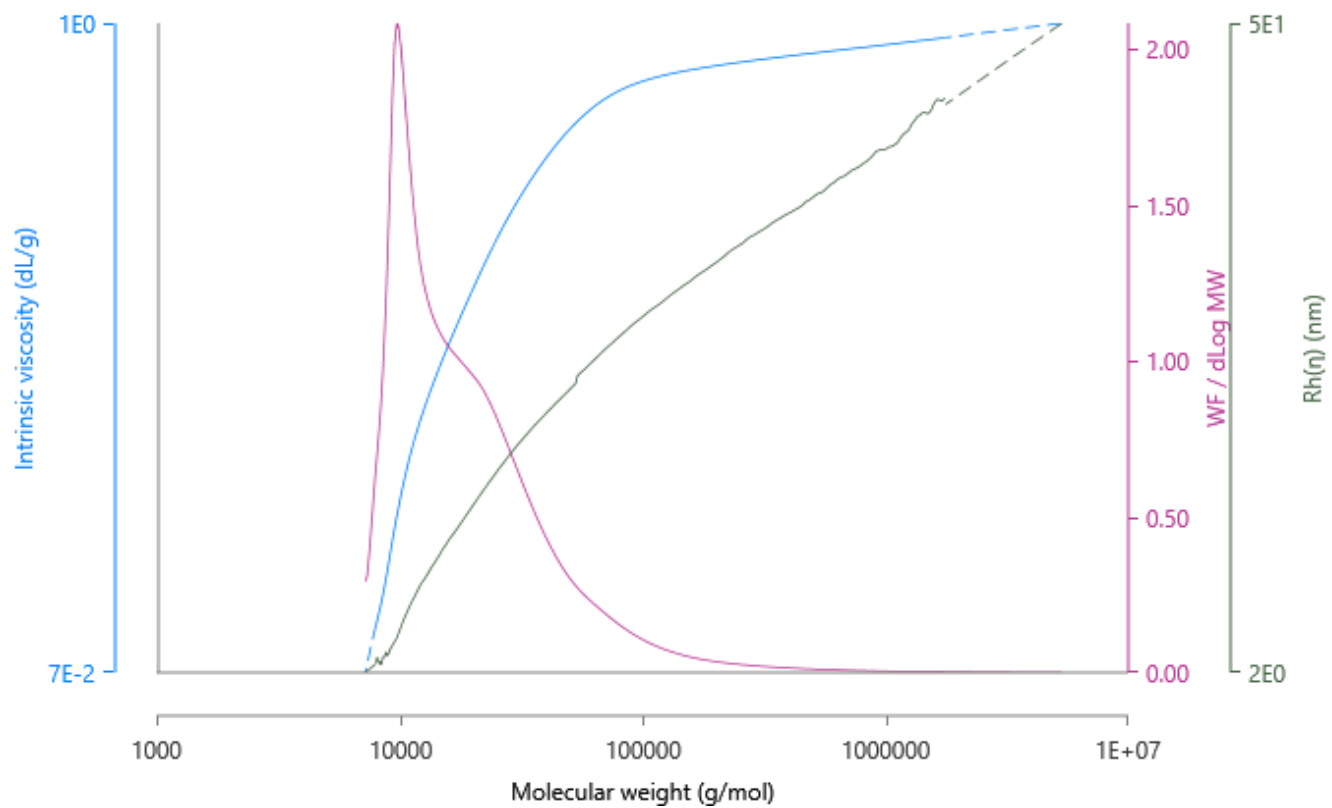
Appendix 8 Molecular Weight m(g/mol) vs Intrinsic viscosity (dL/g), Molecular Weight Distribution (WF/dLog MW) and Hydrodynamic Size (nm) Plot for LP0-120.



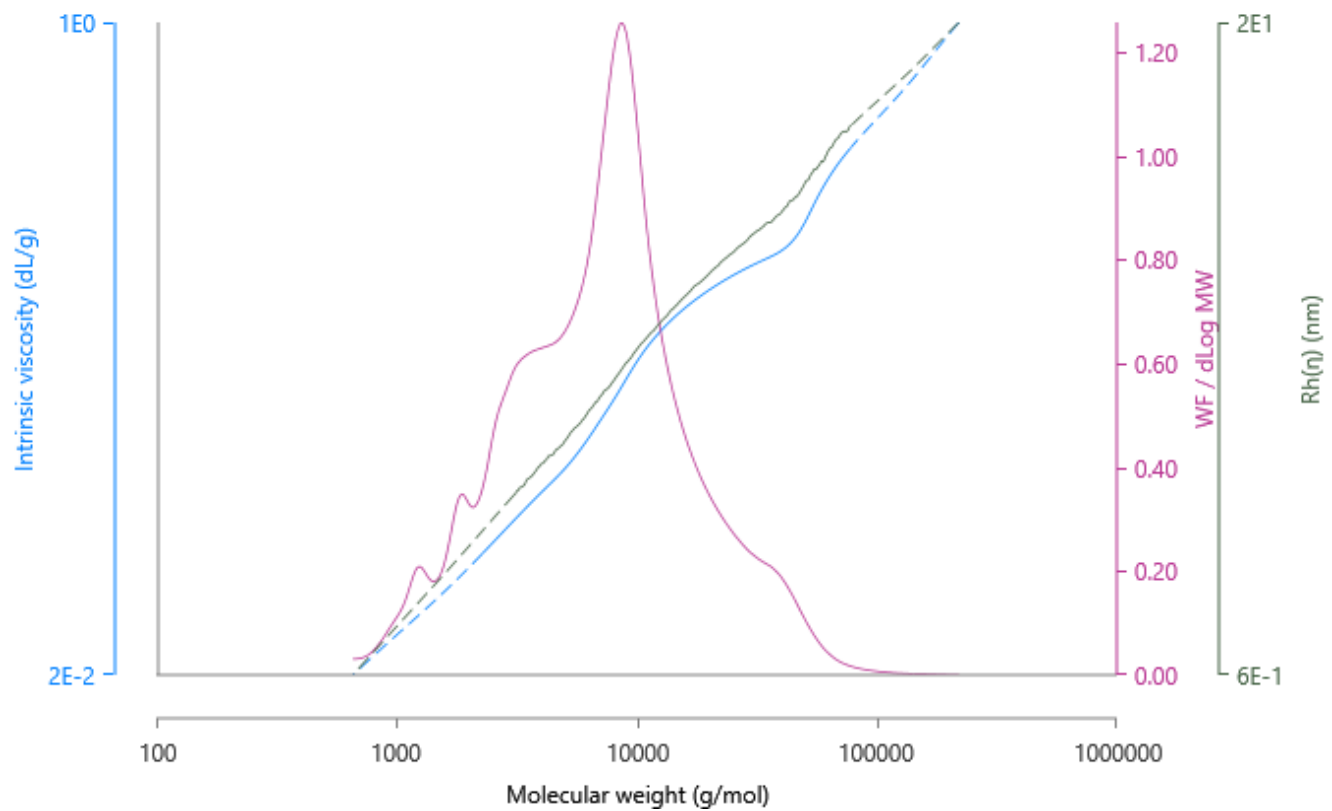
Appendix 9 Molecular Weight m (g/mol) vs Intrinsic viscosity (dL/g), Molecular Weight Distribution (WF/dLog MW) and Hydrodynamic Size (nm) Plot for LP1-120.



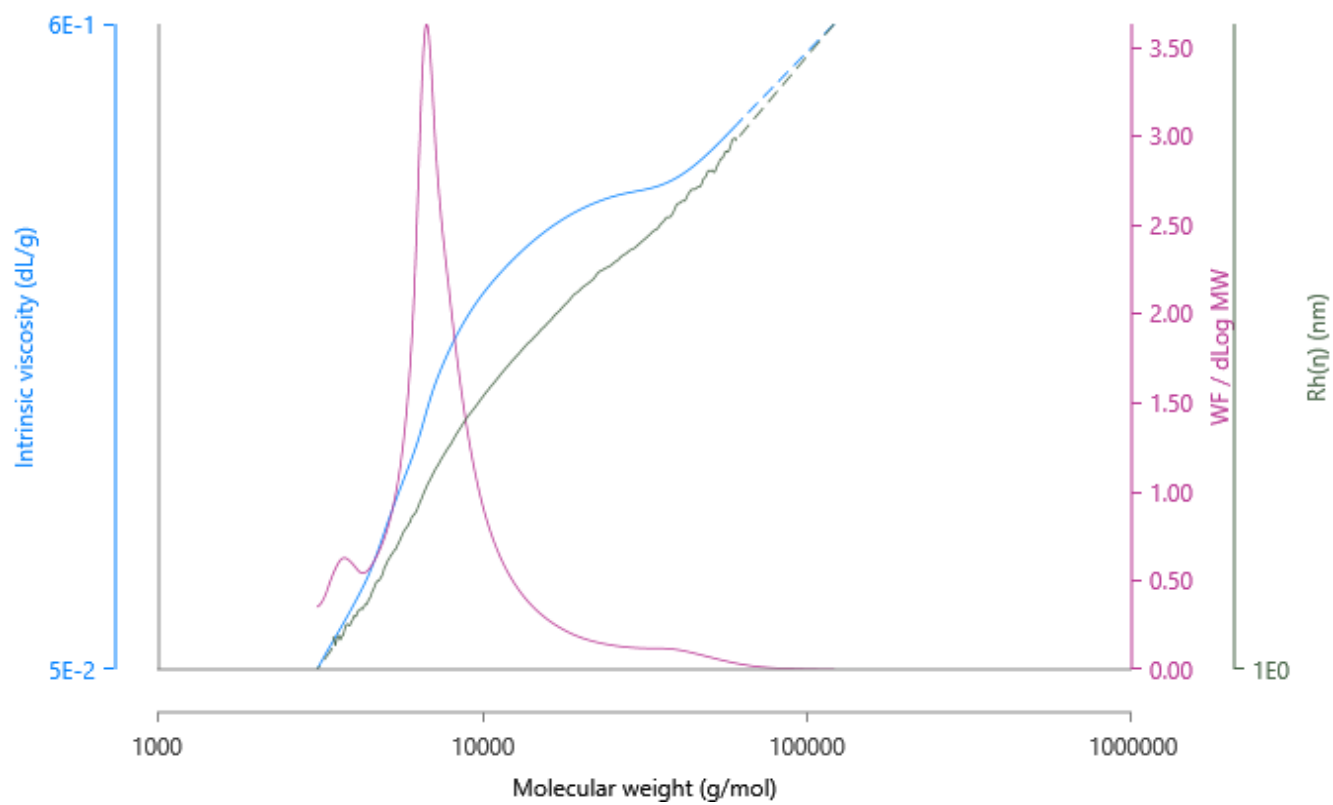
Appendix 10 Molecular Weight m (g/mol) vs Intrinsic viscosity (dL/g), Molecular Weight Distribution (WF/dLog MW) and Hydrodynamic Size (nm) Plot for LP2-140.



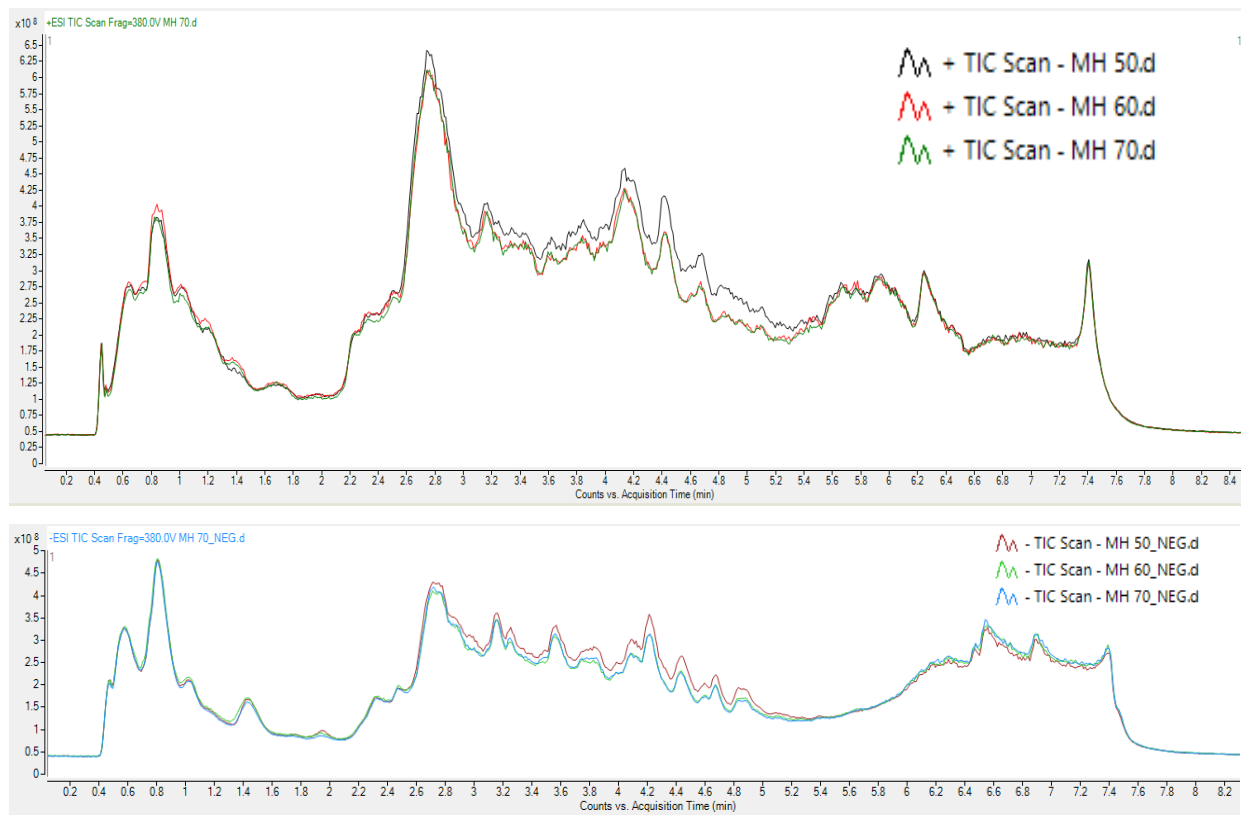
Appendix 11 Molecular Weight m (g/mol) vs Intrinsic viscosity (dL/g), Molecular Weight Distribution (WF/dLog MW) and Hydrodynamic Size (nm) Plot for LP3-160.



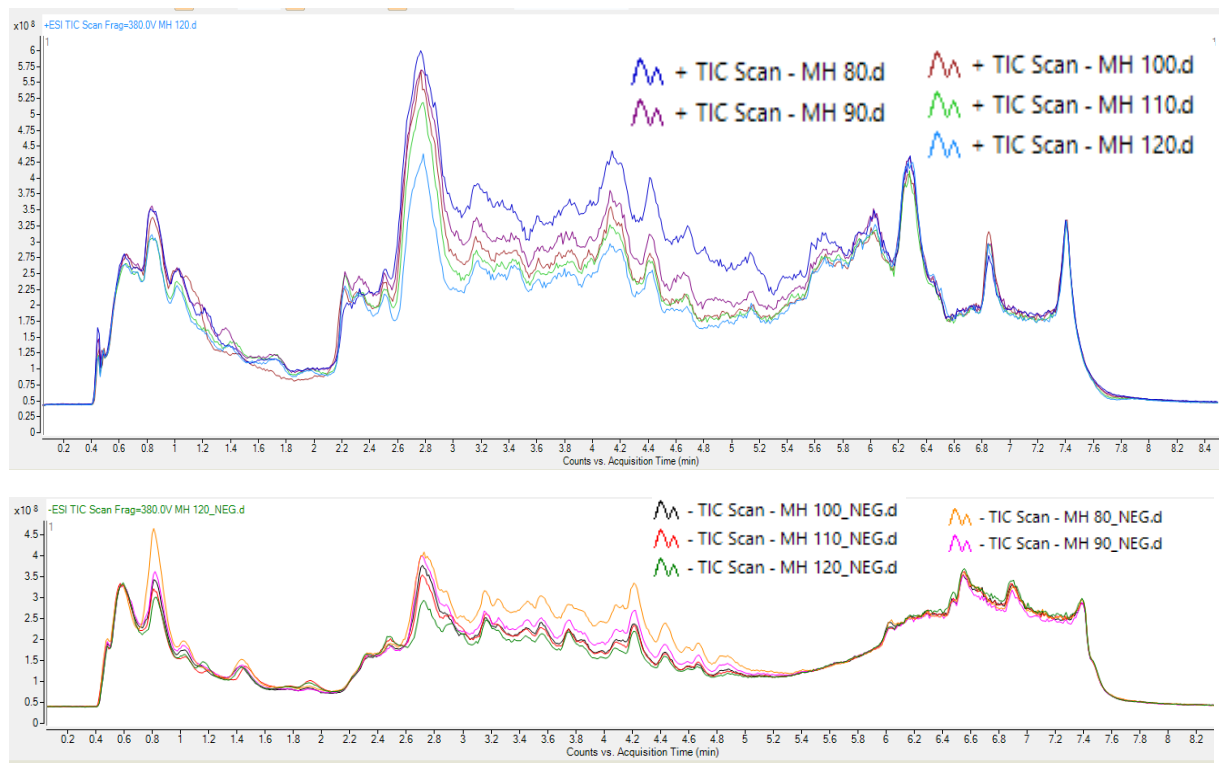
Appendix 12 Molecular Weight m (g/mol) vs Intrinsic viscosity (dL/g), Molecular Weight Distribution (WF/dLog MW) and Hydrodynamic Size (nm) Plot for LP0-160.



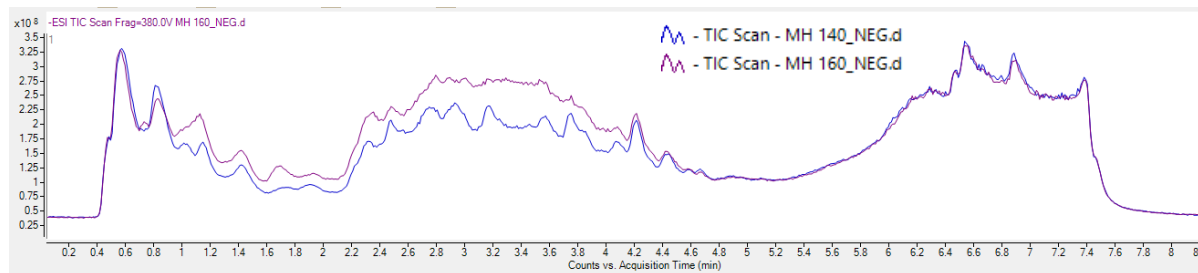
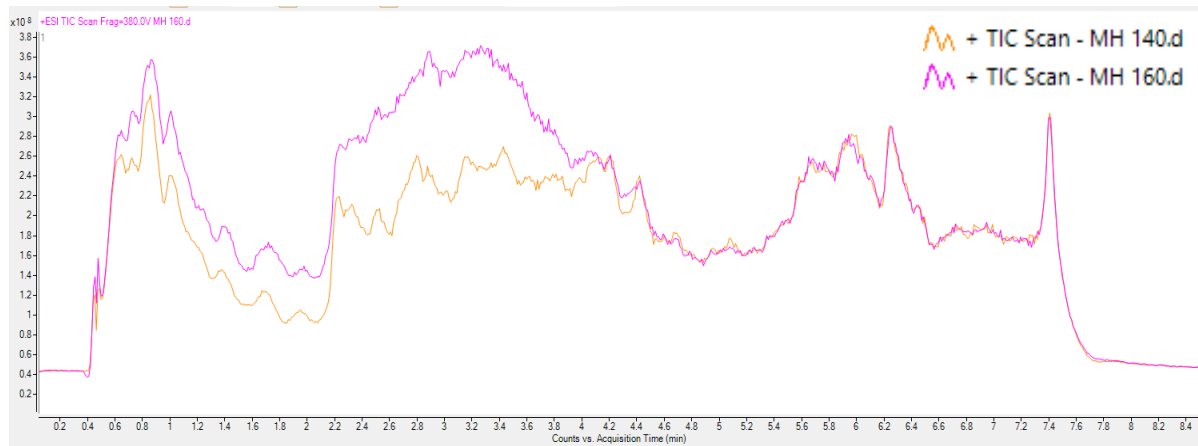
Appendix 13 BCP MH 50-70 positive (top) and negative (bottom) TIC overlay.



Appendix 14 BCP MH 80-120 positive (top) and negative (bottom) TIC overlay.



Appendix 15 BCP MH 140, 160 positive (top) and negative (bottom) TIC overlay



Appendix 16 BCP-MH-50 Positive

Label	Mass	RT	Width	Height	Score
Cpd 1: 2-Amino-3-methyl-1-butanol; C5 H13 N O; 0.588	103.0994	0.588	0.283	8363460	98.86
Cpd 2: bk-DMBDB; C13 H17 N O3; 0.623	235.1213	0.623	0.157	11160153	91.77
Cpd 3: Mefenamic acid metabolite; C15 H15 N O3; 0.854	257.1053	0.854	0.209	10789684	85.98
Cpd 4: Carboxymethyloxysuccinate; C6 H8 O7; 0.856	192.0275	0.856	0.142	8829891	98.05
Cpd 5: (S)-5'-Deoxy-5'-(methylsulfinyl) adenosine; C11 H15 N5 O4 S; 1.230	313.0847	1.23	0.123	8015550	76.49
Cpd 6: Delphinidin 3-glucoside; C21 H21 O12; 2.670	465.1037	2.67	0.14	12571685	97.8
Cpd 7: 5,7,8,3',4'-Pentahydroxyisoflavone; C15 H10 O7; 2.679	302.043	2.679	0.133	8092190	98.57
Cpd 8: Delphinidin 3-rhamnoside 5-glucoside; C27 H31 O16; 2.689	611.1617	2.689	0.154	15339518	99.3
Cpd 9: Kaempferol 7-O-glucoside; C21 H20 O11; 2.791	448.101	2.791	0.233	11074981	99.05
Cpd 10: Kaempferol; C15 H10 O6; 2.796	286.048	2.796	0.19	8993553	99.47
Cpd 11: Biorobin; C27 H30 O15; 2.814	594.1591	2.814	0.264	16443074	97.59
Cpd 12: 15-Acetoxyisoprene-3,4-diol 4-O-a-D-glucopyranoside; C23 H34 O11; 3.345	486.2084	3.345	0.127	8563971	87.95
Cpd 13: 2,6-Dimethyl-6-O-beta-D-quinovopyranosyl-7-octadecenoic acid; C16 H28 O7; 3.447	332.1838	3.447	0.129	10565001	97
Cpd 14: Withaperuvin B; C28 H40 O9; 4.142	520.2654	4.142	0.14	11141149	71.83
Cpd 15: Withaperuvin B; C28 H40 O9; 4.410	520.2657	4.41	0.146	8863352	91.25
Cpd 16: Eugenin; C11 H10 O4; 4.416	206.0583	4.416	0.122	8063819	99.08
Cpd 17: Acetyl tributyl citrate; C20 H34 O8; 6.253	402.2261	6.253	0.172	8798396	97.65
Cpd 18: Palmitic amide; C16 H33 N O; 6.474	255.257	6.474	0.075	8527150	96.75
Cpd 19: Stearamide; C18 H37 N O; 6.940	283.2879	6.94	0.243	8023426	83.73
Cpd 20: Oleamide; C18 H35 N O; 7.404	281.2724	7.404	0.14	8902995	83.45

Appendix 17 BCP-MH-50 Negative

Label	Mass	RT	Width	Height	Score
Cpd 1: sn-glycero-3-phosphoethanolamine; C5 H14 N O6 P; 0.511	215.0569	0.511	0.178	2211724	95.4
Cpd 2: Gulonic acid; C6 H12 O7; 0.546	196.0592	0.546	0.139	5128490	96.07
Cpd 3: L-Altruronic acid; C6 H10 O7; 0.554	194.0436	0.554	0.154	8008744	82.87
Cpd 4: Coriandrone C; C13 H10 O5; 0.573	246.0517	0.573	0.127	2145800	80.45
Cpd 5: 1,2-beta-D-Glucuronosyl-D-glucuronate; C12 H18 O13; 0.586	370.0761	0.586	0.176	1637011	91.67
Cpd 6: Valiolone; C7 H12 O6; 0.590	192.064	0.59	0.142	1932908	84.9
Cpd 7: Tetrahydro-2-methyl-3-thiophenethiol; C5 H10 S2; 0.658	134.0224	0.658	0.108	1802985	68.74
Cpd 8: 0.774	391.0599	0.774	0.115	43073984	
Cpd 9: C14 H12 N5 O7 S; 0.802	394.0464	0.802	0.104	1760334	83.7
Cpd 10: C10 H16 O16; 0.819	392.0428	0.819	0.13	15039763	81.41
Cpd 1: Gallic acid; C7 H6 O5; 1.439	170.0222	1.439	0.153	10855856	96.84
Cpd 2: (-)-Epigallocatechin 7-glucuronide; C21 H22 O13; 2.691	482.1062	2.691	0.138	6023479	99.6
Cpd 3: C22 H20 N13 O9; 2.701	610.151	2.701	0.15	10339582	72.13
Cpd 4: Delphinidin 3-glucosylglucoside; C27 H31 O17; 2.706	627.1572	2.706	0.138	11477425	95.81
Cpd 5: Luteolin 7-neohesperidoside; C27 H30 O15; 2.804	594.1582	2.804	0.14	9679446	78.63
Cpd 6: C21 H26 N9 O13; 2.819	612.164	2.819	0.177	8642021	89.87
Cpd 7: N-Benzooxazol-2-yl-guanidine; C8 H8 N4 O; 2.858	176.0692	2.858	0.157	6422807	92.08
Cpd 8: Phenylmalonic acid; C9 H8 O4; 2.998	180.0422	2.998	0.087	5633746	98.49
Cpd 9: Quercetin-3'-glucuronide; C21 H20 O13; 3.112	480.0913	3.112	0.09	6605382	79.3
Cpd 10: 2,2',3-Trihydroxy-3'-methoxy-5,5'-dicarboxybiphenyl; C15 H12 O8; 3.161	320.0542	3.161	0.083	6207380	95.18
Cpd 11: C9 H8 O3; 3.266	164.0488	3.266	0.128	5458572	77.44
Cpd 12: C7 H14 N3 O3; 3.559	188.1034	3.559	0.112	6002956	92.02
Cpd 13: Norwedelic acid; C15 H10 O8; 3.563	318.0371	3.563	0.174	9973254	89.18

Cpd 14: C15 H12 O9 S; 3.756	368.0205	3.756	0.111	8511407	97.81
Cpd 15: Rhynchosin; C15 H10 O7; 3.852	302.0427	3.852	0.147	7002210	99.52
Cpd 16: C19 H28 N4 O; 4.091	328.2265	4.091	0.137	7322230	82.48
Cpd 17: 17-hydroxyandrostane-3-glucuronide; C25 H40 O9; 4.147	484.2673	4.147	0.102	5502996	78.18
Cpd 18: 11,12,13-trihydroxy-9-octadecenoic acid; C18 H34 O5; 4.224	330.2405	4.224	0.107	11808968	98.17
Cpd 19: C19 H30 N4 O; 4.440	330.2424	4.44	0.108	8915962	94.31
Cpd 20: 8-HpODE; C18 H32 O4; 4.865	312.2304	4.865	0.115	5699078	84.81

Appendix 18 BCP-MH-60 Positive

Label	Mass	RT	Width	Height	Score
Cpd 1: 2-Amino-3-methyl-1-butanol; C5 H13 N O; 0.593	103.0994	0.593	0.286	8846351	99.03
Cpd 2: bk-DMBDB; C13 H17 N O3; 0.625	235.1216	0.625	0.159	10613652	89.48
Cpd 3: Carboxymethyloxysuccinate; C6 H8 O7; 0.856	192.0277	0.856	0.14	8357026	96.82
Cpd 4: bk-DMBDB; C13 H17 N O3; 0.866	235.1214	0.866	0.37	10138709	91.48
Cpd 5: L-Tyrosine; C9 H11 N O3; 0.896	181.0746	0.896	0.131	7599334	79.49
Cpd 6: (S)-5'-Deoxy-5'-(methylsulfinyl)adenosine; C11 H15 N5 O4 S; 1.222	313.0849	1.222	0.133	7561819	76.24
Cpd 7: Delphinidin 3-glucoside; C21 H21 O12; 2.676	465.1038	2.676	0.135	11509479	99.11
Cpd 8: Delphinidin 3-rhamnoside 5-glucoside; C27 H31 O16; 2.695	611.1618	2.695	0.154	15240598	98.14
Cpd 9: Cyanidin-3-O-(6-O-acetyl)pentoside; C21 H21 O11; 2.792	449.1088	2.792	0.21	10417551	99.48
Cpd 10: Kaempferol; C15 H10 O6; 2.797	286.0479	2.797	0.163	8373233	99.42
Cpd 11: Biorobin; C27 H30 O15; 2.813	594.1588	2.813	0.249	16102766	99.12
Cpd 12: Linalool 3,7-oxide beta-primeveroside; C21 H36 O11; 3.345	464.2264	3.345	0.136	8934976	95.09
Cpd 13: 2,6-Dimethyl-6-O-beta-D-quinovopyranosyl-7-octadecenoic acid; C16 H28 O7; 3.449	332.1838	3.449	0.136	10257765	95.52
Cpd 14: Withaperuvin B; C28 H40 O9; 4.141	520.2653	4.141	0.141	11585047	70.74
Cpd 15: Withaperuvin B; C28 H40 O9; 4.415	520.2664	4.415	0.157	9342923	68.02

Cpd 16: (6R)-3,6-Dimethyl-7-((8R,Z)-8-methylhexahydroindolizin-6(5H)-ylidene)heptane-1,2-diol; C18 H33 N O2; 5.654	295.2516	5.654	0.115	7818948	79.7
Cpd 17: Cinitapride; C21 H30 N4 O4; 6.252	402.2262	6.252	0.171	8471087	98.81
Cpd 18: Palmitic amide; C16 H33 N O; 6.473	255.2569	6.473	0.072	8561104	96.81
Cpd 19: Stearamide; C18 H37 N O; 6.943	283.288	6.943	0.247	8010791	94.48
Cpd 20: Oleamide; C18 H35 N O; 7.403	281.2723	7.403	0.145	8789271	84.1

Appendix 19 BCP-MH-60 Negative

Label	Mass	RT	Width	Height	Score
Cpd 1: sn-glycero-3-phosphoethanolamine; C5 H14 N O6 P; 0.513	215.0568	0.513	0.179	2081577	95.34
Cpd 2: Gulonic acid; C6 H12 O7; 0.547	196.0592	0.547	0.14	5528767	96.02
Cpd 3: L-Altruronic acid; C6 H10 O7; 0.554	194.0434	0.554	0.158	7930782	84.23
Cpd 4: Coriandrone C; C13 H10 O5; 0.573	246.0517	0.573	0.129	2022066	80.84
Cpd 5: Valiolone; C7 H12 O6; 0.589	192.064	0.589	0.144	1959676	84.89
Cpd 6: Tetrahydro-2-methyl-3-thiophenethiol; C5 H10 S2; 0.657	134.0224	0.657	0.11	1876172	68.74
Cpd 7: Asn-Asn-OH; C13 H14 N4 O8; 0.718	354.0806	0.718	0.1	1707767	90.99
Cpd 8: C14 H12 N5 O7 S; 0.798	394.0463	0.798	0.107	1825100	69.26
Cpd 9: C4 H8 N4 O3 S; 0.860	192.0316	0.86	0.172	16073302	70.93
Cpd 10: C12 H12 N3 O13; 0.896	406.0364	0.896	0.147	2137944	96.81
Cpd 1: Gallic acid; C7 H6 O5; 1.435	170.0222	1.435	0.162	10790202	96.82
Cpd 2: 2,4-Dihydroxybenzoic acid; C7 H6 O4; 2.480	154.027	2.48	0.087	4937556	99.24
Cpd 3: (-)-Epigallocatechin 7-glucuronide; C21 H22 O13; 2.699	482.1062	2.699	0.133	4985372	99.35
Cpd 4: Kaempferol 3-O-β-D-glucosyl-(1->2)-β-D-glucoside; C27 H30 O16; 2.706	610.1525	2.706	0.146	10015909	72.86
Cpd 5: C21 H27 N9 O14; 2.710	629.1675	2.71	0.116	5911151	97.58
Cpd 6: 2.714	626.1485	2.714	0.136	11036130	
Cpd 7: Luteolin 7-neohesperidoside; C27 H30 O15; 2.806	594.1579	2.806	0.135	9055070	69.69

Cpd 8: C22 H32 N2 O18; 2.819	612.1644	2.819	0.166	8096890	96.06
Cpd 9: 3-Isopropylmalic acid; C7 H12 O5; 2.857	176.0688	2.857	0.157	6748129	93.61
Cpd 10: 5-(4-Acetoxybut-1-ynyl)-2,2'-bithiophene; C14 H12 O2 S2; 2.896	276.0265	2.896	0.114	5424604	69.19
Cpd 11: Phenylmalonic acid; C9 H8 O4; 2.997	180.0425	2.997	0.089	5098232	97.88
Cpd 12: Quercetin-3'-glucuronide; C21 H20 O13; 3.112	480.091	3.112	0.145	5893399	85.64
Cpd 13: 2,2',3-Trihydroxy-3'-methoxy-5,5'-dicarboxybiphenyl; C15 H12 O8; 3.161	320.0542	3.161	0.08	6604758	94.55
Cpd 14: 3-Methylsuberic acid; C9 H16 O4; 3.559	188.1054	3.559	0.113	6191680	98.08
Cpd 15: Norwedelic acid; C15 H10 O8; 3.569	318.0372	3.569	0.165	8890297	97.07
Cpd 16: C15 H12 O9 S; 3.758	368.0204	3.758	0.103	7630386	98.99
Cpd 17: 9,12,13-trihydroxy-10,15-octadecadienoic acid; C18 H32 O5; 4.090	328.2249	4.09	0.138	7053166	84.32
Cpd 18: 17-hydroxyandrostane-3-glucuronide; C25 H40 O9; 4.149	484.2678	4.149	0.107	5840588	82.28
Cpd 19: 11,12,13-trihydroxy-9-octadecenoic acid; C18 H34 O5; 4.223	330.2405	4.223	0.103	11147443	98.3
Cpd 20: C19 H30 N4 O; 4.440	330.2422	4.44	0.105	8149685	96.01

Appendix 20 BCP-MH-70 Positive

Label	Mass	RT	Width	Height	Score
Cpd 1: 2-Amino-3-methyl-1-butanol; C5 H13 N O; 0.598	103.0995	0.598	0.313	8965584	99.33
Cpd 2: bk-DMBDB; C13 H17 N O3; 0.624	235.121	0.624	0.153	9912412	91.87
Cpd 3: Mefenamic acid metabolite; C15 H15 N O3; 0.852	257.105	0.852	0.228	8998760	89.73
Cpd 4: Carboxymethyloxysuccinate; C6 H8 O7; 0.854	192.0277	0.854	0.176	8509456	96.94
Cpd 5: (S)-5'-Deoxy-5'-(methylsulfinyl)adenosine; C11 H15 N5 O4 S; 1.223	313.0849	1.223	0.133	8129584	76.28
Cpd 6: 2.221	102.0473	2.221	0.093	7786305	
Cpd 7: Delphinidin 3-glucoside; C21 H21 O12; 2.674	465.1038	2.674	0.136	11944605	99.1
Cpd 8: Delphinidin 3-rhamnoside 5-glucoside; C27 H31 O16; 2.693	611.1617	2.693	0.208	15363090	98.98
Cpd 9: Cyanidin-3-O-(6-O-acetyl)pentoside; C21 H21 O11; 2.792	449.1088	2.792	0.229	10825373	99.26

Cpd 10: Kaempferol; C15 H10 O6; 2.798	286.048	2.798	0.159	8420502	99.13
Cpd 11: Luteolin 3'-methyl ether 7-arabinosyl-(1->2)-galactoside; C27 H30 O15; 2.815	594.1583	2.815	0.267	16061504	97.74
Cpd 12: Glucosylgalactosyl hydroxylysine; C18 H34 N2 O13; 3.346	486.2084	3.346	0.137	8607316	87.97
Cpd 13: 2,6-Dimethyl-6-O-beta-D-quinovopyranosyl-7-octadecenoic acid; C16 H28 O7; 3.448	332.1838	3.448	0.137	10422333	96.08
Cpd 14: Withaperuvin B; C28 H40 O9; 4.144	520.2656	4.144	0.142	11327804	73.62
Cpd 15: Withaperuvin B; C28 H40 O9; 4.414	520.2658	4.414	0.148	9510527	68.41
Cpd 16: (6R)-3,6-Dimethyl-7-((8R,Z)-8-methylhexahydroindolizin-6(5H)-ylidene)heptane-1,2-diol; C18 H33 N O2; 5.657	295.2517	5.657	0.113	7881637	83.96
Cpd 17: Acetyl tributyl citrate; C20 H34 O8; 6.253	402.2261	6.253	0.17	8517791	98.46
Cpd 18: Palmitic amide; C16 H33 N O; 6.473	255.2569	6.473	0.076	8322457	96.92
Cpd 19: Stearamide; C18 H37 N O; 6.937	283.288	6.937	0.246	7798466	97.26
Cpd 20: 3,4-Epoxy-6,9-octadecadiene; C18 H32 O; 7.401	264.2458	7.401	0.156	8919982	84.73

Appendix 21 BCP-MH-70 Negative

Label	Mass	RT	Width	Height	Score
Cpd 1: Gulonic acid; C6 H12 O7; 0.546	196.0591	0.546	0.137	5025960	96.5
Cpd 2: L-Altruronic acid; C6 H10 O7; 0.554	194.0435	0.554	0.162	7934167	82.7
Cpd 3: Phosphatidyl glycerol; C6 H15 O8 P; 0.573	246.0516	0.573	0.127	1992725	95.03
Cpd 4: 1,2-beta-D-Glucuronosyl-D-glucuronate; C12 H18 O13; 0.588	370.076	0.588	0.177	1718888	92.56
Cpd 5: Valiolone; C7 H12 O6; 0.589	192.0641	0.589	0.141	1833626	84.69
Cpd 6: 9,10-dibromo-stearic acid; C18 H34 Br2 O2; 0.595	440.092	0.595	0.126	1790721	68.29
Cpd 7: Tetrahydro-2-methyl-3-thiophenethiol; C5 H10 S2; 0.658	134.0224	0.658	0.11	1912847	68.68
Cpd 8: C14 H12 N5 O7 S; 0.800	394.046	0.8	0.11	1785301	69.03

Cpd 9: 3-Methyl-2,5-furandione; C5 H4 O3; 0.847	112.0164	0.847	0.151	4330582	86.87
Cpd 10: C12 H12 N3 O13; 0.894	406.0362	0.894	0.143	2161537	97.85
Cpd 1: Gallic acid; C7 H6 O5; 1.438	170.0222	1.438	0.155	10495853	97.21
Cpd 2: 2,4-Dihydroxybenzoic acid; C7 H6 O4; 2.481	154.0268	2.481	0.085	4800928	99.71
Cpd 3: (-)-Epigallocatechin 7-glucuronide; C21 H22 O13; 2.696	482.1061	2.696	0.134	5403884	99.44
Cpd 4: Kaempferol 3-O- β -D-glucosyl-(1->2)- β -D-glucoside; C27 H30 O16; 2.704	610.1519	2.704	0.146	10078628	69.62
Cpd 5: C21 H27 N9 O14; 2.709	629.1676	2.709	0.117	6033551	97.94
Cpd 6: 2.713	626.1487	2.713	0.137	11095666	
Cpd 7: Luteolin 7-neohesperidoside; C27 H30 O15; 2.805	594.1568	2.805	0.146	9135173	66.55
Cpd 8: C22 H32 N2 O18; 2.819	612.165	2.819	0.172	8293390	97.4
Cpd 9: 3-Isopropylmalic acid; C7 H12 O5; 2.855	176.0685	2.855	0.143	6264022	94.39
Cpd 10: Brompheniramine (didemethylated); C14 H15 Br N2; 2.896	290.0418	2.896	0.107	6158214	61.59
Cpd 11: Quercetin-3'-glucuronide; C21 H20 O13; 3.111	480.0905	3.111	0.089	6388868	82.47
Cpd 12: C15 H12 O8; 3.162	320.0522	3.162	0.082	6448423	95.23
Cpd 13: 3-Methylsuberic acid; C9 H16 O4; 3.559	188.1053	3.559	0.114	5781127	98.98
Cpd 14: Norwedelic acid; C15 H10 O8; 3.567	318.0369	3.567	0.18	9452855	95.56
Cpd 15: C15 H12 O9 S; 3.756	368.0203	3.756	0.107	8129832	98.92
Cpd 16: Quercetin; C15 H10 O7; 3.850	302.0425	3.85	0.141	5725391	99.41
Cpd 17: (9R,10S,12Z)-9,10-Dihydroxy-8-oxo-12-octadecenoic acid; C18 H32 O5; 4.087	328.2249	4.087	0.138	6886983	84.54
Cpd 18: 17-hydroxyandrostane-3-glucuronide; C25 H40 O9; 4.143	484.2674	4.143	0.102	5406848	98.15
Cpd 19: 9S,10S,11R-trihydroxy-12Z-octadecenoic acid; C18 H34 O5; 4.221	330.2404	4.221	0.104	11215909	98.17
Cpd 20: 9S,10S,11R-trihydroxy-12Z-octadecenoic acid; C18 H34 O5; 4.438	330.242	4.438	0.105	7937279	90.67

Appendix 22 BCP-MH-80 Positive

Label	Mass	RT	Width	Height	Score
Cpd 1: 2-Amino-3-methyl-1-butanol; C5 H13 N O; 0.582	103.0998	0.582	0.302	9060698	99.74
Cpd 2: bk-DMBDB; C13 H17 N O3; 0.619	235.1216	0.619	0.15	10498961	89.83
Cpd 3: 0.729	118.0284	0.729	0.083	7865860	
Cpd 4: 0.853	214.0096	0.853	0.139	9203772	
Cpd 5: (S)-5'-Deoxy-5'-(methylsulfinyl)adenosine; C11 H15 N5 O4 S; 1.223	313.0842	1.223	0.122	8026598	69.56
Cpd 6: 2.226	102.0472	2.226	0.093	7612130	
Cpd 7: 4-Amino-2-methyl-1-naphthol; C11 H11 N O; 2.521	173.0847	2.521	0.087	7587543	98.01
Cpd 8: Hyperoside; C21 H20 O12; 2.672	464.0959	2.672	0.138	11645791	95.99
Cpd 9: Delphinidin 3-rhamnoside 5-glucoside; C27 H31 O16; 2.691	611.1616	2.691	0.152	15188502	98.09
Cpd 10: Cyanidin-3-O-(6-O-acetyl)pentoside; C21 H21 O11; 2.792	449.1088	2.792	0.219	10689815	98.43
Cpd 11: Kaempferol; C15 H10 O6; 2.799	286.048	2.799	0.176	7797030	99.11
Cpd 12: Biorobin; C27 H30 O15; 2.814	594.1592	2.814	0.237	15805332	98.98
Cpd 13: 15-Acetoxy-scirpene-3,4-diol 4-O- α -D-glucopyranoside; C23 H34 O11; 3.344	486.2084	3.344	0.117	7508904	88.31
Cpd 14: 2,6-Dimethyl-6-O-beta-D-quinovopyranosyl-7-octadecenoic acid; C16 H28 O7; 3.447	332.1838	3.447	0.132	9032520	98.2
Cpd 15: Withaperuvin B; C28 H40 O9; 4.142	520.2655	4.142	0.139	10665418	71.77
Cpd 16: Withaperuvin B; C28 H40 O9; 4.410	520.2657	4.41	0.128	8742552	94.06
Cpd 17: (6R)-3,6-Dimethyl-7-((8R,Z)-8-methylhexahydroindolizin-6(5H)-ylidene)heptane-1,2-diol; C18 H33 N O2; 5.675	295.2516	5.675	0.294	9316060	85.24
Cpd 18: Palmitic amide; C16 H33 N O; 6.472	255.2569	6.472	0.088	8417880	97.11
Cpd 19: Stearamide; C18 H37 N O; 6.939	283.288	6.939	0.245	7401249	98.62
Cpd 20: Oleamide; C18 H35 N O; 7.405	281.2723	7.405	0.13	8313464	85.53

Appendix 23 BCP-MH-80 Negative

Label	Mass	RT	Width	Height	Score
Cpd 1: Gulonic acid; C6 H12 O7; 0.544	196.0591	0.544	0.137	4724674	96.74
Cpd 2: D-Glucuronic acid; C6 H10 O7; 0.555	194.0436	0.555	0.165	7092433	82.35
Cpd 3: 9,10-dibromo-stearic acid; C18 H34 Br2 O2; 0.599	440.0919	0.599	0.117	3041964	68.79
Cpd 4: Tetrahydro-2-methyl-3-thiophenethiol; C5 H10 S2; 0.661	134.0229	0.661	0.11	2069995	77.92
Cpd 5: 0.756	391.0812	0.756	0.056	13393719	
Cpd 6: C22 H9 N4 O2 S; 0.802	393.0442	0.802	0.101	5817096	90.71
Cpd 7: 0.818	391.0441	0.818	0.116	14719474	
Cpd 8: 3-Methyl-2,5-furandione; C5 H4 O3; 0.845	112.0165	0.845	0.144	4174773	86.59
Cpd 9: C12 H4 N2 O; 0.854	192.0311	0.854	0.166	15891592	80.79
Cpd 10: C12 H12 N3 O13; 0.884	406.0364	0.884	0.146	2576030	97.33
Cpd 1: Gallic acid; C7 H6 O5; 1.434	170.0222	1.434	0.152	10027614	96.94
Cpd 2: 2,4-Dihydroxybenzoic acid; C7 H6 O4; 2.480	154.0271	2.48	0.085	4262770	98.6
Cpd 3: (-)-Epigallocatechin 7-glucuronide; C21 H22 O13; 2.694	482.106	2.694	0.133	4690466	99.61
Cpd 4: C20 H18 N16 O8; 2.702	610.1491	2.702	0.145	9634390	71.11
Cpd 5: Delphinidin 3-glucosylglucoside; C27 H31 O17; 2.707	627.1566	2.707	0.134	11063231	97.74
Cpd 6: Kuwanon Z; C34 H26 O10; 2.802	594.1554	2.802	0.134	8960978	61.75
Cpd 7: C20 H20 N16 O8; 2.818	612.1641	2.818	0.169	8084794	93.92
Cpd 8: Brompheniramine (didemethylated); C14 H15 Br N2; 2.896	290.0418	2.896	0.108	6083316	61.48
Cpd 9: Quercetin-3'-glucuronide; C21 H20 O13; 3.112	480.0907	3.112	0.078	5784276	87.07
Cpd 10: 2,2',3-Trihydroxy-3'-methoxy-5,5'-dicarboxybiphenyl; C15 H12 O8; 3.162	320.0545	3.162	0.087	5657216	91.05
Cpd 11: 3-Methylsuberic acid; C9 H16 O4; 3.558	188.1051	3.558	0.071	4703430	99.43
Cpd 12: Myricetin; C15 H10 O8; 3.572	318.0378	3.572	0.162	6909743	96.67
Cpd 13: C15 H12 O9 S; 3.756	368.0204	3.756	0.112	9746564	99.14

Cpd 14: Quercetin; C15 H10 O7; 3.851	302.0425	3.851	0.142	4463222	99.48
Cpd 15: 9,12,13-trihydroxy-10,15-octadecadienoic acid; C18 H32 O5; 4.090	328.225	4.09	0.135	6916427	84.89
Cpd 16: 17-hydroxyandrostane-3-glucuronide; C25 H40 O9; 4.145	484.2673	4.145	0.108	5346648	78.21
Cpd 17: 11,12,13-trihydroxy-9-octadecenoic acid; C18 H34 O5; 4.224	330.2406	4.224	0.103	11309252	85.26
Cpd 18: 9S,10S,11R-trihydroxy-12Z-octadecenoic acid; C18 H34 O5; 4.439	330.242	4.439	0.105	7917022	91.25
Cpd 19: Lauryl hydrogen sulfate; C12 H26 O4 S; 6.035	266.1556	6.035	0.129	7885176	97.62
Cpd 20: C17 H27 Cl N2 O; 6.667	310.1811	6.667	0.131	5800606	80

Appendix 24 BCP-MH-90 Positive

Label	Mass	RT	Width	Height	Score
Cpd 1: 2-Amino-3-methyl-1-butanol; C5 H13 N O; 0.576	103.0996	0.576	0.333	10589851	99.43
Cpd 2: Dihydrocaffeic acid 3-O-glucuronide; C15 H18 O10; 0.618	358.0905	0.618	0.201	9875110	79.5
Cpd 3: bk-DMBDB; C13 H17 N O3; 0.622	235.1216	0.622	0.148	7271737	93.14
Cpd 4: Carboxymethyloxysuccinate; C6 H8 O7; 0.852	192.0277	0.852	0.141	8037768	97.13
Cpd 5: Phenylacrylic acid (Cinnamic acid); C9 H8 O2; 2.228	148.0527	2.228	0.114	7574513	99.32
Cpd 6: 2.230	102.0472	2.23	0.107	11487611	
Cpd 7: 2.338	436.1558	2.338	0.103	7181474	
Cpd 8: 4-Amino-2-methyl-1-naphthol; C11 H11 N O; 2.523	173.0846	2.523	0.084	7310545	98.15
Cpd 9: Delphinidin 3-glucoside; C21 H21 O12; 2.679	465.1038	2.679	0.135	11196059	99.06
Cpd 10: Delphinidin 3-rhamnoside 5-glucoside; C27 H31 O16; 2.697	611.1617	2.697	0.152	14936208	99.52
Cpd 11: Kaempferol 7-O-glucoside; C21 H20 O11; 2.796	448.1009	2.796	0.216	10599666	99.53
Cpd 12: Kaempferol; C15 H10 O6; 2.801	286.048	2.801	0.148	7622397	99.27
Cpd 13: Biorobin; C27 H30 O15; 2.815	594.159	2.815	0.223	15733067	99.12
Cpd 14: 2,6-Dimethyl-6-O-beta-D-quinovopyranosyl-7-octadecenoic acid; C16 H28 O7; 3.450	332.1839	3.45	0.133	9113065	96.52

Cpd 15: Withaperuvin B; C28 H40 O9; 4.140	520.2655	4.14	0.142	10605396	72.04
Cpd 16: Withaperuvin B; C28 H40 O9; 4.413	520.2655	4.413	0.129	8806995	79.4
Cpd 17: (6R)-3,6-Dimethyl-7-((8R,Z)-8-methylhexahydroindolizin-6(5H)-ylidene)heptane-1,2-diol; C18 H33 N O2; 5.654	295.2517	5.654	0.107	7853686	84.17
Cpd 18: Palmitic amide; C16 H33 N O; 6.473	255.2569	6.473	0.081	8549000	97
Cpd 19: Stearamide; C18 H37 N O; 6.938	283.2879	6.938	0.241	7494265	98.83
Cpd 20: Oleamide; C18 H35 N O; 7.400	281.2724	7.4	0.165	8412605	85.28

Appendix 25 BCP-MH-90 Negative

Label	Mass	RT	Width	Height	Score
Cpd 1: Hamamelose; C6 H12 O7; 0.540	196.0591	0.54	0.136	4740292	97.04
Cpd 2: L-Altruronic acid; C6 H10 O7; 0.549	194.0434	0.549	0.151	6186248	83.93
Cpd 3: 1,4-beta-D-Glucan; C18 H32 O18; 0.581	536.1602	0.581	0.128	2890244	73.91
Cpd 4: C13 H19 Cl N4 O7; 0.588	378.0937	0.588	0.133	2649897	97.98
Cpd 5: 9,10-dibromo-stearic acid; C18 H34 Br2 O2; 0.601	440.0914	0.601	0.127	5310341	64.94
Cpd 6: 2-O-a-D-Galactopyranuronosyl-L-rhamnose; C12 H22 O11; 0.648	342.1167	0.648	0.153	3989832	98.99
Cpd 7: Tetrahydro-2-methyl-3-thiophenethiol; C5 H10 S2; 0.666	134.0223	0.666	0.114	2480757	68.69
Cpd 8: 0.805	391.0441	0.805	0.116	10294694	
Cpd 9: 3-Methyl-2,5-furandione; C5 H4 O3; 0.842	112.0164	0.842	0.146	4185402	86.8
Cpd 1: 2,4,6-Trihydroxybenzoic acid; C7 H6 O5; 1.434	170.0221	1.434	0.134	8653697	97.75
Cpd 2: 3-Acetylthiophene; C6 H6 O S; 2.674	126.014	2.674	0.086	4390458	78.31
Cpd 3: C22 H20 N13 O9; 2.707	610.1506	2.707	0.148	8678133	72.3
Cpd 4: C21 H27 N9 O14; 2.711	629.1675	2.711	0.119	4683400	98.06
Cpd 5: Delphinidin 3-glucosylglucoside; C27 H31 O17; 2.712	627.1572	2.712	0.136	9905014	45.99
Cpd 6: 6,8-Di-C-glucopyranosyltricetin; C27 H30 O17; 2.731	626.1488	2.731	0.088	5252970	74.48

Cpd 7: C ₂₄ H ₃₀ N ₆ O ₈ S ₂ ; 2.804	594.1568	2.804	0.127	8291208	82.37
Cpd 8: C ₂₂ H ₃₂ N ₂ O ₁₈ ; 2.821	612.1653	2.821	0.16	7621250	97.66
Cpd 9: 5-(4-Acetoxybut-1-ynyl)-2,2'-bithiophene; C ₁₄ H ₁₂ O ₂ S ₂ ; 2.894	276.0265	2.894	0.104	5278366	67.52
Cpd 10: Quercetin-3'-glucuronide; C ₂₁ H ₂₀ O ₁₃ ; 3.113	480.0906	3.113	0.08	5053886	97.22
Cpd 11: 2,2',3-Trihydroxy-3'-methoxy-5,5'-dicarboxybiphenyl; C ₁₅ H ₁₂ O ₈ ; 3.161	320.054	3.161	0.083	4541946	97.05
Cpd 12: Norwedelic acid; C ₁₅ H ₁₀ O ₈ ; 3.571	318.0375	3.571	0.139	5753409	98.29
Cpd 13: C ₁₅ H ₁₂ O ₉ S; 3.756	368.0198	3.756	0.113	9737935	98.43
Cpd 14: 9,12,13-trihydroxy-10,15-octadecadienoic acid; C ₁₈ H ₃₂ O ₅ ; 4.088	328.225	4.088	0.128	5609551	84.96
Cpd 15: C ₂₈ H ₄₈ O ₆ S ₂ ; 4.145	544.2896	4.145	0.113	4206164	86.19
Cpd 16: 9S,10S,11R-trihydroxy-12Z-octadecenoic acid; C ₁₈ H ₃₄ O ₅ ; 4.221	330.2407	4.221	0.098	10233892	85.24
Cpd 17: 11,12,13-trihydroxy-9-octadecenoic acid; C ₁₈ H ₃₄ O ₅ ; 4.437	330.2408	4.437	0.102	6274320	99.62
Cpd 18: Lauryl hydrogen sulfate; C ₁₂ H ₂₆ O ₄ S; 6.033	266.1556	6.033	0.097	6271741	98.24
Cpd 19: 6.560	117.9362	6.56	0.162	4452398	
Cpd 20: C ₁₄ H ₃₀ Cl ₂ N ₃ ; 6.664	310.1809	6.664	0.135	4281550	82.2

Appendix 26 BCP-MH-100 Positive

Label	Mass	RT	Width	Height	Score
Cpd 1: Dihydrocaffeic acid 3-O-glucuronide; C ₁₅ H ₁₈ O ₁₀ ; 0.626	358.0904	0.626	0.204	10054947	78.53
Cpd 2: Carboxymethyloxysuccinate; C ₆ H ₈ O ₇ ; 0.855	192.0279	0.855	0.144	7802392	95.06
Cpd 3: (S)-5'-Deoxy-5'-(methylsulfinyl)adenosine; C ₁₁ H ₁₅ N ₅ O ₄ S; 1.094	313.0848	1.094	0.087	8131662	71.48
Cpd 4: Adenosine; C ₁₀ H ₁₃ N ₅ O ₄ ; 1.174	267.0967	1.174	0.108	8298248	97.24
Cpd 5: Phenylacrylic acid (Cinnamic acid); C ₉ H ₈ O ₂ ; 2.213	148.0526	2.213	0.115	7925220	99.57
Cpd 6: 2.215	102.0472	2.215	0.11	11609812	
Cpd 7: 2.328	436.1558	2.328	0.107	7818800	
Cpd 8: 4-Amino-2-methyl-1-naphthol; C ₁₁ H ₁₁ N O; 2.519	173.0847	2.519	0.086	7888481	97.86

Cpd 9: Delphinidin 3-glucoside; C21 H21 O12; 2.680	465.1036	2.68	0.137	12083729	99.29
Cpd 10: 5,7,8,3',4'-Pentahydroxyisoflavone; C15 H10 O7; 2.688	302.043	2.688	0.126	7566766	98.77
Cpd 11: Delphinidin 3-rhamnoside 5-glucoside; C27 H31 O16; 2.699	611.1616	2.699	0.153	14507546	99.22
Cpd 12: Cyanidin-3-O-(6-O-acetyl)pentoside; C21 H21 O11; 2.797	449.1088	2.797	0.202	10959584	99.28
Cpd 13: Kaempferol; C15 H10 O6; 2.802	286.048	2.802	0.154	7500514	99.2
Cpd 14: Isopeonidin 3-sambubioside; C27 H31 O15; 2.816	595.1669	2.816	0.217	15552659	98.48
Cpd 15: Valganciclovir; C14 H22 N6 O5; 3.451	354.166	3.451	0.134	9575049	93.47
Cpd 16: Withaperuvin B; C28 H40 O9; 4.139	520.2655	4.139	0.141	10506731	71.2
Cpd 17: Withaperuvin B; C28 H40 O9; 4.413	520.2657	4.413	0.133	8807576	70.8
Cpd 18: (6R)-3,6-Dimethyl-7-((8R,Z)-8-methylhexahydroindolizin-6(5H)-ylidene)heptane-1,2-diol; C18 H33 N O2; 5.707	295.2517	5.707	0.299	7770235	83.93
Cpd 19: Palmitic amide; C16 H33 N O; 6.472	255.2569	6.472	0.092	8356794	96.98
Cpd 20: Oleamide; C18 H35 N O; 7.401	281.2723	7.401	0.168	8103762	84.03

Appendix 27 BCP-MH-100 Negative

Label	Mass	RT	Width	Height	Score
Cpd 1: Hamamelose; C6 H12 O7; 0.540	196.0591	0.54	0.137	4745847	96.59
Cpd 2: L-Altruronic acid; C6 H10 O7; 0.550	194.0434	0.55	0.157	6213776	83.58
Cpd 3: 1,4-beta-D-Glucan; C18 H32 O18; 0.583	536.1604	0.583	0.13	2943022	73.64
Cpd 4: C12 H23 Cl O11; 0.589	378.0936	0.589	0.129	2634250	93.88
Cpd 5: 9,10-dibromo-stearic acid; C18 H34 Br2 O2; 0.600	440.0917	0.6	0.128	5328315	66.47
Cpd 6: 2-O-a-D-Galactopyranuronosyl-L-rhamnose; C12 H22 O11; 0.643	342.1167	0.643	0.154	4214340	99.06
Cpd 7: Tetrahydro-2-methyl-3-thiophenethiol; C5 H10 S2; 0.665	134.0224	0.665	0.113	2327670	68.67
Cpd 8: 0.804	391.044	0.804	0.117	9550070	
Cpd 9: 3-Methyl-2,5-furandione; C5 H4 O3; 0.839	112.0164	0.839	0.159	4059899	86.68

Cpd 10: C ₄ H ₈ N ₄ O ₃ S; 0.847	192.0314	0.847	0.174	15948218	74.1
Cpd 1: 2,4,6-Trihydroxybenzoic acid; C ₇ H ₆ O ₅ ; 1.423	170.022	1.423	0.14	8644203	97.97
Cpd 2: (-)-Epigallocatechin 7-glucuronide; C ₂₁ H ₂₂ O ₁₃ ; 2.697	482.1058	2.697	0.137	4318782	99.17
Cpd 3: C ₂₂ H ₂₀ N ₁₃ O ₉ ; 2.707	610.1504	2.707	0.141	7851936	71.86
Cpd 4: Delphinidin 3-glucosylglucoside; C ₂₇ H ₃₁ O ₁₇ ; 2.711	627.1574	2.711	0.126	9129044	97.41
Cpd 5: Quercetin-3'-glucuronide; C ₂₁ H ₂₀ O ₁₃ ; 2.717	480.0905	2.717	0.085	4922922	80.1
Cpd 6: 6,8-Di-C-glucopyranosyltricetin; C ₂₇ H ₃₀ O ₁₇ ; 2.731	626.1485	2.731	0.089	6105598	74.85
Cpd 7: Kuwanon Z; C ₃₄ H ₂₆ O ₁₀ ; 2.804	594.1562	2.804	0.121	7274180	55.29
Cpd 8: C ₂₂ H ₃₂ N ₂ O ₁₈ ; 2.819	612.1657	2.819	0.152	6556909	97.18
Cpd 9: 5-(4-Acetoxybut-1-ynyl)-2,2'-bithiophene; C ₁₄ H ₁₂ O ₂ S ₂ ; 2.893	276.0267	2.893	0.094	4484414	70.06
Cpd 10: 2,2',3-Trihydroxy-3'-methoxy-5,5'-dicarboxybiphenyl; C ₁₅ H ₁₂ O ₈ ; 2.954	320.0536	2.954	0.096	4656806	99.35
Cpd 11: Quercetin-3'-glucuronide; C ₂₁ H ₂₀ O ₁₃ ; 3.113	480.0909	3.113	0.08	3927760	85.81
Cpd 12: Norwedelic acid; C ₁₅ H ₁₀ O ₈ ; 3.573	318.0375	3.573	0.157	7037726	97.66
Cpd 13: C ₁₅ H ₁₂ O ₉ S; 3.757	368.0201	3.757	0.106	8981554	99.2
Cpd 14: Rhynchosin; C ₁₅ H ₁₀ O ₇ ; 3.866	302.0428	3.866	0.135	4146918	99.32
Cpd 15: (9R,10S,12Z)-9,10-Dihydroxy-8-oxo-12-octadecenoic acid; C ₁₈ H ₃₂ O ₅ ; 4.091	328.2251	4.091	0.127	4946236	85.13
Cpd 16: 17-hydroxyandrostane-3-glucuronide; C ₂₅ H ₄₀ O ₉ ; 4.145	484.2674	4.145	0.11	3817121	78.04
Cpd 17: 9S,10S,11R-trihydroxy-12Z-octadecenoic acid; C ₁₈ H ₃₄ O ₅ ; 4.223	330.2408	4.223	0.094	9442085	85.27
Cpd 18: 11,12,13-trihydroxy-9-octadecenoic acid; C ₁₈ H ₃₄ O ₅ ; 4.440	330.2408	4.44	0.1	5550240	99.43
Cpd 19: Lauryl hydrogen sulfate; C ₁₂ H ₂₆ O ₄ S; 6.028	266.1556	6.028	0.135	7559638	97.99
Cpd 20: C ₁₇ H ₂₇ Cl N ₂ O; 6.661	310.1813	6.661	0.129	6064296	85.9

Appendix 28 BCP-MH-110 Positive

Label	Mass	RT	Width	Height	Score
-------	------	----	-------	--------	-------

Cpd 1: 0.591	103.0987	0.591	0.368	11381903	
Cpd 2: Dihydrocaffeic acid 3-O-glucuronide; C15 H18 O10; 0.619	358.0905	0.619	0.208	10295645	77.99
Cpd 3: 0.738	135.0551	0.738	0.148	7377796	
Cpd 4: Phenylacrylic acid (Cinnamic acid); C9 H8 O2; 2.228	148.0526	2.228	0.12	8603578	99.29
Cpd 5: 2.230	102.0472	2.23	0.112	12348534	
Cpd 6: Fenvalerate; C25 H22 Cl N O3; 2.340	419.1296	2.34	0.107	8125930	66.66
Cpd 7: 4-Amino-2-methyl-1-naphthol; C11 H11 N O; 2.523	173.0847	2.523	0.083	7167502	97.91
Cpd 8: Delphinidin 3-glucoside; C21 H21 O12; 2.687	465.1037	2.687	0.137	11588062	99.37
Cpd 9: Delphinidin 3-rhamnoside 5-glucoside; C27 H31 O16; 2.703	611.1617	2.703	0.148	14259534	98.62
Cpd 10: Cyanidin-3-O-(6-O-acetyl)pentoside; C21 H21 O11; 2.796	449.1087	2.796	0.179	10587481	99.54
Cpd 11: Kaempferol; C15 H10 O6; 2.801	286.048	2.801	0.141	7123005	98.77
Cpd 12: Biorobin; C27 H30 O15; 2.814	594.159	2.814	0.211	15576994	80.6
Cpd 13: 2,6-Dimethyl-6-O-beta-D-quinovopyranosyl-7-octadecenoic acid; C16 H28 O7; 3.449	332.1839	3.449	0.129	8843136	95.04
Cpd 14: Withaperuvin B; C28 H40 O9; 4.134	520.2655	4.134	0.142	9281934	89.57
Cpd 15: Withaperuvin B; C28 H40 O9; 4.411	520.2655	4.411	0.123	7993458	87.79
Cpd 16: (6R)-3,6-Dimethyl-7-((8R,Z)-8-methylhexahydroindolizin-6(5H)-ylidene)heptane-1,2-diol; C18 H33 N O2; 5.654	295.2517	5.654	0.119	7747974	73.11
Cpd 17: Cinitapride; C21 H30 N4 O4; 6.249	402.2262	6.249	0.18	7240740	98.64
Cpd 18: Palmitic amide; C16 H33 N O; 6.472	255.2569	6.472	0.07	8291166	97.29
Cpd 19: Oleamide; C18 H35 N O; 7.402	281.2723	7.402	0.156	8458234	85.09

Appendix 29 BCP-MH-110 Negative

Label	Mass	RT	Width	Height	Score
Cpd 1: L-Altruronic acid; C6 H10 O7; 0.545	194.0434	0.545	0.154	6242958	83.93

Cpd 2: 1,4-beta-D-Glucan; C18 H32 O18; 0.574	536.1602	0.574	0.127	3237019	77.27
Cpd 3: C12 H23 Cl O11; 0.581	378.0936	0.581	0.128	2803152	93.96
Cpd 4: 9,10-dibromo-stearic acid; C18 H34 Br2 O2; 0.592	440.0917	0.592	0.125	5824056	65.85
Cpd 5: 2-O-a-D-Galactopyranuronosyl-L-rhamnose; C12 H22 O11; 0.635	342.1166	0.635	0.155	4591705	99.44
Cpd 6: Tetrahydro-2-methyl-3-thiophenethiol; C5 H10 S2; 0.658	134.0225	0.658	0.113	2699896	82.54
Cpd 7: C14 H16 O11 S; 0.799	392.0409	0.799	0.1	8180953	90.36
Cpd 8: 3-Methyl-2,5-furandione; C5 H4 O3; 0.832	112.0164	0.832	0.142	3967765	87.04
Cpd 9: (E)-1-Propenyl 2-propenyl disulfide; C6 H10 S2; 0.839	146.0225	0.839	0.176	15740357	67.92
Cpd 1: 2,4,6-Trihydroxybenzoic acid; C7 H6 O5; 1.461	170.022	1.461	0.132	8392040	98.17
Cpd 2: Kaempferol 3-O-β-D-glucosyl-(1->2)-β-D-glucoside; C27 H30 O16; 2.706	610.1514	2.706	0.132	7123790	67.99
Cpd 3: Delphinidin 3-glucosylglucoside; C27 H31 O17; 2.710	627.1572	2.71	0.121	8525279	98.07
Cpd 4: Myricetin 3-galactoside; C21 H20 O13; 2.716	480.0899	2.716	0.086	5857574	79.91
Cpd 5: 6,8-Di-C-glucopyranosyltricetin; C27 H30 O17; 2.729	626.1486	2.729	0.086	6856726	75.05
Cpd 6: Biorobin; C27 H30 O15; 2.803	594.1586	2.803	0.108	5885948	89.12
Cpd 7: C23 H28 N6 O14; 2.819	612.1667	2.819	0.155	5624450	91.96
Cpd 8: Myricetin; C15 H10 O8; 2.896	318.0382	2.896	0.099	4400584	82.32
Cpd 9: 2,2',3-Trihydroxy-3'-methoxy-5,5'-dicarboxybiphenyl; C15 H12 O8; 2.958	320.0537	2.958	0.101	8947489	98.23
Cpd 10: Pratenol B; C15 H12 O7; 3.173	304.0594	3.173	0.103	6722863	94.59
Cpd 11: C8 H2 N4; 3.249	154.0277	3.249	0.113	3955319	95.35
Cpd 12: Norwedelic acid; C15 H10 O8; 3.576	318.0375	3.576	0.13	6170453	85.03
Cpd 13: C15 H12 O9 S; 3.756	368.0201	3.756	0.11	9234017	99.47
Cpd 14: Rhynchosin; C15 H10 O7; 3.867	302.0427	3.867	0.137	3920870	98.68
Cpd 15: 9,12,13-trihydroxy-10,15-octadecadienoic acid; C18 H32 O5; 4.090	328.2251	4.09	0.124	4667912	85.2
Cpd 16: 11,12,13-trihydroxy-9-octadecenoic acid; C18 H34 O5; 4.222	330.2406	4.222	0.094	9392320	85.28
Cpd 17: 11,12,13-trihydroxy-9-octadecenoic acid; C18 H34 O5; 4.439	330.2408	4.439	0.1	5321512	99.65
Cpd 18: Lauryl hydrogen sulfate; C12 H26 O4 S; 6.029	266.1556	6.029	0.142	5068642	98.08
Cpd 19: 6.551	117.9363	6.551	0.194	3957197	

Cpd 20: C13 H24 N7 S; 6.664	310.1819	6.664	0.119	3883715	76.1
-----------------------------	----------	-------	-------	---------	------

Appendix 30 BCP-MH-120 Positive

Label	Mass	RT	Width	Height	Score
Cpd 1: 2-Amino-3-methyl-1-butanol; C5 H13 N O; 0.578	103.0994	0.578	0.341	11652300	98.9
Cpd 2: Dihydrocaffeic acid 3-O-glucuronide; C15 H18 O10; 0.615	358.0903	0.615	0.181	9374373	81.54
Cpd 3: bk-DMBDB; C13 H17 N O3; 0.619	235.1212	0.619	0.127	6942568	91.31
Cpd 4: Adenine; C5 H5 N5; 0.736	135.0552	0.736	0.148	8579379	84.55
Cpd 5: 0.849	214.0099	0.849	0.137	7589980	
Cpd 6: Phenylacrylic acid (Cinnamic acid); C9 H8 O2; 2.227	148.0527	2.227	0.115	7858858	99.12
Cpd 7: 2.229	102.0472	2.229	0.11	11641576	
Cpd 8: 2.338	436.156	2.338	0.102	7704511	
Cpd 9: Delphinidin 3-glucoside; C21 H21 O12; 2.696	465.1038	2.696	0.141	9056601	98.91
Cpd 10: Delphinidin 3-rhamnoside 5-glucoside; C27 H31 O16; 2.710	611.162	2.71	0.144	12947053	97.55
Cpd 11: Kaempferol 7-O-glucoside; C21 H20 O11; 2.793	448.1008	2.793	0.142	8131253	99.64
Cpd 12: Isopeonidin 3-sambubioside; C27 H31 O15; 2.810	595.1669	2.81	0.15	14236339	93.97
Cpd 13: 2,6-Dimethyl-6-O-beta-D-quinovopyranosyl-7-octadecenoic acid; C16 H28 O7; 3.452	332.1838	3.452	0.128	8341222	99.25
Cpd 14: Withaperuvin B; C28 H40 O9; 4.130	520.2655	4.13	0.145	8309764	89.43
Cpd 15: Withaperuvin B; C28 H40 O9; 4.410	520.2654	4.41	0.123	7619581	82.75
Cpd 16: (6R)-3,6-Dimethyl-7-((8R,Z)-8-methylhexahydroindolizin-6(5H)-ylidene)heptane-1,2-diol; C18 H33 N O2; 5.653	295.2517	5.653	0.107	7680927	84.21
Cpd 17: Acetyl tributyl citrate; C20 H34 O8; 6.249	402.2261	6.249	0.183	6610539	98.58
Cpd 18: Palmitic amide; C16 H33 N O; 6.472	255.2569	6.472	0.07	8141332	96.78
Cpd 19: Stearamide; C18 H37 N O; 6.933	283.288	6.933	0.238	7063980	94.16
Cpd 20: Oleamide; C18 H35 N O; 7.400	281.2723	7.4	0.22	8424868	85.21

Appendix 31 BCP-MH-120 Negative

Label	Mass	RT	Width	Height	Score
Cpd 1: 1,3-Dimethyluric acid; C7 H8 N4 O3; 0.544	196.0593	0.544	0.134	4101862	95.96
Cpd 2: L-Altruronic acid; C6 H10 O7; 0.554	194.0434	0.554	0.153	6483991	84.13
Cpd 3: 1,4-beta-D-Glucan; C18 H32 O18; 0.584	536.1603	0.584	0.122	2785488	76.36
Cpd 4: C12 H23 Cl O11; 0.590	378.0936	0.59	0.127	2220009	93.48
Cpd 5: 9,10-dibromo-stearic acid; C18 H34 Br2 O2; 0.599	440.0921	0.599	0.12	6024593	67.12
Cpd 6: Tetrahydro-2-methyl-3-thiophenethiol; C5 H10 S2; 0.664	134.0225	0.664	0.114	2775868	82.3
Cpd 7: Phenylmercuric Acetate; C8 H8 Hg O2; 0.806	332.0197	0.806	0.097	6393588	63.64
Cpd 8: 3-Methyl-2,5-furandione; C5 H4 O3; 0.839	112.0164	0.839	0.139	3800593	86.7
Cpd 9: 2,3-Dioxogulonic acid; C6 H8 O7; 0.846	192.0278	0.846	0.169	15654828	90.1
Cpd 10: C12 H12 N3 O13; 0.865	406.0362	0.865	0.134	3037154	81.64
Cpd 1: Norrubrofusarin 6-beta-gentiobioside; C26 H30 O15; 1.171	582.1587	1.171	0.102	4940649	99.75
Cpd 2: 2,4,6-Trihydroxybenzoic acid; C7 H6 O5; 1.435	170.022	1.435	0.132	8695952	98.17
Cpd 3: Norrubrofusarin 6-beta-gentiobioside; C26 H30 O15; 2.477	582.159	2.477	0.081	3037500	97.67
Cpd 4: Kaempferol 3-O-β-D-glucosyl-(1->2)-β-D-glucoside; C27 H30 O16; 2.710	610.1525	2.71	0.123	5291602	73.93
Cpd 5: Myricetin 3-galactoside; C21 H20 O13; 2.716	480.0901	2.716	0.083	4224447	80.37
Cpd 6: C25 H38 Cl2 N3 O7 S2; 2.720	626.1576	2.72	0.101	6225530	38.9
Cpd 7: Luteolin 7-neohesperidoside; C27 H30 O15; 2.802	594.1574	2.802	0.103	3855238	93.45
Cpd 8: Okanin 3',4'-diglucoside; C27 H32 O16; 2.820	612.1684	2.82	0.131	3387845	98.41
Cpd 9: Quinalizarin; C14 H8 O6; 2.897	272.0325	2.897	0.099	4797601	84.06
Cpd 10: 2,2',3-Trihydroxy-3'-methoxy-5,5'-dicarboxybiphenyl; C15 H12 O8; 2.958	320.0534	2.958	0.1	8320507	97.42
Cpd 11: C16 H8 N4 O3; 3.173	304.0599	3.173	0.099	5904040	94.66
Cpd 12: 5,7,8,3',4'-Pentahydroxyisoflavone; C15 H10 O7; 3.181	302.0438	3.181	0.12	4301711	79.45

Cpd 13: C ₈ H ₂ N ₄ ; 3.249	154.0279	3.249	0.097	3646266	96.9
Cpd 14: Myricetin; C ₁₅ H ₁₀ O ₈ ; 3.575	318.0378	3.575	0.144	4971970	94.15
Cpd 15: C ₁₅ H ₁₂ O ₉ S; 3.755	368.0202	3.755	0.11	9576729	99.56
Cpd 16: 9,12,13-trihydroxy-10,15-octadecadienoic acid; C ₁₈ H ₃₂ O ₅ ; 4.090	328.2251	4.09	0.123	4347959	85.15
Cpd 17: 11,12,13-trihydroxy-9-octadecenoic acid; C ₁₈ H ₃₄ O ₅ ; 4.221	330.2408	4.221	0.093	9257447	85.26
Cpd 18: 11,12,13-trihydroxy-9-octadecenoic acid; C ₁₈ H ₃₄ O ₅ ; 4.439	330.2407	4.439	0.1	5193414	99.49
Cpd 19: Lauryl hydrogen sulfate; C ₁₂ H ₂₆ O ₄ S; 6.024	266.1555	6.024	0.088	5604744	98.31
Cpd 20: C ₁₃ H ₂₄ N ₇ S; 6.660	310.1818	6.66	0.121	4326873	75.77

Appendix 32 BCP-MH-140 Positive

Label	Mass	RT	Width	Height	Score
Cpd 1: 2-Amino-3-methyl-1-butanol; C ₅ H ₁₃ N O; 0.591	103.0996	0.591	0.331	11869621	99.68
Cpd 2: Dihydrocaffeic acid 3-O-glucuronide; C ₁₅ H ₁₈ O ₁₀ ; 0.612	358.0902	0.612	0.148	6321863	80.54
Cpd 3: bk-DMBDB; C ₁₃ H ₁₇ N O ₃ ; 0.613	235.1215	0.613	0.122	6490484	89.39
Cpd 4: 0.735	118.0285	0.735	0.13	9605724	
Cpd 5: Carboxymethyloxysuccinate; C ₆ H ₈ O ₇ ; 0.847	192.0278	0.847	0.12	6461338	96.25
Cpd 6: L-Tyrosine; C ₉ H ₁₁ N O ₃ ; 0.891	181.0744	0.891	0.158	9115550	98.6
Cpd 7: Phenylacrylic acid (Cinnamic acid); C ₉ H ₈ O ₂ ; 2.219	148.0527	2.219	0.094	6372625	99.35
Cpd 8: 2.221	102.0472	2.221	0.101	10135599	
Cpd 9: Fenvalerate; C ₂₅ H ₂₂ Cl N O ₃ ; 2.333	419.1298	2.333	0.098	6044991	66.03
Cpd 10: Biorobin; C ₂₇ H ₃₀ O ₁₅ ; 2.803	594.1588	2.803	0.111	6470644	98.85
Cpd 11: 2,6-Dimethyl-6-O-beta-D-quinovopyranosyl-7-octadecenoic acid; C ₁₆ H ₂₈ O ₇ ; 3.455	332.1839	3.455	0.13	6598761	99.26
Cpd 12: Withaperuvin B; C ₂₈ H ₄₀ O ₉ ; 4.406	520.2655	4.406	0.13	6430461	87.07
Cpd 13: (6R)-3,6-Dimethyl-7-((8R,Z)-8-methylhexahydroindolizin-6(5H)-	295.2517	5.66	0.186	7874570	83.74

ylidene)heptane-1,2-diol; C18 H33 N O2; 5.660					
Cpd 14: (6R)-3,6-Dimethyl-7-((8R,Z)-8-methylhexahydroindolizin-6(5H)-ylidene)heptane-1,2-diol; C18 H33 N O2; 5.789	295.2529	5.789	0.24	6492813	37.89
Cpd 15: Spiroxamine; C18 H35 N O2; 5.930	297.2672	5.93	0.162	6292974	98.97
Cpd 16: LY255283; C19 H28 N4 O3; 5.989	360.2155	5.989	0.088	6923958	95.91
Cpd 17: Acetyl tributyl citrate; C20 H34 O8; 6.251	402.2261	6.251	0.165	8601078	98.09
Cpd 18: Palmitic amide; C16 H33 N O; 6.472	255.257	6.472	0.07	8358963	96.79
Cpd 19: Stearamide; C18 H37 N O; 6.935	283.2881	6.935	0.25	7128593	97.22
Cpd 20: Oleamide; C18 H35 N O; 7.407	281.2723	7.407	0.141	8679930	83.96

Appendix 33 BCP-MH-140 Negative

Label	Mass	RT	Width	Height	Score
Cpd 1: C13 H16 N7 O5 S; 0.542	382.0935	0.542	0.068	3756219	65.55
Cpd 2: Hamamelose; C6 H12 O7; 0.546	196.0592	0.546	0.125	4082385	96.07
Cpd 3: L-Altruronic acid; C6 H10 O7; 0.556	194.0434	0.556	0.134	6333205	84.08
Cpd 4: 9,10-dibromo-stearic acid; C18 H34 Br2 O2; 0.594	440.0932	0.594	0.111	5759676	66.71
Cpd 5: Sucrose; C12 H22 O11; 0.629	342.1168	0.629	0.154	2265411	98.72
Cpd 6: Tetrahydro-2-methyl-3-thiophenethiol; C5 H10 S2; 0.661	134.0225	0.661	0.113	2995137	68.64
Cpd 7: PQQH2; C14 H8 N2 O8; 0.806	332.0279	0.806	0.105	3889092	79.81
Cpd 8: 3-Methyl-2,5-furandione; C5 H4 O3; 0.837	112.0164	0.837	0.139	3399668	86.8
Cpd 9: C12 H12 N3 O13; 0.855	406.0362	0.855	0.124	2827971	97.24
Cpd 1: Norrubrofusarin 6-beta-gentiobioside; C26 H30 O15; 1.159	582.1588	1.159	0.101	6091396	99.58
Cpd 2: Dimethylmaleic acid anhydride; C6 H6 O3; 1.418	126.032	1.418	0.145	2120816	99.07
Cpd 3: 2,4,6-Trihydroxybenzoic acid; C7 H6 O5; 1.425	170.022	1.425	0.138	8289699	98.28
Cpd 4: Methyl 2,4,6-trihydroxybenzoate; C8 H8 O5; 1.493	184.0375	1.493	0.135	2480333	86.55

Cpd 5: 2,4-Dihydroxybenzoic acid; C7 H6 O4; 2.306	154.0269	2.306	0.082	2826519	99.38
Cpd 6: Norrubrofusarin 6-beta-gentiobioside; C26 H30 O15; 2.478	582.1589	2.478	0.085	3267331	98.58
Cpd 7: 6,8-Di-C-glucopyranosyltricetin; C27 H30 O17; 2.728	626.1484	2.728	0.085	2346619	75.3
Cpd 8: Prodelphinidin A1; C30 H24 O14; 2.793	608.1168	2.793	0.111	3144353	74.45
Cpd 9: 5-(4-Acetoxybut-1-ynyl)-2,2'-bithiophene; C14 H12 O2 S2; 2.888	276.0276	2.888	0.116	2194385	81.41
Cpd 10: Quinalizarin; C14 H8 O6; 2.895	272.0324	2.895	0.096	3033548	84.06
Cpd 11: 2,2',3-Trihydroxy-3'-methoxy-5,5'-dicarboxybiphenyl; C15 H12 O8; 2.955	320.0533	2.955	0.101	8839287	97.28
Cpd 12: C16 H8 N4 O3; 3.174	304.0599	3.174	0.102	6570658	93.39
Cpd 13: Rhynchosin; C15 H10 O7; 3.182	302.0435	3.182	0.098	2845286	81.23
Cpd 14: Myricetin; C15 H10 O8; 3.576	318.0378	3.576	0.123	5447362	94.3
Cpd 15: C15 H12 O9 S; 3.756	368.0204	3.756	0.114	9390436	99.24
Cpd 16: Rhynchosin; C15 H10 O7; 3.869	302.0429	3.869	0.134	3211222	98.4
Cpd 17: (9R,10S,12Z)-9,10-Dihydroxy-8-oxo-12-octadecenoic acid; C18 H32 O5; 4.091	328.2251	4.091	0.109	3679782	85.15
Cpd 18: 11,12,13-trihydroxy-9-octadecenoic acid; C18 H34 O5; 4.220	330.2408	4.22	0.092	8858130	85.27
Cpd 19: 11,12,13-trihydroxy-9-octadecenoic acid; C18 H34 O5; 4.440	330.2408	4.44	0.099	4751282	99.34
Cpd 20: Lauryl hydrogen sulfate; C12 H26 O4 S; 6.036	266.1555	6.036	0.148	2383016	98.24

Appendix 34 BCP-MH-160 Positive

Label	Mass	RT	Width	Height	Score
Cpd 1: 0.615	103.1016	0.615	0.286	12092458	
Cpd 2: 1H-Pyrrole-2-carboxaldehyde; C5 H5 N O; 0.648	95.0373	0.648	0.108	7731100	99.51
Cpd 3: 0.730	118.0288	0.73	0.121	10315484	
Cpd 4: 0.734	151.0502	0.734	0.108	8297061	
Cpd 5: 2-Acetyl-1-methylpyrrole; C7 H9 N O; 0.822	123.0688	0.822	0.1	6166865	98.93

Cpd 6: L-Tyrosine; C9 H11 N O3; 0.898	181.0744	0.898	0.164	12865713	98.52
Cpd 7: Acetylhydrazinophthalazinone; C11 H11 N3 O2; 1.003	217.0855	1.003	0.119	5468824	86.22
Cpd 8: Adenosine; C10 H13 N5 O4; 1.415	267.0972	1.415	0.142	7437796	96.12
Cpd 9: 5-Acetyl-2,3-dihydro-1H-pyrrolizine; C9 H11 N O; 1.823	149.0846	1.823	0.141	5749212	98.24
Cpd 10: 2.220	102.0472	2.22	0.092	7898457	
Cpd 11: 2.241	253.154	2.241	0.084	7751954	
Cpd 12: [(1R)-1-[(2S,4aR,4bS,7S,8aS)-7-Hydroxy-2,4b,8,8-tetramethyl-4,4a,5,6,7,8a,9,10-octahydro-3H-phenanthren-2-yl]-2-[(2R,3R,4S,5R,6R)-3,4,5-trihydroxy-6-(hydroxymethyl)oxan-2-yl]oxyethyl] acetate; C28 H46 O9; 2.896	526.3119	2.896	0.1	5430653	89.62
Cpd 13: Withaperuvin B; C28 H40 O9; 4.398	520.2654	4.398	0.136	5671010	89.03
Cpd 14: (6R)-3,6-Dimethyl-7-((8R,Z)-8-methylhexahydroindolizin-6(5H)-ylidene)heptane-1,2-diol; C18 H33 N O2; 5.702	295.2517	5.702	0.303	8003365	84.73
Cpd 15: Spiroxamine; C18 H35 N O2; 5.933	297.2671	5.933	0.15	6481095	98.74
Cpd 16: Acetyl tributyl citrate; C20 H34 O8; 6.252	402.2262	6.252	0.164	8382599	98.08
Cpd 17: Palmitic amide; C16 H33 N O; 6.472	255.2569	6.472	0.075	8277398	96.86
Cpd 18: Stearamide; C18 H37 N O; 6.938	283.288	6.938	0.246	7342730	93.62
Cpd 19: 3,4-Epoxy-6,9-octadecadiene; C18 H32 O; 7.403	264.2457	7.403	0.169	8722741	84.68
Cpd 20: Stearamide; C18 H37 N O; 7.406	283.2881	7.406	0.121	5495430	94.62

Appendix 35 BCP-MH-160 Negative

Label	Mass	RT	Width	Height	Score
Cpd 1: C14 H24 O9 S; 0.520	368.1137	0.52	0.044	5179140	91.28
Cpd 2: C14 H12 N11 O S; 0.545	382.0947	0.545	0.059	2930297	67.29
Cpd 3: Gulonic acid; C6 H12 O7; 0.547	196.0592	0.547	0.122	5923586	95.78
Cpd 4: 6-(Hydroxymethyl)-2,4(1H,3H)-pteridinedione; C7 H6 N4 O3; 0.559	194.0437	0.559	0.128	3660900	83.33
Cpd 5: 3,5-Dihydroxyphenyl 1-O-(6-O-galloyl-beta-D-glucopyranoside); C19 H20	440.0935	0.579	0.111	2826797	78.13

O12; 0.579

Cpd 6: 3-Glucosyl-2,3',4,4',6-pentahydroxybenzophenone; C19 H20 O11; 0.595	424.0985	0.595	0.105	3121968	77.4
Cpd 7: Tetrahydro-2-methyl-3-thiophenethiol; C5 H10 S2; 0.657	134.0226	0.657	0.11	3033108	68.48
Cpd 9: 3-Methyl-2,5-furandione; C5 H4 O3; 0.838	112.0164	0.838	0.139	3007537	86.92
Cpd 8: C8 H7 N3 O S; 0.838	193.0307	0.838	0.139	2944193	72.96
Cpd 10: C12 H12 N3 O13; 0.850	406.0361	0.85	0.113	2094176	96.82
Cpd 1: Pratenol B; C15 H12 O7; 1.134	304.0588	1.134	0.125	4075650	97.61
Cpd 2: Norrubrofusarin 6-beta-gentiobioside; C26 H30 O15; 1.154	582.1587	1.154	0.106	4272426	99.63
Cpd 3: Dimethylmaleic acid anhydride; C6 H6 O3; 1.388	126.0319	1.388	0.161	2934737	99.11
Cpd 4: 2,4,6-Trihydroxybenzoic acid; C7 H6 O5; 1.421	170.022	1.421	0.139	9455991	98.39
Cpd 5: Methyl 2,4,6-trihydroxybenzoate; C8 H8 O5; 1.490	184.0377	1.49	0.125	3597902	94.72
Cpd 6: Catechin-4beta-ol; C15 H14 O7; 1.700	306.0742	1.7	0.145	2729970	99.44
Cpd 7: 2,4-Dihydroxybenzoic acid; C7 H6 O4; 2.299	154.0268	2.299	0.085	6542567	99.64
Cpd 8: Myricetin 3-(4"-malonylramnoside); C24 H22 O15; 2.344	550.0954	2.344	0.079	2263649	92.79
Cpd 9: 2,4-Dihydroxybenzoic acid; C7 H6 O4; 2.480	154.0269	2.48	0.099	2578574	99.33
Cpd 10: Catechin-4beta-ol; C15 H14 O7; 2.500	306.0743	2.5	0.083	2280528	99.24
Cpd 11: (+)-Taxifolin; C15 H12 O7; 2.751	304.0579	2.751	0.078	3279997	84.15
Cpd 12: alpha-Furyl methyl diketone; C7 H6 O3; 2.798	138.0318	2.798	0.09	3511119	98.54
Cpd 13: Kaempferol; C15 H10 O6; 2.814	286.0478	2.814	0.087	2264760	84.64
Cpd 14: 3-Isopropylmalic acid; C7 H12 O5; 2.850	176.0686	2.85	0.104	2202861	99.5
Cpd 15: 2-Hydroxy-6-oxo-6-(2-hydroxyphenoxy)-hexa-2,4-dienoate; C12 H10 O6; 3.015	250.0479	3.015	0.093	2084204	96.96
Cpd 16: Myricetin; C15 H10 O8; 3.575	318.0377	3.575	0.154	2680740	98.26
Cpd 17: C15 H12 O9 S; 3.758	368.0204	3.758	0.102	5478355	98.39
Cpd 18: 9,12,13-trihydroxy-10,15-octadecadienoic acid; C18 H32 O5; 4.092	328.2251	4.092	0.13	3755395	78.14
Cpd 19: 11,12,13-trihydroxy-9-octadecenoic acid; C18 H34 O5; 4.220	330.2407	4.22	0.093	8433144	85.3
Cpd 20: 11,12,13-trihydroxy-9-octadecenoic acid; C18 H34 O5; 4.443	330.2407	4.443	0.104	4261238	99.67

Appendix 36 A picture of orange pectin samples.

